AD 748220

# ADAPTIVE PROCESSING FOR ANTENNA ARRAYS

Charles A. Baird, Jr.
George G. Rassweiler
Charles L. Zahm
G. Patrick Martin

Radiation Incorporated

Approved for public release;
distribution unlimited.

## FOREWORD

This final technical report, submitted by the Advanced Systems Operations of Radiation Systems Division, Melbourne, Florida, covers the period March 1971 to March 1972. Research was conducted under Contract F30602-71-C-0173, Job Order Number 45190000, for Rome Air Development Center, Griffiss Air Force Base, New York. Mr. Peter N. Edraos (DCRC) was RADC Project Engineer.

This document has been reviewed by the Office of Information (OI) and is releasable to the National Technical Information Service (NTIS).

This report has been reviewed and is approved.

Approved: Peter N. Edraos
PETER N. EDRAOS
Project Engineer

Approved: Joseph L. Ryerson
JOSEPH L. RYERSON, Technical Director
Communications & Navigation Division

FOR THE COMMANDER: Fred I. Diamond
FRED I. DIAMOND
Acting Chief, Plans Office

UNCLASSIFIED

Security Classification

## DOCUMENT CONTROL DATA - R & D

(Security classification of title, body of abstract and indexing annotation must be entered when the overall report is classified)

| | |
|---|---|
| 1. ORIGINATING ACTIVITY (Corporate author)<br>Radiation Incorporated<br>Melbourne, FL 32901 | 2a. REPORT SECURITY CLASSIFICATION<br>Unclassified<br>2b. GROUP |

3. REPORT TITLE

Adaptive Processing for Antenna Arrays

4. DESCRIPTIVE NOTES (Type of report and inclusive dates)

Final Report - March 71-March 72

5. AUTHOR(S) (First name, middle initial, last name)

Charles A. Baird, Jr; George G. Rassweiler, Charles L. Zahm; G. Patrick Martin

| | | |
|---|---|---|
| 6. REPORT DATE<br>July 1972 | 7a. TOTAL NO. OF PAGES<br>295 | 7b. NO. OF REFS<br>80 |
| 8a. CONTRACT OR GRANT NO.<br>F30602-71-C-0173<br>b.<br>Job Order No.: 45190000<br>c.<br>d. | 9a. ORIGINATOR'S REPORT NUMBER(S)<br>N/A<br>9b. OTHER REPORT NO(S) (Any other numbers that may be assigned this report)<br>RADC-TR-72-174 | |

10. DISTRIBUTION STATEMENT

Approved for public release;
distribution unlimited.

| | |
|---|---|
| 11. SUPPLEMENTARY NOTES | 12. SPONSORING MILITARY ACTIVITY<br>Rome Air Development Center (DCRC)<br>Griffiss AFB NY 13440 |

13. ABSTRACT

This is the final report of a study into adaptive processing techniques for r-f antenna arrays conducted by Radiation Systems Division for Rome Air Development Center. The report reviews the background of adaptive arrays and formulates the basic structure of the array and environment under consideration. Appropriate performance criteria and the derivation of the associated optimal solutions are presented. For very narrowband problems it is shown that the solutions differ only by a scalar gain, and thus have the same output signal-to-noise ratios. Iterative-adaptive computation procedures are then presented, from which it is obvious that a stochastic approximation-steepest gradient algorithm is best suited for real-time arrays. Within the context of this background, the adaptive algorithms which have been presented previously are discussed and compared. From this analysis it is obvious that the most promising algorithms are essentially equivalent. The behavior of the basic LMS type algorithm is analyzed, primarily by the solution of the associated differential equations.

The basic adaptive algorithms examined do not represent complete solutions to many communications problems, because a priori knowledge of signal structure or direction of arrival is assumed. This acquisition problem is studied and techniques to improve the signal-to-noise ratio, in the presence of strong jamming, are presented. These methods allow acquisition of relatively weak desired signals without assuming restrictive a priori knowledge. Computer simulations of these techniques are presented, including the simulation for a specific TDMA scenario. Finally, implementation problems are discussed and breadboard experiments are suggested.

DD FORM 1 NOV 65 1473



UNCLASSIFIED

Security Classification

UNCLASSIFIED

Security Classification

| 14. KEY WORDS | LINK A ROLE | LINK A WT | LINK B ROLE | LINK B WT | LINK C ROLE | LINK C WT |
|---|---|---|---|---|---|---|
| Antenna Arrays | | | | | | |
| Phased Arrays | | | | | | |
| Directional Antennas | | | | | | |
| Steerable Antennas | | | | | | |
| Antenna Radiation Patterns | | | | | | |

SAC--Griffiss AFB NY



UNCLASSIFIED

Security Classification

TABLE OF CONTENTS


| Chapter | Title | Page |
|---|---|---|
| 1.0 | INTRODUCTION | 1-2 |
| 1.1 | The General Null Steering Antenna Array Problem | 1-2 |
| 1.2 | Background Material on Null Steering Antenna Arrays | 1-2 |
| 1.2.1 | Historical Perspectives | 1-2 |
| 1.2.2 | RF Arrays - The Side Lobe Canceller | 1-4 |
| 1.2.3 | More General Adaptive Arrays | 1-7 |
| 1.2.4 | Null Steering Adaptive Array Classification Based Upon A Priori Information | 1-10 |
| 1.3 | The Nature of the Study | 1-12 |
| 1.4 | Outline of the Report | 1-12 |
| 2.0 | GENERAL PROBLEM FORMULATION | 2-2 |
| 2.1 | Environment Structure | 2-2 |
| 2.2 | Signal Structure at the Array | 2-2 |
| 2.3 | Array Processor Models and Their Properties | 2-6 |
| 2.3.1 | The General Transfer Function Model | 2-6 |
| 2.3.2 | Tapped Delay Line Models | 2-8 |
| 2.3.3 | Narrowband Tapped Delay Line Processor: Complex Weight | 2-11 |
| 2.3.4 | Aligned Arrays | 2-14 |
| 2.4 | Array Correlation Functions and Output Relations | 2-17 |
| 2.4.1 | General Representations | 2-17 |
| 2.4.2 | Structure of the Signal and Noise Covariance Matrix | 2-19 |
| 2.4.3 | Basic Array Output Definitions | 2-22 |
| 3.0 | THE OPTIMAL SOLUTIONS | 3-2 |
| 3.1 | The Performance Measures | 3-2 |
| 3.1.1 | Mean Square Error | 3-2 |
| 3.1.2 | Signal-to-Noise Ratio | 3-3 |
| 3.1.3 | The Likelihood Function | 3-4 |
| 3.1.4 | Output Noise Variance | 3-5 |
| 3.2 | Derivation of the Optimal Solutions | 3-6 |
| 3.2.1 | The Minimum Mean Square Error Solution | 3-6 |
| 3.2.2 | The Maximum Signal-to-Noise Ratio Solution | 3-7 |
| 3.2.3 | The Maximum Likelihood Solution | 3-10 |

TABLE OF CONTENTS (Continued)


| Chapter | Title | Page |
|---|---|---|
| 3.2.4 | The Unbiased Minimum Variance Solution | 3-11 |
| 3.3 | Comparison of Solutions | 3-13 |
| 3.3.1 | Mean Square Error Solution Factorization | 3-13 |
| 3.3.2 | Comparison with Other Solutions: Output S/N Ratio | 3-16 |
| 3.3.3 | Maximum Likelihood Versus Minimum Mean Square Error Solutions | 3-18 |
| 4.0 | OPTIMIZATION TECHNIQUES | 4-2 |
| 4.1 | The Search Techniques | 4-2 |
| 4.2 | The Gradient Methods | 4-5 |
| 4.2.1 | General Description | 4-5 |
| 4.2.2 | Steepest Descent Implementations | 4-6 |
| 4.3 | The Higher Order Methods | 4-8 |
| 4.3.1 | General Description - The Newton-Raphson Method | 4-8 |
| 4.3.2 | Application to Mean Square Error Performance Measure | 4-9 |
| 4.4 | The Projection Gradient Method | 4-11 |
| 4.5 | The Method of Stochastic Approximation | 4-13 |
| 4.5.1 | Brief Description of Stochastic Approximation | 4-14 |
| 4.5.2 | Application to Null Steering Adaptive Arrays: Intuitive Agreement | 4-16 |
| 4.6 | Alternative Computational Procedures | 4-17 |
| 5.0 | BASIC ADAPTIVE ARRAY ALGORITHMS | 5-2 |
| 5.1 | Minimum Mean Square Error Algorithm | 5-2 |
| 5.1.1 | The LMS Algorithm | 5-2 |
| 5.1.2 | The Modified LMS Algorithm | 5-6 |
| 5.2 | Signal-to-Noise Ratio Algorithms | 5-7 |
| 5.2.1 | Applebaum's S/N Algorithm | 5-7 |
| 5.2.2 | Other S/N Algorithms | 5-11 |
| 5.3 | Maximum Likelihood Algorithms | 5-11 |
| 5.4 | The Minimum Noise Variance Algorithm | 5-13 |
| 5.4.1 | Derivation of the Projection Operator | 5-13 |
| 5.4.2 | The Use of Signal Corrupted Correlations | 5-14 |
| 5.4.3 | A Two-Dimensional Example | 5-15 |
| 5.4.4 | The General Projection Gradient Algorithm | 5-18 |
| 5.5 | Comparison of the Basic Adaptive Algorithms | 5-20 |
| 5.5.1 | The Removal of Signal Effects | 5-20 |

TABLE OF CONTENTS (Continued)


| Chapter | Title | Page |
|---|---|---|
| 5.5.2 | Basic Processor Differential Equations | 5-21 |
| 6.0 | BEHAVIOR OF ADAPTIVE ARRAYS USING THE LMS ALGORITHM | 6-2 |
| 6.1 | Solution of Basic Differential Equations | 6-2 |
| 6.1.1 | Transient Behavior | 6-2 |
| 6.1.2 | Steady-State Behavior | 6-14 |
| 6.2 | Conventional Array Comparison | 6-24 |
| 6.3 | Optimal Antenna Patterns | 6-34 |
| 7.0 | ACQUISITION TECHNIQUES | 7-2 |
| 7.1 | Mathematical Analysis of Model 1 | 7-5 |
| 7.2 | Large Jammer-to-Signal Power Approximation | 7-8 |
| 7.3 | Analysis of Two Acquisition Models | 7-16 |
| 7.3.1 | Analysis of Model S1 | 7-17 |
| 7.3.2 | Analysis of Model S2 | 7-23 |
| 8.0 | PARAMETRIC STUDIES OF ADAPTIVE ARRAYS | 8-2 |
| 8.1 | Transient Behavior Biased Jammer Suppression | 8-4 |
| 8.1.1 | Typical Results Using Eigenvalue Solutions (vs. Angle, Bandwidth and Bias) | 8-4 |
| 8.1.2 | Typical Simulation Results | 8-8 |
| 8.1.3 | Absolute Time | 8-10 |
| 8.2 | Steady-State Jammer Null Depth for the Jammer Suppression Technique | 8-13 |
| 8.2.1 | Effect of Bandwidth | 8-14 |
| 8.2.2 | Effect of Input Jammer Power | 8-16 |
| 8.2.3 | Effect of Jammer Angle | 8-18 |
| 8.2.4 | Effect of Multiple Jammers | 8-22 |
| 8.3 | Steady-State Output Signal and S/N Improvement-Jammer Suppression Technique | 8-26 |
| 8.3.1 | Null Depth on Signal with Biased Suppression | 8-26 |
| 8.3.2 | Signal-to-Jammer Ratio-Biased Suppression | 8-32 |
| 8.3.3 | Signal-to-Total Noise Ratio-Biased Suppression | 8-34 |
| 8.4 | Several LMS Array Results (Having Signal Removal) | 8-38 |
| 8.5 | Overspecified Arrays (The Numerous Signal Case) | 8-38 |

TABLE OF CONTENTS (Continued)


| Chapter | Title | Page |
|---|---|---|
| 8.6 | Polarization Considerations | 8-38 |
| 9.0 | A UNIFIED TDMA COMMUNICATION - NULL STEERING SYSTEM | 9-2 |
| 9.1 | Introduction | 9-2 |
| 9.2 | System Model | 9-2 |
| 9.2.1 | Geometric Configuration | 9-2 |
| 9.2.2 | Mode of Transmission | 9-2 |
| 9.2.3 | Recognition of Friendlies | 9-4 |
| 9.2.4 | Message Coding | 9-4 |
| 9.2.5 | Message Format | 9-4 |
| 9.2.6 | Jammer Characteristics | 9-4 |
| 9.2.7 | System Synchronization | 9-6 |
| 9.3 | Desired Adaptive Array Properties | 9-6 |
| 9.3.1 | Modes of Operation | 9-8 |
| 9.3.2 | Suppression Mode | 9-8 |
| 9.3.3 | Jammer Strategies | 9-9 |
| 9.3.4 | Sync Mode | 9-13 |
| 9.3.5 | Receive Mode | 9-13 |
| 9.4 | Circuit Description | 9-15 |
| 9.4.1 | Suppression Mode | 9-15 |
| 9.4.2 | Sync Mode | 9-17 |
| 9.4.3 | Receive Modes | 9-18 |
| 9.4.4 | Important Response Times | 9-19 |
| 10.0 | IMPLEMENTATIONS OF ADAPTIVE ARRAYS | 10-2 |
| 10.1 | RF Versus IF Processing | 10-2 |
| 10.1.1 | RF Weighting | 10-2 |
| 10.1.2 | IF Weighting | 10-4 |
| 10.2 | Types of Weights | 10-4 |
| 10.3 | Types of Correlation | 10-6 |
| 10.4 | Weight Control | 10-6 |
| 10.5 | Weight Constraints | 10-8 |
| 10.5.1 | Before Signal Acquisition | 10-8 |
| 10.5.2 | After Signal Acquisition | 10-9 |
| 10.6 | Amplitude and Convergence Rate Control | 10-9 |
| 10.7 | Signal Removal of Spread Spectrum Signals | 10-12 |

TABLE OF CONTENTS (Continued)


| Chapter | Title | Page |
|---|---|---|
| 11.0 | BREADBOARD DESIGNS AND DESIRABLE EXPERIMENTS | 11-2 |
| 11.1 | Preferred Implementations | 11-2 |
| 11.2 | Breadboard Experiments | 11-4 |
| 11.2.1 | Quadrature Channel Experiments | 11-4 |
| 11.2.2 | Complex Weight With IF Correlation | 11-10 |
| 11.3 | Spread Spectrum Signal Removal Experiments | 11-14 |
| 12.0 | CONCLUSIONS | 12-2 |
| 12.1 | Summary of Results | 12-2 |
| 12.2 | Recommendations for Future Work | 12-6 |
| 12.2.1 | Additional Computer Simulation | 12-6 |
| 12.2.2 | Breadboard Tests | 12-7 |
| 12.2.3 | Alternative Algorithm Investigations | 12-7 |
| 12.2.4 | Studies for Specific Applications | 12-7 |
| | APPENDICES | |
| A | Description of Computer Simulation Routines | A -2 |
| B | Simulation Program TDNS | B -2 |
| | References | R -2 |

EVALUATION: FINAL REPORT - "ADAPTIVE PROCESSING FOR ANTENNA ARRAYS"

This is the final technical report of an in-depth comprehensive theoretical investigation carried out for RADC by Radiation, Inc on methods of adaptive array processing. (An adaptive receiving array performs an interference-suppression function, in an environment of spatially-distributed emitters, by adjusting the antenna pattern to place relatively high gains in those directions which contain desired signals, and nulls on all other signal directions.) Some points of significant interest demonstrated during the course of this investigation:

1. The performance measures studied (mean-square-error, signal-to-noise ratio, the likelihood function, and noise variance) are essentially equivalent, the main difference being a scalar factor. The important result of this is that choice of performance measure is mathematically immaterial--the choice will be determined by system application and implementation considerations.

2. The steepest descent approach to an optimum performance measure, coupled with stochastic approximation, is the best available optimization technique within the present state-of-art.

3. The suppression process can be considered to be essentially one of signal equalization--null depth is, roughly, in proportion to signal power (thermal noise is also a controlling factor). The implications of this may be important to TDMA applications, where the mean power of the jammer is significantly higher than that of any single access.

In general, the study provided the fundamental technology on adaptive processing, from which those aspects and features applicable to AF use may be extracted. Although the contract emphasis was on TDMA waveforms (the CNI scenario, parameters, and candidate waveforms were specified for the study), the findings and technical conclusions are in large part very general in applicability, and relevant to other system applications.

Peter N Edraos

PETER N. EDRAOS
PROJECT ENGINEER

# CHAPTER I

# INTRODUCTION

## 1.0 INTRODUCTION

In this introductory chapter the basic problem being addressed, some related background material, and the nature of the study being reported on are presented. The relationship of the adaptive null steering antenna array problem to other technology areas is discussed, and the basic mechanism of the adaptive array is developed within this historical context. This allows the nature of the study to be better defined and leads to an understanding of the relationship between the results presented here and work already accomplished.

### 1.1 The General Null Steering Antenna Array Problem

The null steering antenna array problem can be described in a general context in terms of the diagram in Figure 1-1. In an environment of spatially distributed emitters (including isotropic and thermal noise) it is desired to adjust the antenna pattern of an array of sensors (antennas, hydrophones, seismometers) so as to receive a desired signal in some optimal manner (optimal being defined in terms of some appropriate performance measure). Since the emitters are distributed in space, an array allows the flexibility to perform both spatial and temporal filtering to enhance the desired signal.

This is accomplished by adjusting the antenna pattern to place relatively high gains on those directions and frequencies which contain the desired signal and relatively low gains (nulls) on all other signals. Since this processing is to be conducted in a complicated environment involving emitters capable of relative motion and changing their signal structure (such as turning on and off), a very versatile processing scheme must be used. This leads to the choice of an adaptive processing method for the process controller. Such problems as these arise in sonar and seismic applications, as well as the RF communications context of this study. As such, there is an extensive background of relevant theory and practical devices which must be examined before choosing a specific processing method.

### 1.2 Background Material on Null Steering Antenna Arrays

#### 1.2.1 Historical Perspectives

There has been a considerable amount of work over many years in technology areas related to the general null steering array problem. Some of the earliest work has involved the processing of acoustic signals, both

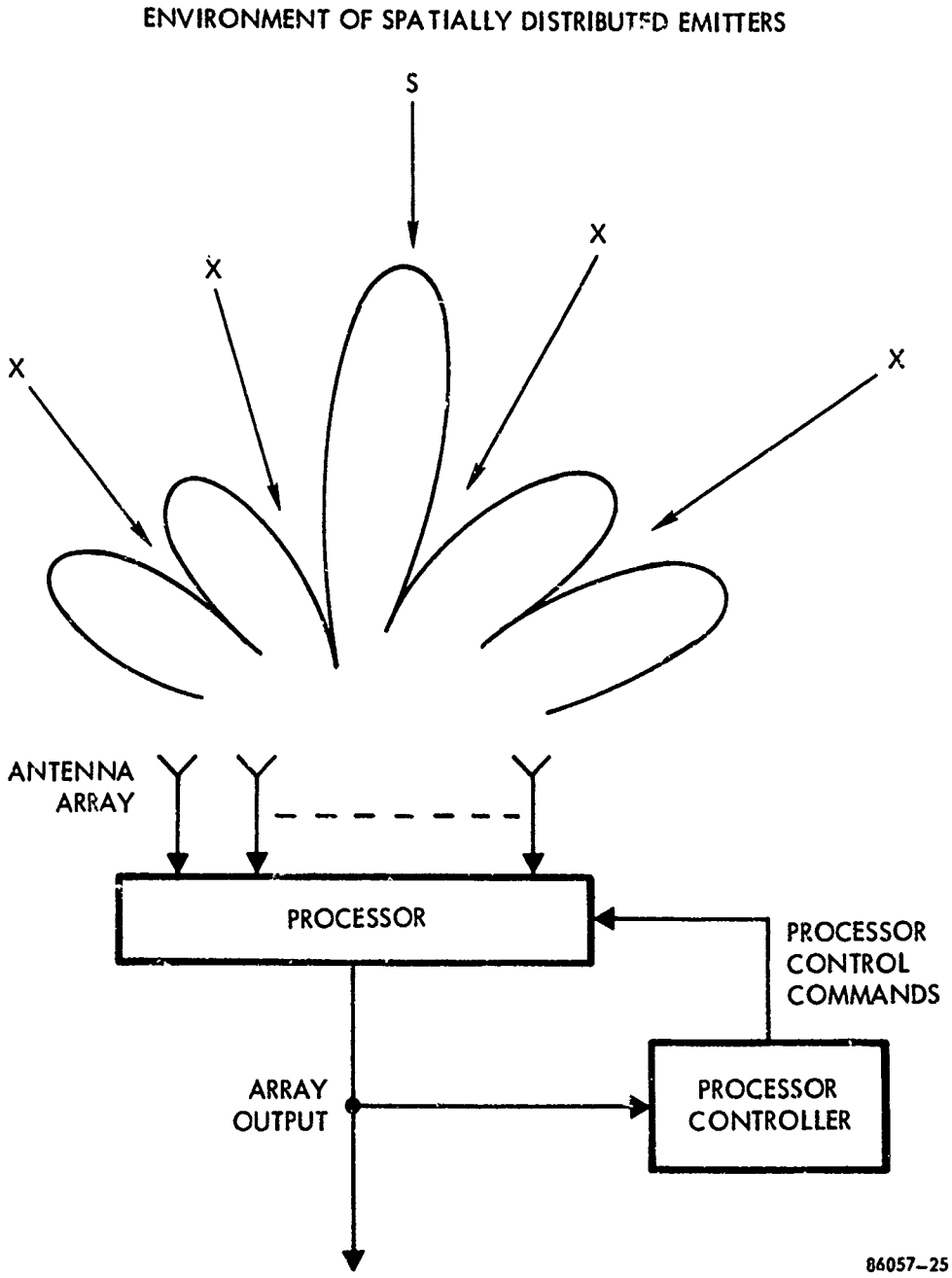


Figure 1-1. General Null Steering System

i. Sonar Signal Processing

and

ii. Seismic Signal Processing for oil exploration and nuclear test detection

Various properties of sonar arrays have received a great deal of attention, from the early work at the Harvard Acoustic Research Laboratory,[36] to the more recent interest of Bryn,[15] Middleton,[57] and Van Trees.[73] Much of this later work has involved the design of optimum arrays, and as such represents an extension of basic Wiener filtering theory to these multidimensional problems. Similar work has proceeded in the area of seismic arrays, with early work being done by Burg,[16] M.I.T. Lincoln Lab,[48,49] and Texas Instruments.[69,70] Much of this acoustic work is detection theory oriented; however, optimal detection design involves the optimal estimation problem of primary concern in this report.[73] Many of the results of this work in acoustic signal processing apply directly to the problems associated with RF communications arrays. For RF arrays, early background material is found in radar side lobe canceller work (discussed in the next section) and the closely related areas of adaptive filtering and pattern recognition.

### 1.2.2 RF Arrays - The Side Lobe Canceller

Early work in the area of RF arrays for interference rejection was done at M.I.T. Lincoln Lab[2] on a nonadaptive interference canceller based on the idea of steering a directional antenna at the interference, and subtracting this, with proper phasing, from the main channel. Unlike the array processors being considered in this study, this procedure requires that the noise be isolated through a separate high-gain antenna; it is not adaptive in nature, and can handle only one jamming source at a time. More recently, Applebaum and others at Syracuse Research Institute[6] have developed side lobe cancellers which are more closely related to the adaptive arrays which are being considered in this study. They are capable of handling both single and multiple jamming sources and use adaptive control circuitry.

To understand the basic mechanism of side lobe cancellers, and thereby see its relationship to the more general adaptive arrays under consideration in this study, consider the simplified diagram of Figure 1-2. The side lobe canceller can be described in terms of adjusting weights to minimize correlation as follows. In Figure 1-2 only one channel of processing is shown; for each channel desired signal, jammer signals and thermal noise form the total ith channel signal, $x_i$, which may go through an IF strip, be weighted for phase and amplitude control, and is summed to form the output, $\gamma$. One channel is assumed to be a high-gain antenna pointed at the desired signal. It is assumed that the desired signal level at each element is very small compared to the jamming, since if this were not so, the high-gain antenna would be able to adequately

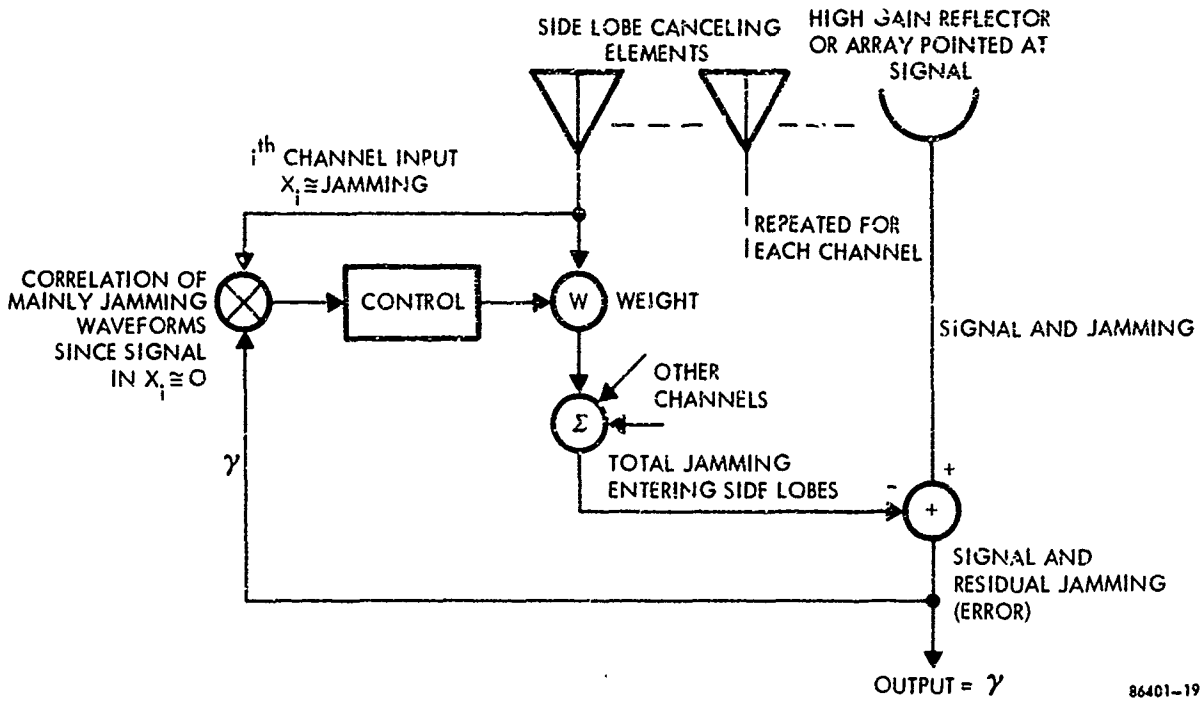


Figure 1-2. The Side Lobe Canceller

suppress the jammer with its side lobe. Figure 1-2 also shows typical control circuitry for the weights. As in almost all adaptive arrays, the output signal (or some error signal derived from the output) is correlated with each ith channel waveform, $x_i$, and filtered to form the control signal for the ith channel weight.

A simplified explanation for jammer cancellation is that, if at some time jamming still exists at the output, a correlation will occur with each ith channel input waveform, $x_i$, which contains the same jamming waveforms. The filtered correlation in the ith channel will change the ith weight, $w_i$. This change will continue until a minimum correlation exists, which means a minimum in jamming signal at the output. Side lobe canceller analysis and design has been greatly refined and generalized by Applebaum[5], but still assumes a priori knowledge of the signals direction-of-arrival and the presence of a high-gain reflector or array antenna.

The adaptive arrays considered in this study differ from the side lobe canceller ideas as follows:

a. There are multiple desired signals which may arrive simultaneously from almost any angle. Thus, one or several "main beams" are not possible in general.

b. There are no well defined side lobes to cancel, due both to the use of low gain (few elements) and to multiple desired signals.

c. The Directions-Of-Arrival (DOA) of the signals are probably not known. Thus, signal processing may not be based on DOA, at least during signal acquisition.

d. If a low gain array is used in the simple side lobe canceller configuration of Figure 1-2, with DOA unknown, a null will be steered on the signal. Simply put, the reason is that the total correlation can only be minimized by eliminating the signal from the output, as well as the jamming.

The more general adaptive arrays to be discussed in the next section utilize various procedures for the elimination of the signal effects from the correlations which control the weight circuits. In this manner they eliminate the interference as the side lobe canceller does, but do not necessarily assume that signal direction of arrival is known and that a high-gain antenna is pointed in that direction.

### 1.2.3 More General Adaptive Arrays

For the application of multiple communication signals with low gain arrays, a more general adaptive array model should be used, such as shown in Figure 1-1. Figure 1-3 shows a different adaptive array type of general adaptive model. There are two basic differences between this array model and Figure 1-2. In the first place, there is no high-gain element; elements are often approximately equal in gain. Secondly, there is formation of an "error" signal "$\epsilon$" by removing the desired signal from the total output. If the desired signal is used to form the error, the error can then be minimized by minimizing jamming and thermal noise alone. If signal is not removed, in general it will be nulled as well as the jammer in order to minimize error. Again, as before, if substantial correlation between $x_i$ and $\epsilon$ exists, the correlation will change the weights, the output and the error until a minimum correlation exists. The signal components in the input channels $x_i$ will not correlate with the error, thus signal will not be minimized. As will be demonstrated, the substantial difference between most of the different types of adaptive arrays is in what a priori information is assumed available about the signals and interference, and how it is used to remove the signal effects from the correlations which drive the weights.

Widrow et al.[76] presented the basic work on the general adaptive arrays which seek to minimize the mean square error between the desired signal and the array output. This work was an extension of Widrow's earlier work on adaptive filtering and pattern recognition [75] and Wiener filtering. Widrow calls his procedure the LMS Algorithm. Their model takes the form shown in Figure 1-3, where the subtraction of the desired signal, as they hypothesize, is not a realistic procedure, since if the desired signal were known there would be no need for further processing. They also suggest an alternative procedure for forming an error channel which requires that the direction-of-arrival of the desired signal is known, rather than the signal itself. A CW reference signal is inserted into each element with phase chosen to simulate an incoming plane wave from the direction of the desired signal. A two mode procedure is then implemented where the array alternatively adapts to the environment with no signal subtracted from the error channel, and then with the inserted reference signal subtracted. However, this procedure does introduce biases into the calculated weights since signal still partially contaminates the error channel. Griffiths [43] has presented a modification to this algorithm which removes the signal effects in a different manner and requires that the spectral density and the direction-of-arrival of the desired signal is known. From these quantities the signal correlation terms in the correlator-weight control circuits can be calculated and subtracted out, so that they will not bias the weights. Actually, Applebaum[5] used a similar procedure before this. This same algorithm was derived using a modified stochastic approximation procedure by Chang and Tutuer[21]. These last procedures were based on the minimization of mean squared error, while other

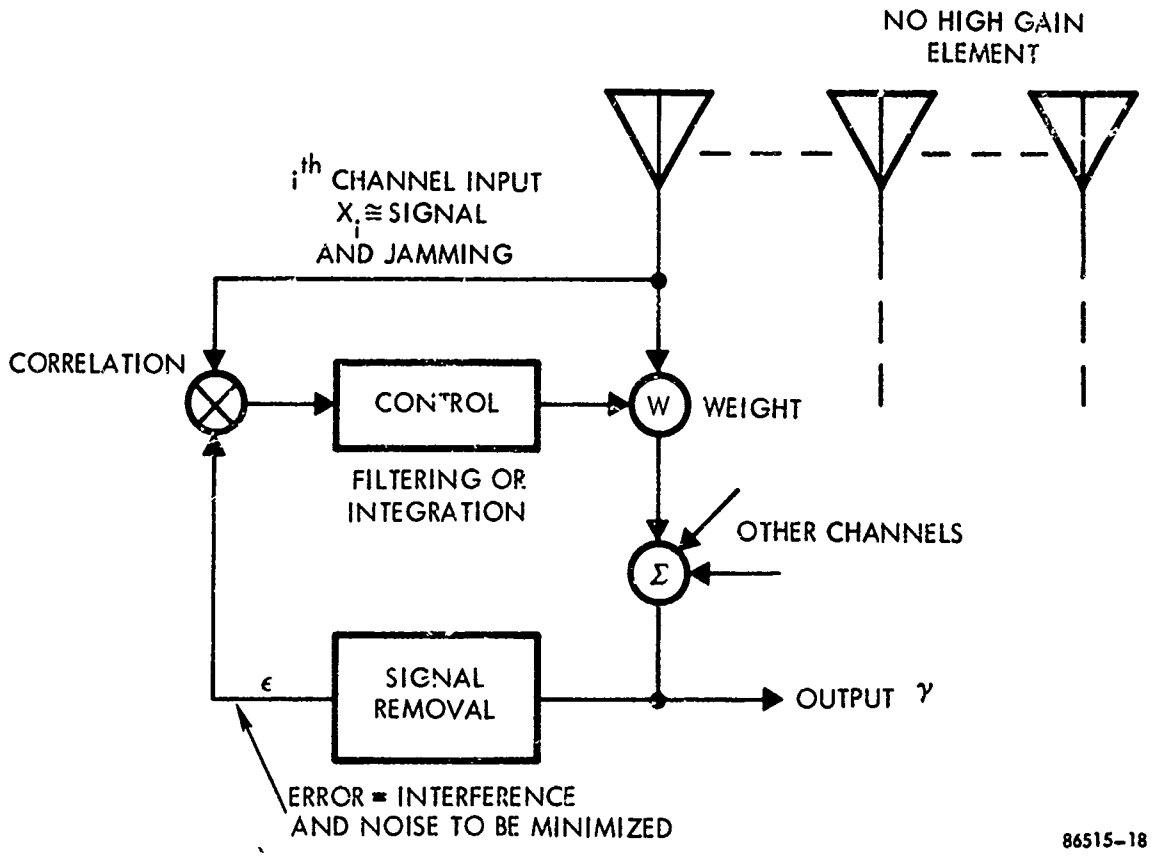


Figure 1-3. General Adaptive Array (Signal Removal Type)

workers have presented similar procedures for maximizing signal-to-noise ratio[1,67], maximizing the likelihood function, [41] and minimizing the output noise variance[52]. As will be demonstrated, in relatively narrowband problems the processors based on these different performance measures are essentially identical.

All of the procedures cited in the last paragraph seek to optimize the performance measure in question utilizing a steepest descent optimization technique, and lead not only to similar final solutions, but also to essentially identical weight control circuitry. However, none of them actually represent a total solution to practical RF communications problems. That is, the basics of the procedures are presented, but questions such as how desired signal, spectral densities or directions-of-arrival are obtained (if at all) must be answered in terms of reasonable assumptions about the specific problem at hand. Initial work on the signal estimation problem was done by Compton and Riegler[26], where they use the basic Widrow LMS Algorithm and demonstrate that only the signal carrier (where the desired signal is assumed to consist of a signal carrier with sidebands) need be known and subtracted from the array output to form the error channel. This, of course, leads to signal biases from the sideband terms, but has been shown experimentally to be an effective procedure. Huff [47] reports further sophistication of this idea for use with spread spectrum waveforms, but he assumes that the coded PN sequence is synchronized at the receiver. More recently [27], Compton has been developing the idea of signal equalization for acquisition, with extensions to this basic idea being presented in this report.

### 1.2.4 Null Steering Adaptive Array Classification Based Upon A Priori Information

With all null steering arrays, it is desired to steer a null on interference, but not on the desired signal; thus, there must be some discrimination of desired signal from interference. For example, with the side lobe canceller, the discrimination was done with the high gain antenna pointed at the signal. With the general signal removal array (Figure 1-3), subtraction or blocking of the desired signal eliminated it from the error channel.

Notice that the interference, not the signal, must be isolated to control the null steering circuitry, which is different and much simpler than the usual signal processing problem of recovering the signal from interference. For example, out-of-band jamming can be separated by simple band stop filtering and minimized to steer nulls on jamming. The a priori knowledge available must govern which technique to use in isolating the interference.

Characteristics of signal and noise that are potentially useful in removing the signal correlation terms from the weight control circuitry are:

Interference (Jammer or RFI) Characteristics

1. Dominant Jammer Power (often greater than the signals)

2. Separable Jammer Power, either by the spectrum (often wider than the signals) or by the time waveform (often continuous if noise-like or broken for look-through if a repeater)

3. Polarization (usually somewhat different from the signals)

Signal Characteristics

1. Known time waveform or spectrum (e.g., spread spectrum code or known frequency channel).

2. Known direction-of-arrival of the signal (obtained a priori or measured).

The most important differences between various adaptive array algorithms stems from how these characteristics are utilized to remove signal effects, if at all. Certain adaptive arrays that result from these differences can generally be classified on the basis of this a priori knowledge, such as:

1. Dominant Jammer Suppression Arrays

   a. Unbiased

   b. Controlled Bias

2. Separable Jammer Arrays

3. Known Signal Arrays

4. Known Signal DOA Arrays

In the dominant jammer technique, no signal effect removal is attempted (much like the side lobe canceller devices). The operation of this type of array is based on the fact that dominance of the jammer power in the control circuitry automatically steers nulls more deeply on the dominant jammer than on a weak signal. Furthermore, the initial suppression of the jammer is very rapid compared to the suppression of weak signals. In fact, with purely integral control in the correlator, it can be shown that the jammer output is suppressed below the signal reciprocally to its incoming ratio of jammer-to-signal. However, at a much later time, signal is gradually nulled too, in order to minimize total error.

In the "unbiased" case of dominant jammer suppression, it is intended to receive the signal completely in the time before nulling, or to derive the signal for a "Known-Signal" mode. With the Controlled Bias case, the jammer and signal can be stopped short of reciprocal suppression in the steady state (possibly equalized, if desired) without great signal loss. Deep nulls are not placed on the jammer, but also are not placed on the signal. A matched filter can then discriminate the signal from uncoded interference.

The Separable Jammer technique relies on separating out pure jammer power, for example out-of-band jamming, perhaps using a band stop filter as mentioned above. The Known Signal and Known Signal DOA techniques are simply the basic LMS adaptive array algorithms as presented by Widrow et al., Griffiths, etc., described above. In these methods, either the signal waveform is subtracted from the output to form the error channel, or signal DOA is used to generate signal correlation which is subtracted after the correlator. These techniques, especially Known Signal, are potentially useful after acquisition of the signal, but are not useful if jamming overwhelms the signal processor that is trying to detect and acquire the signal. However, significant implementation problems exist in the application of Known Signal techniques when matched filters are used for spread spectrum signals.

## 1.3 The Nature of the Study

The first stages of this study have involved the examination of the relevant mathematical techniques, and previously proposed adaptive algorithms (such as those described in Paragraph 1.2.3), which are suitable for the design of null steering array processors in an RF communications problem. This has involved the investigation of the mathematical basis for adaptive optimization techniques, and the adaptive algorithms which have been based on these methods. A major aim is to provide the background for the comparison of available processors, and allow the selection of a promising method for a more detailed parameter analysis. Upon examination of these methods, it is obvious that many of them lead to very similar processors, and that they do not represent viable solutions to the practical problems at hand. Consequently, this background material has been used to develop more practically useful processing algorithms. These methods are based on the fundamental adaptive control algorithm, utilizing steepest descent optimization, common to most such processors, but involves more realistic assumptions concerning available information on signal and environment structure. These newly developed techniques are based on the dominant jammer suppression type of algorithm and have been investigated, both analytically, and through the use of digital computer simulation, to determine the effect of various problem parameters (bandwidth, number of antennas, number of emitters, etc.) on their performance characteristics.

## 1.4 Outline of the Report

With the last several sections as background, the remaining chapters of the report can be briefly described as follows:

### CHAPTER II. GENERAL PROBLEM FORMULATION

In this chapter the basic structure of the problem being examined is defined. The geometrical configurations of the signals and interferences in the array environment are presented, together with the antenna placements. Then the forms which the array processor can take are discussed, from the most general transfer function models, to the tapped delay line models, and the narrow band models using in-phase and quadrature channels. Certain results concerning the general transfer function model are of interest here, but the models most appropriate to the RF communications problems being addressed are seen to be the relatively narrow band ones. These can be studied as complex weight models, and the signal structure at the array can be represented in terms of complex envelopes. In terms of this structure, the correlation functions and output definitions which will be used in the analysis that follows are then defined.

## CHAPTER III. PERFORMANCE MEASURES AND OPTIMAL SOLUTIONS

This chapter discusses the various performance measures which can be used for the choice of the optimum parameters of the complex weight array processor model. Then the associated optimal solutions are derived, where both wideband and narrow band (using zero bandwidth approximations) are presented. In this latter form, various interesting properties are more readily studied. The basic minimum mean square error solution can be factored into a form which includes the other solutions being examined. As such, it can be demonstrated that they all differ only by a scalar gain, and therefore lead to the same output signal-to-noise ratios. A comparison of the maximum likelihood and minimum mean square error solutions is also presented. These solutions are of interest, since they are the forms to which convergent adaptive processors will converge.

## CHAPTER IV. OPTIMIZATION TECHNIQUES

In this chapter, the optimization techniques which can be used for the design of an adaptive processor are presented. These include simple search techniques, gradient methods, and higher order methods. The search techniques and the higher order methods do not lead to the easily implemented algorithms that the steepest descent-gradient method gives. Also discussed is the constrained optimization technique - the projection gradient method, and the method of stochastic approximation, which forms the basis for simplifying the basic form of the adaptive algorithm. From this discussion, it can be seen that the most likely candidate for use in real-time RF communications problems is the steepest descent method utilizing the stochastic approximation simplification. Other computational methods are also briefly discussed.

## CHAPTER V. BASIC ADAPTIVE ARRAY ALGORITHMS

In this chapter, adaptive array algorithms which have been presented in the literature for the optimization of the various performance measures are discussed. It is demonstrated that these algorithms do not represent practical solutions - just the basic forms which must be adapted to the specific problem being solved. Also, it is shown that all of the more practical methods lead to essential similar algorithms, differing only in how the signal effects are removed from the correlation-weight control circuits.

## CHAPTER VI. BEHAVIOR OF ADAPTIVE ARRAYS USING THE LMS ALGORITHM

In this chapter, the equations describing the trajectory of the weights are established with particular emphasis placed on their steady state values. It is from these values that steady state behavior of the array can be evaluated. Descriptions of the optimum array behavior such as

1. Gain

2. Signal-to-noise ratio

and 3. Antenna pattern

are established and compared to conventional arrays.

## CHAPTER VII. ACQUISITION TECHNIQUES

In this chapter two similar, yet different, adaptive models are studied from the point of view of their acquisition properties. In particular, for a two-emitter environment, it is shown that a strong jammer in the presence of weak signal can be suppressed much more than the signal with no additional a priori knowledge, thus permitting desired signal acquisition.

## CHAPTER VIII. PARAMETRIC STUDIES OF ADAPTIVE ARRAYS

This chapter includes detailed numerical studies of the effect of various parameters such as jammer and signal power, bias level, bandwidth, number of elements, and geometry of jammers and signals. Many of the studies will be with only one dominant jammer and one signal, to enable the study of signal-jammer interaction in detail. Then several jammers and signals are studied. This section is not specific to a TDMA signal, but general for "continuous" signals over the time interval computed.

## CHAPTER IX. AN ADAPTIVE ARRAY DESIGN FOR A SPECIFIC TDMA PROBLEM

In this chapter, a functional adaptive array design for a specific TDMA problem is considered. A three-mode approach to the signal acquisition problem is explained, in which 1) a dominant jammer suppression mode is used to lower a very powerful jammer to a level where synchronization can be performed, 2) a signal removal mode is used to prevent nulling friendly signals, and 3) a signal maximization mode (LMS algorithm) is possibly used to further improve output S/N. A block diagram of the functional design is followed by a description and results of a computer program which simulated the performance of the design with a particular input environment.

## CHAPTER X. IMPLEMENTATIONS OF ADAPTIVE ARRAYS

This chapter considers possible implementations of functional adaptive array diagrams, including designs that have been implemented by others, and different

designs that may be useful. Emphasized are processing at RF vs. IF, methods of achieving signal weighting, types of correlators, techniques of spread-spectrum signal removal, convergence rate control, and bias control.

## CHAPTER XI BREADBOARD DESIGNS AND DESIRABLE EXPERIMENTS

This chapter shows more specific diagrams of the implementations in Chapter X that appear most promising. The diagrams appear suitable to form a breadboard experimental test bed that is sufficiently flexible to allow several different implementations of weights and correlators to be tested, and later allow a working several element array to be tested in some detail.

## CHAPTER XII. CONCLUSIONS

This final chapter summarizes the more important esults of the study. Also, suggestions for further work, based on the experience gained during this effort, are presented.

Following these main sections, an extended reference list and appendices describing the computer programs developed during the study are presented.

# CHAPTER 2

# GENERAL PROBLEM FORMULATION

## 2.0 GENERAL PROBLEM FORMULATION

This chapter establishes the basic structure of the adaptive array problem required for the analysis in later chapters. The mathematical formulation of the signal environment is defined, from which the signal structure at the array can be determined in terms of the geometrical configuration of the array. Detailed consideration of the array processor modeling problem is then given, where the use of a complex weight processor is justified. Finally, the correlation functions and output quantities for this processor are defined.

### 2.1 Environment Structure

The signal environment is assumed to be composed of both directional and isotropic signal sources. The desired signal is represented by $\xi(t)$ which is assumed uncorrelated with the directional noise sources $\zeta_i(t)$, $i = 2, 3, \ldots, p$. The isotropic background noise will be lumped with the thermal sensor noise $\zeta_o(t)$ at the front end of the array and is assumed independent from o antenna element to the next. The structure of the desired signal source can include both amplitude and phase modulation of a carrier frequency $\omega_c$ of the form

$$\xi(t) = \alpha_1(t) \cos\left[\omega_c t + \varphi_1(t) + \theta_1\right] \tag{2-1}$$

while the distinct noise sources are given by

$$\zeta_i(t) = \alpha_i(t) \cos\left[\omega_c t + \varphi_i(t) + \theta_i\right], \; i = 2, 3, \ldots, p \tag{2-2}$$

and the terms at each sensor k, due to combined isotropic and thermal noise are

$$\zeta_{ok} = \beta_k(t) \cos\left(\omega_c t + \theta_{ok}\right), \; k = 1, 2, \ldots, m \tag{2-3}$$

The modulations $\alpha_i(t)$, $\beta_k(t)$ and $\varphi_i(t)$ are sample functions of zero mean from independent, ergodic random processes, where the independent random variables $\theta_i$, which are uniformly distributed on $[0, 2\pi]$, are added to ensure stationarity. Also, since the noise terms $\zeta_{ok}(t)$ are desired to be bandlimited white noise, $\beta_k$ is Rayleigh distributed. The directional signals are assumed to propagate as plane waves in a medium which is linear with its only effect on the signals being time delay.

### 2.2 Signal Structure at the Array

In terms of the environment defined above, the signal received by the $k^{th}$ sensor can be written as

$$x_k(t) = \xi\left(t - \tau_{1k}\right) + \sum_{i=2}^{p} \zeta_i\left(t - \tau_{ik}\right) + \zeta_{ok}(t) \tag{2-4}$$

where $\tau_{ik}$ represents the delay of the $i^{th}$ signal at the $k^{th}$ sensor relative to the geometric center of the array. If the direction of arrival of the $i^{th}$ signal with respect to the center of the array is denoted by the unit vector $a_i$ (see Figure 2-1), then $\tau_{ik}$ is given by[†]

$$\tau_{ik} = \frac{\langle a_i, b_k \rangle}{v} \tag{2-5}$$

where v is the velocity of the signal in the medium under consideration. Since the signals composing $x_k(t)$ are represented as amplitude and phase modulation of a carrier frequency, it is only necessary to consider their complex envelopes in the analysis. Denoting the complex envelope by ′, $x_k'(t)$ is written as

$$x_k'(t) = \xi'\left(t - \tau_{1k}\right) + \sum_{i=2}^{p} \zeta_i'\left(t - \tau_{ik}\right) + \zeta_{ok}'(t) \tag{2-6}$$

(For notational convenience the primes will be deleted, where the use of complex envelopes is understood throughout the report.) Defining the m dimensional vectors s(t) and n(t) as

$$s(t) = \begin{bmatrix} \xi\left(t - \tau_{11}\right) e^{-i\omega_c \tau_{1i}} \\ \xi\left(t - \tau_{12}\right) e^{-i\omega_c \tau_{12}} \\ \vdots \\ \xi\left(t - \tau_{1m}\right) e^{-i\omega_c \tau_{1m}} \end{bmatrix} \tag{2-7}$$

[†]Where $\langle a, b \rangle$ denotes inner product.

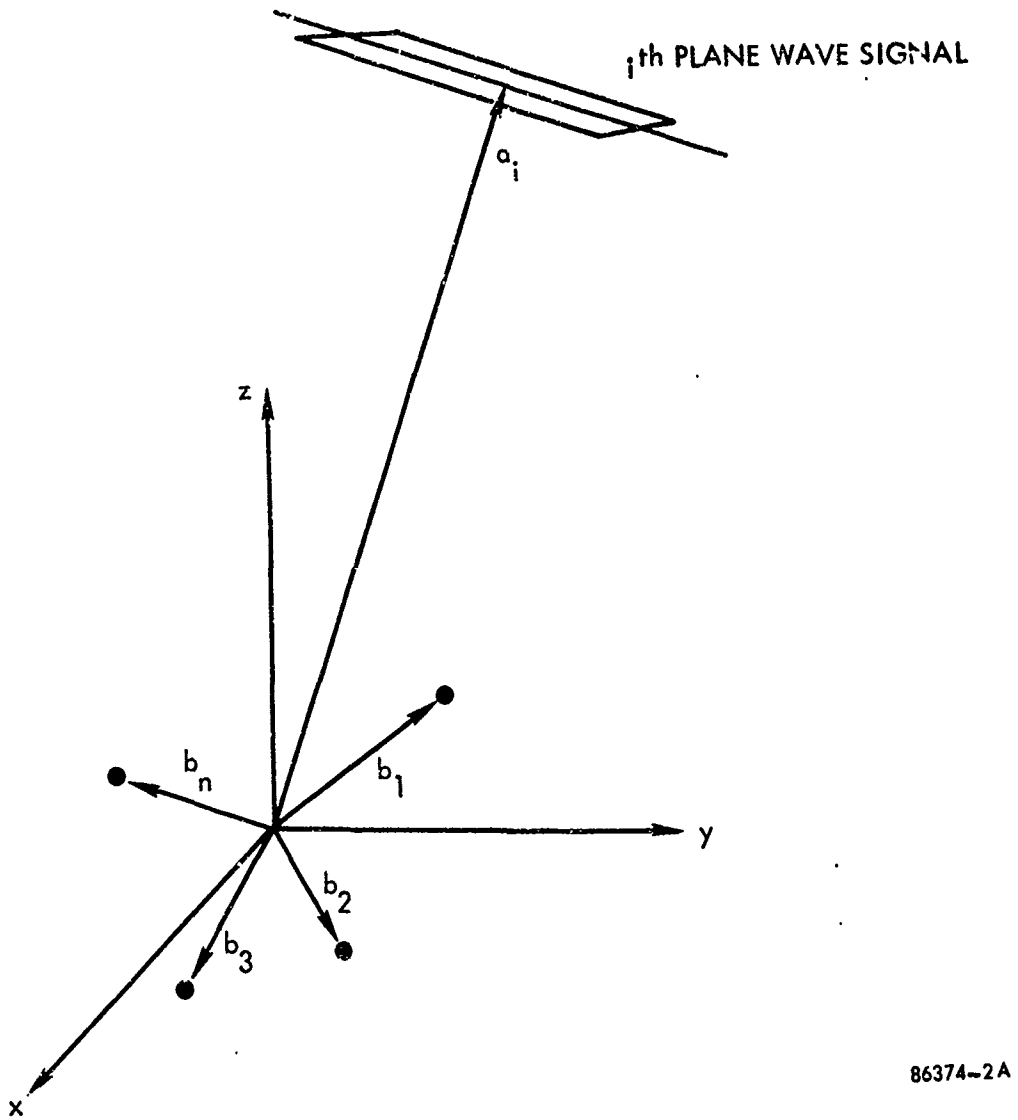


Figure 2-1. Geometrical Configuration of Sensors and Signals

$$n(t) = \sum_{i=2}^{p} \begin{bmatrix} \zeta_i\left(t - \tau_{i2}\right) e^{-j\omega_c \tau_{i1}} \\ \zeta_i\left(t - \tau_{i2}\right) e^{-j\omega_c \tau_{i2}} \\ \vdots \\ \zeta_i\left(t - \tau_{im}\right) e^{-j\omega_c \tau_{im}} \end{bmatrix} + \begin{bmatrix} \zeta_{o1}(t) \\ \zeta_{o2}(t) \\ \vdots \\ \zeta_{om}(t) \end{bmatrix} \tag{2-8}$$

then the m sensor signals can be collected in the m-dimensional vector x(t) as

$$x(t) = s(t) + n(t) \tag{2-9}$$

If the signals are narrow band in the sense that time delays $\tau_{ik}$ encountered by them between the sensor elements are insignificant relative to the slowly varying amplitude and phase modulations, then these representations can be simplified by writing

$$s(t) = \xi(t) v_1 \tag{2-10}$$

$$n(t) = \sum_{i=2}^{p} \zeta_i(t) v_i + n_t(t) \tag{2-11}$$

where $n_t(t)$ represents the collection of thermal noise terms $\zeta_{ok}(t)$ and

$$v_i = \begin{bmatrix} e^{-j\omega_c \tau_{i1}} \\ e^{-j\omega_c \tau_{i2}} \\ \vdots \\ e^{-j\omega_c \tau_{im}} \end{bmatrix} \tag{2-12}$$

In terms of these quantities

$$x(t) = s(t) + n(t) = \xi(t)\, v_1 + \sum_{i=2}^{p} \zeta_i(t)\, v_i + n_t(t) \quad . \tag{2-13}$$

## 2.3 Array Processor Models and Their Properties

In this section several models for the array processor will be considered. The most general linear processor, consisting of transfer functions in each element of the array, will be discussed, together with some interesting results concerning the optimal form of this model. This model is not appropriate to our purposes, since it is not adjustable for use in an adaptive procedure, but some observations in this general context will be relevant. A discrete-time approximation to these general transfer functions can be constructed using tapped delay line filters, where the weights associated with each tap can be adjusted using adaptive procedures. These two models are seen to be appropriate for wideband array problems, whereas for the relatively narrowband problem considered in this study, the tapped delay line reduces to a single time delay per channel, which can be approximated by a complex weight in each channel. Finally, a model which utilizes direction of arrival information to align the desired signal is presented.

### 2.3.1 The General Transfer Function Model

In relatively wideband systems which do not require that the array control be adaptive, the most general linear model for the array processor takes the form of a transfer function in each channel as shown in Figure 2-2. In this form the input vector x is related to the output signal $\gamma$ by

$$\gamma(t) = \int_{t_o}^{t} h^T(t-\tau)\, x(\tau)\, d\tau \tag{2-14}$$

or in the frequency domain

$$\gamma(\omega) = H^T(\omega) x(\omega) . \tag{2-15}$$

Such arrays have been studied extensively for applications in seismic and sonar fields (where the bandwidths are much larger and the constraint to operate in real time is not

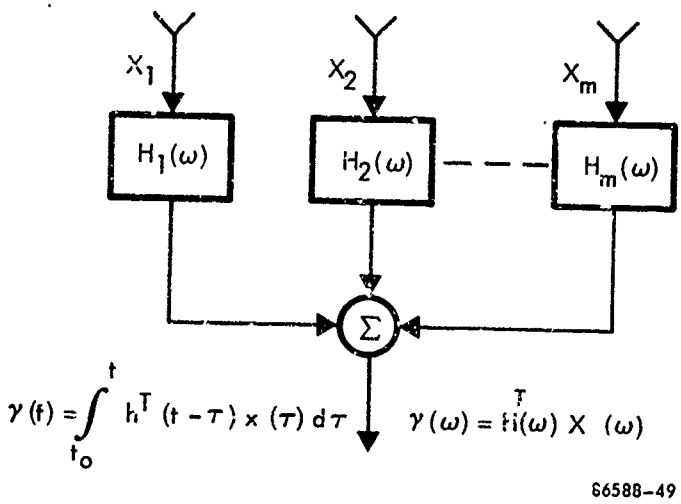


Figure 2-2. Transfer Function Processor Model

necessarily present) by many investigators, e.g., Van Trees[73]. Although much of this work is slanted toward the detection problem, which we are not addressing, some forms of the optimum detector can be shown to require the implementation of an optimal estimator. In Van Trees' work it is shown that the array processor produces a minimum mean square error estimate of the signal and takes the form shown in Figure 2-3. (His analysis uses the general transfer function model and the signal aligning concept discussed in a later section.) In this form, an interesting factorization of the problem is seen where the overall optimal processor factors into a "spatial" filter and a "temporal" filter. The spatial filter (which also includes temporal characteristics of the noise) is a linear matrix filter dependent only on the noise statistics and signal propagation effects, and within a scalar factor $\Lambda(\omega)$ gives a minimum noise, distortionless output; that is, for Gaussian signals it gives the maximum likelihood signal estimate given that there is no spectral information about the signal available. If the spectral density of the signal is known, then the minimum mean square error signal can be found by the addition of a scalar Wiener filter. Cox[29] has also observed this factorization, where he interprets the spatial filter as performing a prewhitening operation (typical of the solution methods used for colored noise filtering problems where the coloring here is due to the spatial distribution of the noise sources) prior to the use of the standard Wiener filter for a MMSE† estimate.

The explicit design equations for the factored form of the processor shown in Figure 2-3 can be obtained from the cited references. However, the general properties of this solution are of primary interest since even though this is not the model to be used for our problem, these general observations will be relevant to the more specific case under consideration. Since the model incorporating general transfer functions does not admit to real-time adjustment via adaptive algorithms, it cannot be directly used for problems involving time varying statistics, i.e., problems where emitters may be moving, turning off and on, and changing their characteristics.

### 2.3.2 Tapped Delay Line Models

A tapped delay line approximation to the general transfer function can be used in each channel of the array, where such a processor is illustrated in Figure 2-4. As the number of taps becomes very large and the time delays become very small, this approximation approaches the ideal of the general transfer function.

For this model we can represent the signals and the weights at any time t and for each of the tap points j as the real vectors,

†MMSE will be used throughout this report as an abbreviation for Minimum Mean Square Error.

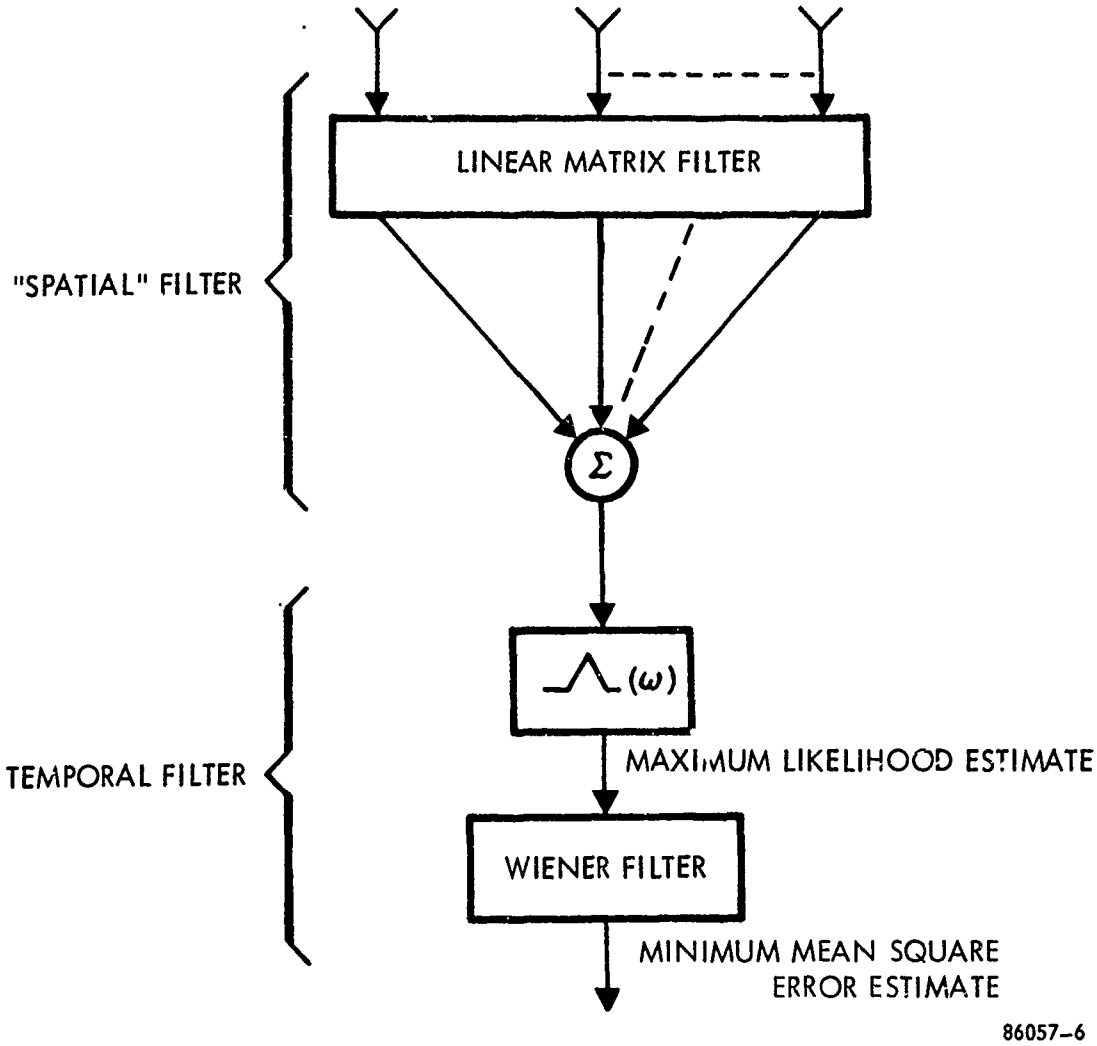


Figure 2-3. Factored Form of Transfer Function Model

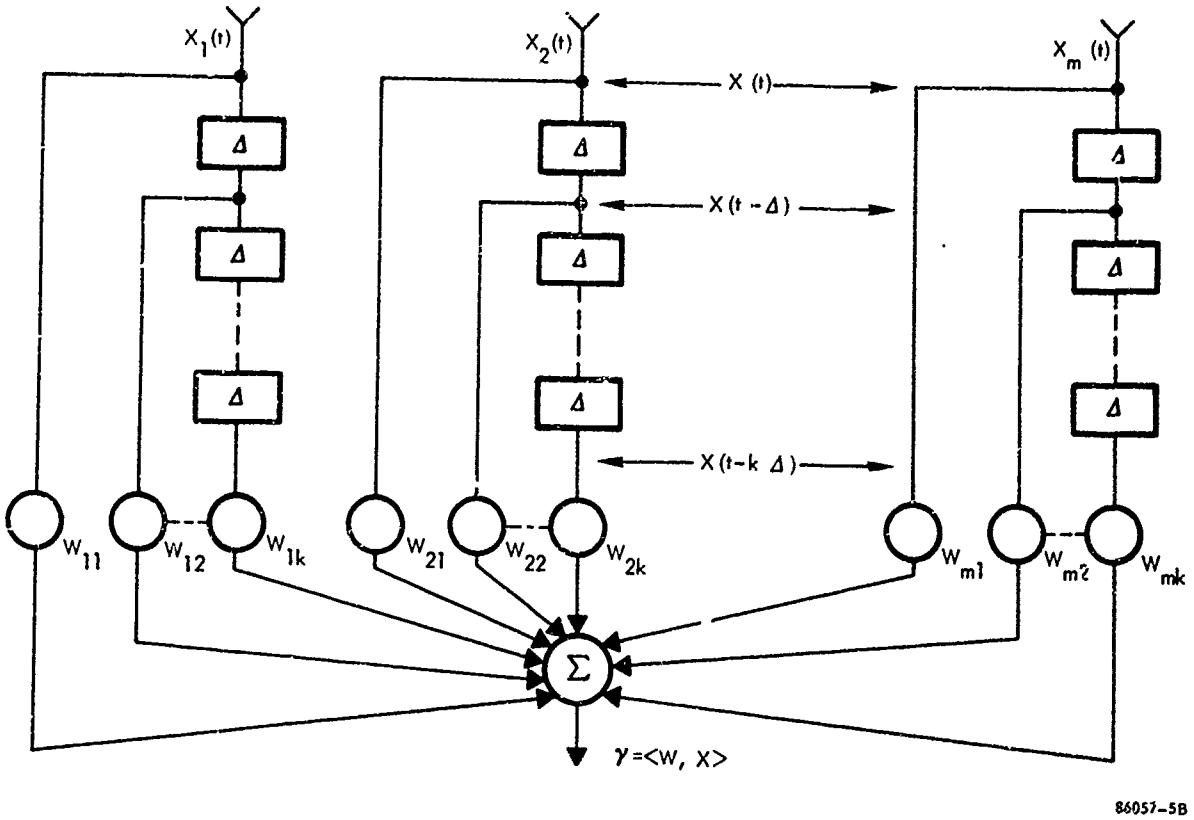


Figure 2-4. Tapped Delay Line Model

$$x(t - j\Delta) = \begin{vmatrix} x_1(t - j\Delta) \\ x_2(t - j\Delta) \\ \vdots \\ x_m(t - j\Delta) \end{vmatrix} \text{ and } w(t - j\Delta) = \begin{bmatrix} w_1(t - j\Delta) \\ w_2(t - j\Delta) \\ \vdots \\ w_m(t - j\Delta) \end{bmatrix}, \; j = 0, 1, \ldots, k$$

so that the output of the array becomes

$$y = w^T(t)\, x(t) + w^T(t-\Delta)\, x(t-\Delta) + \ldots + w^T(t-k\Delta)\, x(t-k\Delta) \qquad (2\text{-}16)$$

(where the tap spacings are chosen equal for notational convenience, but can be variable).

In terms of the augmented vectors W and X defined as

$$W = \begin{bmatrix} w(t) \\ w(t-\Delta) \\ \vdots \\ w(t-k\Delta) \end{bmatrix} \quad \text{and } X = \begin{bmatrix} x(t) \\ x(t-\Delta) \\ \vdots \\ x(t-k\Delta) \end{bmatrix} \qquad (2\text{-}17)$$

the output becomes

$$\gamma = \langle W, X \rangle = W^T X \qquad (2\text{-}18)$$

The exact number of taps and the size of the time delays must be chosen for any particular application. These choices will be determined by tradeoffs involving signal bandwidth and overall system complexity. For the narrow band problems contemplated in RF communications and radar systems, it is generally adequate to consider only one time delay per channel and the array takes the form illustrated in Figure 2-5.

### 2.3.3 Narrowband Tapped Delay Line Processor: Complex Weight

As mentioned above, for relatively narrowband problems the tapped delay line array can be reduced to the model in Figure 2-5 with a single time delay per channel. This processor has the obvious advantage of simplicity over the multitap processor, thereby reducing the complexity of the adaptive circuitry which is used to control the array. The time delay for each tap is shown to be $\tau = \frac{f_c}{4}$, or 90 degrees phase shift at the

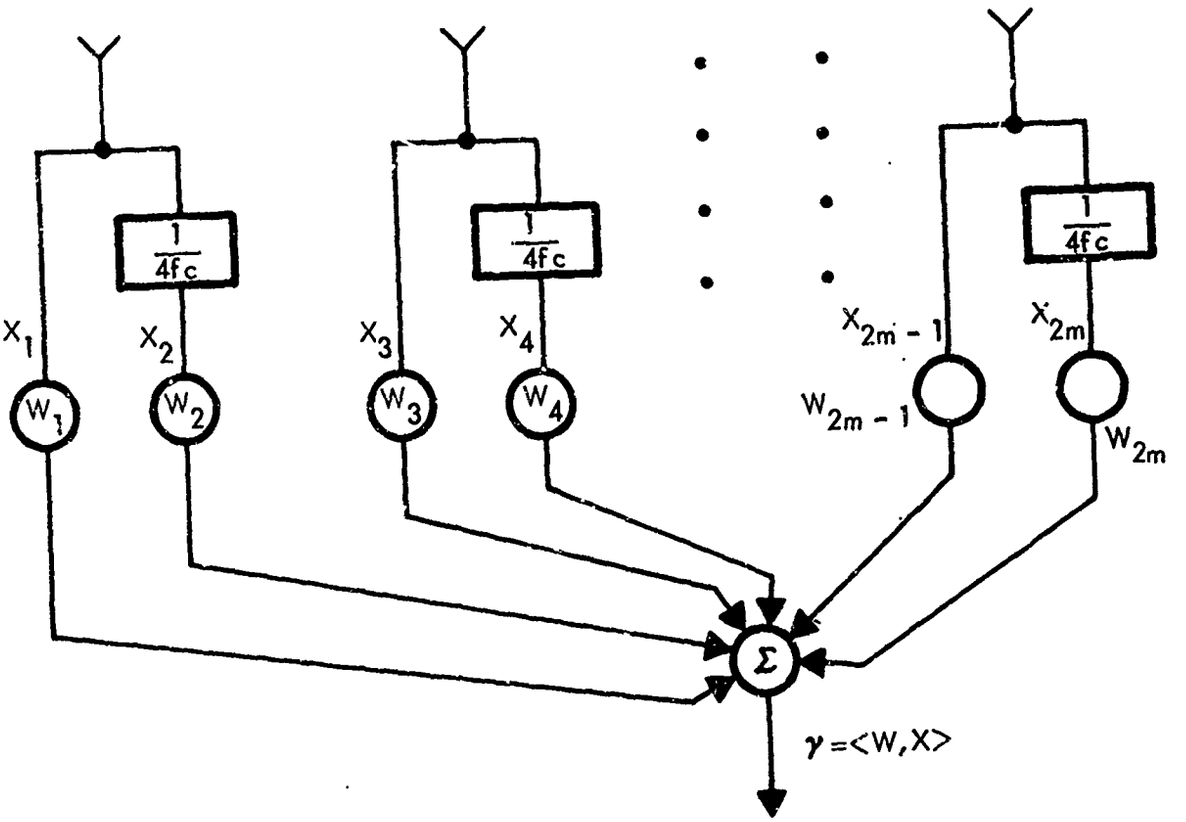


Figure 2-5. In-Phase and Quadrature Channel Model

carrier frequency. Over the relatively narrow bandwidth addressed here, we will assume that the time delay is in fact a broadband phase shifter providing a $90^{\circ}$ phase shift over the frequency band of interest.

The benefits of this type of phase shifter have a substantial impact on the mathematical development of the phased array. By eliminating the signal diffusion through the $90^{\circ}$ phase shifter we are able to represent the weights as members of an m-dimensional complex Euclidean space. Consider for example the signal processing channel associated with the kth sensor element shown in Figure 2-6, with $\gamma_k$ representing that portion of the total output due to the kth channel.

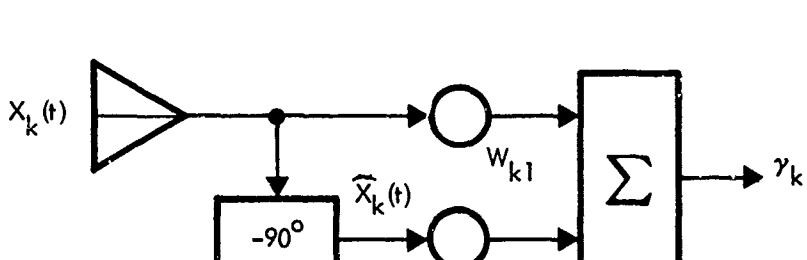


Figure 2-6. Kth Element Processing

Let $x_k(t)$ be represented in the form

$$x_k(t) = \mathrm{Re}\{x_k'(t)\, e^{-j\omega_c t}\} \tag{2-19}$$

then the partial response of the array output can be written as

$$\gamma_k(t) = w_{k1} x_k(t) + w_{k2} \widehat{x}_k(t) \tag{2-20}$$

where $\widehat{x}_k(t)$ is the response of the broadband $-90^{\circ}$ phase shifter to $x_k(t)$.

The functional form of $\widehat{x}(t)$ is easily determined by taking the Fourier transform of $x_k(t)$

$$X_k(\omega) = A(\omega) e^{j\phi(\omega)} \tag{2-21}$$

where A and $\phi$ represent the amplitude and phase of each frequency component. Since the phase shifter provides a $-90^{\circ}$ phase shift at every frequency, the Fourier transform of $\hat{x}_k(t)$ is then obtained by

$$\hat{X}_k(\omega) = A(\omega)\ [-je^{j\phi(\omega)}] = -jA(\omega)e^{-j\phi(\omega)} = -jX_k(\omega)\ . \qquad (2\text{-}22)$$

Taking the inverse transform we arrive at

$$\hat{x}(t) = \mathrm{Re}\{-jx_k{}'(t)e^{-j\omega_c t}\}, \qquad (2\text{-}23)$$

thus

$$\gamma_k(t) = \mathrm{Re}\{\ w_{k1}x_k{}'(t)e^{-j\omega_c t} - jw_{k2}x_k{}'(t)e^{-j\omega_c t}\} \qquad (2\text{-}24)$$

$$= \mathrm{Re}\{(w_{k1} - jw_{k2})x_k{}'(t)e^{-j\omega_c t}\}.$$

From this expression we recognize that we need only consider the complex envelopes of the signals as well as the obvious complex representation of the weights to determine the array output. We can now represent the array output in the simplified form

$$\gamma(t) = \mathrm{Re}\{<w, x'>\ e^{-j\omega_c t}\} = \mathrm{Re}\{<\gamma'(t)e^{-j\omega_c t}\} \qquad (2\text{-}25)$$

where $<w, x'>$ denotes the usual inner product in a complex Eucledian space. For the remainder of our presentation we shall require only the envelope of the output and for notational convenience we again drop the prime representation and denote the output by

$$\gamma = <w, x> \qquad (2\text{-}26)$$

The complex weight model corresponding to this simplification is shown in Figure 2.7.

### 2.3.4 Aligned Arrays

For many array problems it can be assumed that the direction of arrival of the desired signal is known or measured. In this case the time delays required to align (or co-phase) the desired signal terms in each channel can be computed and inserted as a Spatial Correction Filter (SCF) as shown in Figure 2-8a. (Even if these time delays are not known, it is often mathematically convenient to consider factoring out SCF's from the general model weights).

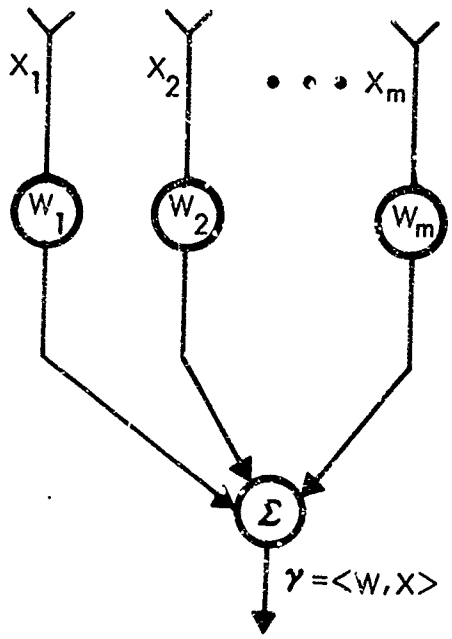


86057-4A

Figure 2-7. Complex Weight Model

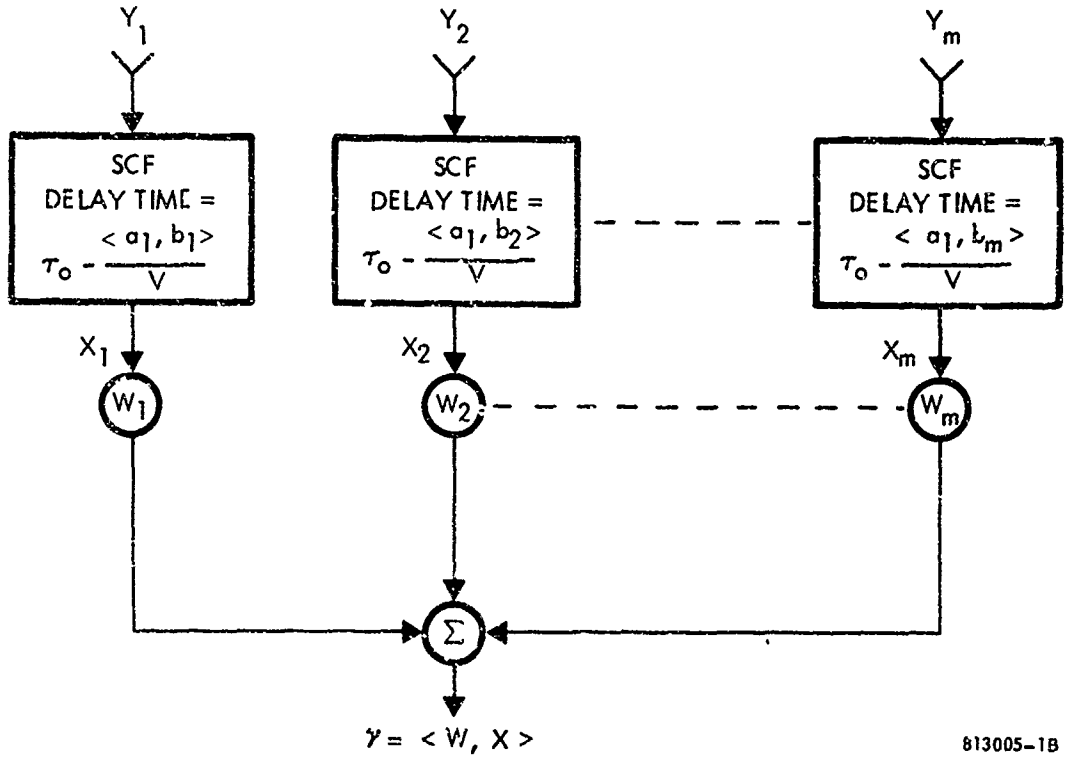


Figure 2-8a. Signal Aligned Array Model

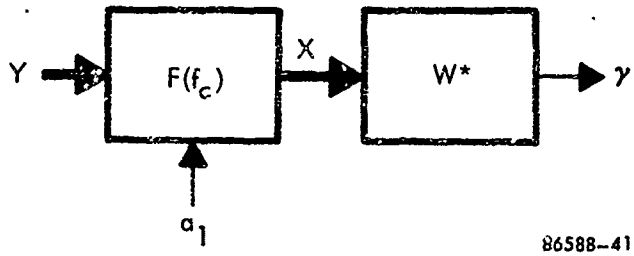


Figure 2-8b. Functional Representation

Mathematically we will represent this operation as

$$x(t) = f\,y(t) \tag{2-27}$$

where f is the vector valued function representing the spatial correction filters with a transform function matrix given by

$$F(\omega) = \begin{bmatrix} \mathrm{Exp}\left[-j\omega\left(\tau_o - \frac{\langle a_1, b_1\rangle}{V}\right)\right] & 0 & \cdots & 0 \\ 0 & \mathrm{Exp}\left[-j\omega\left(\tau_o - \frac{\langle a_1, b_2\rangle}{V}\right)\right] & \cdots\cdots & 0 \\ \vdots & & & \\ 0 & 0 & \cdots & \mathrm{Exp}\left[-j\omega\left(\tau_o - \frac{\langle a_1, b_m\rangle}{V}\right)\right] \end{bmatrix} \tag{2-28}$$

where $y = s+n$ denotes the m-dimensional signal and noise vector at the input to the array. In the absence of the spatial correction filters $x(t)$ is exactly equal to $y(t)$. In this form the vector x always represents the input to the complex weights. The term $\tau_o$ is a constant delay whose addition is to ensure the physical realizability of f, however, without loss of generality we shall omit its use in the sequel.

After the SCF's the signal can again be represented as x vector, which takes the simplified form

$$x(t) = \xi(t)\,\underline{1} + \tilde{n}(t) \tag{2-29}$$

where $\underline{1} = [1, 1, \ldots, 1]^T$ and $\tilde{n}(t)$ represents the noise terms after the SCF's.

## 2.4 Array Correlation Functions and Output Relations

### 2.4.1 General Representations

For the analysis of the models presented in the last several paragraphs, the correlation matrices associated with the various signals will be required. The correlation matrix of the received signal and noise vector will be defined as

$$R_x = E\left[x(t)x^*(t)\right] \tag{2-30}$$

where $^*$ represents the adjoint matrix (i.e., the complex conjugate transpose). Since the desired signal is assumed to be uncorrelated with the noise signals in the array, this matrix can be decomposed into the sum of two positive matrices

$$R_x = R_s + R_n \tag{2-31}$$

where

$$R_n = E\left[n(t)n^*(t)\right] \tag{2-32}$$

and is assumed positive definite when thermal noise is present, and where

$$R_s = E\left[s(t)s^*(t)\right]. \tag{2-33}$$

The complex matrix $R_x$ may also be decomposed into its real and imaginary parts

$$R_x = C + jD \tag{2-34}$$

and since $R_x$ is self adjoint we see from the following identity chain that

$$\begin{aligned} \langle x, (C+jD)x\rangle &= \langle x, Cx\rangle + j\langle x, Dx\rangle = \langle (C+jD)x, x\rangle \\ &= \langle Cx, x\rangle - j\langle Dx, x\rangle. \end{aligned} \tag{2-35}$$

Thus by equating the real and imaginary parts it is evident that

a. C is positive definite

b. D is skew symmetric

The cross-correlation vector between the desired signal $\xi(t)$ and the received signal vector $x(t)$ is given by

$$r_{x\xi} = E\left[\xi^*(t)x(t)\right]. \tag{2-36}$$

If spatial correction filters are used, then the covariance matrices are related by

$$R_y = R_s + R_n \tag{2-37}$$

and after the SCF's

$$R_x = S\,\underline{1}\,\underline{1}^T + R_{\tilde{n}} \tag{2-38}$$

where for narrow band signals

$$R_{\tilde{n}} = F(f_c)\,R_n\,F(f_c) \tag{2-39}$$

## 2.4.2 Structure of the Signal and Noise Covariance Matrix

In this section we will focus our attention on the functional form of the entries of the matrix $R_x$ for an environment consisting of wide-band as well as narrow band emitters. The approach used in this development is to formulate a more realistic model of the low pass nature of each sensor channel relative to the complex signal envelopes and its effects on these signals. Consider the functional diagram of the kth channel shown in Figure 2-9, where H is an ideal low-pass filter. Let $\nu_k(t)$ be an arbitrary complex signal contained in $x_k(t)$, where in terms of the geometrical center of the array

$$\nu_k(t) = \nu(t-\tau_k)e^{-j2\pi f_c \tau_k} \tag{2-40}$$

where

$$\tau_k = \frac{\langle a_\nu b_k \rangle}{v} \tag{2-41}$$

which for a uniform linear array can be written as

$$\tau_k = \left(\frac{m+1}{2} - k\right)\frac{\rho}{v}\cos\theta_\nu \tag{2-42}$$

where $\rho$ represents the spacing between antenna elements and $\theta_\nu$ represents the angle to the emitter relative to the axis of the array. The ij entry of the correlation matrix due to this emitter is then easily seen to be (where ~ represents the signal after the bandpass filter H only in this section).

$$r_{ij} = E[\tilde{\nu}_i(t)\tilde{\nu}_j^*(t)] = e^{-j2\pi f_c(\tau_i-\tau_j)}E[\tilde{\nu}(t-\tau_i)\tilde{\nu}^*(t-\tau_j)] \tag{2-43}$$

$$= e^{-j2\pi f_c(\tau_i-\tau_j)}R_{\tilde{\nu}}(\tau_i-\tau_j).$$

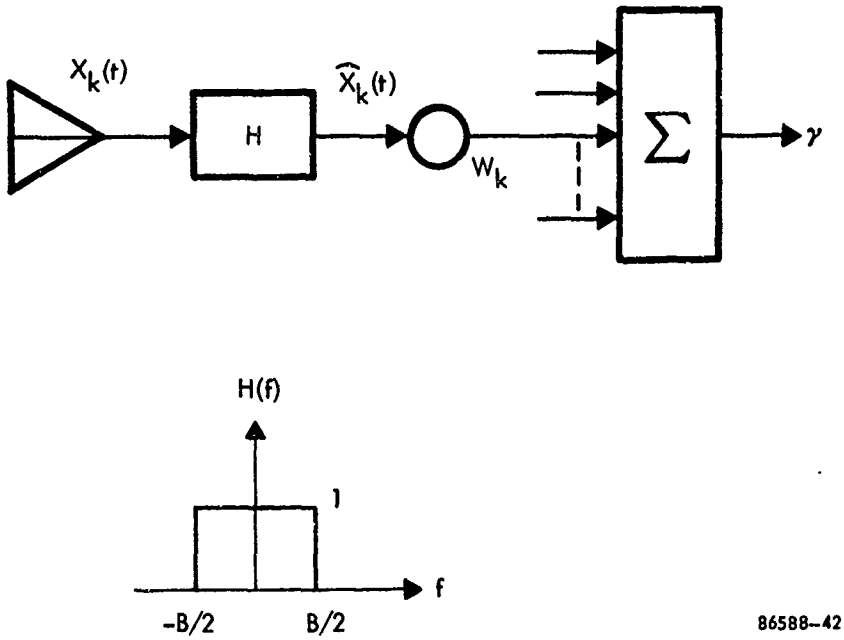


Figure 2-9. Functional Diagram of Kth Channel in the Complex Weight Array

However,

$$R_{\tilde{\nu}}(\tau_j - \tau_i) = \int_{-\infty}^{\infty} S_{\tilde{\nu}}(f) e^{j2\pi f(\tau_j - \tau_i)} df \tag{2-44}$$

$$= \int_{-\infty}^{\infty} S_{\nu}(f) \left| H(f) \right|^2 e^{j2\pi f(\tau_j - \tau_i)} df.$$

Since $\left| H(f) \right|$ is zero for $\left| f \right| > B/2$

$$R_{\tilde{\nu}}(\tau_j - \tau_i) = \int_{-B/2}^{B/2} S_{\nu}(f) e^{j2\pi f(\tau_j - \tau_i)} df \tag{2-45}$$

thus we write

$$r_{ij} = e^{-j2\pi f_c(\tau_j - \tau_i)} \int_{-B/2}^{B/2} S_{\nu}(f) e^{j2\pi f(\tau_j - \tau_i)} df. \tag{2-46}$$

Since all the emitters are assumed uncorrelated the ij entry of $R_x$ is the sum of the entries due to each emitter.

For an illustrative example let us evaluate $r_{ij}$ due to an emitter which has a constant power spectral density of $\frac{N_\nu}{b}$ over a bandwidth b (b<B) and a zero otherwise. Then it is easily seen that

$$r_{ij} = N_\nu e^{-j2\pi f_c(\tau_j - \tau_i)} \frac{\sin\left[\pi(\tau_j - \tau_i) b\right]}{\pi(\tau_j - \tau_i) b} \tag{2-47}$$

For very narrow bandwidths

$$\frac{\sin \pi(\tau_j - \tau_i) b}{\pi(\tau_j - \tau_i) b} \approx 1 \tag{2-48}$$

which permits us to write the correlation matrix due to the signal $\nu(t)$ as

$$R_\nu = N_\nu v_\nu v_\nu^* . \tag{2-49}$$

if the entire environment is narrow band with equal thermal noise power in each antenna element then the structure of correlation matrices take on the simple form

$$R_s = S v_1 v_1^* \tag{2-50}$$

$$R_n = \sum_{i=2}^{p} N_i v_i v_i^* + \sigma^2 I \tag{2-51}$$

$$r_{x\xi} = S v_1 \tag{2-52}$$

where $S = E[\xi^*(t)\xi(t)]$, the desired signal power, and where $N_i = E[\zeta_i(t)\zeta_i^*(t)]$, the received power from the ith directional noise source. Note that for the signal aligned array $v_1 = \underline{1}$,† for wideband as well as narrow band signals.

### 2.4.3 Basic Array Output Definitions

Throughout this report the basic parameters which are used in analyzing the array behavior are quantities such as: output signal power, output signal to noise power ratio, output gain and the array antenna pattern. These concepts are well known as fundamental array descriptions and therefore, perhaps need no further discussion. However, since a portion of the discussion centers around signals of finite bandwidth, the generalization to this environment may not be too familar. Therefore, these concepts are presented in this section for arrays with and without spatial correction filters.

For the array shown in Figure 2-7, the average power out of the array is given by

$$\text{Output Power} = P_o = E\,|y|^2 = E|\langle w,x\rangle|^2 = E\,\langle w,x\rangle\,\langle x,w\rangle$$

$$= Ew^*xx^*w = w^* R_x w = \langle w, R_x w\rangle . \tag{2-53}$$

Since the signals are uncorrelated the output power is the sum of the powers due to each source. Thus, we can write

† Where $\underline{1}$ denotes $(1, 1, \ldots 1,)^T$.

$$P_o = P_s + P_n = \langle w, R_s w \rangle + \langle w, R_n w \rangle \tag{2-54}$$

$$= \langle w, R_s w \rangle + \sum_{i=2}^{p} \langle w, R_{n_i} w \rangle + P_{n_t}$$

(where $P_{n_t}$ is the power due to thermal and isotropic noise) for the narrowband environment this reduces to

$$P_o = S \langle w, v_1 v_1^* w \rangle + \sum_{i=2}^{p} N_i \langle w, v_i v_i^* w \rangle + P_{n_t}$$

$$= S \left| \langle w, v_1 \rangle \right|^2 + \sum_{i=2}^{p} N_i \left| \langle w, v_i \rangle \right|^2 + P_{n_t}. \quad (2\text{-}55) \tag{2-55}$$

The output signal-to-noise ratio is then simply the output power due to the desired signal divided by the output power due to all the noise. That is, by definition,

$$\frac{P_s}{P_n} \triangleq \frac{\langle w, R_s w \rangle}{\langle w, R_n w \rangle} \tag{2-56}$$

For an array incorporating spatial correction filters, if the signal and noise covariance matrices of the signals at the output of the spatial correction filters are known, then these can be used in place of $R_s$ and $R_n$ in the above expressions. If on the other hand it is desired to determine the output power explicitly in terms of the signals impinging on the array, then it can be shown that

$$P_s = S \langle \underline{1}, \underline{1} \rangle \tag{2-57}$$

$$P_n = \int_{-\infty}^{\infty} \langle w, S_n(f) w \rangle df = \int_{-\infty}^{\infty} \langle w, F(f) S_n(f) F^*(f) w \rangle df \tag{2-58}$$

where $S_n(f)$ is the noise power spectral density matrix i.e.,

$$S_n(f) = E\left[n(f) n^*(f)\right] \tag{2-59}$$

where n is the noise at the input to the spatial correction filters. For narrowband signals $P_n$ reduces to

$$P_n = \langle w, F(f_c) R_n F^*(f_c) w \rangle \tag{2-60}$$

The concept of array gain as used in this report is the output signal-to-noise power ratio divided by the signal-to-noise power ratio per sensor. That is, the gain G is

$$G = \frac{\text{S/N at the array output}}{\text{S/N per sensor}} \tag{2-61}$$

or

$$G = \frac{\langle w, R_s w \rangle / \langle w, R_n w \rangle}{S/(\sum_i N_i + \sigma^2)} \tag{2-62}$$

where $\sigma^2$ is the power at each sensor (assumed equal) due to thermal noise. Another useful concept is that of antenna pattern, which can be defined in terms of the covariance matrix of a linear array with fixed weights. The antenna pattern $\psi(\phi\mu)$ is defined as the output power of the array due to an arbitrary emitter $\mu$ of unity power with azimuth $\phi\mu$. That is,

$$\psi = P_\mu(\phi_\mu) = \langle w, R_\mu(\phi) w \rangle \tag{2-63}$$

where $R_\mu(\phi_\mu)$ is the covariance matrix of received signal vector due to emitter $\mu$. Thus, the antenna pattern is not only a function of the angular location of the emitter $\mu$ but also its spectral content. For a broadband environment it is necessary to use a broadband emitter $\mu$ consistent with the environment in order to obtain an accurate representation of the pattern.

# CHAPTER 3

# THE OPTIMAL SOLUTIONS

## 3.0 THE OPTIMAL SOLUTIONS

In this chapter, several solutions for the optimal weight vector for the complex weight processor discussed in the last chapter will be derived and discussed. To define an optimal solution a performance criterion must be selected, and several appropriate measures will be presented, each appropriate for certain specific types of problems and objectives. For each of these performance measures the optimum weight vectors will be found. Several interesting features about these solutions will be examined. For very narrowband signals it will be shown that the minimum mean square error processor will factor in much the same way described for the general transfer function model. In this form a linear matrix filter will compose the spatial filter, which will be shown to be common to each of the optimal solutions. Moreover, each of these solutions will be seen to differ only by a scalar factor, which leads to the result that they each have identical signal-to-noise ratios at their outputs.

### 3.1 The Performance Measures

Four separate performance measures will be discussed: mean square error, signal-to-noise ratio, the likelihood function, and the output noise variance. Within the context of the more general wideband array problem each of these performance measures would have a specific use. The minimum mean square error measure is utilized when it is desired to reproduce the desired signal as accurately as possible. This measure assumes that the signal is represented as a random process and requires knowledge of the second order statistics of the signals and the noises. The signal-to-noise ratio criterion seeks to maximize the signal power in the output while minimizing the noise power. This form is not concerned with reproducing the signal accurately, and hence can lead to signal distortion.[41] It also assumes the signal is modeled statistically and requires knowledge of the second order statistics of the signal and noise. The maximum likelihood measure is utilized when the signal is assumed to be an unknown deterministic signal. Its use requires that the noise is assumed to be Gaussianly distributed with known second order statistics; however, no signal characteristics need be known. Likewise, the minimum variance performance measure assumes no statistical knowledge of the signal, and only second order noise statistics. However, its use is restricted to the signal aligned arrays where an undistorted estimate of the signal is desired. As will be demonstrated below, for very narrowband signals many of these differences will manifest themselves only in the form of a scalar factor at the output of a common linear matrix filter.

#### 3.1.1 Mean Square Error

The mean square error at the output of the array is defined in terms of the difference between the array output $\gamma(t)$ and the desired received signal $\xi(t)$ in the form

### 3.1.3 The Likelihood Function

Given that a particular vector x (t) has been received by the array, it is desired to choose an estimate $\hat{s}$ (t) of the signal as the most likely waveform. That is, we choose $\hat{s}$ to maximize the conditional probability density function p [x/s], i.e.,

$$\hat{s} = \max_{s} p\ [x/s] \tag{3-7}$$

which, when considered to be a function of s, is called the likelihood function. This conditional density can be written as

$$p[x/s] = \frac{p[x, s]}{p[s]}$$

and making a change of variables this becomes

$$p[x/s] = \frac{p[x, s]}{p[s]} = \frac{p[s, n]}{p[s]} = \frac{p[s]\ p[n]}{p[s]} = p[n] \tag{3-8}$$

consequently, to maximize the likelihood function, s must be chosen to maximize

$$p\ [n] = p_n\ [x-s] = \exp\ [-1/2\ (x-s)^* R_n^{-1}\ (x-s)] \tag{3-9}$$

(assuming the noise is Gaussianly distributed with covariance $R_n$) which is maximized by the minimization of the exponent, and gives

$$\begin{aligned} J_{ml} &= (x-s)^* R_n^{-1}\ (x-s) \\ &= \langle (x-s),\ R_n^{-1}\ (x-s) \rangle \end{aligned} \tag{3-10}$$

The obvious minimum value of this function is zero when the estimate is chosen as the received signal. This result is expected, since we have hypothesized very little knowledge of the signal, and the best we can do is to use the received vector for the estimate.

For this to be a well-posed problem we must insert some knowledge of signal structure. This can be accomplished for relatively wideband signals if direction of arrival is known and spatial correction filters are used to align the desired signal. In this case the signal vector $s = \xi\ (t)\ \underline{1}$ and the likelihood function performance measure becomes

$$J_{ml} = (x - \xi \underline{1})^* R_n^{-1}\ (x-\xi\underline{1}) = \langle (x-\xi\underline{1}),\ R_n^{-1}\ (x-\xi\underline{1}) \rangle . \tag{3-11}$$

For very narrowband signals where there is no dispersion across the array, the signals need not be aligned and we can write $s = \xi v_1$. For this case $J_{m1}$ becomes

$$J_{m1} = (x-\xi v_1)^* R_n^{-1} (x-\xi v_1) = \langle (x-\xi v_1), R_n^{-1} (x-\xi v_1) \rangle \ . \tag{3-12}$$

### 3.1.4 Output Noise Variance

This type of performance measure is appropriate only for those processors which utilize direction of arrival information to align the desired signal components. As shown, for such an array the received vector $x(t) = \xi(t)\,\underline{1} + n(t)$ and the output $\gamma(t)$ becomes

$$\gamma(t) = w^* x = \xi(t)\, w^* \underline{1} + w^* n(t) \ . \tag{3-13}$$

In this equation $w^*\underline{1} = \sum_{i=1}^{m} w_i^*$ and if this summation is constrained to equal 1[+], i.e.,

$$w^*\underline{1} = \sum_{i=1}^{m} w_i^* = 1 = \langle w, \underline{1} \rangle \tag{3-14}$$

then the output can be written as

$$\gamma(t) = \xi(t) + w^* n(t) \ . \tag{3-15}$$

In this form $\gamma(t)$ is seen to be an unbiased estimate of $\xi(t)$, that is, for zero mean noise

$$E[\gamma(t)] = E[\xi(t) + w^* n(t)] = E[\xi(t)] = \xi(t) \tag{3-16}$$

and the noise variance in $\gamma(t)$ is

$$\mathrm{Var}\ \gamma(t) = w^* R_n w \ . \tag{3-17}$$

Consequently, the minimum variance performance measure can be written as

$$J_{mv} = w^* R_n w = \langle w, R_n w \rangle \tag{3-18}$$

---

[+]Note that this implies $\sum_i \mathrm{Re}(w_i) = 1$ and $\sum_i \mathrm{Im}(w_i) = 0$.

subject to the constraint

$$\sum_{i=1}^{m} w_i^* = 1 = \langle w, \underline{1} \rangle \quad .$$

## 3.2 Derivation of the Optimal Solutions

In this section the complex weight vectors, which optimize the four performance criteria discussed previously, will be determined. Various optimization techniques could be used to obtain these solutions; however, the methods which appear best suited to this task, particularly since we desire to utilize a general representation with complex signals and weights, are to place the problem in a Hilbert space format and utilize the geometrical concept of orthogonality. The Hilbert space in which we shall formulate our solutions is consistent with the implied space used in establishing the performance measures, namely an m-dimensional complex Euclidean space which we shall denote as H.

### 3.2.1 The Minimum Mean Square Error Solution

The mean square error performance criteria has been presented in the form

$$J_{mse}(w) = \langle w, R_x w \rangle - 2\mathrm{Re}\ \langle w, r_{x\xi} \rangle + S \tag{3-19}$$

where we must find $w_{mse}$, the complex weight vector which minimizes $J_{mse}$. The vector which minimizes $J_{mse}$ is equivalent to that which minimizes the quadratic form

$$J_1(w) = \langle w, R_x w \rangle - 2\mathrm{Re}\ \langle w, r_{x\xi} \rangle \tag{3-20}$$

since S is not a function of w.

Consider the quadratic form given by

$$\begin{aligned} J_2(w) &= \langle w - w_o, Q(w - w_o) \rangle \\ &= \langle w, Qw \rangle - 2\mathrm{Re}\ \langle w, Qw_o \rangle + \langle w_o, Qw_o \rangle \end{aligned} \tag{3-21}$$

where Q is an arbitrary positive definite matrix. The performance measure $J_2(w)$ takes on its minimum value of zero only when $w = w_o$, which also minimizes

$$J_3(w) = \langle w, Qw \rangle - 2\mathrm{Re}\langle w, Qw_o \rangle . \tag{3-22}$$

Returning to the original problem, we see that the minimization of $J_1(w)$ is equivalent to the minimization of $J_3(w)$ if we have:

$$\text{(a)} \quad Qw_o = r_{x\xi} \tag{3-23}$$

$$\text{(b)} \quad Q = R_x . \tag{3-24}$$

Equations (a) and (b) give the explicit form of the weight vector which minimizes $J_{mse}(w)$ as

$$R_x w = r_{x\xi} \tag{3-25}$$

and since $R_x$ is positive definite, its inverse exists, and gives

$$w_{mse} = R_x^{-1} r_{x\xi} . \tag{3-26}$$

### 3.2.2 The Maximum Signal-to-Noise Ratio Solution

The performance measure for the maximum signal-to-noise ratio has been shown to be

$$J_{s/n}(w) = \frac{\langle w, R_s w \rangle}{\langle w, R_n w \rangle} . \tag{3-27}$$

To determine the weight which optimizes this cost function we shall utilize the positive square root [44] of $R_n$ so that

$$J_{s/n}(w) = \frac{\langle w, R_s w \rangle}{\langle R_n^{\frac{1}{2}} w, R_n^{\frac{1}{2}} w \rangle} = \frac{\langle w, R_s w \rangle}{\| R_n^{\frac{1}{2}} w \|^2} . \tag{3-28}$$

Making the substitution

$$v = R_n^{\frac{1}{2}} w \tag{3-29}$$

we can rewrite the above expression as

$$J_{s/n}(u) = \frac{\langle u, R_n^{-\frac{1}{2}} R_s R_n^{-\frac{1}{2}} u \rangle}{\| u \|^2} . \tag{3-30}$$

Thus, the problem reduces to finding the u of norm one that maximizes the inner product $\langle u, R_n^{-\frac{1}{2}} R_s R_n^{-\frac{1}{2}} u \rangle$. We will now show that the maximum value of this inner product is $\lambda_{max}$ (the maximum eigenvalue of $R_n^{-\frac{1}{2}} R_s R_n^{-\frac{1}{2}}$), where $u_{opt}$ belongs to the eigenspace associated with $\lambda_{max}$.

Consider the following inequality chain with $\| u \| = 1$

$$\langle u, R_n^{-\frac{1}{2}} R_s R_n^{-\frac{1}{2}} u \rangle \leq \| R_n^{-\frac{1}{2}} R_s R_n^{-\frac{1}{2}} u \| \, \| u \| = \| R_n^{-\frac{1}{2}} R_s R_n^{-\frac{1}{2}} u \| \tag{3-31}$$

By the Buniakovskii inequality[55], the above inequality reduces to equality if and only if u is colinear to $R_n^{-\frac{1}{2}} R_s R_n^{-\frac{1}{2}} u$. Thus, equality holds if and only if

$$R_n^{-\frac{1}{2}} R_s R_n^{-\frac{1}{2}} u = \lambda u, \tag{3-32}$$

so that u is an eigenvector of $R_n^{-\frac{1}{2}} R_s R_n^{-\frac{1}{2}}$ and $\lambda$ is the associated eigenvalue. When u is an eigenvector we have

$$\langle u, R_n^{-\frac{1}{2}} R_s R_n^{-\frac{1}{2}} u \rangle = \lambda \| u \|^2 = \lambda . \tag{3-33}$$

Thus, the inner product is maximized when $\lambda$ is the maximum eigenvalue. The optimum weight vector then takes the form

$$w_{s/n} = R_n^{-\frac{1}{2}} u_{opt} \tag{3-34}$$

where $u_{opt}$ is a vector of unity norm belonging to the eigenspace associated with $\lambda_{max}$ and

$$J_{s/n}(w_{s/n}) = \lambda_{max}. \tag{3-35}$$

If the desired signal is narrowband or if spatial correction filters are used to cophase the desired signal in each channel, the optimum weight vector takes on a much simpler form. If the desired signal is narrowband then the performance measure can be written as

$$J_{s/n}(u) = \frac{S < u, R_n^{-\frac{1}{2}} v_1 v_1^* R_n^{-\frac{1}{2}} u>}{\| u \|^2} = \frac{S \, |<u, R_n^{-\frac{1}{2}} v_1>|^2}{\| u \|^2} . \tag{3-36}$$

We now decompose H into two disjoint subspaces $Q_1$ and $Q_2$ such that

$$H = Q_1 + Q_2 . \tag{3-37}$$

These spaces explicity consist of

$$Q_1 = \{ u_1 \mid u_1 = \alpha R_n^{-\frac{1}{2}} v_1 \}, \alpha \text{ an arbitrary scalar}$$

$$Q_2 = \{ u_2 \mid < u_1, u_2 > = 0 \} . \tag{3-38}$$

Given this orthogonal decomposition we can uniquely express any element of H as an element from $Q_1$ and $Q_2$. Let u be such an element, then

$$u = u_1 + u_2 \tag{3-39}$$

where $u_1 \epsilon Q_1$ and $u_2 \epsilon Q_2$. Then

$$J_{s/n}(u) = \frac{S|< u_1 + u_2, R_n^{-1} v_1>|^2}{\| u_1 \|^2 + \| u_2 \|^2} = \frac{S|< u_1, R_n^{-1} v_1>|^2}{\| u_1 \|^2 + \| u_2 \|^2}$$

$$= \left(\frac{S}{\alpha^2}\right) \frac{\| u_1 \|^4}{\| u_1 \|^2 + \| u_2 \|^2} \tag{3-40}$$

which takes on its maximum value when $\| u_2 \|$ is zero. Thus

$$u_{opt} = \alpha R_n^{-\frac{1}{2}} v_1 \tag{3-41}$$

If the desired signal is narrowband or if spatial correction filters are used to cophase the desired signal in each channel, the optimum weight vector takes on a much simpler form. If the desired signal is narrowband then the performance measure can be written as

$$J_{s/n}(u) = \frac{S < u, R_n^{-\frac{1}{2}} v_1 v_1^* R_n^{-\frac{1}{2}} u>}{\| u \|^2} = \frac{S \, |<u, R_n^{-\frac{1}{2}} v_1>|^2}{\| u \|^2} . \tag{3-36}$$

We now decompose H into two disjoint subspaces $Q_1$ and $Q_2$ such that

$$H = Q_1 + Q_2 . \tag{3-37}$$

These spaces explicity consist of

$$Q_1 = \{ u_1 \mid u_1 = \alpha R_n^{-\frac{1}{2}} v_1 \}, \alpha \text{ an arbitrary scalar}$$

$$Q_2 = \{ u_2 \mid < u_1, u_2 > = 0 \} . \tag{3-38}$$

Given this orthogonal decomposition we can uniquely express any element of H as an element from $Q_1$ and $Q_2$. Let u be such an element, then

$$u = u_1 + u_2 \tag{3-39}$$

where $u_1 \epsilon Q_1$ and $u_2 \epsilon Q_2$. Then

$$J_{s/n}(u) = \frac{S|< u_1 + u_2, R_n^{-1} v_1>|^2}{\| u_1 \|^2 + \| u_2 \|^2} = \frac{S|< u_1, R_n^{-1} v_1>|^2}{\| u_1 \|^2 + \| u_2 \|^2}$$

$$= \left(\frac{S}{\alpha^2}\right) \frac{\| u_1 \|^4}{\| u_1 \|^2 + \| u_2 \|^2} \tag{3-40}$$

which takes on its maximum value when $\| u_2 \|$ is zero. Thus

$$u_{opt} = \alpha R_n^{-\frac{1}{2}} v_1 \tag{3-41}$$

which implies that the optimum weight vector is

$$w_{s/n} = \alpha R_n^{-1} v_1 \tag{3-42}$$

with a signal-to-noise ratio of

$$J_{s/n}(w_{opt}) = \frac{S\alpha^2 |< R_n^{-1} v_1, v_1 >|^2}{\alpha^2 < R_n^{-1} v_1, R_n R_n^{-1} v_1 >} = S < v_1, R_n^{-1} v_1 > . \tag{3-43}$$

For a wideband desired signal that is cophased in each channel, the optimum weights are easily seen to be

$$w_{s/n} = \alpha R_n^{-1} \underline{1} \tag{3-44}$$

when $R_n$ is the covariance matrix of the noise vector after the spatial correction filters.

### 3.2.3 The Maximum Likelihood Solution

For relatively wideband desired signals the likelihood function has been derived as

$$J_{ml}(\xi) = < x - \xi \underline{1}, R_n^{-1} (x - \xi \underline{1}) > \tag{3-45}$$

which may be written in the form

$$J_{ml}(\xi) = || u ||^2 \tag{3-46}$$

where $u = R_n^{-\frac{1}{2}} (x - \xi \underline{1})$. The problem now becomes that of finding the scalar $\xi$ which minimizes the norm of $u$. Let us decompose H into the direct sum of subspaces $Q_1$ and $Q_2$ where

$$Q_1 = \{ u_1 | u_1 = \alpha R_n^{-\frac{1}{2}} \underline{1} \}, \alpha \text{ an arbitrary scalar}$$

$$Q_2 = \{ u_2 | < u_1, u_2 > = 0 \} . \tag{3-47}$$

In terms of these subspaces the vector $R_n^{-\frac{1}{2}} x$ has the unique representation

$$R_n^{-\frac{1}{2}} x = \alpha_1 R_n^{-\frac{1}{2}} \underline{1} + u_2 \tag{3-48}$$

where $u_2 \in Q_2$. Then u can be represented by

$$u = (\xi - \alpha_1) R_n^{-\frac{1}{2}} \underline{1} + u_2. \tag{3-49}$$

Thus, u has minimum norm when $\xi = \alpha_1$, and $\xi$ can be obtained by taking the inner product of $R_n^{-\frac{1}{2}} x$ with $R_n^{-\frac{1}{2}} \underline{1}$

$$< R_n^{-\frac{1}{2}} \underline{1}, R_n^{-\frac{1}{2}} x > = \xi < R_n^{-\frac{1}{2}} \underline{1}, R_n^{-\frac{1}{2}} \underline{1} > + < R_n^{-\frac{1}{2}} \underline{1}, u_2 > . \tag{3-50}$$

Since the last term in this expression is zero, we have the maximum likelihood signal as

$$\xi = \frac{< R_n^{-1} \underline{1}, x >}{< \underline{1}, R_n^{-1} \underline{1} >} \tag{3-51}$$

Since the output of the array is to be formed as

$$\xi = < w, x > \tag{3-52}$$

the optimum weight vector must take the form

$$w_{ml} = \frac{R_n^{-1} \underline{1}}{< \underline{1}, R_n^{-1} \underline{1} >} . \tag{3-53}$$

If the desired signal is narrowband, then we see from the performance measure given by Equation 3-12 a simple replacement of $\underline{1}$ with $v_1$ will yield the optimum weight vector.

### 3.2.4 The Unbiased Minimum Variance Solution

The performance measure for this solution was presented as

$$J_{mv}(w) = < w, R_n w > \tag{3-54}$$

subject to the equality constraint $\langle w, \underline{1} \rangle = 1$. The solution of this problem follows the same general pattern as the others. First, we define a vector u related to w by

$$u = R_n^{\frac{1}{2}} w \tag{3-55}$$

and note that

$$J_{mv}(w) = \langle w, R_n w \rangle = \| u \|^2 . \tag{3-56}$$

Hence the problem reduces to finding the vector of minimum norm such that

$$\langle R_n^{-\frac{1}{2}} u, \underline{1} \rangle = 1 . \tag{3-57}$$

Intuitively we know that the solution of this problem is a vector u that is colinear to $R_n^{-\frac{1}{2}} \underline{1}$. To show this is the case, we again decompose H into the direct sum of spaces $Q_1$ and $Q_2$ where

$$Q_1 = \{ u_1 \mid u_1 = \alpha R_n^{-\frac{1}{2}} \underline{1} \}, \ \alpha \text{ an arbitrary scalar}$$

$$Q_2 = \{ u_2 \mid \langle u_1, u_2 \rangle = 0 \} . \tag{3-58}$$

If u is any element of H, then we may write u uniquely as

$$u = u_1 + u_2 \tag{3-59}$$

where $u_1 \in Q_1$ and $u_2 \in Q_2$ such that

$$1 = \langle u_1 + u_2, R_n^{-\frac{1}{2}} \underline{1} \rangle = \langle u_1, R_n^{-\frac{1}{2}} \underline{1} \rangle = \alpha \| R_n^{-\frac{1}{2}} \underline{1} \|^2 . \tag{3-60}$$

Thus $\alpha$ is given by

$$\alpha = \frac{1}{\| R_n^{-\frac{1}{2}} \underline{1} \|^2} \tag{3-61}$$

which yields $u_1$ as

$$u_1 = \frac{1}{\left\| R_n^{-\frac{1}{2}} \underline{1} \right\|^2} R_n^{-\frac{1}{2}} \underline{1} . \tag{3-62}$$

From the performance measure we can conclude that $u_2$ is zero since

$$J_{mv}(u) = \left\| u_1 + u_2 \right\|^2 = \left\| u_1 \right\|^2 + \left\| u_2 \right\|^2 \geq \left\| u_1 \right\|^2 . \tag{3-63}$$

Thus the optimum weight vector is

$$w_{mv} = \frac{1}{< \underline{1}, R_n^{-1} \underline{1} >} R_n^{-1} \underline{1} . \tag{3-64}$$

## 3.3 Comparison of Solutions

### 3.3.1 Mean Square Error Solution Factorization

In this section the solutions obtained in the last section will be examined under the assumption of very narrowband signals. First, the minimum mean square error weights will be examined and it will be shown that these weights define a solution which can be factored into much the same form as that described for the general transfer function solution of Van Trees[73]. By examining the other optimal solutions, it will be seen that the S/N and the maximum likelihood solutions are part of this factorization and, as a special case, also the unbiased, minimum variance solution. It is shown that all these performance measures give weights which differ only by a scalar factor and, therefore, they all lead to identical signal-to-noise ratios.

The complex weight vector for the minimum mean square error processor was found to be

$$w_{mse} = R_x^{-1} r_{x\xi} . \tag{3-65}$$

For very narrowband signals this can be written as

$$w_{mse} = (Sv_1 v_1^* + R_n)^{-1} Sv_1 , \tag{3-66}$$

and using the matrix inversion lemma

$$w_{mse} = S \left[ R_n^{-1} - \frac{SR_n^{-1} v_1 v_1^* R_n^{-1}}{1 + Sv_1^* R_n^{-1} v_1} \right] v_1$$

$$= \frac{S}{1 + Sv_1^* R_n^{-1} v_1} R_n^{-1} v_1 = \beta_{mse} R_n^{-1} v_1 \tag{3-67}$$

where

$$\beta_{mse} = \frac{S}{1 + Sv_1^* R_n^{-1} v_1} . \tag{3-68}$$

In this form the processor can be drawn as shown in Figure 3-1 where the linear matrix filter $R_n^{-1} v_1$ can be interpreted as a "spatial" filter since it incorporates the spatial correlation of the noise and the propagation effects on the signal. $\beta_{mse}$ will be interpreted below.

The noise power at the output of the spatial filter can be written as

$$P_n = w^* R_n w = (R_n^{-1} v_1)^* R_n R_n^{-1} v_1$$

$$= v_1^* R_n^{-1} v_1 \tag{3-69}$$

and the signal power is

$$P_s = w^* R_s w = (R_n^{-1} v_1)^* R_s R_n^{-1} v_1$$

$$= v_1^* R_n^{-1} S v_1 v_1^* R_n^{-1} v_1$$

$$= SP_n^2 \tag{3-70}$$

In these expressions we see that the weights are proportional to $R_n^{-1} v_1$, that is they are inversely proportional to the input noise power (note that if $v_1 = \underline{1}$ then $v_1^* R_n^{-1} v_1$ is equal to the sum of the terms in the inverse noise correlation matrix). Consequently, the output noise power decreases as the input noise increases. This could also be interpreted

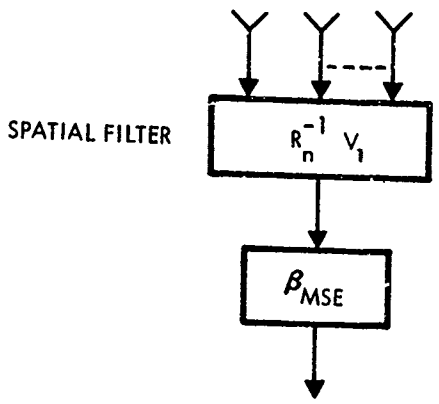


Figure 3-1. The MMSE Processor

from the point of view that the array is able to place deeper nulls on better defined noise sources. Using these expressions for $P_n$ and $P_s$, $\beta_{mse}$ can be written as

$$\beta_{mse} = \frac{S}{1 + Sv_1^* R_n^{-1} v_1} = \frac{P_n^2}{P_n^2} \left(\frac{S}{1 + SP_n}\right)$$

$$= \frac{1}{P_n} \left(\frac{SP_n^2}{P_n + SP_n^2}\right) = \frac{1}{P_n} \left(\frac{P_s}{P_n + P_s}\right) \tag{3-71}$$

and the weights become

$$w_{mse} = \frac{1}{P_n} \frac{P_s}{P_n + P_s} R_n^{-1} v_1 \tag{3-72}$$

### 3.3.2 Comparison with Other Solutions: Output S/N Ratio

In terms of the quantities defined above, the other optimal weights can be rewritten in a form which illustrates their relationship to the minimum mean square error solution. The optimal S/N weights were found as

$$w_{s/n} = \alpha R_n^{-1} v_1 \tag{3-73}$$

and hence, $\beta_{s/n} = \alpha$, where $\alpha$ is an arbitrary constant. The maximum likelihood weights were found as

$$w_{ml} = \frac{R_n^{-1} v_1}{v_1^* R_n^{-1} v_1} = \beta_{ml} R_n^{-1} v_1 \tag{3-74}$$

$$\beta_{ml} = \frac{1}{v_1^* R_n^{-1} v_1} = \frac{1}{P_n} \quad . \tag{3-75}$$

In terms of these quantities, the minimum mean square error processor of Figure 3-1 is seen to factor into the form shown in Figure 3-2.

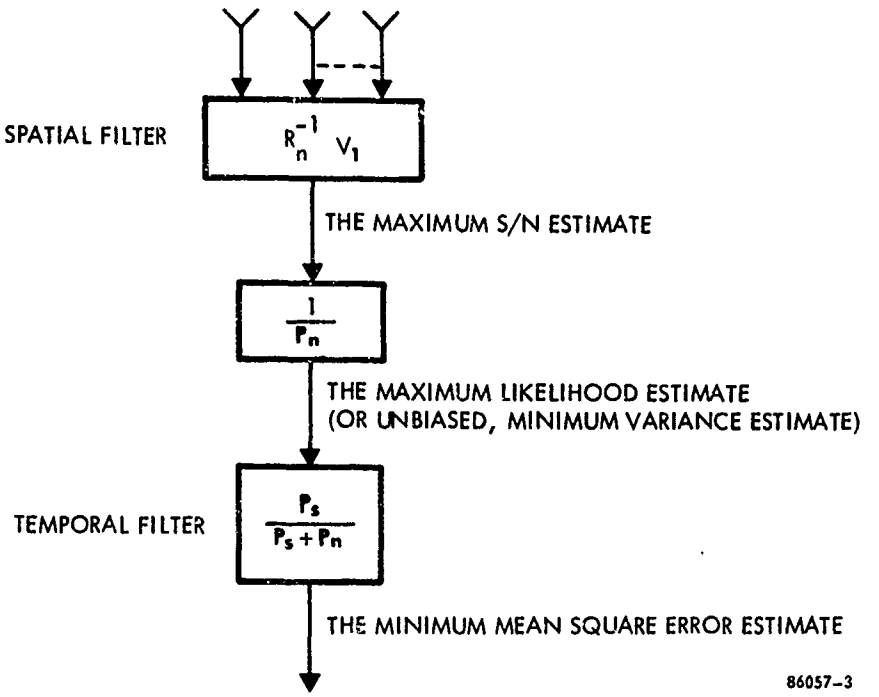


Figure 3-2. The Factored Processor

If the desired signal terms were aligned in the array, either through the use of spatial correction filters in each channel, or because it happened to be broadside to the array, then the signal propagation vector $v_1$ would simply be the vector $\underline{1}$. In this case, the maximum likelihood weights $w_{m1}$ are seen to reduce to the unbiased minimum variance weights, a result previously established for the more general processor models [23]. That is,

$$w_{m1}\Big|_{v_1 = \underline{1}} = \frac{R_n^{-1}\underline{1}}{\underline{1}^* R_n^{-1}\underline{1}} = w_{mv} \tag{3-76}$$

Similarly, the other optimal weights for the signal aligned case can be found simply by replacing $v_1$ by $\underline{1}$. Notice also that for the signal aligned array the results of this section can be extended to relatively wideband problems since the correlation functions $R_s$ and $r_{x\xi}$ can be factored as $R_s = S\,\underline{1}\,\underline{1}^*$ and $r_{x\xi} = S\,\underline{1}$. This is due to the fact that when the desired signal in broadside there is no dispersion along the array since it arrives at each antenna simultaneously. For all the cases examined above, the optimal complex weight vectors are seen to differ only by a scalar factor $\beta$. Consequently, all the different processors have the same output signal-to-noise ratios given by

$$P_s/P_n = \frac{w^* R_s w}{w^* R_n w} = \frac{\beta v_1^* R_n^{-1} S v_1 v_1^* \beta R_n^{-1} v_1}{\beta v_1^* R_n^{-1} R_n \beta R_n^{-1} v_1}$$

$$= S v_1^* R_n^{-1} v_1 \tag{3-77}$$

### 3.3.3 Maximum Likelihood Versus Minimum Mean Square Error Solutions

As previously discussed in Paragraph 3.1, the various performance criteria are generally useful in different situations. For example, the maximum likelihood criteria is used when the desired signal is modelled as a deterministic, but unknown signal. In this case it is not necessary to assume any knowledge of the signal statistics, but the noise must be Gaussian. On the other hand, the mean square error criterion is generally used when the desired signal is modelled as a random process. This requires the second order statistics of both the signal and the noise to be known or measured. However, if the desired signal's statistics are not known or are difficult to measure, then one could resort to the use of a maximum likelihood processor. This section will examine the tradeoff between these two processors.

To compare these two processors, the optimal weights associated with each can be substituted back into the expression for the mean square error given in Equation 3-5:

$$J_{mse} = \frac{1}{2}[\langle w, R_x w\rangle - 2\mathrm{Re}\,\langle w, r_{x\xi}\rangle + S] \tag{3-78}$$

In this manner $\bar{J}_{mse}$, the mean square error associated with the minimum mean square error weights, normalized by letting signal power S equal unity, can be written (using Equation 3-70) as

$$\bar{J}_{mse} = \frac{1}{1 + P_n} \quad . \tag{3-79}$$

Also, the normalized mean square error associated with the maximum likelihood weights can be found as

$$\bar{J}_{mse}\Big|_{ml} = \frac{1}{P_n} \tag{3-80}$$

Recalling from Equation 3-70 that the output noise power $P_n$ is inversely proportional to the input noise, N, we can write

$$\bar{J}_{mse} \sim \frac{N}{N + 1} \tag{3-81}$$

and

$$\bar{J}_{mse}\Big|_{ml} \sim N. \tag{3-82}$$

From these expressions we see that the mean square error associated with each of these processors becomes nearly equal when $N << 1$; that is, large input signal-to-noise ratios, a result previously noted by Griffiths [41]. Also, from Equation 3-81 it is apparent that for large input noise power the normalized mean square error associated with the minimum mean square error solution is relatively constant.

# CHAPTER 4

# OPTIMIZATION TECHNIQUES

## 4.0 OPTIMIZATION TECHNIQUES

This chapter examines candidate optimization methods for the optimization of a given array performance measure J (w). The methods to be examined can generally be classified as either search techniques, gradient (first order) methods, or the higher order methods. The search techniques utilize only information about the values of the performance measure at neighboring weight settings to compute successively better weights. The gradient methods utilize knowledge of the performance measure gradient at a particular weight setting in order to change that setting to an improved value, while the higher order techniques require knowledge of the higher order derivatives of the performance measure. From this examination it will be apparent that the gradient technique known as steepest descent is the most practical method for the implementation of adaptive null steering arrays - the other techniques do not lead to simple and effective circuitry. Also, since the minimum noise variance performance criterion requires a constraint on the weights, a constrained gradient method, the projection gradient method, will be presented. These optimization techniques are designed for the optimization of the performance criteria as presented in the preceding chapters, which require the evaluation of appropriate correlation matrices. It will be demonstrated through the method of stochastic approximation, and intuitive arguments, that instantaneous error quantities can be effectively used, avoiding the necessity to consider averaged quantities and resulting in much simpler implementations.

### 4.1 The Search Techniques

The search type techniques for optimization are essentially refined trial and error methods. They proceed by evaluating the performance measure for several values of the independent variable (the weights in the adaptive antenna problem) and from these calculations an improved estimate of the weights is made. For example, consider the two situations illustrated in Figure 4-1 for the initial weight approximation $w_1$. If the optimum can be bounded by the interval $[\alpha, \beta]$, then a smaller bounding region can be established as follows. Let $\alpha < w_1 < w_2 < \beta$, then for

$$\text{i)} \quad J(w_1) > J(w_2) \rightarrow w_{opt} \in [w_1, \beta]$$

$$\text{ii)} \quad J(w_1) < J(w_2) \rightarrow w_{opt} \in [\alpha, w_2].$$

The next trial is then compared to $J(w_2)$ for case i) or $J(w_1)$ for case ii) and the process continues until the corrections become small.

i) $J(w_1) > J(w_2)$

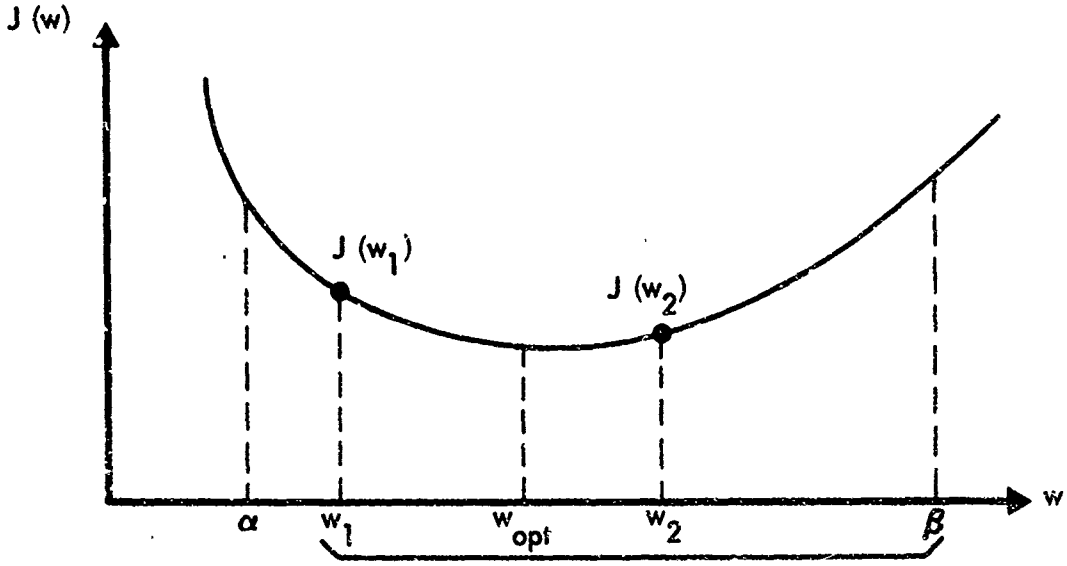


ii) $J(w_1) < J(w_2)$

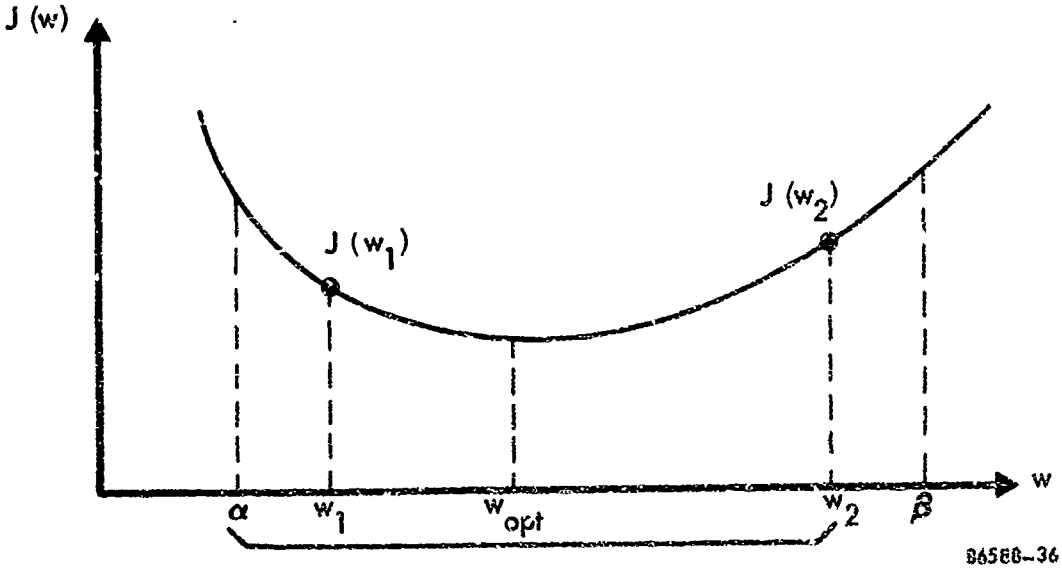


Figure 4-1. General Search Method

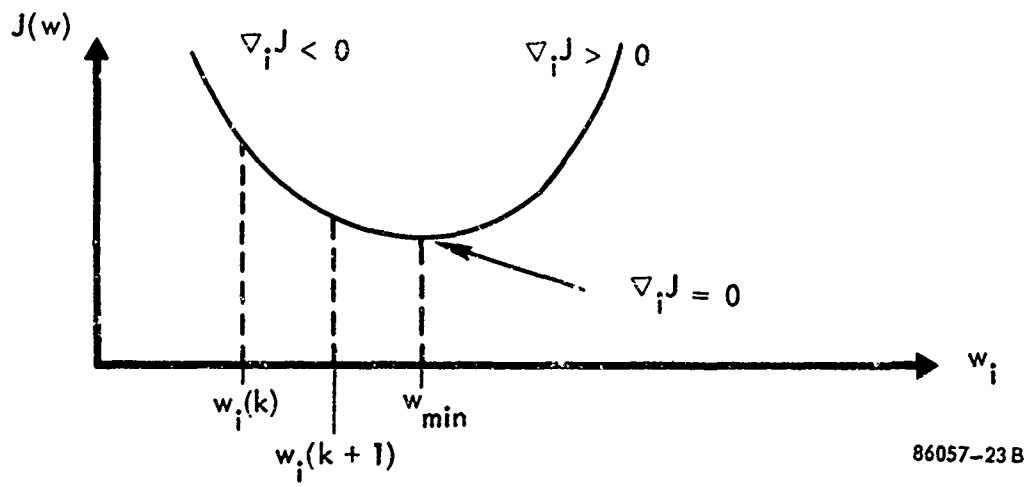


Figure 4-2. Geometrical Illustration of Steepest Descent Procedure

The method for choosing the next trial point within the new interval defines the algorithm, e.g., the golden section or the Fibonacci search. Extensions of these ideas can be obtained for multivariable problems [51] such as the simplex method which constructs successively smaller geometrical regions which contain the optimum solution. These methods, however, have two distinct disadvantages which disqualify them for use as computational procedures for finding the optimum array processor weights. First, they require that the precise functional form of the performance measure be known [to calculate the trial values $J(w_i)$], which requires that the correlation functions for our problem be known. And secondly, they generally require a digital computer for implementation and do not lead to practical circuitry.

## 4.2 The Gradient Methods

### 4.2.1 General Description

To obtain better convergence properties and more implementable solutions, the gradient type optimization techniques can be used. These methods utilize the slope of the performance measure for a candidate weight setting to generate an improved estimate of the weight. This general procedure is best illustrated geometrically. Figure 4-2 shows the performance measure surface for one component of the weight vector. From this figure we see that to the left of the minimum the slope or gradient of the error curve (or generally, a surface) is negative, while to the right the gradient is positive. This property suggests the following algorithm to update an initial approximation $w_i(0)$

$$w_i(k+1) = w_i(k) - \alpha \nabla_i J \Big|_{w_i(k)} \tag{4-1}$$

or

$$w(k+1) = w(k) - \alpha \nabla J \Big|_{w(k)}, \quad k = 0, 1, 2, \ldots \tag{4-2}$$

where $\alpha$ is a positive constant and $\nabla J$ is the column vector $\left(\frac{\partial J}{\partial w_1}, \frac{\partial J}{\partial w_2}, \ldots, \frac{\partial J}{\partial w_m}\right)^T$.

It is apparent that the choice of the constant $\alpha$ is critical to the success of this algorithm. If $\alpha$ is too large, then the correction terms $[\alpha \nabla_i J]$

will be so large that the updated values will oscillate on each side of the minimum. On the other hand, if $\alpha$ is too small, then the approximations will converge too slowly. Also, it is apparent that the gradient becomes very small (approaches zero) as the minimum is approached, and hence the convergence rate slows down, dictating an increase in the magnitude of $\alpha$ as the solution is approached. Another consideration is that certain components of w may be more sensitive to adjustment than others and it might be appropriate to consider a matrix of constants A in the modified algorithm

$$w(k+1) = w(k) - A\nabla J \Big|_{w(k)}, \quad k = 0, 1, 2, \ldots \tag{4-3}$$

The choice of the convergence factor must be made within the context of the particular problem to be solved. In the section on stochastic approximation it will be seen that a set of equations which this factor must satisfy will also be specified. Also, in the section on higher order methods the matrix A discussed above will appear as the inverse of the matrix of second partial derivatives of J with respect to w. While this is too complex for practical solutions, it does give an indication of how A might be chosen. The method of steepest descent, as presented here, is seen to require the evaluation of the gradient of the performance measure, but not the performance measure itself, at each value of the weight setting. As will be demonstrated in Chapter V, the method used to perform this evaluation will be one of the critical differences between the various implementations of this method. As presented, the method of steepest descent changes the weight (in the direction of the gradient) an amount dependent on the magnitude of the convergence factor. Other descent methods differ from this in that they often use different directions, e.g., the conjugate gradient method [32]. Also, some of these other methods do not change the weight a fixed amount, but calculate the exact minimum in the descent direction [51]. However, similar to the search techniques, these methods are primarily suited for digital computer applications and do not lead to readily implemented circuitry.

### 4.2.2 Steepest Descent Implementations

The algorithm in Equation 4-1 can be implemented directly in terms of discrete elements in the form of Figure 4-3a, or the equivalent analog representation of Figure 4-3b can be used. This alternate form can be derived from the differential equation

$$\frac{dw}{dt} = -\alpha\nabla J, \; w(t_0) = w_0, \; t \geq t_0 \tag{4-4}$$

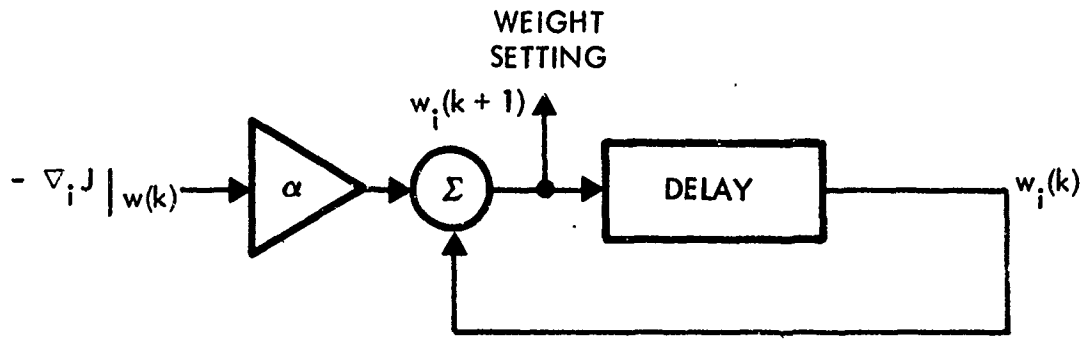


Figure 4-3a. Digital Implementation of Steepest Descent

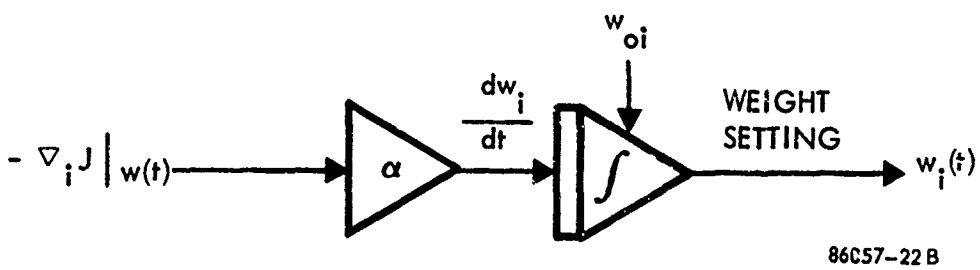


Figure 4-3b. Analog Implementation of Steepest Descent

whose solution will approach the equilibrium point $dw/dt = \underline{0}$ at the minimizing value of w where $\nabla J$ is zero. The solution of this differential equation, represented in Figure 4-3b, is

$$w(t) = w_0 - \alpha \int_{t_0}^{t} \nabla J ds. \tag{4-5}$$

Again, the choice of the gain factor $\alpha$ is seen to be critical if proper balance between stability and speed of response is to be maintained.

## 4.3 The Higher Order Methods

### 4.3.1 General Description - The Newton-Raphson Method

The higher order optimization techniques are characterized by their use of higher order derivatives of the performance measure, rather than just the first derivative as is required in the steepest descent method. An example of this type of method can be derived by using the Newton-Raphson root finding technique. This procedures is primarily designed for the determination of the roots of an algebraic equation. To utilize it for the problem at hand we must apply it to finding the roots of the equations specified by the necessary conditions. That is, we seek the root $\hat{w}$ of the equation

$$\nabla J(w) = \underline{0} \tag{4-6}$$

which defines $\hat{w}$ which optimizes the performance measure J. The method proceeds by constructing a linear approximation to the function $\nabla J(w)$ at some approximation $w = w_0$ for the desired root. That is, the nonlinear functional $\nabla J(w)$ is replaced by a Taylor series expansion truncated after the linear terms, giving the equation

$$\nabla J(w) = \nabla J(w_0) + [H(w_0)](w-w_0) + \ldots \tag{4-7}$$

where $H(w_0) = [\frac{\partial^2 J(w_0)}{\partial w_i \partial w_j}]$ is the Hessian matrix of second partial derivatives. The zero of this approximation is solved for, giving

$$\hat{w} = w_0 - H^{-1}(w_0) \nabla J \Big|_{w_0} \tag{4-8}$$

which leads to the general sequence of approximations

$$w(k+1) = w(k) - H^{-1}(w_0)\ \nabla J \Big|_{w(k)}, \quad k = 0, 1, 2, \ldots \tag{4-9}$$

These ideas are presented graphically for a simple scalar problem in Figure 4-4.

The algorithm of Equation 4-9 is a second order method for the optimization of the performance measure J since it requires the use of second order partial derivatives of J. Generally these procedures yield faster convergence rates; however, not only must these derivatives be evaluated, but the inverse must be computed. These two operations must be done at each stage of the algorithm, an obviously tedious process. Some variations on this method can be used, which utilize the same matrix inverse for several steps, but the algorithm is still too involved for practical implementation. As will be demonstrated in the next paragraph, this method is essentially the evaluation of the closed form solution for the minimum mean square error case, a procedure which has already been discounted as computationally unattractive. Methods using even higher order derivatives are conceivable (for higher order performance measures), but would lead to even more complex calculations.

### 4.3.2 Application to Mean Square Error Performance Measure

It is interesting to examine the application of the Newton-Raphson algorithm to the computation of the optimal weights for the minimum mean square error processor. For this case the performance measure was given in Equation 3-5 as

$$J(w) = \frac{1}{2}\left[\langle w, R_x w\rangle - 2\mathrm{Re}\langle w, r_{x\xi}\rangle + S\right] \tag{4-10}$$

and the necessary condition for the optimum becomes

$$\nabla J = \underline{0} = R_x w - r_{x\xi} \tag{4-11}$$

the solution of which can be computed as $w = R_x^{-1} r_{x\xi}$. Alternatively, the Newton-Raphson algorithm of Equation 4-9 can be applied to this problem in the form of finding the roots (solution) to Equation 4-11.

Since the performance measure is quadratic in the weights w, the necessary conditions of Equation 4-11 yield the solution which is a unique minimum. However, since it is quadratic, the first partials in Equation 4-11 are linear and the linear approximation defined by the Newton-Raphson method is seen to be exact. (This can also be

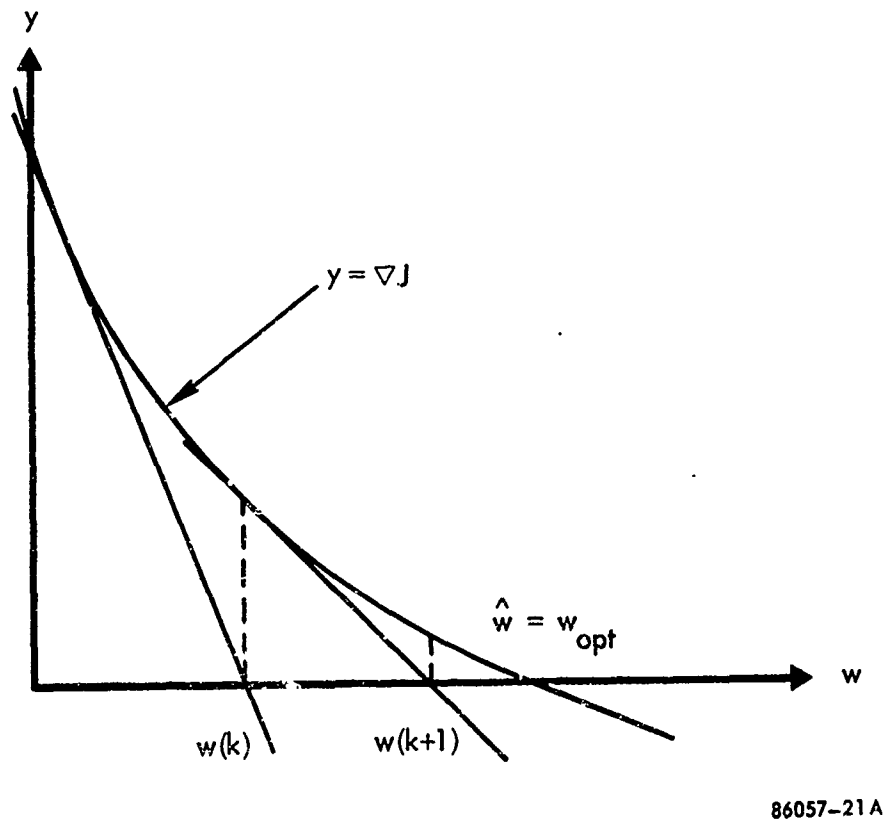


Figure 4-4. The Newton-Raphson Method

thought of as the "approximation" of the original performance measure, which is quadratic, with a quadratic function.) This means that the Newton-Raphson method converges in one step - it is an exact procedure for this application. These facts can be demonstrated by an examination of the equations required by the procedure. The matrix of second partial derivatives in Equation 4-9 becomes $H(w) = R_x$ and the algorithm is written as

$$w(k+1) = w(k) - R_x^{-1}\left[R_x w(k) - r_{x\xi}\right] = R_x^{-1} r_{x\xi}. \tag{4-12}$$

This is, of course, the exact solution of the set of linear equations given in Equation 4-11. In other words, the application of the Newton-Raphson method to this problem is trivial; however, it is interesting to obtain these equations because of their relationship to the steepest descent equations and the implications they have on the choice of the convergence factor.

## 4.4 The Projection Gradient Method

In the past several sections candidate optimization techniques have been discussed and it is apparent that the method of steepest descent is most appropriate for adaptive antenna problems. Since the minimum variance performance measure requires that the weights be constrained, then a constrained optimization method must also be presented. The projection gradient method is a steepest descent procedure for iteratively (adaptively) computing the optimum of a constrained optimization problem. The procedure is best described in terms of the geometric presentation of Figure 4-5. This figure represents a two-dimensional optimization problem where the optimal w is required to lie on the line (hyperplane)

$$w_1 + w_2 = 1, \left(\sum_{i=1}^{2} w_i = 1 = \langle w, \underline{1}\rangle\right). \tag{4-13}$$

And since the performance measure J is convex, constant J surfaces are closed about the origin. As shown there, the point on the line $w_1 + w_2 = 1$ which is on the smallest constant J surface (i.e., the smallest value of performance measure) occurs where that surface is tangential to the constraint set and is characterized by the fact that the gradient of the performance measure is orthogonal (perpendicular) to the constraint set. Thus, the necessary condition for an unconstrained optimum, i.e., that the gradient is zero, is replaced by the condition that the gradient be orthogonal to the constraint set - that is, that the projection of the gradient onto the constraint set is zero.

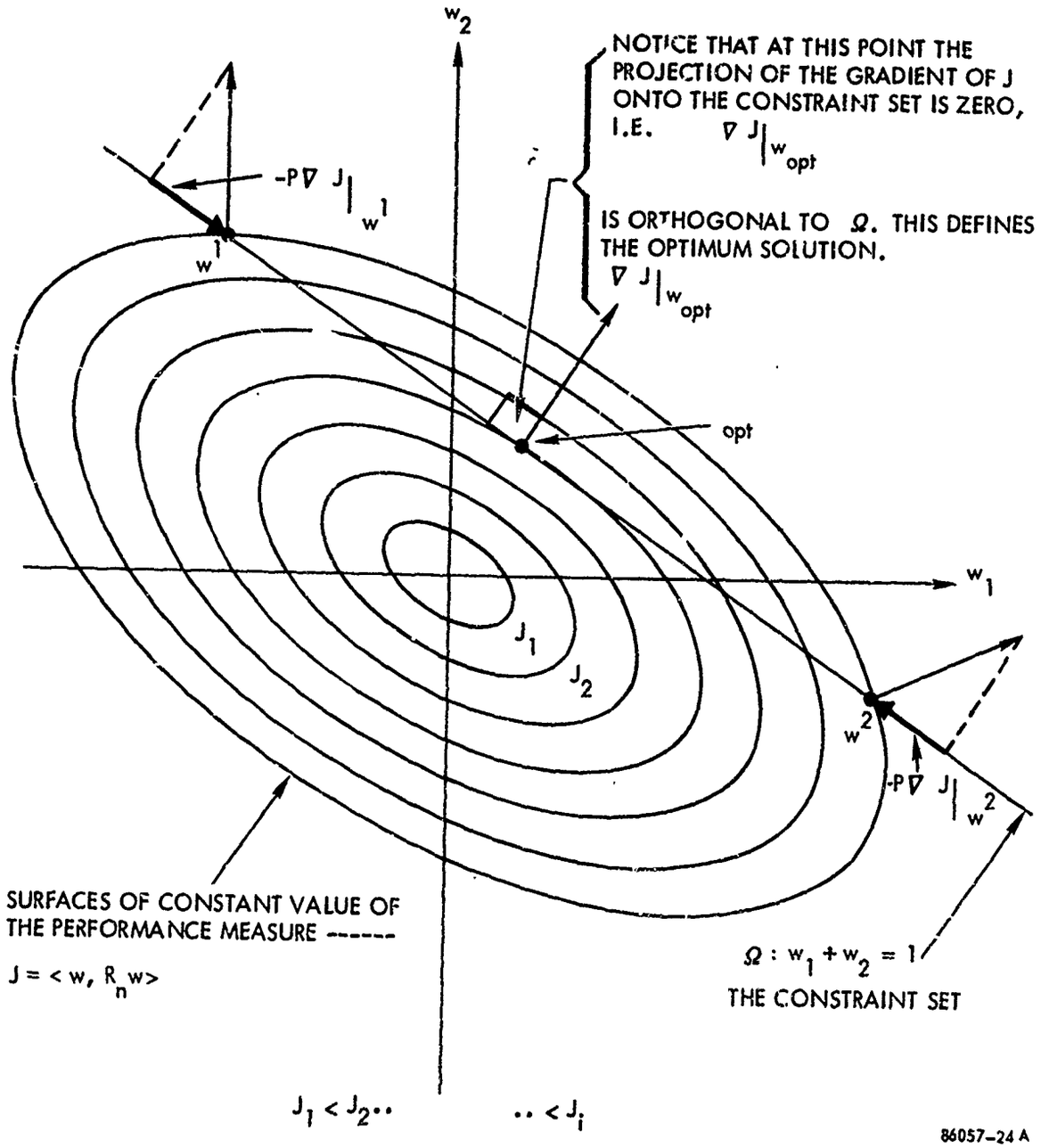


Figure 4-5. Geometric Interpretation of Projection Gradient Method

This illustration also indicates a procedure which could be used in an iterative fashion, exactly analogous to the unconstrained method of steepest descent. Looking at the gradient vector evaluated at the two points $w^1$ and $w^2$ shows that the negative of the projection (orthogonal) onto the constraint set always points in the direction of the optimum, so rather than using the standard steepest descent algorithm of Equation 4-2 we use the modified form

$$w(k+1) = w(k) - \alpha P \nabla J \Big|_{w(k)} \tag{4-14}$$

where P is a projection operator. It is interesting to note that the form of this projection operator is quite simple (for this case it takes the form $P = \left(I - \frac{\underline{1}\,\underline{1}^T}{m}\right)$, and the resulting algorithm can lead to as simple an implementation as the standard steepest descent solution of using an unconstrained performance measure. The application of this procedure to the minimum variance performance measure is presented in Chapter V.

## 4.5 The Method of Stochastic Approximation

The techniques developed in this chapter are designed primarily to optimize the performance measures in the forms presented in Chapter 3. In particular, the steepest descent procedure, the obvious candidate for practical implementation, requires the gradient of these performance measures. These gradient expressions require the a priori knowledge or evaluation of the signal correlation functions. Generally, these correlations are not known and their evaluation would require more complex implementations. However, the method of stochastic approximation avoids these problems. Using this procedure, the instantaneous signals available at the array can be used directly in the optimization algorithm. This avoids the requirement to compute averaged quantities, thereby eliminating additional integrators from the circuitry.

For example, the gradient of the mean square error performance measure takes the form:

$$\nabla J = R_x w - r_{x\xi} \tag{4-15}$$

where $R_x$ and $r_{x\xi}$ are generally not known, but can be evaluated as finite time averages. That is:

$$R_x \approx \frac{1}{T} \int_T x(t)^* (t)dt = \overline{x(t)x^*(t)} \tag{4-16}$$

and

$$r_{x\xi} \approx \frac{1}{T} \int_T \xi^*(t)x(t)\, dt = \overline{\xi^*(t)x(t)}. \tag{4-17}$$

Denoting averaging by overbar, $\nabla J$ becomes

$$\nabla J = \overline{x(t)x^*(t)}w(t) - \overline{\xi^*(t)x(t)}. \tag{4-18}$$

Consequently, to obtain these correlations an additional integrator must be used in the implementation shown in Figure 4-3b to obtain $\nabla J$. However, if the signal bandwidths and the convergence factor $\alpha$ are chosen correctly, this additional integration can be avoided. In this form the gradient of $\hat{J}$, the instantaneous error squared (rather than J, the mean square error) can be used and takes the form (dropping the overbar above):

$$\begin{aligned} \nabla J &= x(t)x^*(t)w(t) - \xi^*(t)x(t) \\ &= x(t)y^*(t) - \xi^*(t)x(t) \\ &= x(t)\,[y^*(t) - \xi^*(t)] \end{aligned} \tag{4-19}$$

This simplification can be justified using either stochastic approximation [33] or intuitive arguments, both of which are discussed briefly below. Also, these methods will be illustrated in application to specific adaptive algorithms in Chapter 5.

### 4.5.1 Brief Description of Stochastic Approximation

Consider the problem of finding the extrema of

$$\hat{J}(x_1, x_2, \ldots, x_m; w_1, w_2, \ldots, w_m) = \hat{J}(x, w) \tag{4-20}$$

where $\hat{J}$ is a function of the deterministic quantities w - the weights, and the statistical quantities x - the signals received by the array. Since $\hat{J}$ is a function of variables which are known only in a probabilistic sense, then the extremization of this function implies the extremization of J which is the expected value of $\hat{J}$, that is,

$$J = E[\hat{J}(x, w)] = \int \hat{J}(x, w)\, p(x)\, dx \approx 1/T \int_T \hat{J}(x, w)\, dt. \tag{4-21}$$

The extrema of this expression are specified by the zeros of the gradient vector

$$\nabla J = \underline{0} \tag{4-22}$$

and the steepest descent type adaptation scheme would take the form of Equation 4-2

$$w(k+1) = w(k) - \alpha \nabla J \Big|_{w(k)} \tag{4-23}$$

Since the probability density function $p(x)$ is generally not known, and its approximation by a time average is often tedious, $J$ and $\nabla J$ are often difficult to compute. However, the stochastic approximation algorithm involving the gradient of the instantaneous function $\hat{J}$ is often utilized, and takes the form

$$w(k+1) = w(k) - \alpha(k) \nabla \hat{J} \Big|_{w(k)} \tag{4-24}$$

In this form of algorithm, it might be expected that the relaxation of the requirement to compute an averaged gradient term (requiring knowledge of the correlation functions) might necessitate a more stringent set of requirements on the specification of the convergence factor. These requirements generally take the following form:

1. $\sum_{k=1}^{\infty} \alpha(k) = \infty$ which ensures that there is an unlimited amount of correction effort if required; and,

2. $\sum_{k=1}^{\infty} [\alpha(k)]^2 < \infty$ which ensures that the correction terms go to zero so that the process converges.

It can be established that under these conditions the stochastic approximation algorithm converges both in mean square

$$\lim_{k \to \infty} E\,[w(k) - w_{opt}]^2 = \underline{0} \tag{4-25}$$

and with probability one.

### 4.5.2 Application to Null Steering Adaptive Arrays: Intuitive Argument

The use of instantaneous quantities for performance criteria has been applied to adaptive array design in the past and been justified both through the explicit use of stochastic approximation and more directly through intuitive reasoning. This will be illustrated in the discussion of specific algorithms in the next chapter, but generally this reasoning can be illustrated as follows. Considering the control loop of Figure 4-3b for the algorithm

$$\frac{dw}{dt} = -\alpha \nabla J(w), \; w(t_o) = w_o \tag{4-26}$$

the weights $w$ are given by Equation 4-5 as

$$w(t) = w_o - \alpha \int_{t_o}^{t} \nabla J(w)\, ds \tag{4-27}$$

For the mean square error performance measure of Equation 3-5 $\nabla J(w)$ is given by

$$\nabla J(w) = R_x w - r_{x\xi} \tag{4-28}$$

which requires that $R_x$ and $r_{x\xi}$ be known or calculated from quantities available at the array. Alternatively we could use instantaneous quantities as

$$\nabla \hat{J}(w) = xx^*w - \xi^* x. \tag{4-29}$$

In this form, Equation 4-26 becomes

$$\frac{dw}{dt} = -\alpha \nabla \hat{J}(w) = -\alpha \left[ xx^*w - \xi^* x \right] \tag{4-30}$$

Notice from Equation 4-30 that if $\alpha$ is small enough, then $w(t)$ will remain relatively constant and $w$ will be essentially independent of $\nabla \hat{J}(w)$ and $x(t)$. (This can also be argued that if $\alpha$ is small enough, the loop bandwidth of the control loop is much smaller than the bandwidth of the received signal $x(t)$ and the weights will vary slowly compared to these signals.) For this case, the equation for the average weights $\bar{w}$ comes directly from Equation 4-30 as

$$\frac{d\overline{w}}{dt} = -\alpha\,\overline{xx^*}\,\overline{w} + \alpha\,\overline{\xi^* x} \tag{4-31}$$

$$= -\alpha R_x \overline{w} + \alpha r_{x\xi} = -\alpha \nabla J(\overline{w})$$

That is, for $\alpha$ small, the average weights computed using instantaneous values are governed by the steepest descent equation for the averaged performance measure.

## 4.6 Alternative Computational Procedures

In this chapter the mathematical optimization techniques required for the design of adaptive null steering arrays have been presented. These procedures avoid the necessity to know the correlation functions at the array and since they are continually being updated they can be used in time varying environments. Alternatively, if the correlation functions are known or measured, then the solutions could be computed directly and the optimal filter could be constructed. However, these solutions require the computation of a matrix inverse, often a tedious computational procedure, particularly if the array has many elements. For some of the solutions the matrix which must be inverted is Toeplitz, a fact which can be used to construct more efficient inversion routines[77]. However, if the statistics change due to a time varying environment, such as moving emitters, jammers, and signals turning on and off, or changing signal structure, then the solutions must all be recalculated and a new filter constructed.

Another class of iterative computation techniques for the optimal processors are the recursive methods. These procedures both measure and perform the required inversions and matrix computations using efficient procedures which make use of recursive estimation methods to introduce the effects of new data and avoid the requirement to re-invert the correlation matrix. Mantey and Griffiths[56] and Baird[7] have presented such processors which converge to the minimum mean square error solutions, while Baird and Rickard[9] have developed a similar procedure for the unbiased, minimum variance solution. These procedures are suitable for problems with time varying statistics since the solutions are continually updated. Also, they have the property that they are optimal at each stage of the iterative process, based on the data used, whereas the steepest descent processors are merely asymptotically optimal. These are a promising class of processing methods; however, they require further development before practical implementations competitive with the steepest descent methods can be designed.

# CHAPTER 5

# BASIC ADAPTIVE ARRAY ALGORITHMS

## 5.0 BASIC ADAPTIVE ARRAY ALGORITHMS

In the past several chapters the mathematical techniques required for the development of optimum adaptive array processors have been presented. The optimal solutions have been discussed, together with the adaptive optimization methods which can be used to efficiently calculate these solutions in a complex time-varying environment. As has been demonstrated, the most appropriate optimization procedure is the method of steepest descent, which coupled with stochastic approximation ideas allows the simplification of using instantaneous performance measures, rather than averaged measures.

In this chapter the adaptive algorithms which have been presented in the literature are described. The majority of these procedures utilize the basic steepest descent-stochastic approximation solution. They differ according to which performance measure they are designed to optimize, however, as was demonstrated in Chapter 3, for narrow band systems these lead to identical steady state solutions. Furthermore, it will be apparent that they will exhibit essentially similar transient behavior. The basic algorithm takes the form

$$\frac{dw}{dt} = - \alpha \nabla \hat{J} \quad , w(t_o) = w_o \qquad 5\text{-}1$$

where $\hat{J}$ is the performance measure based on instantaneous quantities and a general block diagram is shown in Figure 5-1. In this diagram the array output, a priori information, and array inputs are utilized to calculate the instantaneous performance measure gradient, which is then used in the steepest descent optimization algorithm of Equation 5-1 to find the optimum weights. The procedures discussed in this chapter are primarily signal known or DOA known type methods, with little consideration as to how accurate approximations for these quantities are acquired. In other words, these algorithms represent basic solution methods, but do not qualify as practical solution techniques since they do not solve the acquisition problem. This problem will be considered in detail in later chapters of this report.

### 5.1 Minimum Mean Square Error Algorithm

In this section basic algorithms which have been designed to minimize mean square error will be presented. Two such procedures will be illustrated, a signal known type and a signal DOA known method.

#### 5.1.1 The LMS Algorithm

Widrow, et al.[76], have presented an algorithm which minimizes the mean square error at the array output and is designed using the instantaneous error

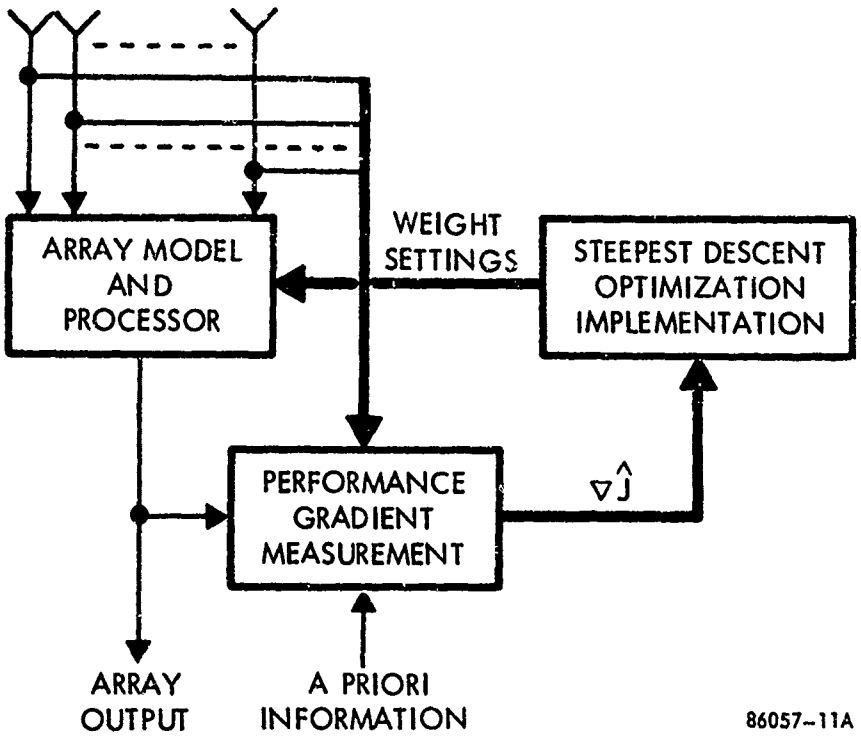


Figure 5-1. General Adaptive Null Steering System

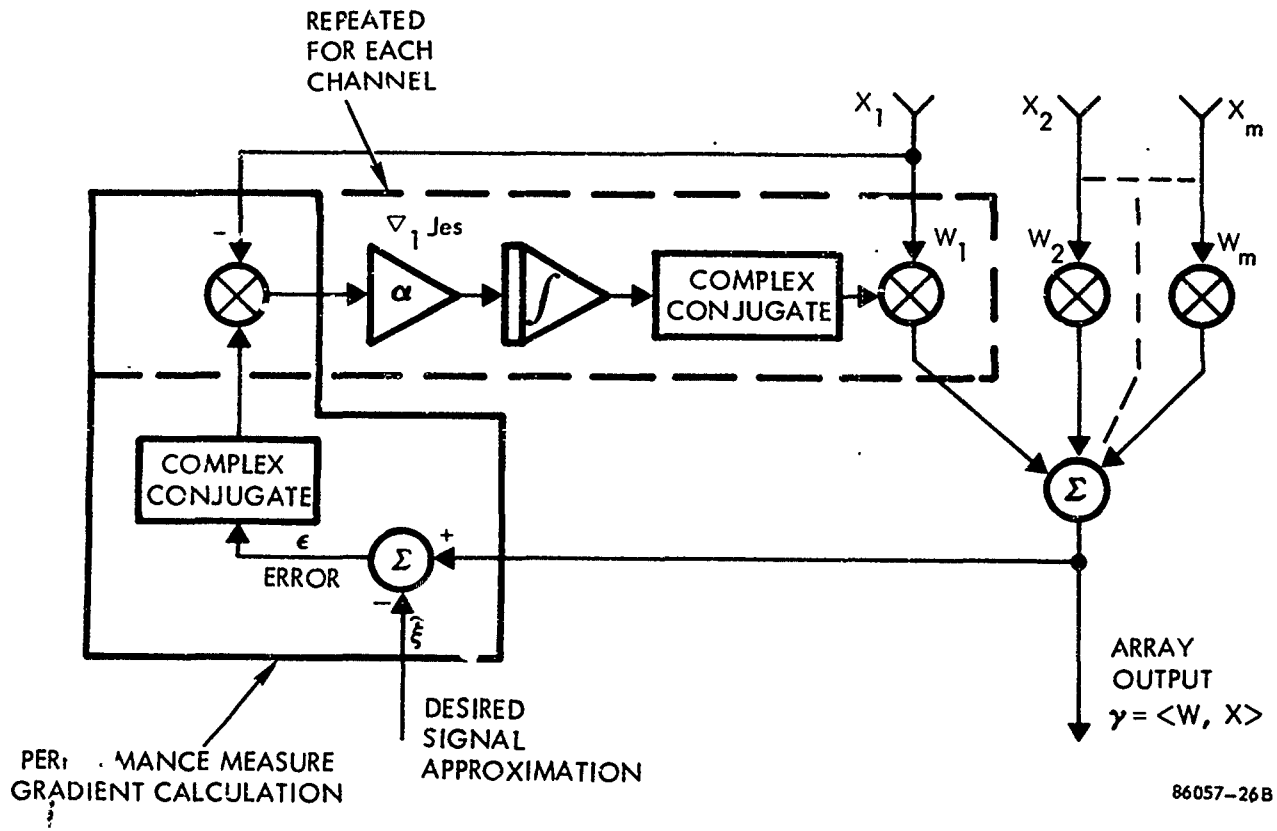


Figure 5-2. The LMS Algorithm

squared criterion. Considering the error between the array output and an approximation $\tilde{\xi}$ for the desired signal, this criterion is

$$J_{es} = \tfrac{1}{2} \left| \epsilon \right|^2 = \tfrac{1}{2} \left| \langle w, x \rangle - \tilde{\xi} \right|^2 \qquad 5\text{-}2$$

(where the ½ is introduced in the performance measures of this chapter to simplify the gradient expressions). The gradient of this expression is

$$\nabla J_{es} = (\langle w, x \rangle - \tilde{\xi})^* x = \epsilon^* x \qquad 5\text{-}3$$

and the analog implementation (based on Figure 4-3b) becomes

$$\frac{dw}{dt} = - \alpha \, \epsilon^* x, \qquad w(t_o) = w_o \qquad 5\text{-}4$$

This type of algorithm has been studied extensively since it was first suggested for antenna array problems by Widrow, et al.[76] (They also present an investigation of the choice of the convergence factor $\alpha$.) Using the implementation detailed in Figure 4.3b this algorithm can be constructed as shown in Figure 5-2, where the integrator shown integrates both the real and complex components for the weight $w_1 = w_{1re} + jw_{1im}$.

In the form presented above, the LMS algorithm is seen to require precise knowledge of the desired signal in order to construct the performance measure gradient. This is, of course, an unrealistic assumption (since it would obviate the need for an array), however, several fixes have been suggested. Compton and Riegler[26] suggested that only partial knowledge of the desired signal is necessary here, and an approximation $\tilde{\xi}$ for $\xi$ (such as the carrier frequency) can be used. They have also developed more sophisticated techniques for use with spread spectrum signals[47]. The construction of a useful approximation for this form of algorithm is also discussed under the topic of acquisition in later sections of this report. Widrow, et al.[76] suggested a two-mode algorithm which requires direction-of-arrival and alternatively adapts to the environment and an inserted pilot signal constructed to appear as though it came from the desired direction. In this form the array alternatively steers a beam towards the desired signal, and then tries to steer nulls on all signals (including the desired signal), leading to a compromise solution which does not approach the optimal weights.

### 5.1.2 The Modified LMS Algorithm

Another variation of the LMS algorithm has been developed by Griffiths[43] and uses a mixed strategy of instantaneous and average quantities in the gradient calculation. The gradient of the mean square error is given by

$$\nabla J_{mse} = R_x w - r_{x\xi} \qquad 5\text{-}5$$

and Griffiths suggests that if we have estimates for the desired signals direction-of-arrival and spectral density then we can calculate $\tilde{r}_{x\xi}$, an estimate for $r_{x\xi}$. He then argues that instantaneous quantities can be used in place of $R_x$ and writes $\nabla J_{mse}$ as

$$\nabla J_{mse} = xx^* w - \tilde{r}_{x\xi} \qquad 5\text{-}6$$

and constructs the algorithm (where $y^* = x^* w$)

$$\frac{dw}{dt} = -\alpha (x y^* - \tilde{r}_{x\xi}), \qquad w(t_o) = w_o \qquad 5\text{-}7$$

It can be shown[43] that for sufficiently small constants $\alpha$ that the average value of the weights computed using this algorithm will converge to the optimal weights.

Chang and Tutuer[21] present an alternative, and perhaps more rigorous derivation of this modified LMS algorithm using a modified stochastic approximation argument. If the performance measure $\hat{J}$ is decomposed into two parts (where $\hat{J}$ is formed using instantaneous quantities)

$$\hat{J}(x, w) = J_1(x, w) + J_2(x, w) \qquad 5\text{-}8$$

They demonstrate that under certain conditions the algorithm

$$\frac{dw}{dt} = -\alpha(k) \left[ \nabla J_1 + \nabla \overline{J_2} \right], \qquad w(t_o) = w_o \qquad 5\text{-}9$$

(where overbar denotes averaging), converges both in probability and mean square.

To illustrate the use of this idea, again consider the performance measure of error squared in the form

$$J_{es}(x, w) = \tfrac{1}{2} \left| \langle w, x \rangle - \xi \right|^2 \qquad 5\text{-}10$$

Since the received signals $x$ are noisy, one would generally consider the minimization of the mean squared error, however, a stochastic approximation type algorithm is simpler to implement. Expanding this expression gives

$$J_{es} = \tfrac{1}{2} < w, xx^*w > + ( \tfrac{1}{2} | \xi |^2 - \mathrm{Re} < w, \xi^* x > ) \qquad 5\text{-}11$$

where this can be decomposed into $J_1$ and $J_2$ as follows

$$J_{es} = J_1 + J_2 = \tfrac{1}{2} < w, xx^*w > + ( \tfrac{1}{2} | \xi |^2 - \mathrm{Re} < w, \xi^* x > ) \qquad 5\text{-}12$$

The required gradients for the modified algorithm become

$$\nabla J_1 = xx^*w = x\gamma^* \qquad 5\text{-}13$$

where $\gamma = x^*w = < x, w >$ is the complex conjugate of the array output and

$$\nabla J_2 = - \overline{\xi^* x} = - r_{x\xi} \qquad 5\text{-}14$$

where $r_{x\xi}$ is the signal correlation across the array. The algorithm then takes the form

$$\frac{dw}{dt} = - \alpha (k) [ x\gamma^* - \tilde{r}_{x\xi} ], \qquad w (t_o) = w_o \qquad 5\text{-}15$$

where $\tilde{r}_{x\xi}$ is an estimate for $r_{x\xi}$. This algorithm is implemented as shown in Figure 5-3 where only estimates for the signal correlation (or spectral density) function and direction-of-arrival need to be known, a reasonable assumption in many practical problems.

## 5.2 Signal-to-Noise Ratio Algorithms

### 5.2.1 Applebaum's S/N Algorithm

Applebaum[5] presents an algorithm which is an extension of his side lobe canceller work and is designed to maximize the signal-to-noise ratio at the output of an adaptive array. He does not explicitly utilize steepest descent, but develops his control loop using side lobe canceller circuitry (to solve the set of algebraic equations for the optimum weights), which leads to an essentially similar design. Also, he considers that the desired signal components in the array signals are negligible compared to the

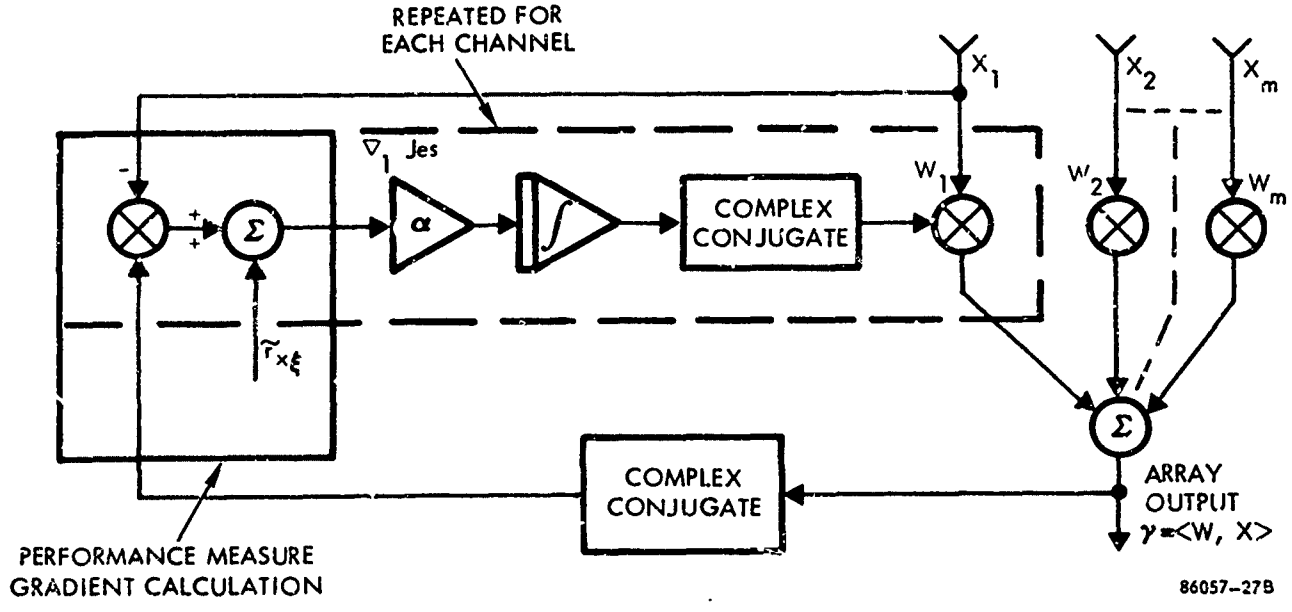


Figure 5-3. The Modified LMS Algorithm

noise terms (the side lobe canceller argument), but this assumption is unnecessary. To implement his algorithm, he assumes a low-pass filter (with time constant $\tau$) and a high gain amplifier (with gain G), are connected as shown in Figure 5-4. Before the amplifier he adds the signal $\tilde{r}_{x_\xi}$, which corresponds to the signal cross-correlation, but he also considers the use of other quantities here to give particular antenna patterns in the absence of directional noise. For this circuit, the $k^{th}$ weight is given by

$$w_k = \left[ - \overline{x_k \langle x, w \rangle} + \tilde{r}_{x_\xi} \right] G \qquad 5\text{-}16$$

where overbar indicates averaging in the low-pass filter. Assuming the loop bandwidth is small compared to the bandwidth of the complex envelope signal, this leads to the vector equation (i.e. w varies relatively slowly)

$$\begin{aligned} w &= \left[ - \overline{xx^* w} + \tilde{r}_{x_\xi} \right] G \\ &\approx - G R_x w + G \tilde{r}_{x_\xi} \end{aligned} \qquad 5\text{-}17$$

or

$$\left[ R_x + \frac{1}{G} \right] w = \tilde{r}_{x_\xi} \qquad 5\text{-}18$$

Notice, that if G is large, then this reduces to the Wiener-Hopf Equation [Equation 3-26], which gives the minimum mean square error weights. In Applebaum's analysis, he assumes $x \approx n$ (noise only) and his equation takes the form

$$\left[ R_n + \frac{1}{G} \right] w = \tilde{r}_{x_\xi} \qquad 5\text{-}19$$

however, as shown in Chapter 3.0, Equation 5-18 also gives the optimal signal-to-noise ratio, that is, one need not make the assumption $x \approx n$.

The dynamics of this control circuitry is given by the differential equation (5)

$$\frac{dw}{dt} + \frac{1}{\tau} \left[ G R_x + I \right] w = \frac{G}{\tau} \tilde{r}_{x_\xi}, \qquad w(t_o) = w_o \qquad 5\text{-}20$$

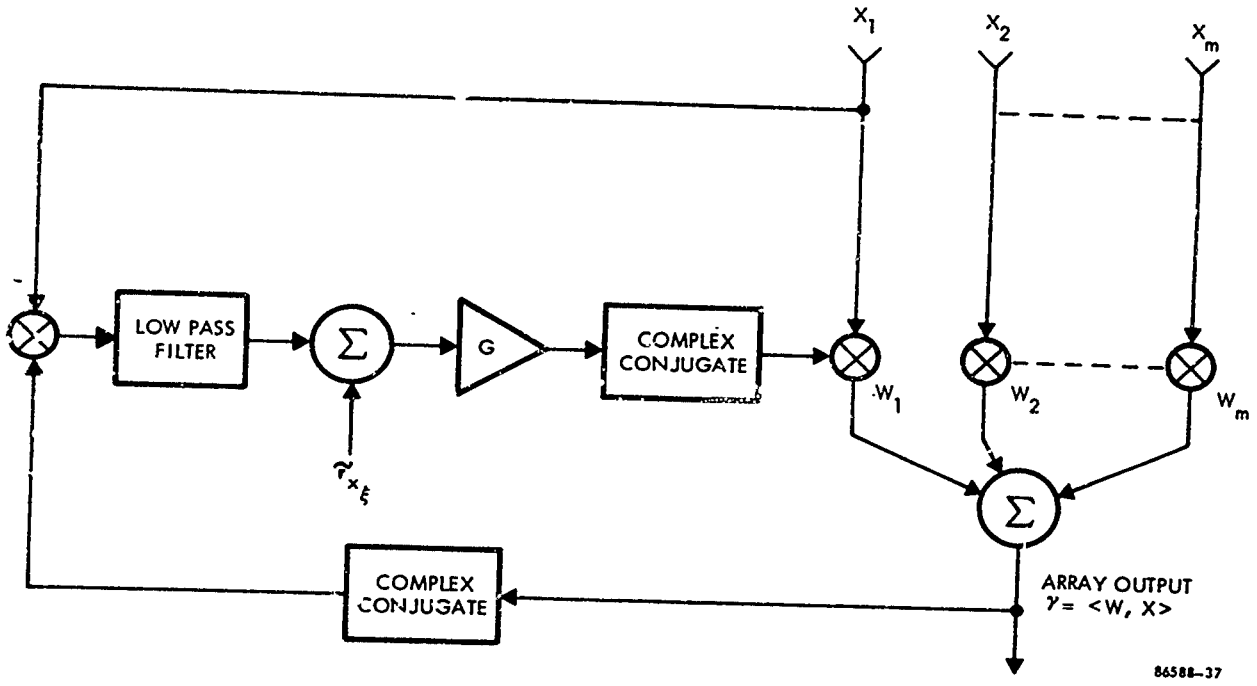


Figure 5-4. Applebaum's $\overline{S/N}$ Algorithm

Assuming $1 \ll GR_x$ this becomes

$$\frac{dw}{dt} + \frac{G}{\tau} R_x w = \frac{G}{\tau} r_{x\xi}, \qquad w(t_o) = w_o \qquad 5\text{-}21$$

which has the desired steady state solution $\left(\frac{dw}{dt} = 0\right)$

$$w = R_x^{-1} r_{x\xi} \qquad 5\text{-}22$$

This differential equation is essentially the same as that suggested by Griffiths and Chang and Tutuer. If we consider the average value of the weights in their equation (Equation 5-15), then we will obtain this same equation (see Section 5.5). Notice then, that subtracting the signal correlation after a low-pass filter gives the same form as subtracting it before an assumed perfect integrator. That is, Figures 5-3 and 5-4 lead to the same general form for the loop differential equation.

### 5.2.2 Other S/N Algorithms

Several other investigators have proposed algorithms designed to maximize signal-to-noise ratio. Shor[67] presents a standard steepest descent formulation, where he proposes to measure the required gradients using correlation techniques. However, these measurements require the separation of signal and noise. His method of doing this is to insert a strong pilot signal in the direction of the desired signal to measure signal correlation, and to measure noise correlations when there is no target (a sonar problem) present. This is similar to Widrow's two-mode procedure, and as such does not offer a practical solution in a communications context.

Adams [1] has also developed a S/N algorithm, where he suggests a more practically oriented procedure. He measures the gradient of the S/N ratio by calculating S/N at incremental values of the weights, which is found using a S/N ratio detector, illustrated with his control loop in Figure 5-5. Unfortunately, this procedure is limited since the S/N detector is designed only for use where a wideband signal is operating against a narrow band signal.

## 5.3 Maximum Likelihood Algorithms

The maximum likelihood type algorithms which have been suggested have not led to the practical circuitry which would be necessary for the problem being addressed by this study. Griffiths[41] suggests such an algorithm, but it requires the injection of a pilot signal, and as such, offers no more than the two pilot signal type solutions suggested by Widrow and Shor, and is more complicated to construct.

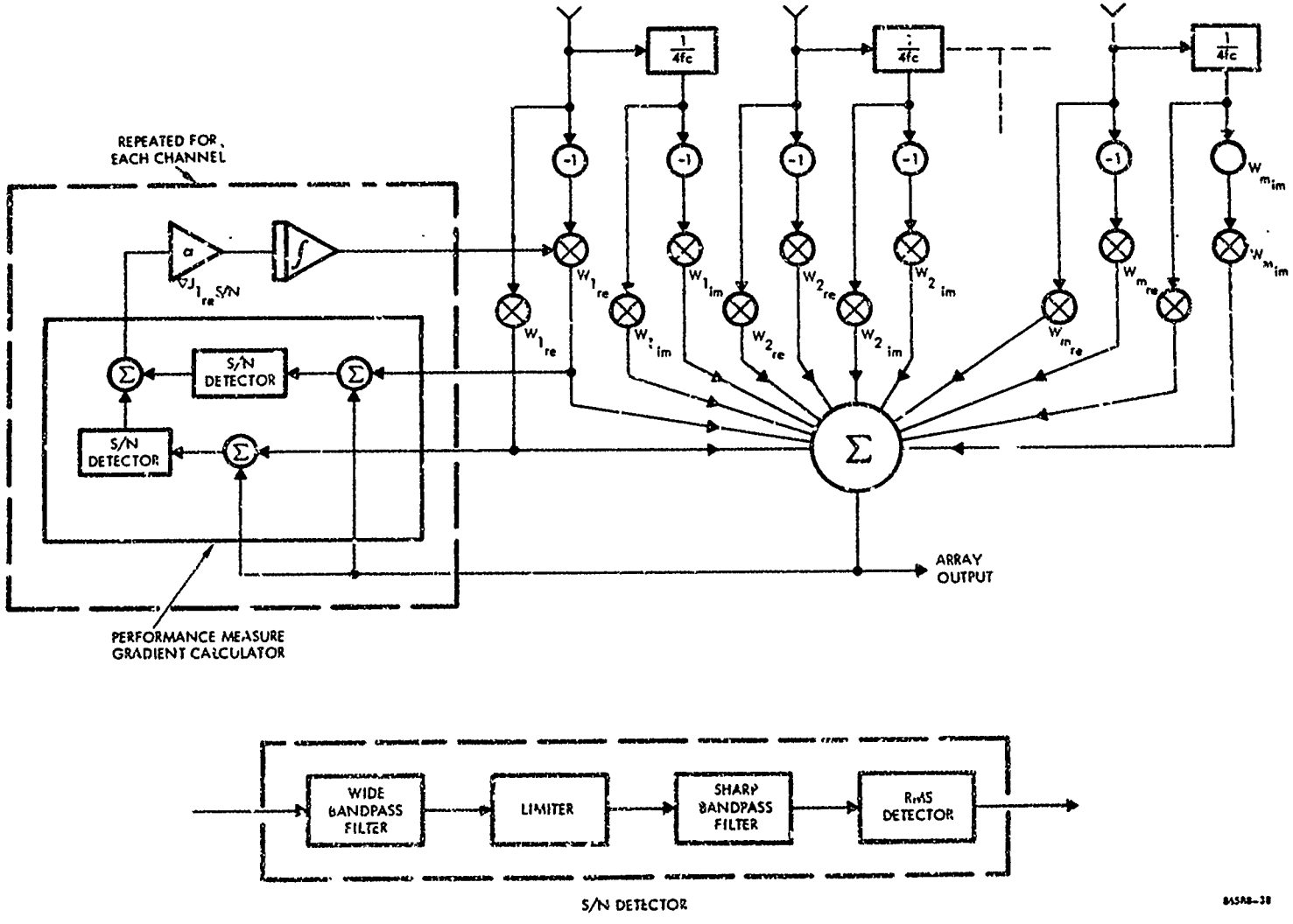


Figure 5-5. Adams' S/N Algorithm

## 5.4 The Minimum Noise Variance Algorithm

One final algorithm, which is based on the minimum noise variance performance measure, is seen to lead to an interesting adaptive array processor. This algorithm, suggested by Lacoss[52], is based on the projection gradient method discussed previously and takes the general form

$$\frac{dw}{dt} = -\alpha P \nabla J_{mv}, \quad w(t_o) = w_o \qquad 5\text{-}23$$

where the gradient of the noise variance is $\frac{\partial J_{mv}}{\partial w} = R_n w$ and the algorithm becomes

$$\frac{dw}{dt} = -\alpha P R_n w, \qquad w(t_o) = w_o \qquad 5\text{-}24$$

The projection operator $P$ is designed to give the projection of the gradient onto the constraint set $\langle w, \underline{1} \rangle = 1$ and is derived below. It should be noted that the average performance measure is used here, which requires an additional integration in the final implementation, but can be eliminated using stochastic approximation ideas under appropriate bandwidth assumptions. Also, the difficulty of obtaining $R_n$ in the presence of signal is shown to be avoided by a unique property of the projection operator.

### 5.4.1 Derivation of the Projection Operator

To derive the projection operator it is noted that the constraint set $\langle w, \underline{1} \rangle = 0$ defines an m-1 dimensional hyperplane in the m dimensional complex space of the array weights. Any vector in this space can be decomposed into a component in a one-dimensional space $W_1$ spanned by the vector $\underline{1} + j\,\underline{0}$ and a component in the m-1 dimensional space $W_2$ formed by all the vectors which are orthogonal to this vector. That is

$$W_1 = \{ x \mid x = \alpha \underline{1} \} \qquad 5\text{-}24$$

$$W_2 = \{ x \mid \langle x, \underline{1} \rangle = 0 \} . \qquad 5\text{-}25$$

We can write any vector $w$ as $w = w^2 + \alpha \underline{1}$ and we have

$$\langle w, \underline{1} \rangle = \langle w^2 + \alpha \underline{1}, \underline{1} \rangle = 0 + \alpha \langle \underline{1}, \underline{1} \rangle \qquad 5\text{-}26$$

which gives

$$\alpha = \frac{\langle w, \underline{1} \rangle}{\langle \underline{1}, \underline{1} \rangle} = \frac{\langle w, \underline{1} \rangle}{m} \qquad 5\text{-}27$$

The projection operator $P_1$, that gives the orthogonal projection of any vector $w$ onto $W_1$ gives

$$P_1 w = P_1 \left( w^2 + \alpha \underline{1} \right) = \alpha \underline{1} = \frac{\langle w, \underline{1} \rangle}{m} \underline{1} \qquad 5\text{-}28$$

and in Euclidian space we can write,

$$P_1 w = \frac{\langle w, \underline{1} \rangle}{m} \underline{1} = \frac{\underline{1}\,\underline{1}^T}{m} w \; . \qquad 5\text{-}29$$

The orthogonal projection $P$ onto $W_2$ is equivalent to the projection on the hyperplane defined by $\langle w, \underline{1} \rangle = 1$, since it is merely a translate of $W_2$. This projection can then be written as

$$P w = (I - P_1) w = \left( I - \frac{\underline{1}\,\underline{1}^T}{m} \right) w \qquad 5\text{-}30$$

and the required projection operator is

$$P = I - \frac{\underline{1}\,\underline{1}^T}{m} \; . \qquad 5\text{-}31$$

### 5.4.2 The Use of Signal Corrupted Correlations

The algorithm as stated in Equation 5-24 is seen to require the noise correlation matrix $R_n$ which must be calculated from measured data. This data will generally contain both signal and noise terms, however, if the inputs $x$ do not contain signal terms, $R_n$ can be approximated by

$$\bar{R}_n = \bar{R}_x \approx \frac{1}{T} \int_0^T x(s)\, x^*(s)\, ds \qquad 5\text{-}32$$

for T sufficiently large. In this case, it can be shown that the projection operator allows the use of signal contaminated $x$'s. In general

$$R_x = R_n + R_s \qquad 5\text{-}33$$

and for the signal aligned array (See Equation 2-50)

$$R_s = S\,\underline{1}\,\underline{1}^T \qquad 5\text{-}34$$

The expected value of the approximation based on the finite time average in Equation 5-32 will be

$$E\,[\bar{R}_x] = R_x = R_n + S\,\underline{1}\,\underline{1}^T \qquad 5\text{-}35$$

If the projection operator is used

$$E\,[P\bar{R}_x] = PR_x = PR_n + SP\,\underline{1}\,\underline{1}^T \qquad 5\text{-}36$$

where

$$P\,[\underline{1}\,\underline{1}^T] = [I - \frac{\underline{1}\,\underline{1}^T}{m}]\,\underline{1}\,\underline{1}^T \qquad 5\text{-}37$$

$$= \underline{1}\,\underline{1}^T - \frac{m\,\underline{1}\,\underline{1}^T}{m} = 0$$

then

$$E\,[P\bar{R}_x] = PR_x = PR_n \approx P\,[\frac{1}{T}\int_0^T x\,(s)\,x^*\,(s)\,ds] \qquad 5\text{-}38$$

Consequently, we see that on the average the projection operator allows the estimation of $PR_n$ to be made from $P\bar{R}_x$.

### 5.4.3 A Two-Dimensional Example

As derived above, the projection operator required for the implementation of the projection gradient method is seen to be a constant matrix of simple form. Consequently, its use will be seen to lead to little complication of the standard gradient algorithm. To demonstrate this, we can examine the circuitry required for the implementation of a simple two-dimensional example. This is, of course, a trivial case,

but the general form is the same for higher order arrays. In this case, we must choose the complex weights $w_1$ and $w_2$ to minimize

$$J_{mv} = \langle w, R_n \; w \rangle = \frac{1}{2} \; [w_1^*, w_2^*] \; R_n \begin{bmatrix} w_1 \\ w_2 \end{bmatrix} \qquad 5\text{-}39$$

subject to $w_1 + w_2 = 1$. The projection operator as derived above becomes

$$P = I - \frac{\begin{bmatrix} 1 & 1 \\ 1 & 1 \end{bmatrix}}{2} = \begin{bmatrix} \frac{1}{2} & -\frac{1}{2} \\ -\frac{1}{2} & \frac{1}{2} \end{bmatrix} \qquad 5\text{-}40$$

Using the results of Section 5.4.2 the algorithm of Equation 5-24 can be written for this example as

$$\frac{dw}{dt} = -\alpha P R_n w \approx -\frac{\alpha}{T} P \int_0^T x(s) x^*(s) ds \, w(t),$$
$$w(t_o) = w_o \qquad 5\text{-}41$$

Assuming that $w$ varies slowly compared to the complex envelopes $x$, and noting that $x^*(s) w = \gamma^*(s)$ this becomes

$$\frac{dw}{dt} = \frac{-\alpha}{T} P \int_0^T x(s) \gamma^*(s) ds, \qquad w(t_o) = w_o \qquad 5\text{-}42$$

For the two-dimensional example this becomes

$$\frac{dw}{dt} = \frac{-\alpha}{T} \begin{bmatrix} \frac{1}{2} & -\frac{1}{2} \\ -\frac{1}{2} & \frac{1}{2} \end{bmatrix} \int_0^T x(s) \gamma^*(s) ds, \qquad w(t_o) = w_o \qquad 5\text{-}43$$

or

$$\frac{dw_1}{dt} = -\frac{\alpha}{T} \int_0^T \frac{x_1(s) - x_2(s)}{2} \gamma^*(s) ds, \qquad w_1(t_o) = w_{1o} \qquad 5\text{-}44$$

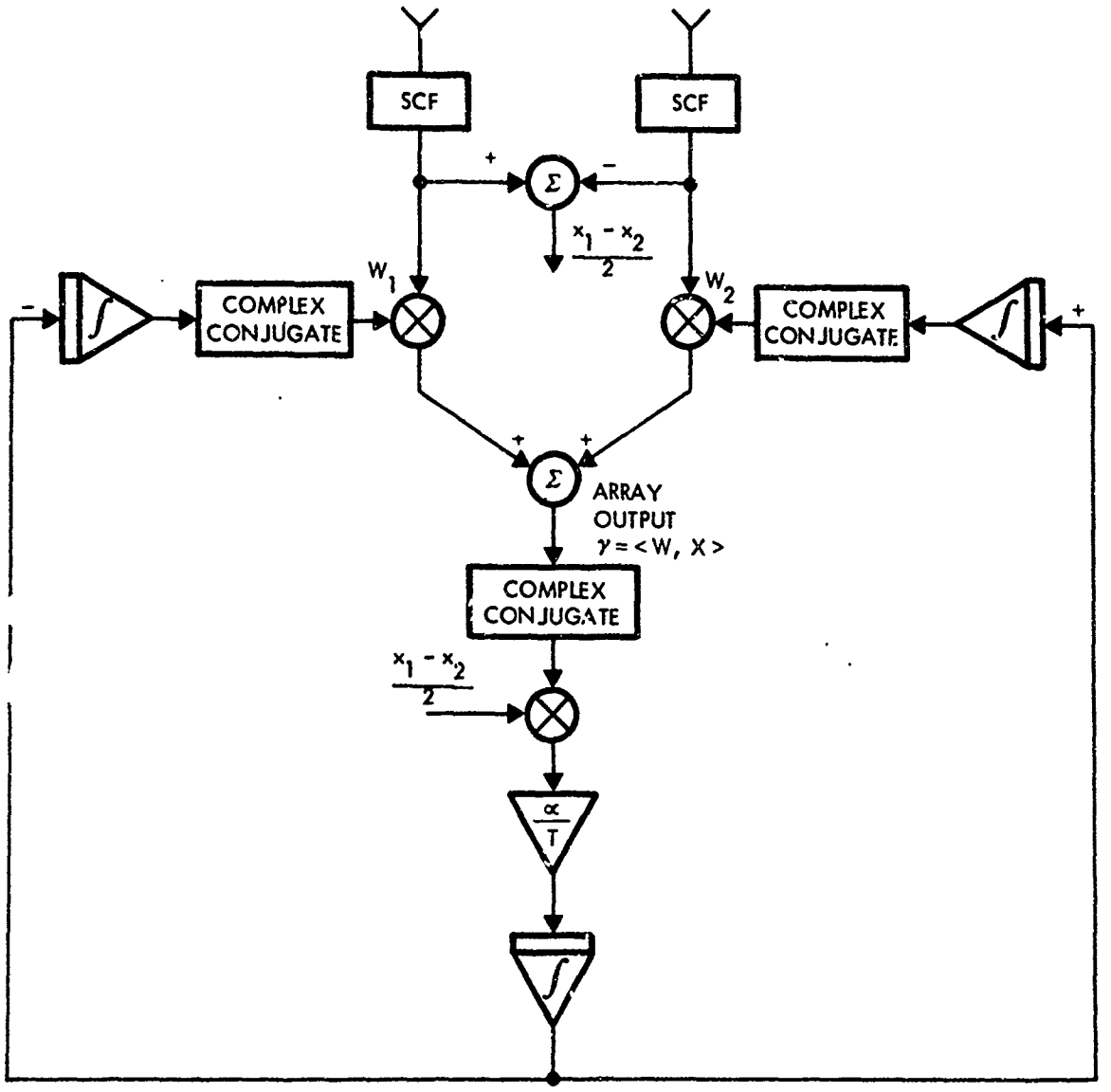


Figure 5-6. Projection Gradient Algorithm Implementation - Two-Dimensional Example

and

$$\frac{dw_2}{dt} = + \frac{\alpha}{T}\int_0^T \frac{x_1(s)-x_2(s)}{2}\,\gamma^*(s)\,ds, \quad w_2(t_o) = w_{2o} \qquad 5\text{-}45$$

which can be implemented using the circuitry illustrated in Figure 5-6.

### 5.4.4 The General Projection Gradient Algorithm

The simple two-dimensional example clearly indicates that the use of the projection operator leads to easily implemented circuitry. To compare this method to the others presented in this chapter we must place it in similar form. Using the stochastic approximation arguments the use of the averaged noise variance can be replaced by instantaneous quantities which will eliminate one of the integrators in the algorithm implementation. For the general m-dimensional problem the algorithm then becomes

$$\begin{aligned}\frac{dw}{dt} &= -\alpha P\, x(t)\, x^*(t)\, w \\ &= -\alpha\left[I - \frac{\underline{1}\,\underline{1}^T}{m}\right] x(t)\,\gamma^*(t) \\ &= -\alpha\left[x(t) - \frac{1}{m}\sum_{i=1}^{m} x_i(t)\,\underline{1}\right]\gamma^*(t), \qquad w(t_o) = w_o \qquad 5\text{-}46\end{aligned}$$

For the first complex weight in the array we write

$$\frac{dw_1}{dt} = -\alpha\left[x_1(t) - \frac{1}{m}\sum_{i=1}^{m} x_i(t)\right]\gamma^*(t),$$

$$w_1(t_o) = w_{1o} \qquad 5\text{-}47$$

which is illustrated in Figure 5-7. In this form the term $\frac{1}{m}\sum_{i=1}^{m} x_i(t)$ can be interpreted as an estimate $\tilde{\xi}$ for the desired signal. This gives

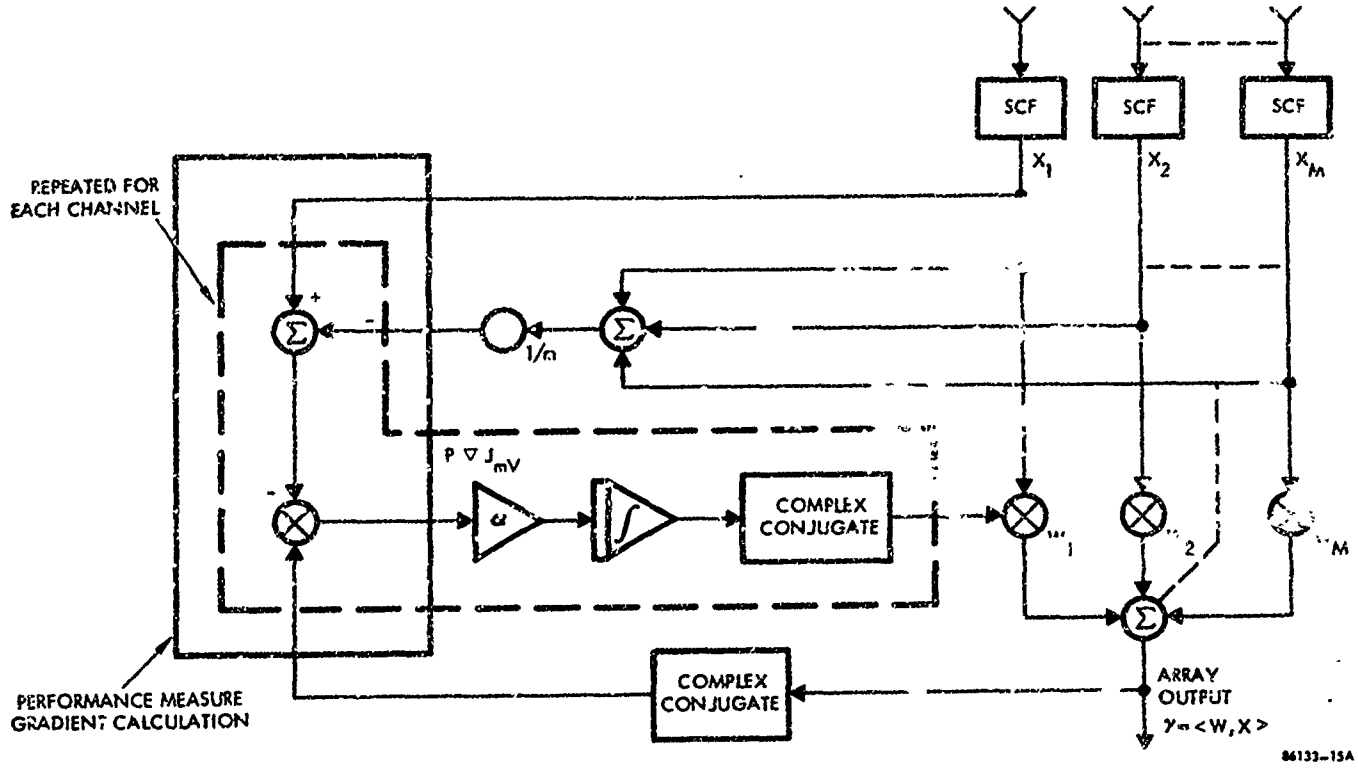


Figure 5-7. General Projection Gradient Algorithm

$$\tilde{\xi} = \frac{1}{m} \sum_{i=1}^{m} x_i(t) = \frac{1}{m} \sum_{i=1}^{m} [\xi_i(t) + n_i(t)]$$

$$= \xi(t) + \frac{n_1(t) + n_2(t) + \ldots + n_m(t)}{m} \qquad 5\text{-}48$$

where the $\xi_i(t)$ are all identical and add coherently since the array is pointed at the desired signal, and the directional noise terms enter through the side lobes.

## 5.5 Comparison of the Basic Adaptive Algorithms

### 5.5.1 The Removal of Signal Effects

Most of the algorithms presented in this chapter have been developed as applications of steepest descent-stochastic approximation principles. However, as indicated in the descriptions of the fundamental behavior of side lobe cancellers and general adaptive arrays in Chapter One, an alternative interpretation in terms of correlation methods can also be used to describe their behavior. Examination of the more promising processors presented here indicates that they are all basically performing a correlation of the array inputs with the array output and driving the weights from this correlator. That is, they are attempting to eliminate the noise terms in the array output by correlating it with the array inputs and driving the appropriate weights. This procedure is valid if the noises are not correlated with the desired signal (generally a valid assumption) and if the signal correlations can be removed so that they do not affect the weights. The basic difference between most of the algorithms presented here can be interpreted in terms of how they remove these signal effects.

Widrow's basic Signal Know Type LMS algorithm presented in Figure 5-1 avoids the signal correlation terms by subtracting (or perhaps blocking) the desired signal using a priori knowledge about the signal structure. Consequently, the output of the multiplier (correlator) will not contain terms due to the signal, and the integrator is driven by noise correlation terms until the weights are set such that these terms are zero. That is, the noise terms are removed from the array output. For the modified LMS algorithm, a DOA Known method, shown in Figure 5-2, the signal effects are seen to be removed after the correlation has taken place. The cross correlation between the desired signal and the received signals are computed from the signal's DOA (and spectrum if relatively wideband) and are removed by subtraction. Applebaum's processor also removes the desired signal effects after the correlator (See Figure 5-3) with somewhat different circuitry, but the procedure leads to an essentially identical

algorithm, as is evident from comparing the differential equations associated with the two approaches. Finally, the projection gradient algorithm (Figure 5-7) is also a DOA known type method, where DOA information is used to align the desired signal terms, from which an approximation for the desired signal is found (Equation 5-48) and subtracted from the received signal. Thus, the desired signal effects can be removed at any of three different points in the processor (as illustrated in Figure 5-8):

1. At the array output (basic LMS algorithm).

2. After the correlation (both the modified LMS algorithm and Applebaum's S/N algorithm).

3. At the array inputs (projection gradient algorithm).

This interpretation of the adaptive array, in terms of a correlation device, indicates that the various algorithms are indeed quite similar. Thus, not only do they lead to the same S/N ratios at their outputs, as mentioned in Chapter Three, but they are all performing basically the same correlation operation. This similarity will be even more apparent in the next section where the differential equations associated with the above processors are examined.

### 5.5.2 Basic Processor Differential Equations

An examination of the differential equations associated with the processors discussed in the last section also indicates the similarity of these algorithms. For the basic LMS algorithm the equation was given in Equation 5-4 as

$$\frac{dw}{dt} = -\alpha\, \epsilon^* x = -\alpha (x x^* w - \tilde{\xi}^* x) \qquad 5\text{-}49$$

Generally, these control loops are designed (i.e., $\alpha$ is chosen) so that the weights vary slowly compared to the complex envelopes of the signals. In that case, the expected value of the weights are governed by the equation

$$\frac{d\overline{w}}{dt} = -\alpha \left[ \overline{x x^*}\, \overline{w} - \overline{\tilde{\xi}^* x} \right] \qquad 5\text{-}50$$

or

$$\frac{d\overline{w}}{dt} + \alpha R_x \overline{w} = \alpha \tilde{r}_{x\xi} \qquad 5\text{-}51$$

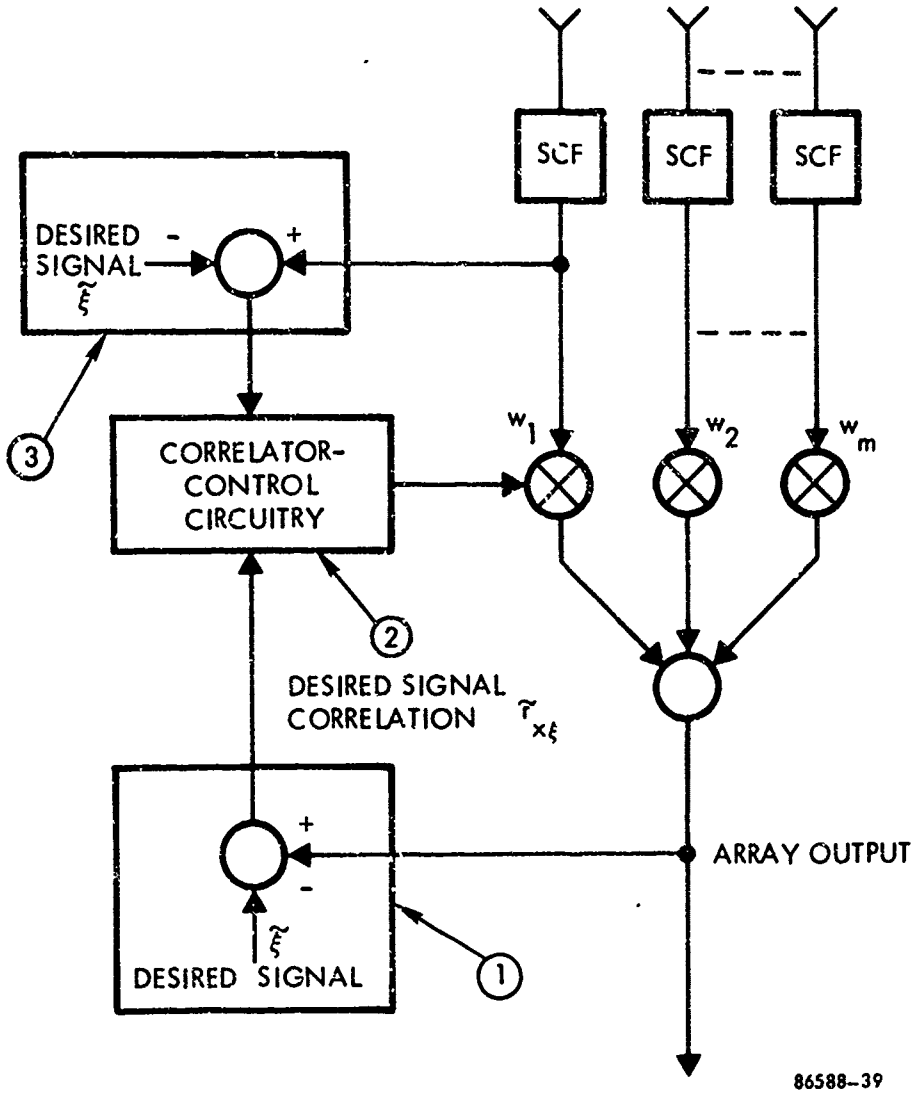


Figure 5-8. Desired Signal Effect Removal

For the modified LMS algorithm of Equation 5-15 the equction is

$$\frac{dw}{dt} = -\alpha(xx^*w - \tilde{r}_{x\xi}) \qquad 5\text{-}52$$

and the expected value equation again becomes

$$\frac{d\overline{w}}{dt} + \alpha R_x \overline{w} = \alpha \tilde{r}_{x\xi} \qquad 5\text{-}53$$

Notice that this is the same form as Applebaum's control law of Equation 5-21 where

$$\alpha \sim \frac{G}{\tau}. \qquad 5\text{-}54$$

The differential equation for the generalized projection gradient algorithm was given in Equation 5-46 as

$$\frac{dw}{dt} = -\alpha\left[x(t) - \frac{1}{m}\sum_{i=1}^{m} x_i(t)\underline{1}\right]\gamma^*(t) \qquad 5\text{-}55$$

$$= -\alpha\left[x(t) - \tilde{\xi}(t)\underline{1}\right]\gamma^*(t)$$

Since $\gamma^*(t) = x^*(t)w$ this becomes

$$\frac{dw}{dt} = -\alpha xx^*w + \alpha\tilde{\xi}(t)\underline{1}x^*w$$

$$= -\alpha xx^*w + \alpha\tilde{\xi}(t)\begin{bmatrix} w^T \\ w^T \\ \vdots \\ w^T \end{bmatrix}(\xi^*\underline{1} + \underline{n}^*) \qquad 5\text{-}56$$

Using the fact that the weights are constrained such that $w^T\underline{1} = 1$ this becomes

$$\frac{dw}{dt} = -\alpha xx^*w + \alpha\left[\tilde{\xi}\xi^*\underline{1} + \tilde{\xi}w^T n^*\underline{1}\right] \qquad 5\text{-}57$$

Since the desired signal is uncorrelated with the noise, the expected value of the weights is governed by the equation

$$\frac{d\overline{w}}{dt} = -\alpha R_x \overline{w} + \alpha \tilde{S} \underline{1} \qquad 5\text{-}58$$

where $\tilde{S} \underline{1}$ is the form for the desired signal cross correlation for the signal aligned array. Thus, the differential equation again takes the form

$$\frac{d\overline{w}}{dt} + \alpha R_x \overline{w} = \alpha \tilde{r}_{x_\xi} . \qquad 5\text{-}59$$

where $\tilde{r}_{x_\xi} = \tilde{S} \underline{1}$ .

For all of these procedures, the differential equation is seen to take the same general form, indicating that not only are the steady state solutions identical (with respect to output signal-to-noise ratio for relatively narrow band problems), but the transient behavior is also the same. It is important to realize that the algorithms presented here do not represent practical solutions, but merely define the basic form (the differential equation, Equation 5-59) of the processor. To implement them effectively, good estimates $\tilde{\xi}$ for the desired signal or its direction-of-arrival must be obtained. This problem is dealt with in Chapter Seven, while the behavior of the basic array (described by the differential equation - Equation 5-59) is discussed in the next chapter.

# CHAPTER 6

# BEHAVIOR OF ADAPTIVE ARRAYS USING THE LMS ALGORITHM

## 6.0 BEHAVIOR OF ADAPTIVE ARRAYS USING THE LMS ALGORITHM

In this chapter we focus attention on the time behavior of an adaptive array using the LMS algorithm and determine the transient as well as steady state response using spectral techniques. The steady state results will then be used in evaluating the array performance described by the output signal to noise power and gain.

### 6.1 Solution of Basic Differential Equations

#### 6.1.1 Transient Behavior

Recall from Equation (4-31) that the differential equation which describes the trajectory of the m dimensional complex weight vector through the m+1 dimensional weight-time space is given by

$$\frac{dw}{dt} + \alpha R_x w = \alpha r_{x\xi} ; \qquad w(o) = w_o , \tag{6-1}$$

where $R_x$ represents the correlation matrix of the vector valued input x and is assumed to be positive definite, whereas $r_{x\xi}$ represents the m dimensional correlation vector between the desired signal $\xi(t)$ and x.

The approach we shall use in solving this differential equation is to utilize finite-dimensional spectral theory so that the vector w can be expressed in terms of the eigenvalues and eigenvectors and/or projection operators associated with the positive definite matrix $R_x$. This technique, although perhaps not well known among practicing engineers, is very powerful and for our problems easily yields results for narrowband environments with arbitrary array geometries. Let H denote the m-dimensional complex Euclidean space on which the matrix $R_x$ is defined, and let $\lambda_1, \ldots \lambda_\ell$ denote the distinct eigenvalues of $R_x$ with corresponding eigenspaces $Q_1, \ldots, Q_\ell$. If $E_p$ represents the orthogonal projection from H onto $Q_p$, then we can write $R_x$ as[44]

$$R_x = \sum_{p=1}^{\ell} \lambda_p E_p , \tag{6-2}$$

where the projection operators have the properties:

$$E_i E_j = 0 \qquad i \neq j \tag{6-3}$$

$$E_i E_j = E_i \qquad i = j \tag{6-4}$$

and

$$\sum_{p=1}^{\ell} E_p = I. \tag{6-5}$$

With this representation in hand, consider now the equation describing the unforced response of the antenna system, namely:

$$\frac{dw}{dt} + \alpha R_x w = 0 ; \qquad w(o) = w_o . \tag{6-6}$$

It is well known that the solution of this differential equation can be written as

$$w(t) = e^{-\alpha R_x t} w_o \tag{6-7}$$

where the expression $e^{-\alpha R_x t}$ is defined as

$$e^{-\alpha R_x t} = I - \alpha R_x t + (\alpha R_x)^2 \frac{t^2}{2!} - \ldots + (-1)^n (\alpha R_x)^n \frac{t^n}{n!} + \ldots \tag{6-8}$$

Substituting Equation (6-2) into Equation (6-8) and using Equations (6-3), (6-4), and (6-5), we write $e^{-\alpha R_x t}$ in terms of the eigenvalues and projection operators, namely:

$$e^{-\alpha R_x t} = \sum_{p=1}^{\ell} e^{-\alpha \lambda_p t} E_p . \tag{6-9}$$

Thus the unforced response can be written as

$$w(t) = \sum_{p=1}^{\ell} e^{-\alpha \lambda_p t} E_p w_o . \tag{6-10}$$

It is evident that the unforced response is well behaved; in fact the origin is asymptotically stable since

$$\|w(t)\| \leq \sum_{p=1}^{\ell} e^{-\alpha \lambda_p t} \|E_p w_o\| \longrightarrow 0 \text{ as } t \longrightarrow \infty$$

where we have used the fact that all the eigenvalues are greater than zero.

Focusing now on the forced response we first multiply Equation (6-1) by $e^{-\alpha R_x t}$ and integrate, obtaining

$$w(t) = \alpha \int_0^t e^{-\alpha R_x (t-\tau)} r_{x\xi} \, d\tau = \alpha \int_0^t \sum_{p=1}^{\ell} e^{-\alpha \lambda_p (t-\tau)} E_p r_{x\xi} \, d\tau .$$

Since the vector $r_{x_\xi}$ is time invariant and since $\ell$ is finite, we can write

$$w(t) = \alpha \sum_{p=1}^{\ell} \left( \int_0^t e^{-\alpha \lambda_p (t-\lambda)} d\lambda \right) E_p r_{x\xi} \tag{6-11}$$

which becomes

$$w(t) = \sum_{p=1}^{\ell} \frac{1}{\lambda_p} \left(1 - e^{-\alpha \lambda_p t}\right) E_p r_{x\xi} \; . \tag{6-12}$$

Thus the complete time response of the weight trajectory is obtained by adding Equation (6-10) to Equation (6-12)

$$w(t) = \sum_{p=1}^{\ell} e^{-\alpha \lambda_p t} E_p w_o + \sum_{p=1}^{\ell} \frac{1}{\lambda_p} \left(1 - e^{-\alpha \lambda_p t}\right) E_p r_{x\xi} \; . \tag{6-13}$$

As $t \to \infty$, the weight vector approaches the optimum value

$$w = R_x^{-1} r_{x\xi}$$

which in terms of this development is clearly

$$w = R_x^{-1} r_{x\xi} = \sum_{p=1}^{\ell} \frac{1}{\lambda_p} E_p r_{x\xi} . \tag{6-14}$$

To demonstrate the utility of this development we consider the following two examples:

<u>Example 1:</u>

Consider a narrowband environment consisting of one emitter, the desired emitter, and an arbitrary m element adaptive sensor system with narrowband

white noise in each sensor channel which is uncorrelated from one sensor to the next with equal variance $\sigma^2$ in each channel. With reference to the nomenclature developed in Chapter 2, the covariance matrix becomes

$$R_x = \sigma^2 I + S\, v_1 v_1^* \tag{6-15}$$

with

$$r_{x\xi} = S v_1 \quad .$$

To determine the eigenvectors and eigenvalues corresponding to this matrix we proceed as follows. Consider the vector

$$c_1 = \alpha v_1 \quad . \tag{6-16}$$

This vector is clearly an eigenvector since

$$R_x \alpha v_1 = (\sigma^2 I + S v_1 v_1^*)(\alpha v_1) = \alpha(\sigma^2 + Sm) v_1 \tag{6-17}$$

where we have recognized that $v_1^* v_1 = m$. Thus $c_1$ is an eigenvector with $\sigma^2 + Sm$ as its associated eigenvalue. The eigenspace $Q_1$ is the linear space spanned by $c_1$. Consider, now any other eigenvector $c_p$ belonging to the arbitrary eigenspace $Q_p$. Since $c_p$ is orthogonal to $c_1$ it is also orthogonal to $v_1$; hence,

$$R_x c_p = (\sigma^2 I + S\, v_1 v_1^*)\, c_p = \sigma^2 c_p . \tag{6-18}$$

Thus, the eigenvalue corresponding to the remaining m-1 eigenvectors is $\sigma^2$. Therefore, there are only two eigenspaces for this example, the first being $Q_1$, and the second being that linear space spanned by the m-1 eigenvectors corresponding to the eigenvalue $\sigma^2$. The array response can then be written as

$$w(t) = e^{-\alpha\lambda_1 t} E_1 w_o + e^{-\alpha\lambda_2 t} (I - E_1) w_o + \frac{1}{\lambda_1}(1 - e^{-\alpha\lambda_1 t}) E_1 S v_1$$

$$+ \frac{1}{\lambda_2}(1 - e^{-\alpha\lambda_2 t})(I - E_1) S v_1 \tag{6-19}$$

where

$$\lambda_1 = \sigma^2 + Sm \tag{6-20}$$

$$\lambda_2 = \sigma^2 . \tag{6-21}$$

Since $E_1 v_1 = v_1$ we can write Equation (6-19) as

$$w(t) = e^{-\alpha\sigma^2 t} \left[ (e^{-\alpha Smt} - 1) E_1 w_o + w_o \right]$$

$$+ \frac{S}{Sm+\sigma^2} \left[ 1 - e^{-\alpha(\sigma^2 + Sm)t} \right] v_1 \tag{6-22}$$

Thus it is evident that the larger the signal power the more quickly the weights converge to their steady state value which is given by

$$w = \frac{S/\sigma^2}{1 + mS/\sigma^2} \; v_1 \tag{6-23}$$

The corresponding steady state output signal power and noise power are seen to be given by

$$P_S = E\left| < w, s(t) > \right|^2 = < w, R_S w > = S\left| < w, v_1 > \right|^2 \tag{6-24}$$

$$= S \left( \frac{mS/\sigma^2}{1+mS/\sigma^2} \right)^2 \tag{6-25}$$

and

$$P_{n_t} = E\left| < w, n(t) > \right|^2 = < w, R_n w > = \sigma^2 \left|\left| w \right|\right|^2 \tag{6-26}$$

$$= \sigma^2 m \left( \frac{S/\sigma^2}{1+mS/\sigma^2} \right)^2 \tag{6-27}$$

respectively. The output signal to noise power ratio is then easily given by

$$\frac{P_S}{P_{n_t}} = m\left(\frac{S}{\sigma^2}\right) . \tag{6-28}$$

Thus we have established the well known result that the output signal to noise power ratio is equal to the number of antenna elements multiplied by the input signal to noise ratio at one sensor element.

Example 2:

In this example we assume the same signal environment as in Example 1 except that we now include a directional jamming source which is assumed uncorrelated from the signal. Utilizing spectral theory we now develop the weight trajectory governed by Equation (6-1) for an arbitrary antenna array whose elements are symmetrical about the geometric center.

For this environment the correlation matrix becomes

$$R_x = \sigma^2 I + Sv_1v_1^* + Jv_2v_2^* \tag{6-29}$$

where J corresponds to the jamming power at one sensor element. Our first order of business is to establish the eigenvalues and corresponding eigenvectors of $R_x$. Considering the vector

$$c_1 = \alpha_1 v_1 + v_2 \tag{6-30}$$

as a candidate, then from the following equality chain

$$R_x(\alpha_1 v_1 + v_2) = (\sigma^2 I + Sv_1v_1^* + Jv_2v_2^*)(\alpha_1 v_1 + v_2) \tag{6-31}$$

$$= \left[\alpha_1\sigma^2 + \alpha_1 Sm + S\langle v_1, v_2\rangle\right]v_1 + \left[\sigma^2 + Jm + \alpha_1 J\langle v_1, v_2\rangle\right]v_2 \tag{6-32}$$

$$= \lambda(\alpha_1 v_1 + v_2) \tag{6-33}$$

We see by equating the coefficients of $v_1$ and $v_2$ that

$$\lambda = \sigma^2 + Jm + \alpha_1 J < v_1, v_2 > \tag{6-34}$$

$$\alpha_1 \lambda = \alpha_1 \sigma^2 + \alpha_1 Sm + S < v_1, v_2 > \tag{6-35}$$

Substituting Equation (6-35) into (6-34) and solving for $\lambda$ we obtain the quadratic

$$\lambda^2 - \left[2\sigma^2 + m(S+J)\right] \lambda + \sigma^4 + \sigma^2 m(S+J) + SJm^2 \left(1 - \frac{<v_1, v_2>^2}{m^2}\right) = 0 \tag{6-36}$$

whose solutions are given by

$$\lambda_1 = \sigma^2 + \frac{m}{2}(S+J) + \left[\frac{m^2}{4}(S-J)^2 + SJ<v_1, v_2>^2\right]^{\frac{1}{2}} \tag{6-37}$$

and

$$\lambda_2 = \sigma^2 + \frac{m}{2}(S+J) - \left[\frac{m^2}{4}(S-J)^2 + SJ<v_1, v_2>^2\right]^{\frac{1}{2}} \tag{6-38}$$

The eigenvectors corresponding to these eigenvalues are easily determined from Equations (6-34) and (6-30) as

$$c_1 = \left\{ \frac{m(S-J) + \left[m^2(S-J)^2 + 4SJ<v_1, v_2>^2\right]^{\frac{1}{2}}}{2J<v_1, v_2>} \right\} v_1 + v_2 \tag{6-39}$$

$$c_2 = \left\{ \frac{m(S-J) - \left[m^2(S-J)^2 + 4SJ<v_1, v_2>^2\right]^{\frac{1}{2}}}{2J<v_1, v_2>} \right\} v_1 + v_2 \, . \tag{6-40}$$

To solve for the remaining m-2 eigenvectors, we note that any vector which is orthogonal to $c_1$ and $c_2$ is also orthogonal to $v_1$ and $v_2$ (provided the emitters are distinct). If $c_3$ is such a vector then

$$R_x c_3 = (\sigma^2 I + S v_1 v_1^* + J v_2 v_2^*) c_3 = \sigma^2 c_3 \tag{6-41}$$

Hence $c_3$ is an eigenvector with $\sigma^2$ as its eigenvalue. This process can be continued until all the remaining m-3 eigenvectors associated with $\sigma^2$ are found, however, we shall find that explicit knowledge of these vectors is not necessary.

The eigenspaces corresponding to the three distinct eigenvalues for $R_x$ are now seen to be

$$Q_1 = \left\{ \text{one dimensional subspace spanned by } c_1 \right\}$$

$$Q_2 = \left\{ \text{one dimensional subspace spanned by } c_2 \right\}$$

$$Q_3 = \left\{ \text{m-2 dimensional subspace spanned by the eigenvectors associated with } \sigma^2 \right\}.$$

The term $< v_1, v_2 >$ represents the spatial factor of the array. For a linear array with spacing $\rho$, $< v_1, v_2 >$ can be shown to be

$$< v_1, v_2 > = \frac{\sin\left[\frac{m\pi\rho}{\lambda_c}(\cos\theta_1 - \cos\theta_2)\right]}{\sin\left[\frac{\pi\rho}{\lambda_c}(\cos\theta_1 - \cos\theta_2)\right]} \tag{6-42}$$

where $\theta_i$ and $\lambda_c$ represent the angle between the axis of the array and the ith emitter, and the wavelength of the carrier respectively.

Returning now to Equation (6-13) and using the identity

$$I = E_1 + E_2 + E_3 \tag{6-43}$$

we can write

$$\begin{aligned} w(t) = {} & e^{-\alpha\lambda_1 t} E_1 w_o + \frac{1}{\lambda_1}(1 - e^{-\alpha\lambda_1 t}) E_1 S v_1 + e^{-\alpha\lambda_2 t} E_2 w_o \\ & + \frac{1}{\lambda_2}(1 - e^{-\alpha\lambda_2 t}) E_2 S v_1 + e^{-\alpha\sigma^2 t}(I - E_1 - E_2) w_o \\ & + \frac{1}{\sigma^2}(1 - e^{-\alpha\sigma^2 t})(I - E_1 - E_2) S v_1 \end{aligned} \tag{6-44}$$

which we note is only a function of the orthogonal projection operators on $Q_1$ and $Q_2$. Thus explicit knowledge of the eigenvectors belonging to the subspace $Q_3$ is not necessary. To determine the components of $w_o$ in the subspaces $Q_1$ and $Q_2$ we recognize that $w_o$ can be uniquely written as the sum of vectors

$$w_o = \alpha_1 c_1 + \alpha_2 c_2 + c_3 \tag{6-45}$$

where $\alpha_1$ and $\alpha_2$ are scalars yet to determined and $c_3$ is a vector belonging to the subspace $Q_3$. The components in $Q_1$ and $Q_2$ being given by

$$E_1 w_o = \alpha_1 c_1 = \frac{\langle c_1, w_o \rangle}{\|c_1\|^2} c_1 \tag{6-46}$$

$$E_2 w_o = \alpha_2 c_2 = \frac{\langle c_2, w_o \rangle}{\|c_2\|^2} c_2 . \tag{6-47}$$

The components of $v_1$ in each of these subspaces are computed correspondingly and will not be explicitly presented. Substituting these results in Equation (6-44) we finally arrive at

$$\begin{aligned} w(t) = {} & e^{-\alpha\sigma^2 t} w_o + (e^{-\alpha\lambda_1 t} - e^{-\alpha\sigma^2 t}) \frac{\langle c_1, w_o \rangle}{\|c_1\|^2} c_1 \\ & + (e^{-\alpha\lambda_2 t} - e^{-\alpha\sigma^2 t}) \frac{\langle c_2, w_o \rangle}{\|c_2\|^2} c_2 \\ & + S\left[\frac{1}{\lambda_1}(1-e^{-\alpha\lambda_1 t}) - \frac{1}{\sigma^2}(1-e^{-\alpha\sigma^2 t})\right] \frac{\langle c_1, v_1 \rangle}{\|c_1\|^2} c_1 + \\ & S\left[\frac{1}{\lambda_2}(1-e^{-\alpha\lambda_2 t}) - \frac{1}{\sigma^2}(1-e^{-\alpha\sigma^2 t})\right] \frac{\langle c_2, v_1 \rangle}{\|c_2\|^2} c_2 \\ & + \frac{S}{\sigma^2}(1-e^{-\alpha\sigma^2 t}) v_1 \end{aligned} \tag{6-48}$$

We point out that since the weights are dependent on $\sigma^2$, which is normally much smaller than $\lambda_1$ or $\lambda_2$, they take a considerable time to converge to their steady state. However, the output power of the array due to the desired emitter and jammer given by

$$P_S(t) = S \left| \langle w, v_1 \rangle \right|^2 \tag{6-49}$$

$$P_J(t) = J \left| \langle w, v_2 \rangle \right|^2 \tag{6-50}$$

are independent of $\lambda_3$ and thus converge more quickly. This fact is readily apparent since

$$E_3 v_1 = E_3 v_2 = 0 ; \tag{6-51}$$

hence we may write

$$P_S = S \left| e^{-\alpha\lambda_1 t} \frac{\langle c_1, w_o \rangle}{\|c_1\|^2} \langle c_1, v_1 \rangle + e^{-\alpha\lambda_2 t} \frac{\langle c_2, w_o \rangle}{\|c_2\|^2} \langle c_2, v_1 \rangle \right.$$

$$\left. + \frac{S}{\lambda_1} (1 - e^{-\alpha\lambda_1 t}) \frac{\langle c_1, v_1 \rangle^2}{\|c_1\|^2} + \frac{S}{\lambda_2} (1 - e^{-\alpha\lambda_2 t}) \frac{\langle c_2, v_1 \rangle^2}{\|c_2\|^2} \right|^2 \tag{6-52}$$

$$P_J = J \left| e^{-\alpha\lambda_1 t} \frac{\langle c_1, w_o \rangle}{\|c_1\|^2} \langle c_1, v_2 \rangle + e^{-\alpha\lambda_2 t} \frac{\langle c_2, w_o \rangle}{\|c_2\|^2} \langle c_2, v_2 \rangle \right.$$

$$+ \frac{S}{\lambda_1} (1 - e^{-\alpha\lambda_1 t}) \frac{\langle c_1, v_1 \rangle}{\|c_1\|^2} \langle c_1, v_2 \rangle$$

$$\left. + \frac{S}{\lambda_2} (1 - e^{-\alpha\lambda_2 t}) \frac{\langle c_2, v_1 \rangle}{\|c_2\|^2} \langle c_2, v_2 \rangle \right|^2 \tag{6-53}$$

As an example, let us consider the simple case when the initial weight vector is zero with the signal power equal to the jamming power. From this example

we see that

$$\lambda_1 = \sigma^2 + mS\left(1 + \left|\frac{\langle v_1, v_2\rangle}{m}\right|\right)$$

$$\lambda_2 = \sigma^2 + mS\left(1 - \left|\frac{\langle v_1, v_2\rangle}{m}\right|\right)$$

$$c_1 = \frac{\langle v_1, v_2\rangle}{|\langle v_1, v_2\rangle|} v_1 + v_2$$

$$c_2 = -\frac{\langle v_1, v_2\rangle}{|\langle v_1, v_2\rangle|} v_1 + v_2$$

$$\langle c_1, v_1\rangle = -\frac{\langle v_1, v_2\rangle}{|\langle v_1, v_2\rangle|} m + \langle v_1, v_2\rangle$$

$$\langle c_2, v_1\rangle = -\frac{\langle v_1, v_2\rangle}{|\langle v_1, v_2\rangle|} m + \langle v_1, v_2\rangle$$

$$\langle c_1, c_1\rangle = \|c_1\|^2 = 2m\left(1 + \frac{|\langle v_1, v_2\rangle|}{m}\right)$$

$$\langle c_2, c_2\rangle = 2m\left(1 - \frac{|\langle v_1, v_2\rangle|}{m}\right).$$

The weight vector for this example can then be written as

$$w(t) = \frac{S}{2\sigma^2}\left\{\frac{1}{1+\frac{mS}{\sigma^2}\left(1+\frac{|\langle v_1, v_2\rangle|}{m}\right)}\left(1-e^{-\alpha\sigma^2\left[1+\frac{mS}{\sigma^2}\left(1+\frac{|\langle v_1, v_2\rangle|}{m}\right)\right]t}\right)\bullet\right.$$

$$\left(v_1+\frac{\langle v_1, v_2\rangle}{|\langle v_1, v_2\rangle|}v_2\right)+\frac{1}{1+\frac{mS}{\sigma^2}\left(1-\frac{|\langle v_1, v_2\rangle|}{m}\right)}\left(1-e^{-\alpha\sigma^2\left[1+\frac{mS}{\sigma^2}\left(1-\frac{|\langle v_1, v_2\rangle|}{m}\right)\right]t}\right)\bullet$$

$$\left.\left(v_1-\frac{\langle v_1, v_2\rangle}{|\langle v_1, v_2\rangle|}v_2\right)\right\} \qquad (6\text{-}54)$$

with corresponding output powers of

$$P_S(t) = S\left(\frac{S}{2\sigma^2}\right)^2\left\{\frac{m+|\langle v_1, v_2\rangle|}{1+\frac{mS}{\sigma^2}\left(1+\frac{|\langle v_1, v_2\rangle|}{m}\right)}\left(1-e^{-\alpha\sigma^2\left[1+\frac{|\langle v_1, v_2\rangle|}{m}\right]t}\right)\right.$$

$$\left.+\frac{m-|\langle v_1, v_2\rangle|}{1+\frac{mS}{\sigma^2}\left(1-\frac{|\langle v_1, v_2\rangle|}{m}\right)}\left(1-e^{-\alpha\sigma^2\left[1+\frac{mS}{\sigma^2}\left(1-\frac{|\langle v_1, v_2\rangle|}{m}\right)\right]t}\right)\right\}^2 \qquad (6\text{-}55)$$

$$P_J(t) = S\left(\frac{S}{2\sigma^2}\right)^2\left\{\left(\frac{\langle v_1, v_2\rangle + m\langle v_1, v_2\rangle/|\langle v_1, v_2\rangle|}{1+\frac{mS}{\sigma^2}\left(1+\frac{|\langle v_1, v_2\rangle|}{m}\right)}\right)\left(1-e^{-\alpha\sigma^2\left[1+\frac{mS}{\sigma^2}\left(1+\frac{|\langle v_1, v_2\rangle|}{m}\right)\right]t}\right)\right.$$

$$\left.+\left(\frac{\langle v_1, v_2\rangle - m\langle v_1, v_2\rangle/|\langle v_1, v_2\rangle|}{1+\frac{mS}{\sigma^2}\left(1-\frac{|\langle v_1, v_2\rangle|}{m}\right)}\right)\left(1-e^{-\alpha\sigma^2\left[1+\frac{mS}{\sigma^2}\left(1-\frac{|\langle v_1, v_2\rangle|}{m}\right)\right]t}\right)\right\}^2 \qquad (6\text{-}56)$$

At steady state, the ratio of $P_S$ to $P_J$ is easily seen to be

$$\frac{P_S}{P_J} = \frac{1 + \left(\frac{mS}{\sigma^2}\right)\left(1 - \frac{\langle v_1, v_2\rangle^2}{m^2}\right)}{\langle v_1, v_2\rangle / m}, \tag{6-57}$$

thus, the larger the powers the greater $P_S/P_J$ becomes. From an antenna pattern point of view the adaptive array is placing a null in the direction of the jammer while attempting to maintain a large gain in the direction of the desired signal. This point will be explored in further detail in the next chapter. However, before focusing on the steady state behavior we present the Figures 6-1 and 6-2 which illustrate the time behavior of a four element linear array with half wavelength spacing at the carrier frequency using the LMS algorithm. The environment consists of two emitters, the desired signal at an angle of 70° with respect to the array axis with $S/\sigma^2 = 10$ and a jammer at 60° with $J/\sigma^2 = 1000$. In Figure 6-1, both emitter and jammer are very narrowband, whereas, in Figure 6-2, they both have constant power spectral densities over 10 percent of the carrier frequency and zero otherwise. The antenna pattern is initially omnidirectional, since $w_o$ is chosen as $[1, 0, 0, \ldots, 0]^*$, and then steers in such a manner as to attempt to place a maximum on the desired signal while placing a null in the direction of the jammer. It is evident that the wider bandwidth reduces the capability of the array to place a null in the direction of the jammer since the jammer no longer appears as a point source to the array.

### 6.1.2 Steady State Behavior

The most important insight into the behavior of the adaptive array, for many situations, is not obtained from the transient response but rather from its steady state behavior. By taking the limit as $t \longrightarrow \infty$ in Equation (6-13) we can analytically examine many important characteristics of the array response for environments consisting of relatively few emitters. For denser environments we must resort to a digital computer simulations, however, the additional insight provided here is marginal at best for narrow band environments. For wide band environments the problem is far too complicated to be analyzed analytically except for one very interesting case which we shall present shortly, and thus, we must resort to computer simulations in order to compare the array performance in the wide band and narrowband environments.

We begin our discussion by considering an environment containing two very narrow band emitters, a desired emitter and one interference source. The antenna array is assumed to consist of m antenna elements arbitrarily placed but symmetric with respect to the geometric center of the array. We will also assume that thermal noise is

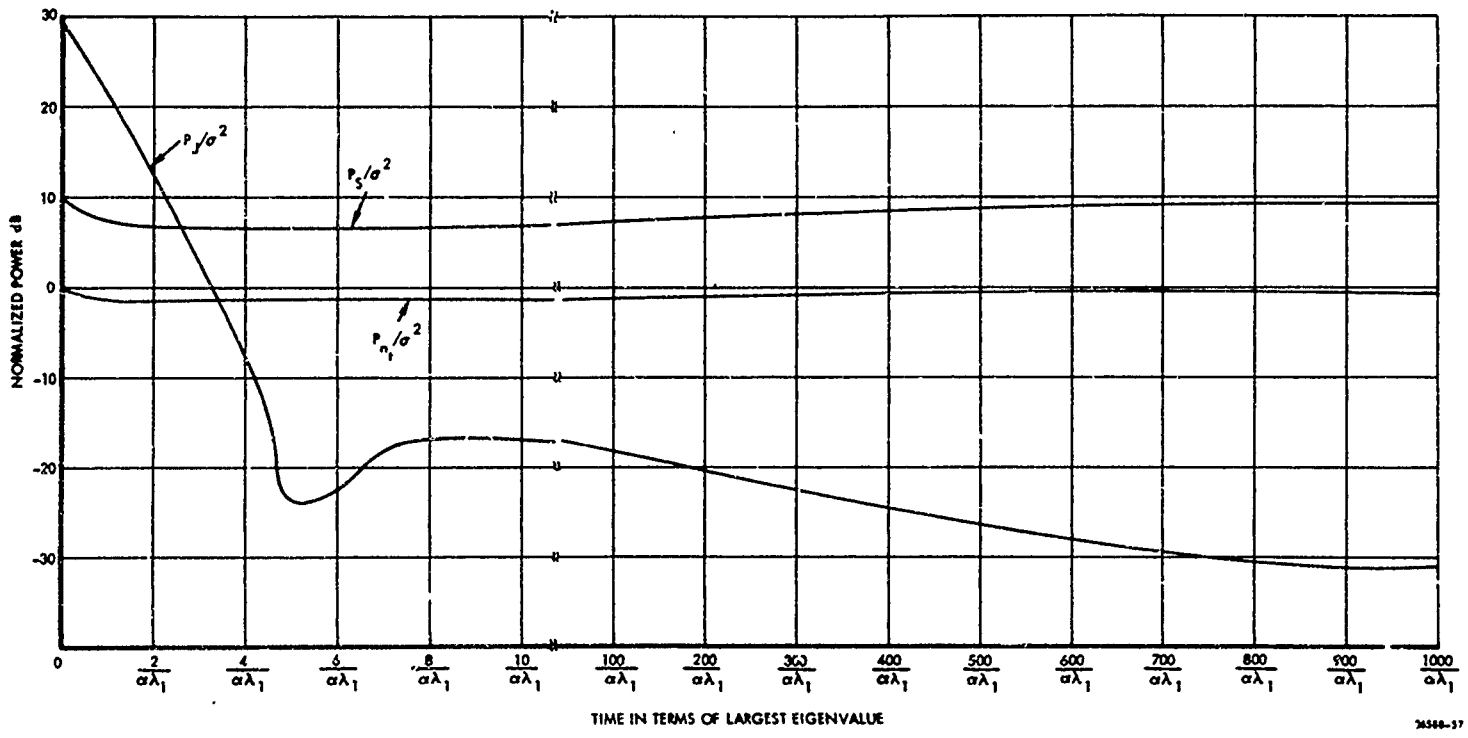


Figure 6-1. Transient Response for a Four Element Linear Array Using the LMS Algorithm for Very Narrowband Signals

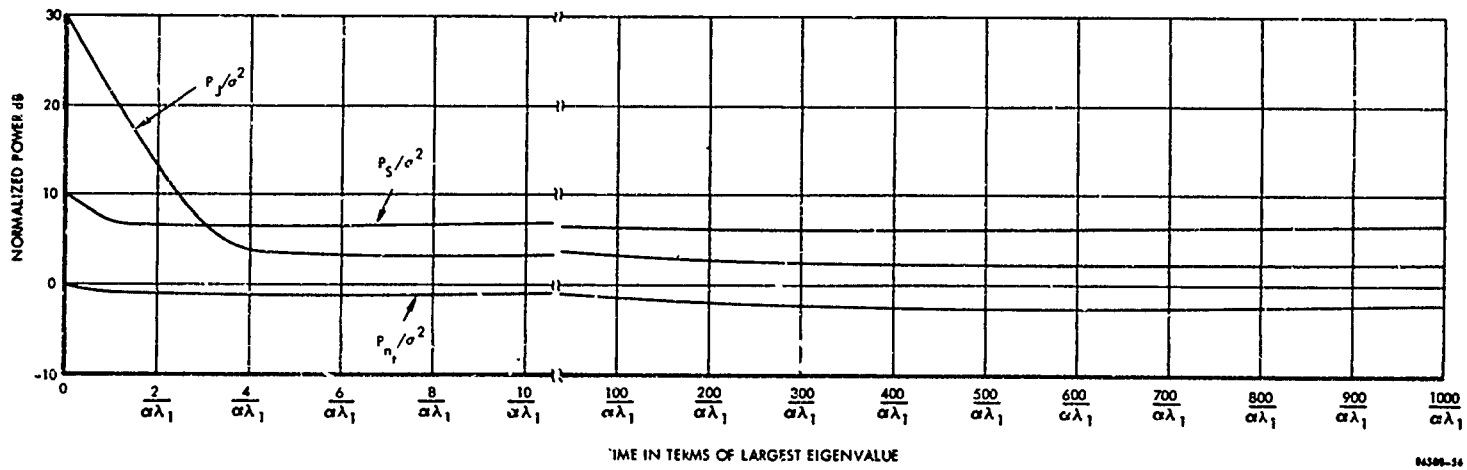


Figure 6-2. Transient Response for a Four Element Linear Array Using the LMS Algorithm for Signals with 10% Bandwidth

present in each antenna element and is uncorrelated from one antenna to the next with equal variance. Given this format we now proceed to develop the power out of the array due to the jammer, desired signal and thermal noise and evaluate the antenna gain, signal-to-noise power ratio and antenna patterns. We will then compare these results for wide band signals.

Recall that the steady state output signal powers of the array are obtained by taking the limit as $t \longrightarrow \infty$ in Equations (6-52) and (6-53). By taking this limit we arrive at

$$P_S = S\left(\frac{S}{\sigma^2}\right)^2 \left\{ \frac{1 + \frac{m^2 J}{2}\left(1 - \frac{\langle v_1, v_2\rangle}{m^2}\right)}{1 + \frac{mS}{\sigma^2} + \frac{mJ}{\sigma^2} + \left(\frac{mJ}{\sigma^2}\right)\left(\frac{mS}{\sigma^2}\right)\left(1 - \frac{\langle v_1, v_2\rangle^2}{m^2}\right)} \right\}^2 \tag{6-58}$$

and

$$P_J = J\left(\frac{S}{\sigma^2}\right)^2 \left\{ \frac{\langle v_1, v_2\rangle}{1 + \frac{mS}{\sigma^2} + \frac{mJ}{\sigma^2} + \left(\frac{mS}{\sigma^2}\right)\left(\frac{mJ}{\sigma^2}\right)\left(1 - \frac{\langle v_1, v_2\rangle^2}{m^2}\right)} \right\}^2 . \tag{6-59}$$

The output thermal noise power can be computed in a similar manner since

$$P_{n_t} = \sigma^2 \, ||w||^2 . \tag{6-60}$$

By taking the limit as $t \longrightarrow \infty$ in Equation 6-13 and substituting into the above equation we see that

$$P_{n_t} = \sigma^2 \frac{\left[m\left(\frac{S}{\sigma^2}\right)^2 + \left(\frac{S}{\sigma^2}\right)\left(\frac{mS}{\sigma^2}\right)\left(\frac{mJ}{\sigma^2}\right)\left(2 + \frac{mJ}{\sigma^2}\right)\left(1 - \frac{\langle v_1, v_2\rangle^2}{m^2}\right)\right]}{\left[1 + \frac{mJ}{\sigma^2} + \frac{mS}{\sigma^2} + \left(\frac{mS}{\sigma^2}\right)\left(\frac{mJ}{\sigma^2}\right)\left(1 - \frac{\langle v_1, v_2\rangle^2}{m^2}\right)\right]^2} \tag{6-61}$$

It is of interest to evaluate these expressions as a function of the power of the interference source and ascertain their general behavior. From Figures 6-3, 6-4, and 6-5 we note that as the jamming power increases the output signal power and thermal noise power approach a nonzero constant whereas $P_J$ approaches zero. Moreover, the smaller the level of thermal noise the less $P_J$ becomes. In the limit as $\sigma^2 \longrightarrow 0$ the output power due to the jammer becomes identically zero. Thus, a perfect spatial null is placed in the direction of the jammer. This is generally true even in a dense emitter environment as we demonstrate in the following example.

Example 3

Consider a narrow band environment containing p emitters $p < m$, a desired emitter and p-1 jammers. If $v_1$ is not a linear combination of $v_2, \ldots, v_p$ then the jammer power out of an arbitrary m element array is zero.

To show this is the case, we recall that w satisfies the equation

$$R_x w = S v_1 \tag{6-62}$$

or

$$(S v_1 v_1^* + \sum_{i=2}^{p} J_i v_i v_i^*)\, w = S v_1, \tag{6-63}$$

Since the dimension of the space spanned by $v_i$, $i=2, \ldots, p$ is at most p-1, any weight vector w belonging to the null space of $R_n$, which is at least of dimension m-p+1, such that

$$\langle v_1, w \rangle = 1 \tag{6-64}$$

will do.

It is also of interest to note that the output power due to the jammer is normally much smaller than the output thermal noise power provided that the relative angular displacement between the jammer and desired emitter is sufficiently large. If we take the ratio of Equations (6-59) and (6-61) we find that $P_J/P_{n_t}$ takes on its maximum value when

$$\frac{J}{\sigma^2} = \frac{1}{m\sqrt{1 - \frac{\langle v_1, v_2 \rangle^2}{m^2}}} \tag{6-65}$$

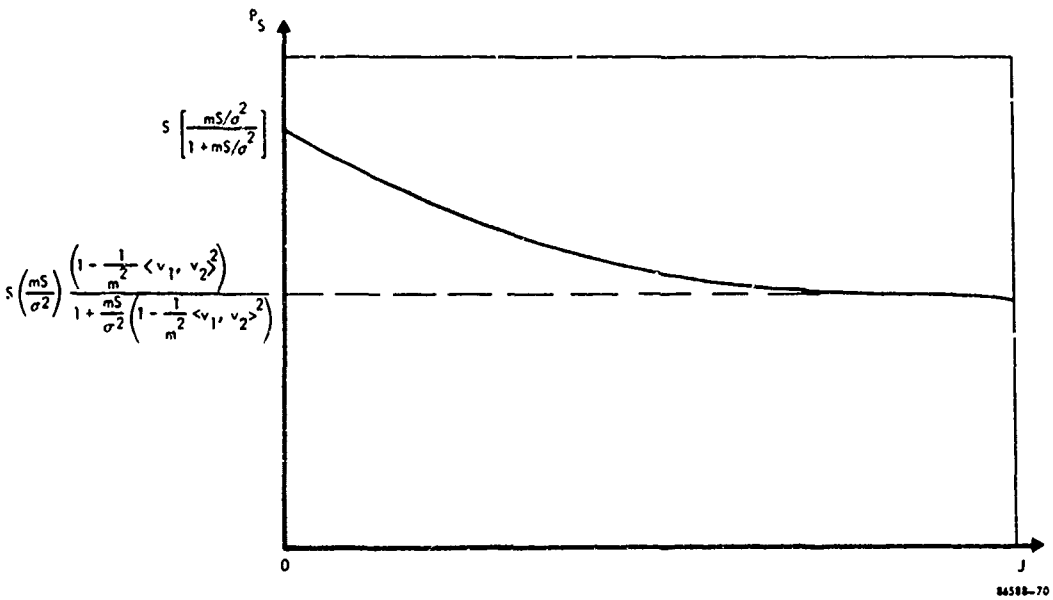


Figure 6-3. Steady State Output Signal Power Behavior

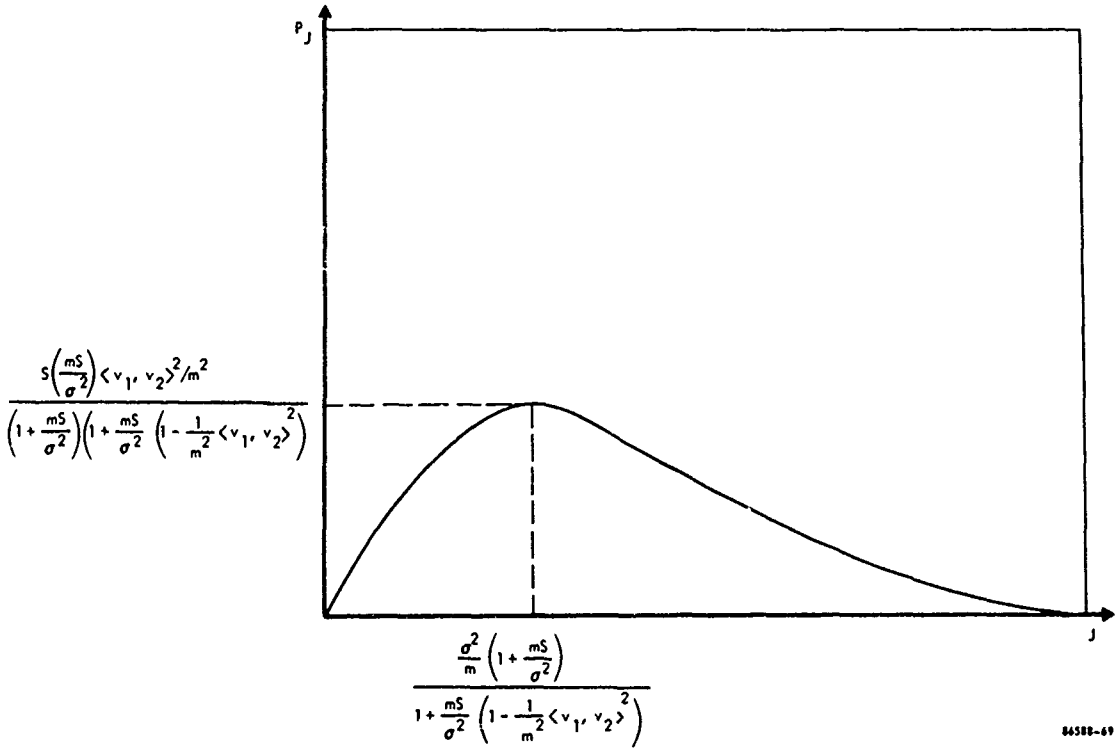


Figure 6-4. Steady State Output Jammer Power Behavior

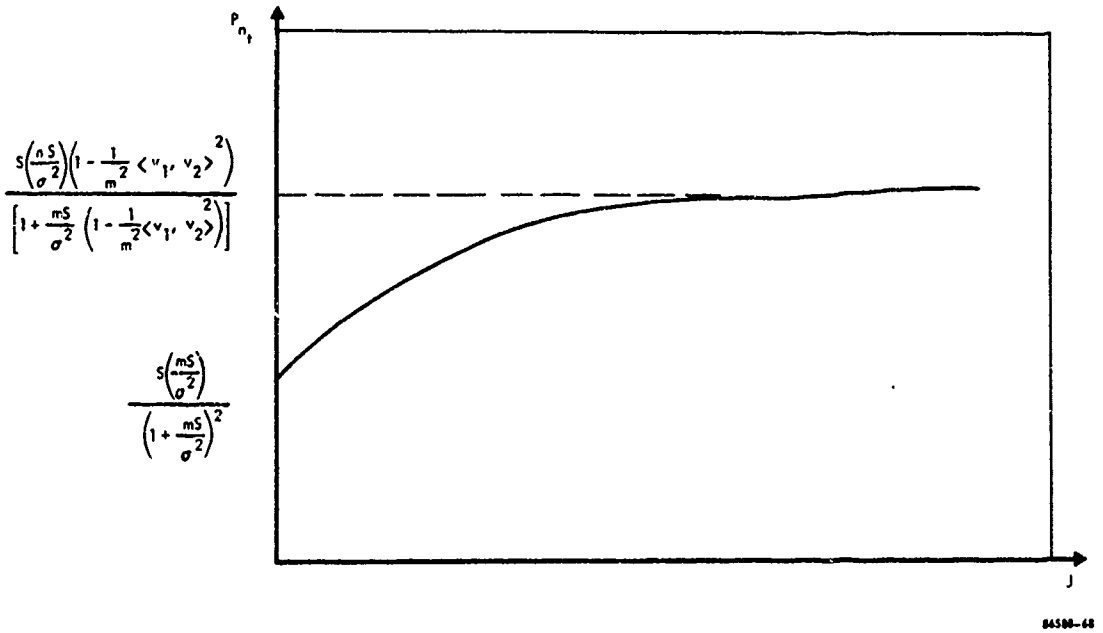


Figure 6-5. Steady State Output Thermal Noise Behavior

and is given by

$$\left.\frac{P_J}{P_{n_t}}\right|_{max} = \frac{\langle v_1, v_2\rangle^2/m^2}{2\left[1 - \frac{\langle v_1, v_2\rangle^2}{m^2} + \sqrt{1 - \frac{\langle v_1, v_2\rangle^2}{m^2}}\right]} \quad . \tag{6-66}$$

This ratio is always less than one provided that $\langle v_1, v_2\rangle^2/m^2 < 8/9$. (For a four element linear array with half wavelength spacing with a desired emitter at $90^\circ$ relative to the array axis, these equations imply that if the jammer is displaced by more than $7.5^\circ$ from the desired signal then $\left.\frac{P_J}{P_{n_t}}\right|_{max} < 1$.) This behavior is shown in Figure 6-6.

Returning to Figures 6-3 and 6-4, we see that since $P_J$ goes to zero as J becomes larger the output signal-to-noise power ratio approaches a constant value while the output gain, which is the ratio of the output signal-to-noise power ratio to the input signal-to-noise power ratio per sensor, increases as J increases. Explicit relationships for the output signal-to-noise ratio and optimum gain are easily obtained since

$$\frac{S}{N_o} = S\langle v_1, R_n^{-1} v_1\rangle \tag{6-67}$$

$$G_o = \frac{S\langle v_1, R_n^{-1} v_1\rangle}{\frac{S}{J+\sigma^2}} = (J+\sigma^2)\langle v_1, R_n^{-1} v_1\rangle \quad . \tag{6-68}$$

To evaluate these equations we see that for the two emitter environment the noise covariance matrix reduces to

$$R_n = \sigma^2 I + J v_2 v_2^* \tag{6-69}$$

which has an inverse of

$$R_n^{-1} = \sigma^{-2} I - \frac{J\sigma^{-4} v_2 v_2^*}{1 + mJ\sigma^{-2}} \quad . \tag{6-70}$$

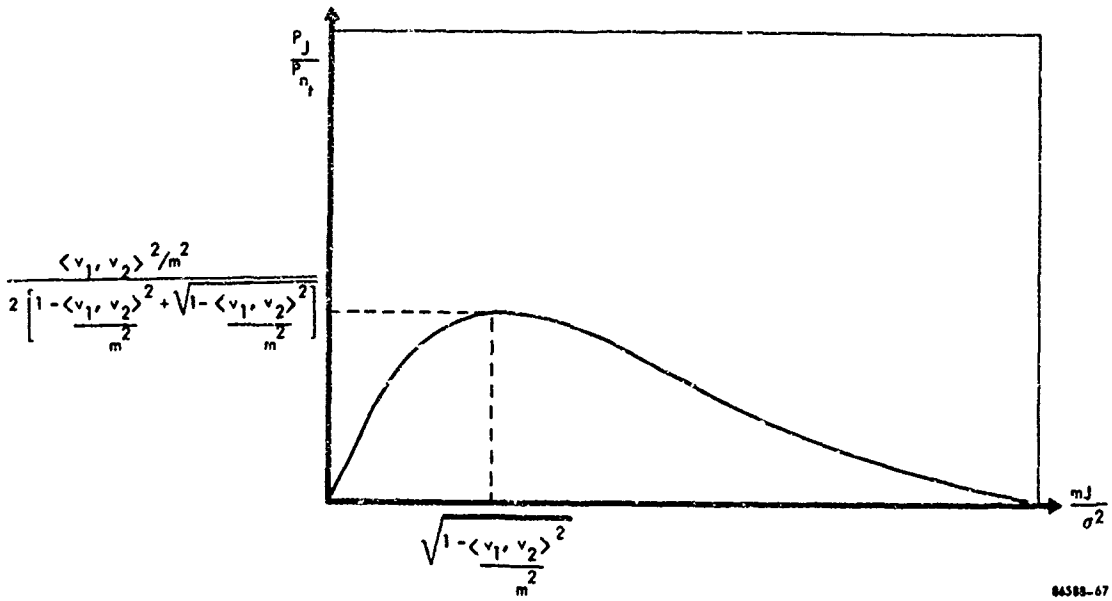


Figure 6-6. Steady State Output Jammer to Thermal Noise Behavior

Performing the indicated innerproduct we see that

$$\frac{S}{N_o} \approx \frac{\left(\frac{mS}{\sigma^2}\right)\left[1 + \frac{mJ}{\sigma^2}\left(1 - \frac{\langle v_1, v_1\rangle^2}{m^2}\right)\right]}{1 + \frac{mJ}{\sigma^2}} \tag{6-71}$$

and

$$G_o = m \frac{\left(1 + \frac{J}{\sigma^2}\right)}{\left(1 + \frac{mJ}{\sigma^2}\right)} \left\{1 + \frac{mJ}{\sigma^2}\left(1 - \frac{\langle v_1, v_2\rangle^2}{m^2}\right)\right\}, \tag{6-72}$$

Thus for large J, the signal-to-noise power ratio and optimum gain become

$$\frac{S}{N_o} \longrightarrow \frac{mS}{\sigma^2}\left(1 - \frac{\langle v_1, v_2\rangle^2}{m^2}\right) \tag{6-73}$$

and

$$G_o \longrightarrow 1 + \frac{mJ}{\sigma^2}\left(1 - \frac{\langle v_1, v_2\rangle^2}{m^2}\right). \tag{6-74}$$

As the relative angular separation of the desired signal and jammer becomes small $\frac{\langle v_1, v_2\rangle^2}{m^2} \longrightarrow 1$ resulting in a degradation in array performance as expected.

## 6.2 Conventional Array Comparison

In order to obtain a meaningful understanding of the magnitude of this degradation it is convenient to compare the response of the optimum array with an array which cannot adapt to a changing noise environment. An array which would provide a very desirable comparitive base would be one using a Dolph-Tchebyscheff weighting yielding low side lobes. However, the Dolph-Tchebyscheff weighting provides about the same performance as a "conventional array" as the relative angular displacement of

jammer and the desired emitter becomes small. Since the conventional array, which denotes an array which cophases the desired signal in each sensor element and coherently adds these signals to yield the array output, is more simply evaluated analytically we shall use it as our comparison base. A functional representation of these arrays are shown in Figure 6-7. With the presence of the spatial correctional filters, the signal-to-noise power ratio for the optimum array and conventional array become*

$$\frac{S}{N_o} = S \langle \underline{1}, R_{\hat{n}}^{-1} \underline{1} \rangle \tag{6-75}$$

$$\frac{S}{N_c} = \frac{\frac{S}{m} \langle \underline{1}, \underline{1} \rangle}{\frac{1}{m^2} \langle \underline{1}, R_{\hat{n}} \underline{1} \rangle} = \frac{m^2 S}{\langle \underline{1}, R_{\hat{n}} \underline{1} \rangle} \tag{6-76}$$

which in terms of the input noise covariance matrix becomes

$$\frac{S}{N_o} = S \langle \underline{1}, (F R_n F^*)^{-1} \underline{1} \rangle = S \langle F^* \underline{1}, R_n^{-1} F^* \underline{1} \rangle \tag{6-77}$$

$$\frac{S}{N_c} = \frac{m^2 S}{\langle F^* \underline{1}, R_n F^* \underline{1} \rangle} \tag{6-78}$$

where we have made use of the fact that F is unitary. Recognizing that

$$F^* \underline{1} = \begin{bmatrix} e^{-j2\pi f_c \tau_{11}} \\ e^{-j2\pi f_c \tau_{12}} \\ \vdots \\ e^{-j2\pi f_c \tau_{1m}} \end{bmatrix} = v_1 \tag{6-79}$$

*The subscripts o and c refer to the optimal and conventional arrays, respectively.

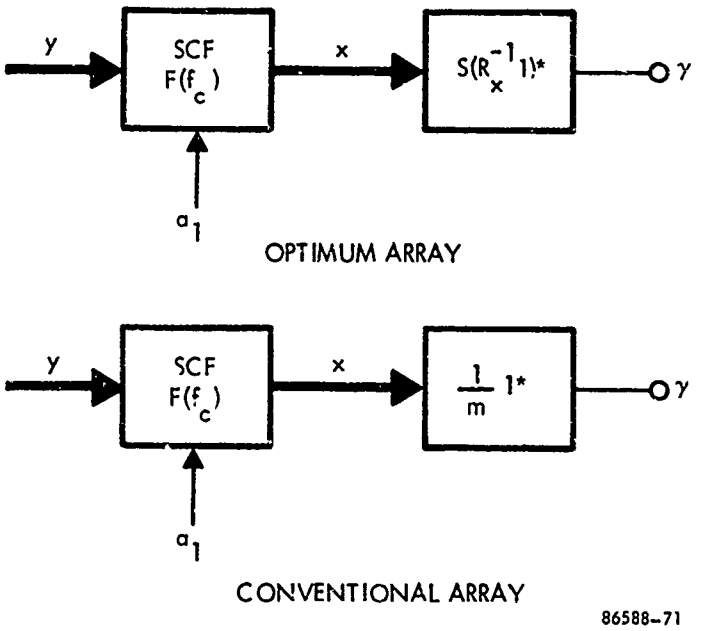


Figure 6-7. Functional Diagram of Optimal and Conventional Arrays

we can reduce the above equation set to

$$\frac{S}{N_o} = S \langle v_1, R_n^{-1} v_1 \rangle , \tag{6-80}$$

which we see is equivalent to the S/N ratio without the spatial connection filters, and

$$\frac{S}{N_c} = \frac{m^2 S}{\langle v_1, R_n v_1 \rangle} . \tag{6-81}$$

The gain advantage of the optimum processor relative to the conventional processor is now easily computed since

$$\frac{G_o}{G_c} = \frac{S/N_o}{S/N_c} = \frac{\langle v_1, R_n^{-1} v_1 \rangle \langle v_1, R_n v_1 \rangle}{m^2} \leq (\lambda^{-1}{}_{min})(\lambda\, max) \tag{6-82}$$

Where $\lambda_{min}$ and $\lambda_{max}$ represent the maximum and minimum eigenvalues of $R_n$ respectively. We note that this ratio becomes unity when the noise field is temporally and spatially white. Thus, the two processors have the same gain m in every direction.

With the completion of this development we now return to the two emitter environment and compare the performance of the conventional array in the two emitter environment considered previously. The signal-to-noise power ratio as well as gain is now easily seen to be

$$\frac{S}{N_c} = \frac{mS/\sigma^2}{1 + (\frac{mJ}{\sigma^2}) \frac{\langle v_1, v_2 \rangle^2}{m^2}} \tag{6-83}$$

and

$$G_c = \frac{m\,(1 + J/\sigma^2)}{1 + (\frac{mJ}{\sigma^2}) \frac{\langle v_1, v_2 \rangle^2}{m^2}} . \tag{6-84}$$

A comparison of the behavior of the conventional array and the optimal can be performed by comparing Equations 6-71 and 6-72 with Equations 6-83 and 6-84. Figures 6-8 and 6-9 illustrate this comparison. From these figures and equations we make the following observations:

a. For J=0, $G_o = G_c = m$

b. As $J \longrightarrow \infty$, $G_c$ monotonically increases or decreases to $\frac{m^2}{<v_1,v_2>^2}$ depending on whether $\frac{m^2}{<v_1,v_2>^2}$ is larger or smaller than m.

c. As $J \longrightarrow \infty$, $G_o$ asymptotically approaches the line $+ \frac{mJ}{\sigma^2}(1 - \frac{1}{m^2} <v_1,v_2>^2)$

d. For all J, $G_o > G_c$

e. For J=0, $\frac{S}{N_o} = \frac{S}{N_c} = \frac{mS}{\sigma^2}$

f. As $J \longrightarrow \infty$, $\frac{S}{N_c}$ monotonically approaches zero while $\frac{S}{N_o}$ monotonically approaches $\frac{mS}{\sigma^2}[1 - \frac{1}{m^2} <v_1,v_2>^2]$. Moreover, for $\frac{mJ}{\sigma^2} = 1$, $\frac{S}{N_o}$ is equal to $\frac{mS}{\sigma^2}(1 - \frac{1}{2m^2} <v_1,v_2>^2)$.

That is, the signal-to-noise power ratio has dropped to 50 percent of its asymptotic value.

g. As the relative angular separation between the desired signal and jammer becomes small, both gains and signal-to-noise power ratios become equally poor.

Thus, for very narrowband environments a very desirable signal-to-noise ratio and gain are obtainable from the adaptive array regardless of jammer power

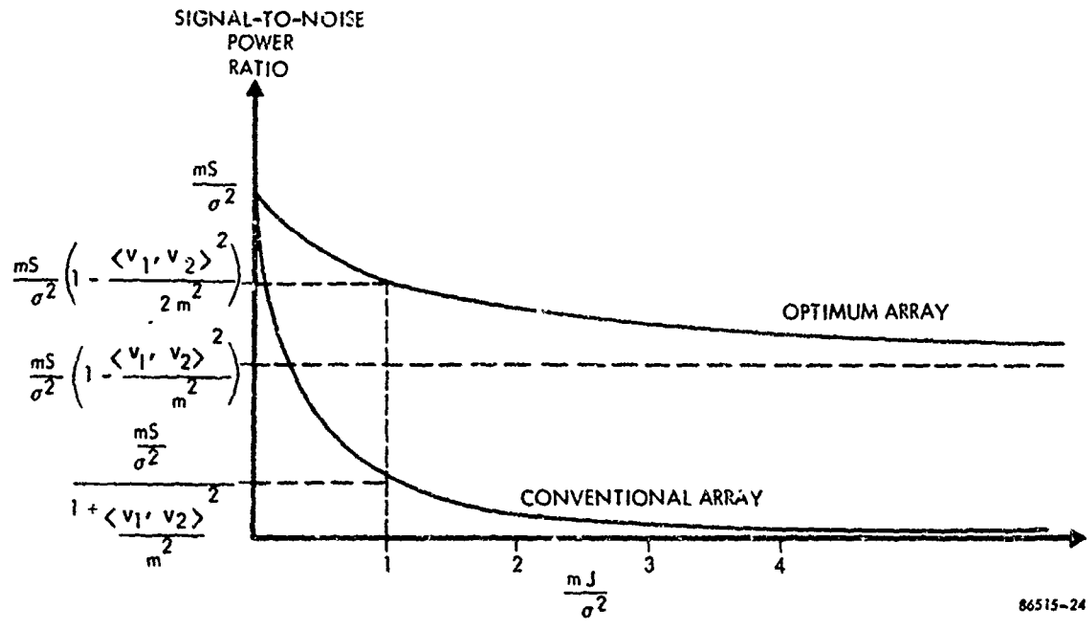


Figure 6-8. Optimal and Conventional Signal-To-Noise Ratio

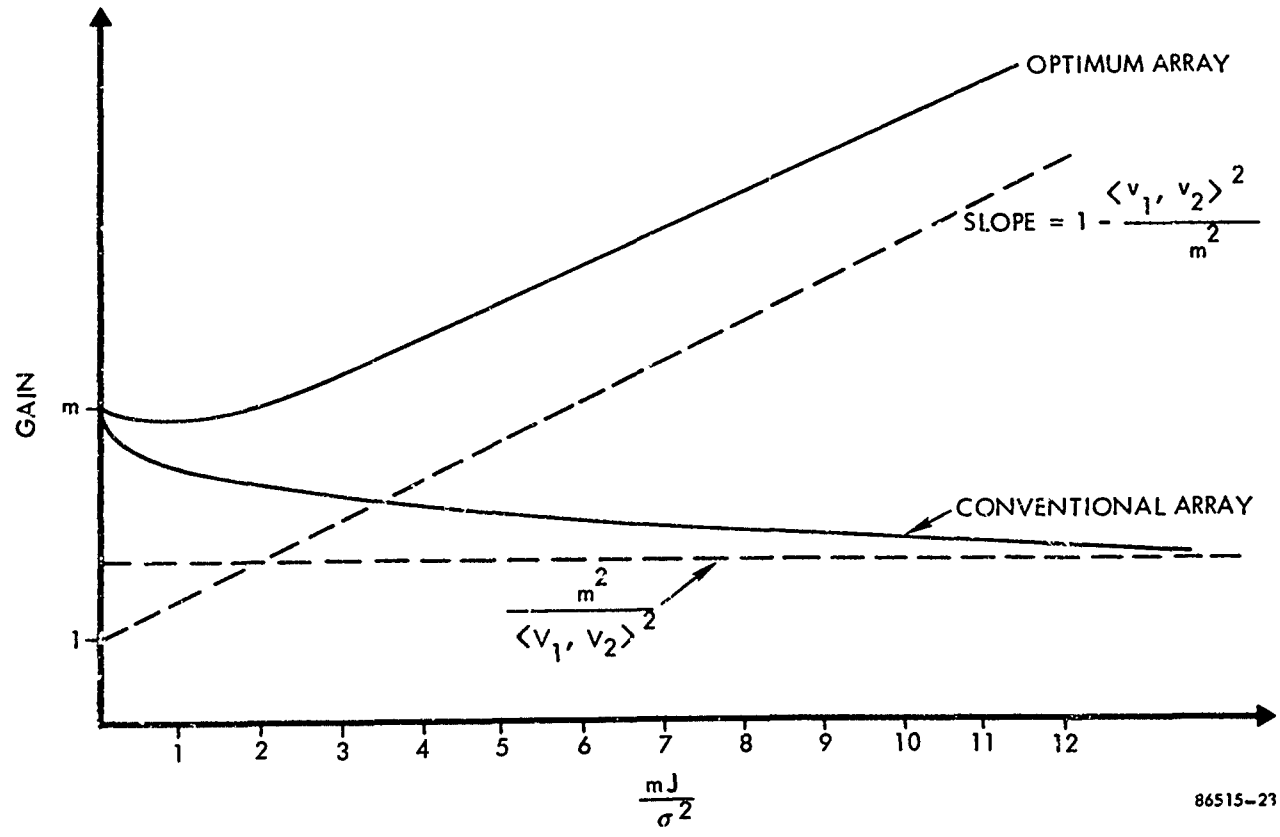


Figure 6-9. Optimal and Conventional Array Gain

provided sufficient angular separation exists. In wideband environments diffusion of the signals across the array deteriorates the performance. The diffusion has the effect of decorrelating signals between widely spaced antenna elements due to each emitter. As the bandwidth increases the signals arriving at different antenna elements due to each emitter become nearly uncorrelated resulting in each emitter behaving as though it were isotropic noise. Thus, with increased bandwidth the emitters evolve from point sources to distributed sources. The corresponding covariance matrix then approaches a diagonal matrix. Intuitively, we can see that if the desired signal is wideband and the jammers are also wideband, then placing antenna pattern nulls in the direction of the jammers will not completely negate their power from the array output since they are effectively distributed sources.

Let's consider a simple wideband case of a linear or planer array with the desired emitter broadside to the array and one jammer. We shall approximate the covariance matrix for this example as

$$R_x = (\sigma^2 + J)\, I + S\, \underline{1}\,\underline{1}^*. \tag{6-85}$$

The output signal-to-noise power ratio and gain for this example then becomes

$$\frac{S}{N_o} = \frac{mS}{\sigma^2 + J} \tag{6-86}$$

$$G_o = m. \tag{6-87}$$

Thus, as the jammer power increases the output signal-to-noise ratio goes to zero with the gain remaining constant at m. From this simple example we can expect that the amount of jammer suppression obtainable for finite bandwidth signals will certainly be less than that given in the equations developed in this chapter.

An extensive study of the effects of bandwidth will be presented in Chapter VIII, however, we present Figures 6-10 and 6-11 to demonstrate the effects of bandwidth on the performance of a four element linear array with half wavelength spacing of the carrier frequency. The desired signal and jammer have azimuths of $70^\circ$ and $60^\circ$ respectively as measured from the axis of the array. Both emitters have a constant power spectral density over a 10 percent bandwidth about the carrier with $S/\sigma^2 = 10$ and $J/\sigma^2 = 1000$. Here we see the effects of dispersion of the jammer in the array. As the jamming power increases, an increasing amount of the jamming power appears at the array output reducing the signal-to-noise ratio and gain relative to the very narrowband case. This performance degradation can also be seen in the antenna patterns which we now present.

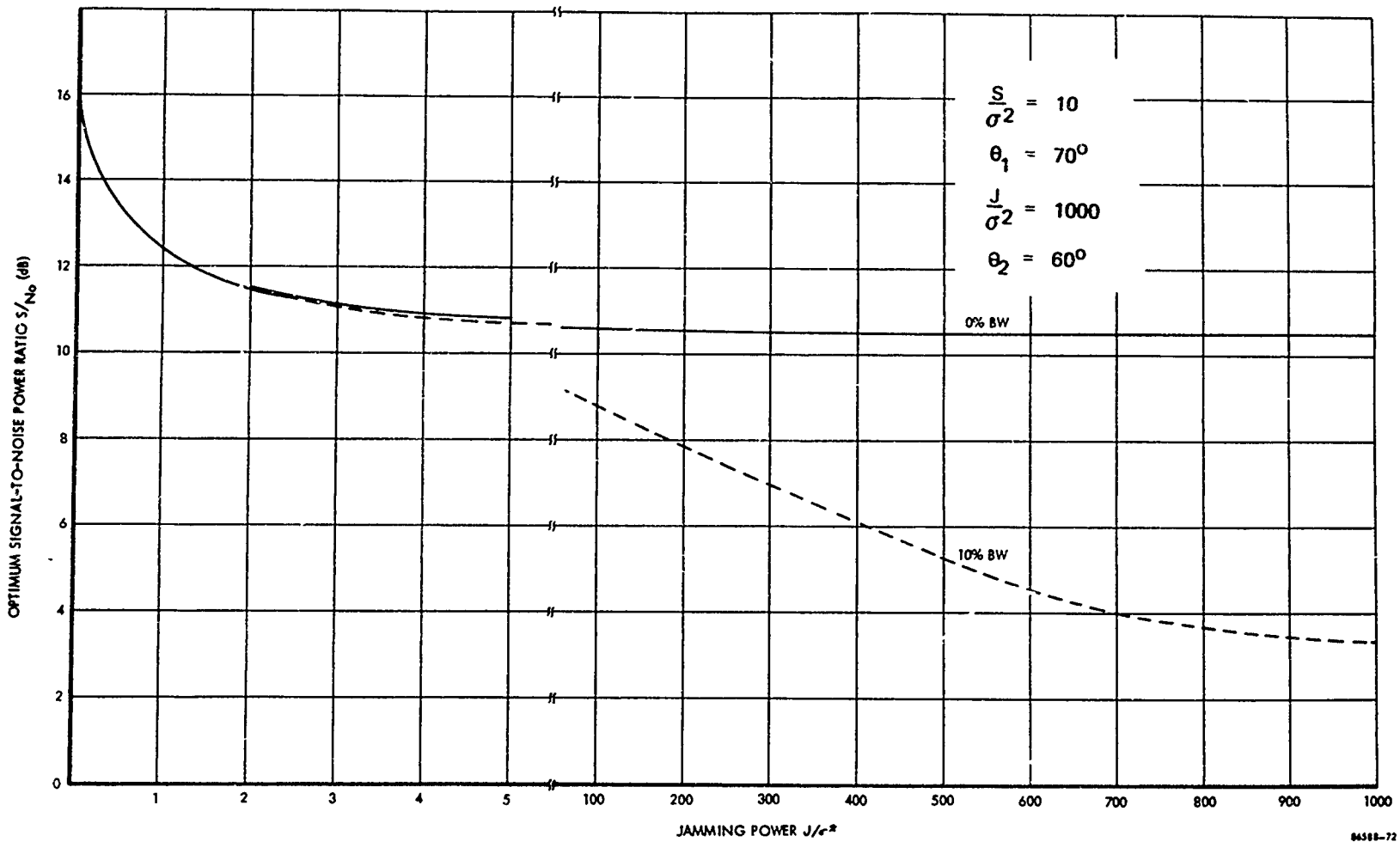


Figure 6-10. Optimal Signal-to-Noise Power Ratio

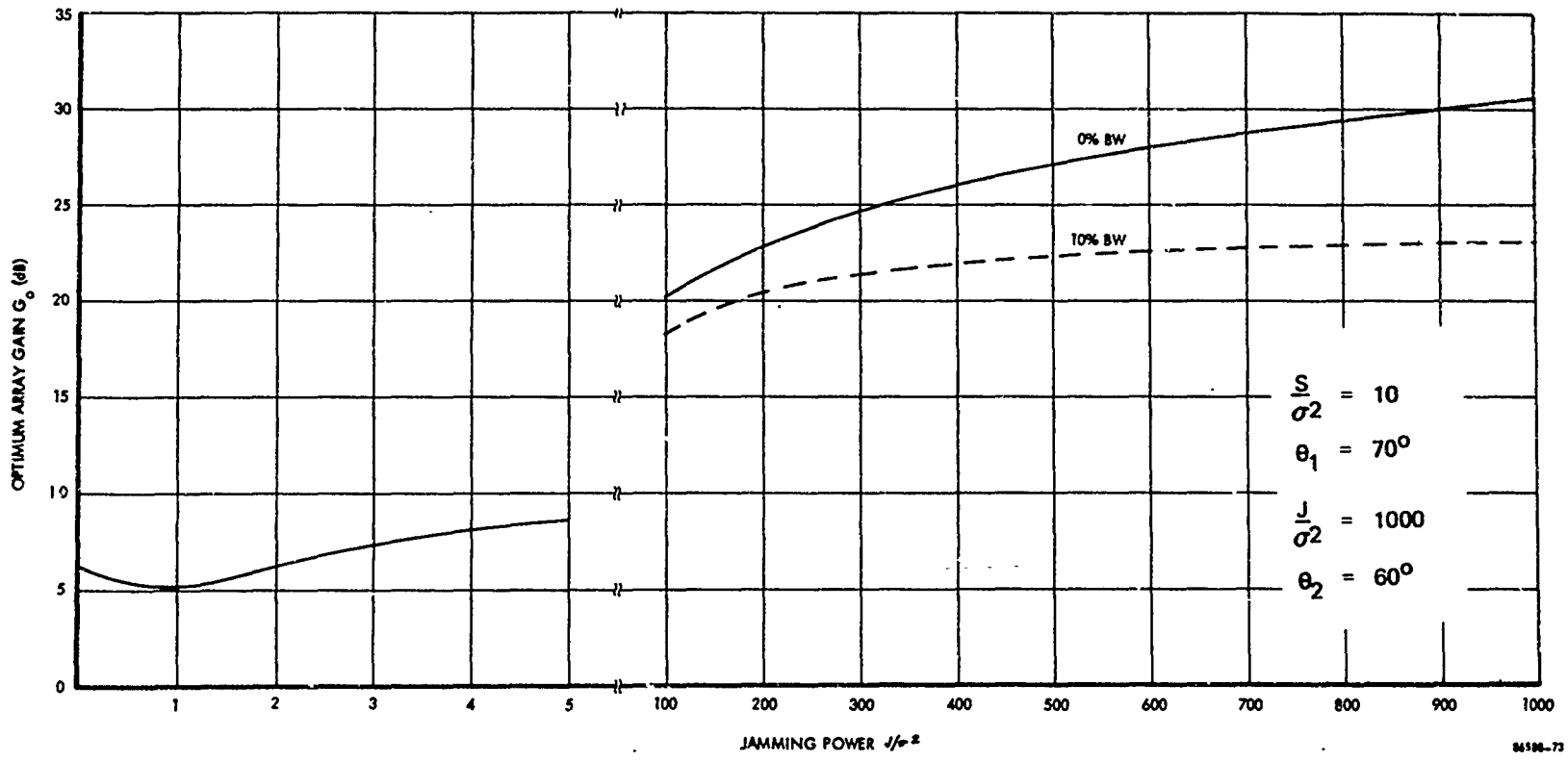


Figure 6-11. Optimal Array Gain

## 6.3 Optimal Antenna Patterns

In the previous section we addressed the influence of a jammer on an adaptive array in a narrowband environment by examining the two descriptors: signal-to-noise power ratio and gain. In this section we shall derive the expression for the antenna pattern for the two emitter environment considered previously and show how the antenna pattern can be decomposed into two partial patterns; one in the direction of the desired signal and one in the direction of the jammer. We will then see how these two patterns result in a null in the direction of the jammer.

Recall from Chapter 2 that the antenna pattern for an arbitrary array was defined as

$$\psi = \langle w, R_\mu w \rangle \tag{6-88}$$

where $R_\mu$ is the covariance matrix of a ficticious source of unity power. In our narrowband environment $R_\mu$ can be written as

$$R_\mu = v_\mu v_\mu^* \tag{6-89}$$

which together with the fact that $w = S R_x^{-1} v_1$, enables us to write the pattern as

$$\psi = \langle w, v_\mu v_\mu^* w \rangle = \left| \langle w, v_\mu \rangle \right|^2 = S^2 \left| \langle R_x^{-1} v_1, v_\mu \rangle \right|^2 .$$

For the environment consisting of a desired emitter and one jammer, the pattern takes the form

$$\psi(v) = \frac{\left(\frac{S}{\sigma^2}\right)^2 \left| \left(1 + \frac{mJ}{\sigma^2}\right) \langle v_1, v_\mu \rangle - \left(\frac{J}{\sigma^2}\right) \langle v_1, v_2 \rangle \langle v_2, v_\mu \rangle \right|^2}{\left| 1 + \frac{mJ}{\sigma^2} + \frac{mS}{\sigma^2} + \left(\frac{mS}{\sigma^2}\right)\left(\frac{mJ}{\sigma^2}\right) \left[1 - \frac{1}{m^2} \langle v_1, v_2 \rangle^2\right] \right|^2} \tag{6-90}$$

The terms $\langle v_1, v_\mu \rangle$ and $\langle v_2, v_\mu \rangle$ represent the antenna beams in the direction of the desired emitter and jammer respectively. In fact, it can be shown that for p emitters ($p < m$); the antenna will form p individual beams, one on each emitter.

Figure 6-12 illustrates this decomposition for a four element linear array with half wavelength spacing. In this figure the jammer is located at broadside with $\frac{J}{\sigma^2} = 1000$ where as the desired signal makes an angle of 86° with respect to the axis of the array with $S/\sigma^2 = 10$.

The gains in the direction of the jammer and desired signal are easily computed by letting $v_\mu$ approach $v_2$ and $v_1$ respectively. In particular

$$\psi(v_1) = \frac{P_S}{S} = \frac{\left(\frac{mS}{\sigma^2}\right)^2 \left| 1 + \frac{mJ}{\sigma^2}\left(1 - \frac{\langle v_1, v_2\rangle^2}{m^2}\right)\right|^2}{\left|1 + \frac{mJ}{\sigma^2} + \frac{mS}{\sigma^2} + \left(\frac{mS}{\sigma^2}\right)\left(\frac{mJ}{\sigma^2}\right)\left(1 - \frac{1}{m^2}\langle v_1, v_2\rangle^2\right)\right|^2} \tag{6-91}$$

whereas

$$\psi(v_2) = \frac{P_J}{J} = \frac{\left(\frac{S}{\sigma^2}\right)^2 \langle v_1, v_2\rangle^2}{\left|1 + \frac{mS}{\sigma^2} + \frac{mJ}{\sigma^2} + \left(\frac{mS}{\sigma^2}\right)\left(\frac{mJ}{\sigma^2}\right)\left(1 - \frac{1}{m^2}\langle v_1, v_2\rangle^2\right)\right|^2} \tag{6-92}$$

A sequence of antenna patterns for the linear four element array is given in Figures 6-13 for narrowband emitters and 6-14 for wideband emitters with 10 percent bandwidth. Again we note the predominant effect of bandwidth, namely that the array is no longer capable of reducing the output jammer power to the same degree as for the very narrowband environment.

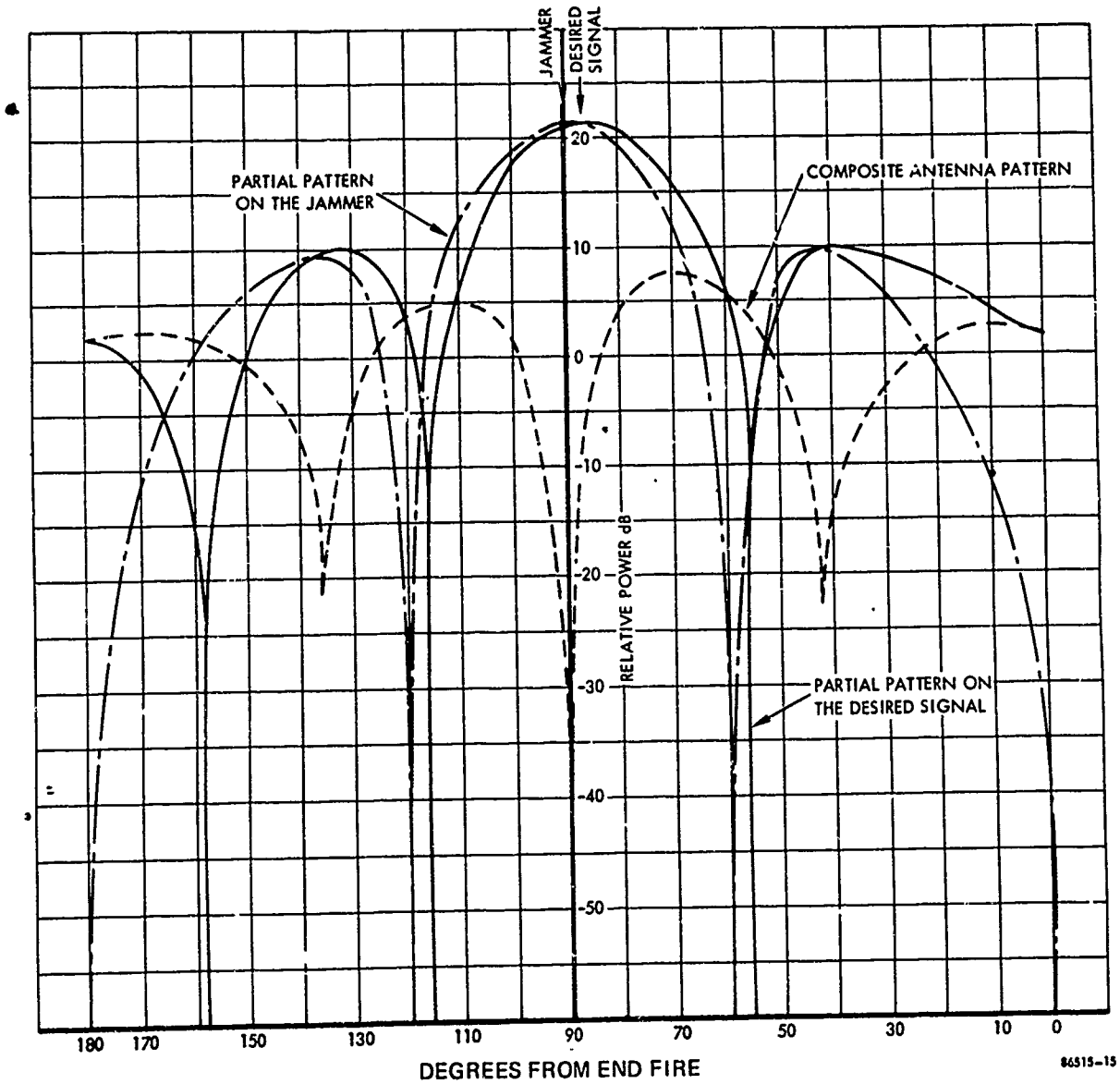


Figure 6-12. Antenna Pattern Decomposition

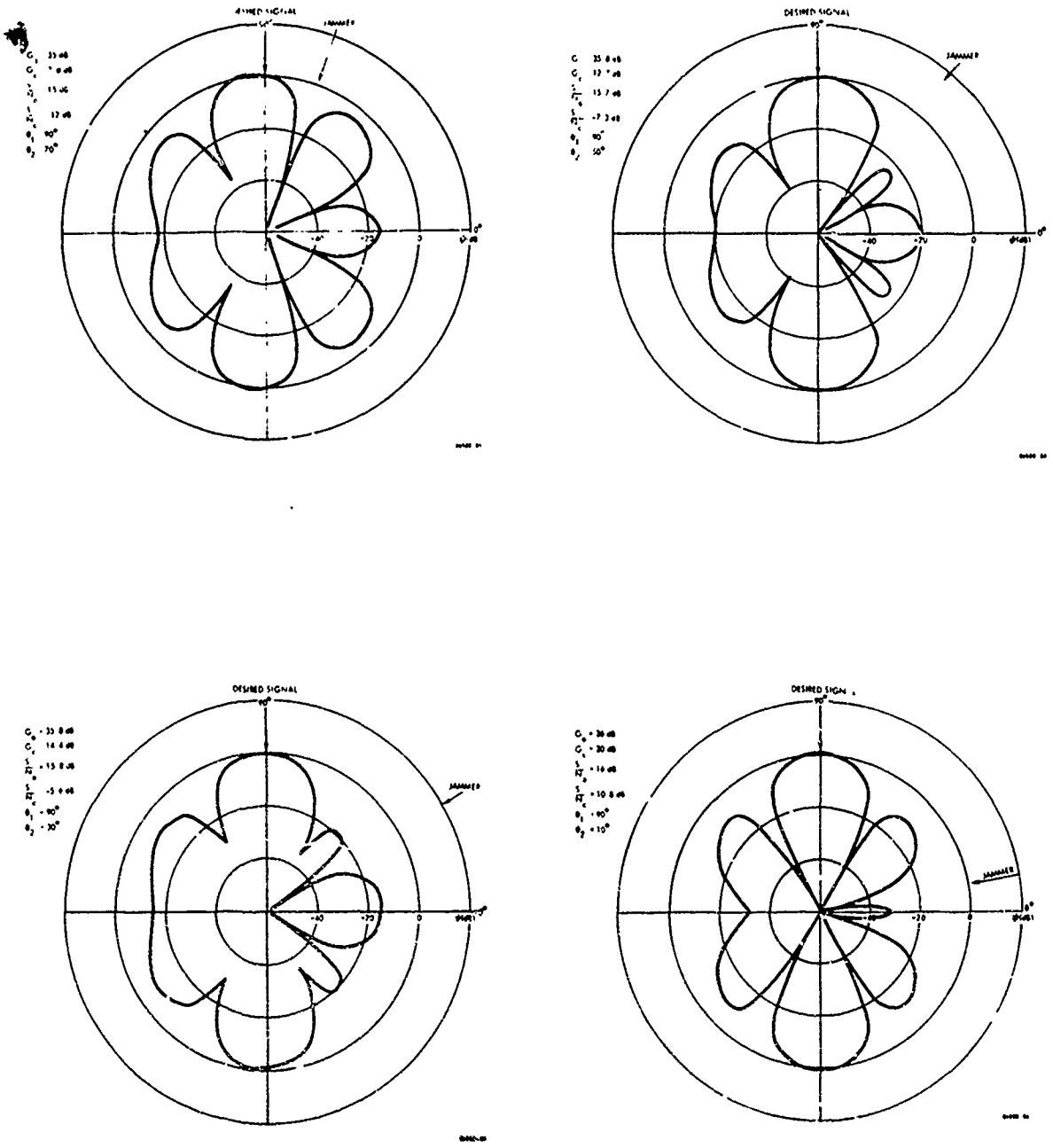


Figure 6-13. Antenna Patterns for Two Emitters with Very Narrow Bandwidth

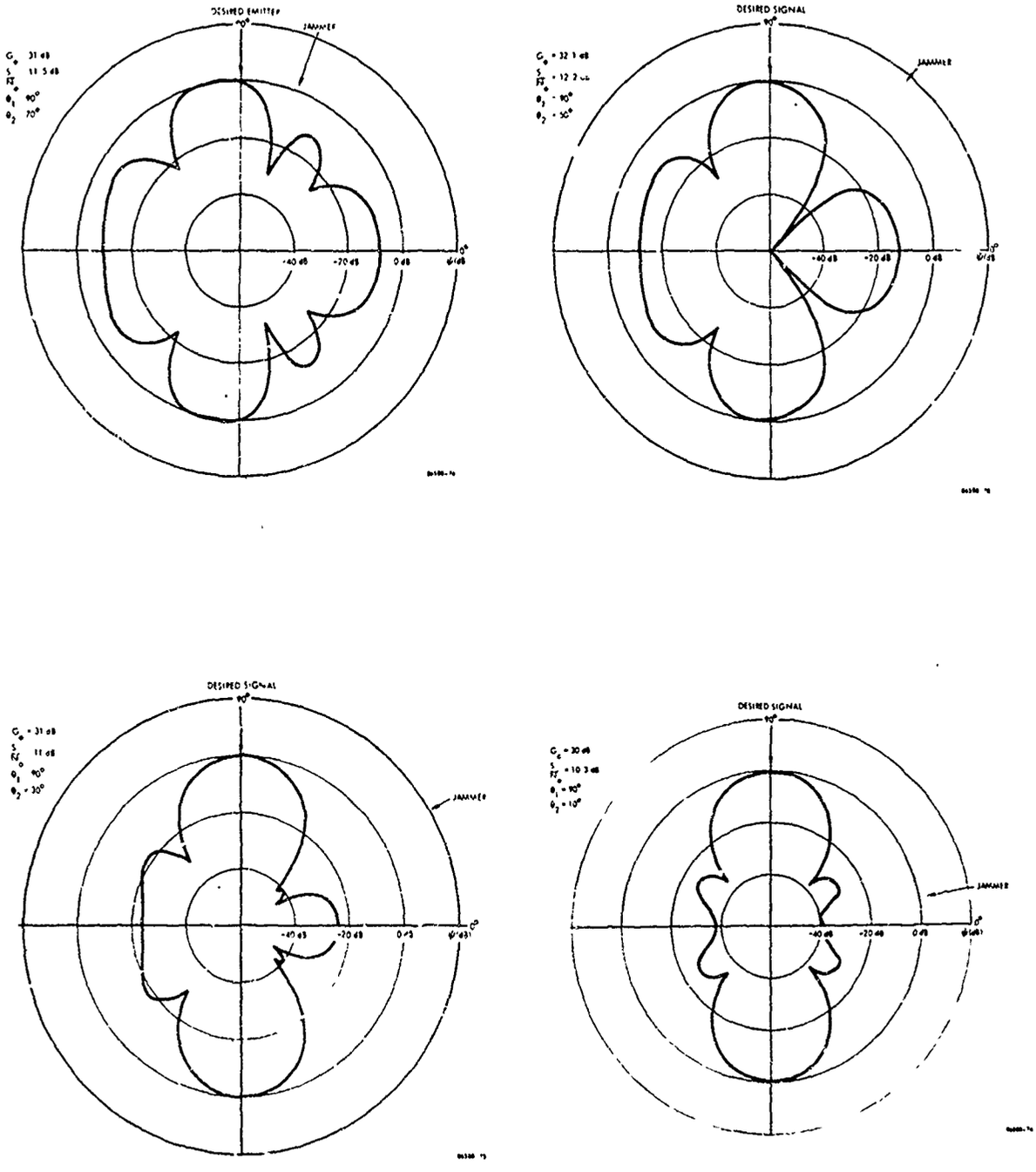


Figure 6-14. Antenna Patterns for Emitters with 10% Bandwidth

# CHAPTER 7

# ACQUISITION TECHNIQUES

## 7.0 ACQUISITION TECHNIQUES

In this chapter we shall address the difficult problem of acquiring a weak desired signal in the presence of strong jamming or interference by use of adaptive arrays. The intent is to develop a technique using adaptive arrays which will protect coded communication systems from strong jamming during the prelockup phase before code timing has been established.

One of the most notable researchers in adaptive null steering arrays is R. T. Compton, Jr., of Ohio State University . He formulated the initial concept of a power equalization technique for adaptive arrays which was based on proportional feedback control. He has shown that for a two-element array with two correlated CW signals and no thermal noise, the desired signal power and jamming power can be equalized, thus permitting matched filter acquisition of the desired signal of the array output. One of the most interesting features about this technique is that it requires no knowledge of the signal structures.

Although the signal and array model utilized by Dr. Compton was rather restrictive it at least demonstrated that it was possible to provide a favorable signal-to-jammer power ratio so that acquisition could be obtained. We have also addressed this problem and have analyzed and simulated different techniques which suppress dominant jammers to a point where acquisition of a weak desired signal is possible. This study was performed for arbitrary antenna arrays with wideband as well as narrowband signals in the presence of thermal noise.

Two models evolved during our study denoted by S1 and S2, and are shown in functional form in Figures 7-1 and 7-2 respectively. Initially, our investigation centered about the model S1 shown in Figure 7-1 with the absence of the bias signal $\eta$ and the steering command vector $z$. It was with this model that we demonstrated that in a narrowband environment strong emitters were suppressed below weak emitters at the array output which thus provided antijam protection for weak sources. In fact we shall show that the signal-to-jammer power ratio out of the array is proportional to the jammer-to-signal power ratio in one sensor. That is,

$$\frac{P_S}{P_J} = \beta\left(\frac{J}{S}\right) \qquad (7\text{-}1)$$

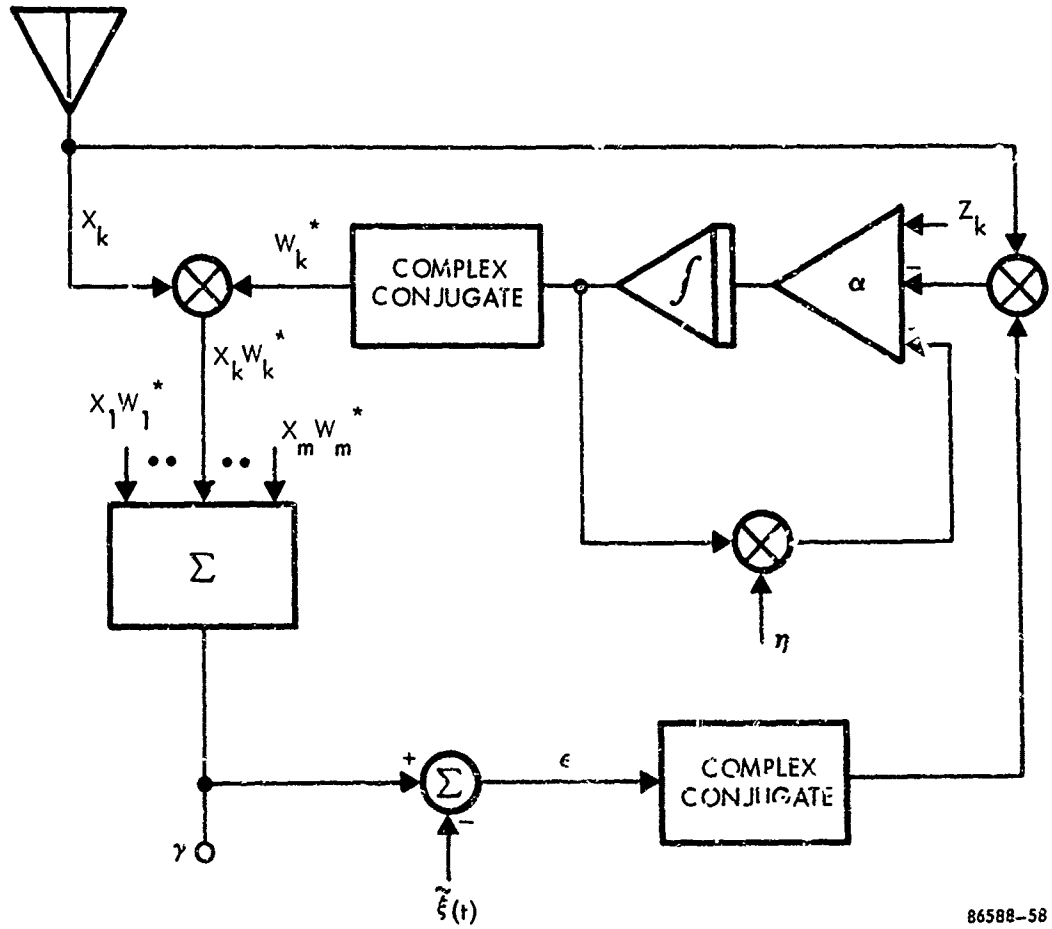


Figure 7-1. Functional Diagram of Model S1

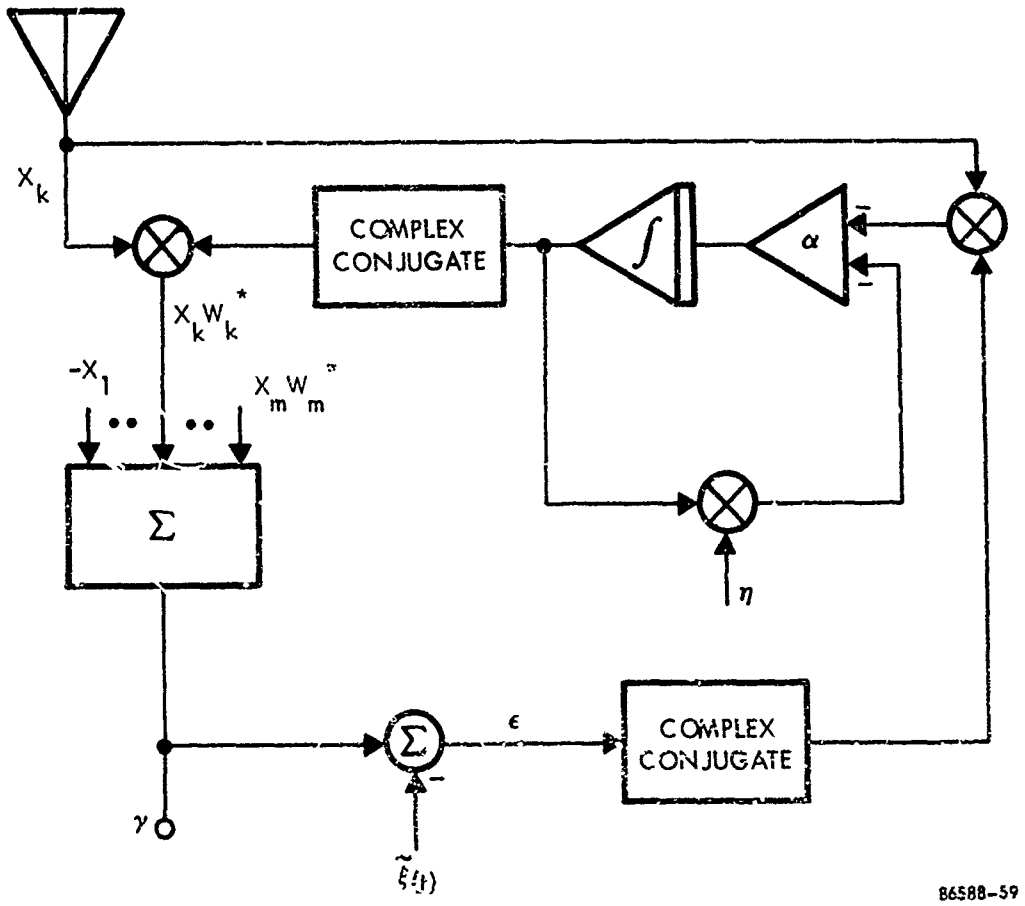


Figure 7-2. Functional Diagram of Model S2

where $\beta$ is a function of the number of antenna elements and the spatial factor of the array. The major drawback with this technique is that eventually $P_S$ and $P_J$ become zero which requires that the adaptive array must be reinitialized if acquisition is not obtained. Once acquisition is obtained, the demodulated coded carrier is used as the reference signal $\tilde{\xi}(t)$ in the array which then steers the array in the direction of the desired emitter while placing spatial nulls on the interfering sources.

## 7.1 Mathematical Analysis of Model 1

We now focus attention on the development of equation 1. Consider an arbitrary m element array in a narrowband environment consisting of a weak desired emitter and a strong interference source whose complex envelopes are denoted by $\xi(t)$ and $\zeta(t)$ respectively. If $x(t)$ denotes the m dimensional vector of signals entering the sensor elements then as developed in Chapter 2 we may write

$$x(t) = s(t) + n(t)$$

where

$$s(t) = \xi(t)v_1$$

$$n(t) = \zeta(t)v_2 + n_f(t)$$

given that $n_f(t)$ represents the vector valued thermal noise at the array input. In terms of these signals the complex envelope of the array output can be written as

$$\gamma(t) = \left[\sum_{k=1}^{m}(w_{1k} - jw_{2k})x_k\right](t)$$

or in the usual Euclidian inner product notation as

$$\gamma(t) = \langle w, x \rangle .$$

The error signal $\epsilon(t)$ formed by subtracting the reference signal $\tilde{\xi}(t)$ from $\gamma(t)$ is fed back into the system input. The integral control thus steers the array until $|\epsilon^2(t)|$ is minimized. In the absence of thermal noise $\epsilon(t)$ will become zero provided the reference signal exactly correlates with the desired signal. That is, perfect spatial nulls are placed on the unwanted interference sources.

Referring again to Figure 7-1 we see that the $k^{th}$ input signal $s_k$ is multiplied by $w_k^*$ and the result summed with the other weighted envelopes. The reference signal is now subtracted from this resultant forming the error $\epsilon$. In the absence of the reference signal as well as $\eta$ and z, the complex weight $w_k$ is governed by the differential equation

$$\frac{dw_k}{dt} = \alpha\epsilon^* x_k = -\alpha x_k \langle x, w \rangle ; \; k = 1, \ldots, m \tag{7-2}$$

or in vector notation as

$$\frac{dw}{dt} + \alpha x x^* w = 0; \; w(0) = w_o . \tag{7-3}$$

By controlling the weights in this fashion, the instantaneous magnitude of the squared error is minimized at every time t. This was accomplished by selecting $\frac{dw}{dt}$ to be equal to $-\nabla|\epsilon(t)|^2$ as developed in Chapter 4. That is, the weights move along the path of steepest descent. Normally, the bandwidth of the control circuitry is much smaller than the bandwidth of the complex envelopes. In this case the trajectory of the weights is sufficiently filtered so that w(t) is approximately equal to the average value of w(t) denoted by $\overline{w}(t)$. The average weights are then governed by equation (7-3) by taking the expectation over all the random variables resulting in

$$\frac{d\overline{w}}{dt} + \alpha R_x \overline{w} = 0 ; \overline{w}(0) = w_o \tag{7-4}$$

where $R_x$ is the covariance matrix defined by

$$R_x = E(R_x) . \tag{7-5}$$

Henceforth, we shall drop the $\overline{\phantom{w}}$ notation recognizing that we shall always be using average quantities.

If the initial weight vector $w_o$ is now selected so that the antenna pattern is initially omnidirectional, then the correlator output channel is dominated by the strong emitters. Intuitively speaking, the adaptive weights then initially move in a direction to reduce these strong emitters, the weaker signals being reduced later. Thus, there should be some point in time, say $t_1$, in which the array output consists primarily of the weakest signal. If it is known that the desired signal is weaker than the surrounding jamming sources, then there should be a significant time interval in which the signal-to-jamming power ratio is sufficient for acquisition.

Let us now focus attention on the solution of the vector differential equation 7-4 with

$$w_o = \begin{bmatrix} 1 \\ 0 \\ 0 \\ \vdots \\ 0 \end{bmatrix}$$

which describes the average array behavior. The approach used for this analysis is given in example 2 of Chapter 6 and we shall so draw from this example for this presentation.

From equations (6-48), (6-52), and (6-53) we see that the weight trajectory, output signal power and output jammer are given by

$$w(t) = \epsilon^{-\alpha\lambda_1 t} \frac{\langle c_1, w_o \rangle}{\| c_1 \|^2} c_1 + \epsilon^{-\alpha\lambda_2 t} \frac{\langle c_2, w_o \rangle}{\| c_2 \|^2} c_2$$

$$+ \epsilon^{-\alpha\lambda_3 t} \left[ w_o - \frac{\langle c_1, w_o \rangle}{\| c_1 \|^2} c_1 - \frac{\langle c_2, w_o \rangle}{\| c_2 \|^2} c_2 \right] \tag{7-6}$$

$$P_S(t) = S \left| \epsilon^{-\alpha\lambda_1 t} \frac{\langle c_1, w_o \rangle \langle c_1, v_1 \rangle}{\| c_1 \|^2} + \epsilon^{-\alpha\lambda_2 t} \frac{\langle c_2, w_o \rangle \langle c_2, v_1 \rangle}{\| c_2 \|^2} \right|^2 \tag{7-7}$$

and

$$P_J(t) = J \left| \epsilon^{-\alpha\lambda_1 t} \frac{\langle c_1, w_o \rangle \langle c_1, v_2 \rangle}{\| c_1 \|^2} + \epsilon^{-\alpha\lambda_2 t} \frac{\langle c_2, w_o \rangle \langle c_2, v_2 \rangle}{\| c_2 \|^2} \right|^2 \tag{7-8}$$

## 7.2 Large Jammer-to-Signal Power Approximation

The equations developed so far, although they are exact for our model, provide little insight into the problem we have been addressing. The desired goal is to obtain analytical expressions for $P_S$ and $P_J$ in terms of the signal power, jamming power, and relative angular displacements that are simple enough to permit an accurate interpretation of the behavior of the array without resorting to a detailed computer study. This is the problem we now address, the only assumptions being that $S \ll J$ and that the array is symmetrical about its geometric center. This last assumption is not necessary, but simplifies procedures since $\langle v_1, v_2 \rangle$ is now real.

Under these assumptions $\lambda_1 \gg \lambda_2 > \lambda_3$ and can be approximated by

$$\lambda_1 \approx \sigma^2 + mJ \left[ 1 + \frac{S}{J} \cdot \frac{\langle v_1, v_2 \rangle^2}{m^2} \right] \tag{7-9}$$

$$\lambda_2 \approx \sigma^2 + mS \left[ 1 - \frac{\langle v_1, v_2 \rangle^2}{m^2} - \frac{\langle v_1, v_2 \rangle^2}{m^2} \frac{S}{J} \right] \tag{7-10}$$

$$\lambda_3 = \sigma^2 \tag{7-11}$$

with a signal power and noise power given by

$$\begin{aligned} P_S \cong S \Big\{ & \left[ 1 - \frac{2}{m} \langle v_1, v_2 \rangle \cos(\phi_1 - \phi_2) + \frac{\langle v_1, v_2 \rangle^2}{m^2} \right] e^{-2\alpha\lambda_2 t} \\ & + 2 \frac{\langle v_1, v_2 \rangle}{m} \left[ \cos(\phi_1 - \phi_2) - \frac{\langle v_1, v_2 \rangle}{m} \right] e^{-\alpha(\lambda_1 + \lambda_2)t} + \frac{\langle v_1, v_2 \rangle^2}{m^2} e^{-2\alpha\lambda_1 t} \Big\} \end{aligned} \tag{7-12}$$

$$P_J \cong S\left(\frac{S}{J}\right)\frac{\langle v_1, v_2\rangle^2}{m^2}\left|1 - \frac{2}{m}\langle v_1, v_2\rangle\cos(\phi_1-\phi_2) + \frac{\langle v_1, v_2\rangle^2}{m^2}\right| e^{-\alpha\lambda_2 t}$$

$$+2S\frac{\langle v_1,v_2\rangle}{m}\left\{\frac{\langle v_1,v_2\rangle}{m}\left[1 - \frac{S}{J}\left(\frac{\langle v_1,v_2\rangle^2}{m^2} + 1\right)\right]\right.$$

$$\left. + \left(\frac{2S}{J}\frac{\langle v_1, v_2\rangle^2}{m^2} - 1\right)\cos(\phi - \phi_2)\right\} e^{-2\alpha(\lambda_1+\lambda_2)t}$$

$$+ J\left\{\left[1 - \frac{S}{J}\frac{\langle v_1, v_2\rangle^2}{m^2}\right]^2 + \frac{\langle v_1,v_2\rangle^2}{m^2}\left(\frac{S}{J}\right)^2\right.$$

$$\left. + 2\left[1 - \frac{\langle v_1, v_2\rangle^2}{m^2}\right]\frac{S}{J}\frac{\langle v_1, v_2\rangle}{m}\cos(\phi_1 - \phi_2)\right\} e^{-2\alpha\lambda_1 t} \qquad (7\text{-}13)$$

where $\phi_i = \frac{2\pi}{\lambda_c}\langle a_i, b_1\rangle$ ; $i = 1,2$.

When $S/J \ll 1$ terms involving $e^{-\alpha(\lambda_1+\lambda_2)t}$ and $e^{-\alpha 2\lambda_1 t}$ decay very rapidly compared with the term containing $e^{-\alpha 2\lambda_2 t}$. Thus, after a short period of time say $t_1$, the signal power exceeds the jamming power, the expressions being given by

$$P_S = S\left\{1 - \frac{2}{m}\langle v_1, v_2\rangle\cos(\phi_1 - \phi_2) + \frac{\langle v_1, v_2\rangle^2}{m^2}\right\} e^{-2\alpha\lambda_2 t} \qquad (7\text{-}14)$$

$$P_J = S\left(\frac{S}{J}\right)\frac{\langle v_1, v_2\rangle^2}{m^2}\left\{1 - \frac{2}{m}\langle v_1, v_2\rangle^2\cos(\phi_1 - \phi_2) + \frac{\langle v_1, v_2\rangle^2}{m^2}\right\} e^{-2\alpha\lambda_2 t} \quad ; t > t_1 \qquad (7\text{-}15)$$

These equations illustrate that the jamming power is suppressed relative to the signal power by the ratio

$$\frac{P_S}{P_J} = \left(\frac{J}{S}\right)\frac{m^2}{\langle v_1, v_2\rangle^2} \qquad (7\text{-}16)$$

Thus over the time interval in which $t > t_1$ not only is the jammer suppressed below the signal by at least the same amount it exceeded the signal before adaptation of the array, but it is also reduced by the square of the normalized spatial factor. The processing gain obtained in this fashion cannot be achieved for all angular displacements between the jammer and desired emitter since it is limited by the basic resolution of the array. That is, as the emitter and jammer become closer with respect to the array, the term

$$1 - \frac{2}{m}\langle v_1, v_2\rangle \cos(\phi_1 - \phi_2) + \frac{\langle v_1, v_2\rangle^2}{m^2} \tag{7-17}$$

reflects the degradation of $P_S$ due to proximity of the jammer, whereas

$$\frac{\langle v_1, v_2\rangle^2}{m^2}\left\{1 - \frac{2}{m}\langle v_1, v_2\rangle \cos(\phi_1 - \phi_2) + \frac{\langle v_1, v_2\rangle^2}{m^2}\right\} \tag{7-18}$$

reflects the degradation of $P_J$ due to the proximity of the desired signal. For a four element array with half wavelength spacing as shown in Figure 7-3, we have plotted the two expressions given by (7-17) and (7-18) in Figures 7-4 and 7-5 in order to place proper perspective on the influence of the azimuth of the two emitters on $P_S$ and $P_J$.

It is also of interest to note that $P_S(t)$ and $P_J(t)$ are even functions of the difference in the angles of arrival of the two signals and therefore exchanging location of the weak emitter with the strong jammer has no effect on $P_S(t)$ and $P_J(t)$.

For the purposes of illustrating the time behavior of an adaptive array, we will again focus attention on a four element linear array with half wavelength spacing between sensors. We shall examine the case when the desired signal makes an angle of $\theta_1 = 70^\circ$ with $S/\sigma^2 = 10$ whereas the jammer has an angle $\theta_2 = 60^\circ$ with $J/\sigma^2 = 1000$. Figure 7-6 illustrates the time response of the array in terms of $P_S(t)/\sigma^2$ and $P_J(t)/\sigma^2$. We note that the desired signal power relative to the noise variance dominates the array output after $t \simeq 3/\alpha\lambda_1$ and remains about 27 dB above the jammer power over the useful time which terminates when $P_S$ drives below thermal noise at $t \simeq 400/\alpha\lambda_1$. We point out that for linear adaptive arrays this desired performance that has been exhibited in this example deteriorates as $\theta_1$ and $\theta_2$ approach zero. This is because the array places a much wider null on jammer when it is close to endfire and thus greatly reduces the gain in the direction of the desired emitter. Finally, Figure 7-7 illustrates the time history of the antenna pattern. Significant from this figure is the formation of the deep null in the direction of the strong emitter.

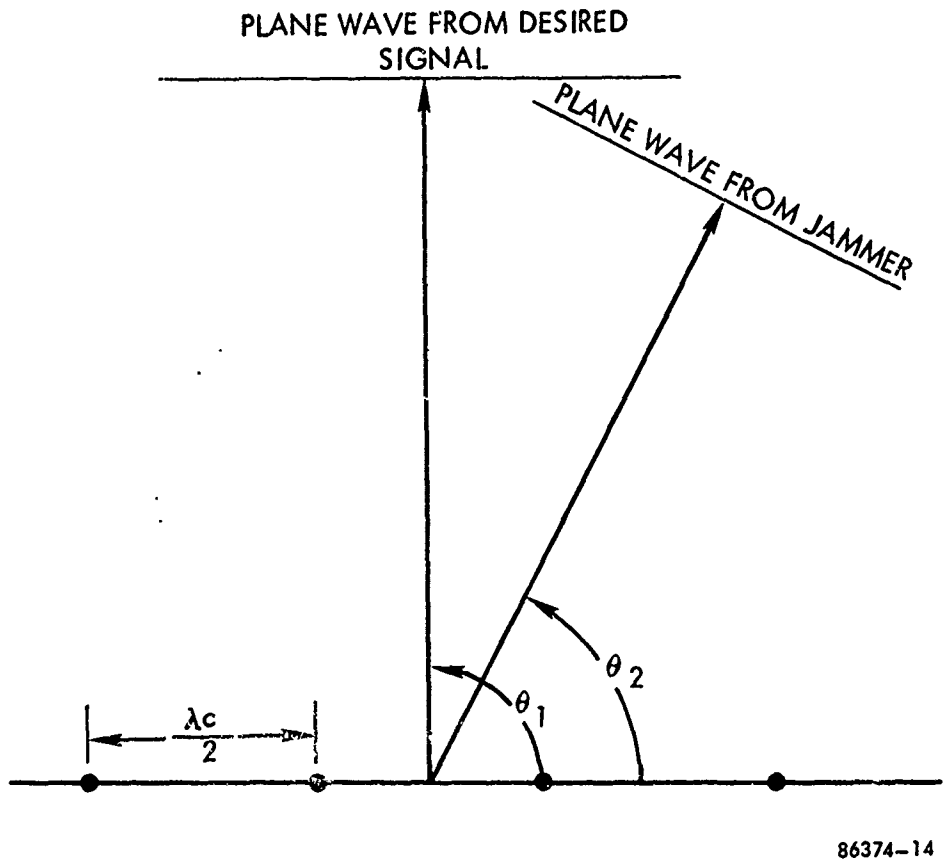


Figure 7-3. Geometry of the Signal and Jammer Impinging on a Linear Array

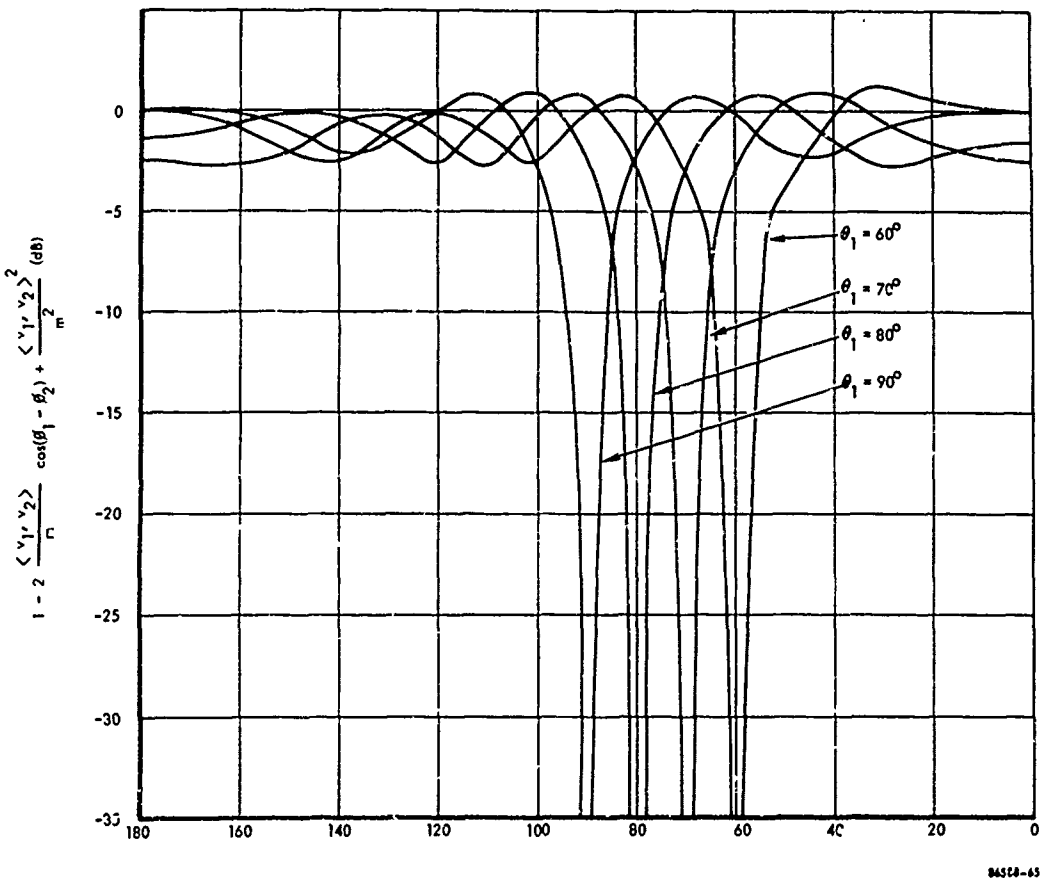


Figure 7-4. Desired Signal Degradation Factor

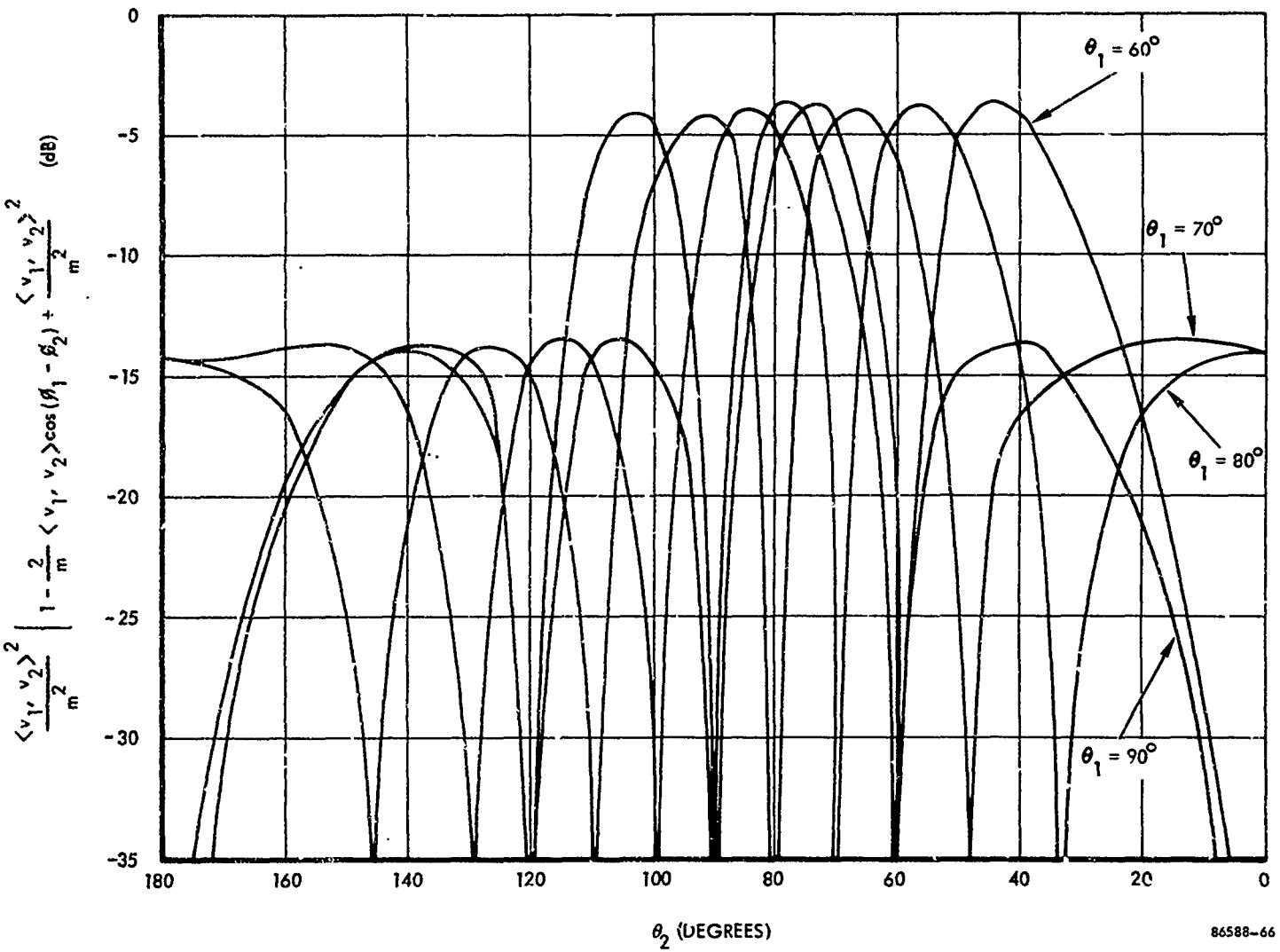


Figure 7-5. Jammer Degradation Factor

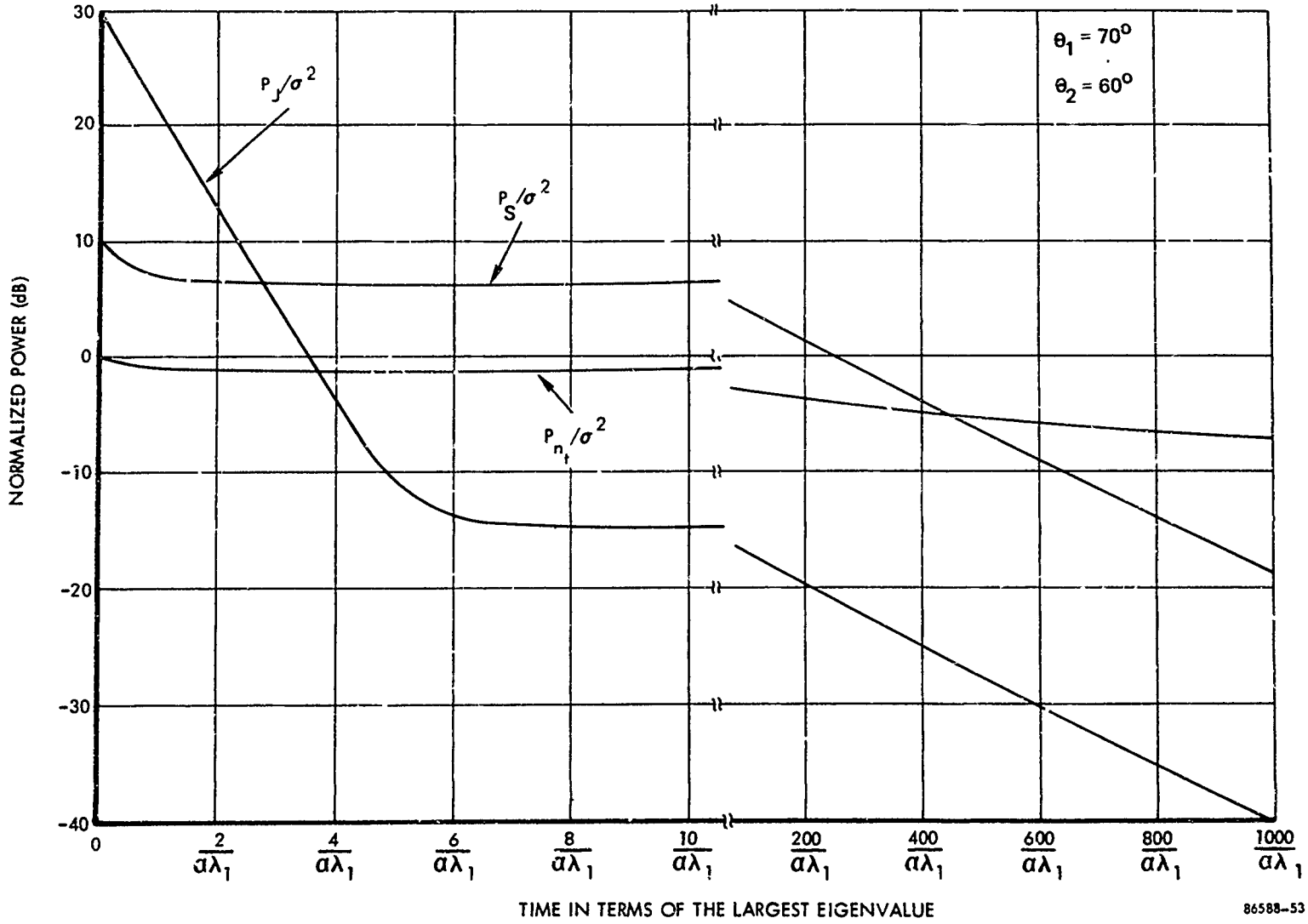


Figure 7-6. Transient Response of Model S1 for Very Narrowband Signals with $\delta = 0$ and $\eta = 0$

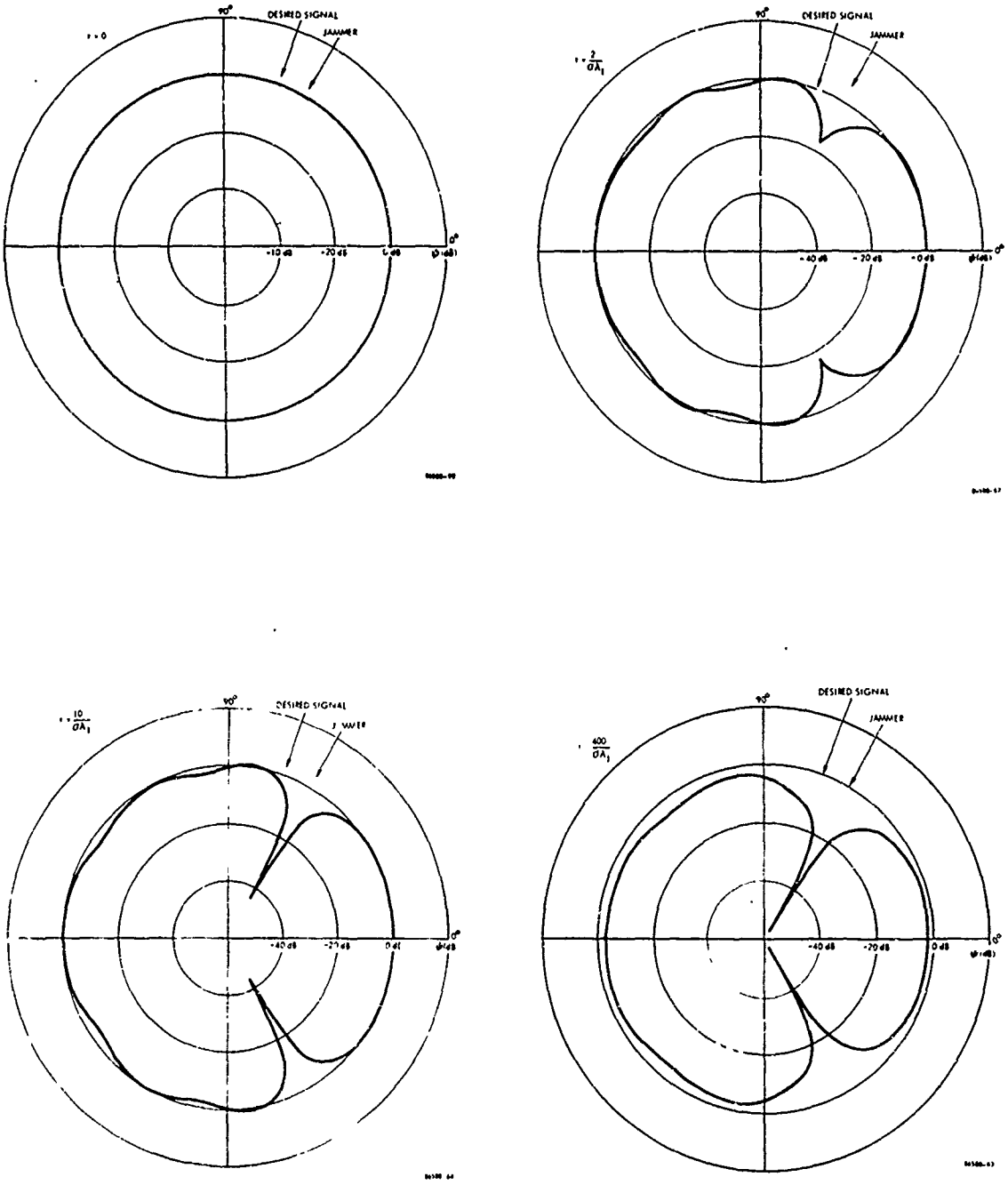


Figure 7-7. Antenna Pattern Time Behavior

## 7.3 Analysis of Two Acquisition Models

The obvious undesirable feature of the adaptive circuitry just analyzed is that the weights tend towards zero. Thus, if acquisition is not obtained shortly, the array must be reinitialized and the process repeated.

To eliminate this undesirable characteristic two similar but different approaches were evaluated. These approaches center around models S1 and S2 with the absence of the bias signal $\eta$ which shall be discussed shortly. In reference to model S1 a steering command $z$ was applied to the adaptive circuitry which has the form

$$z = \begin{bmatrix} \delta \\ 0 \\ \vdots \\ 0 \end{bmatrix}$$

where $\delta$ is an arbitrary gain, whereas in model S2 one of the weights was fixed to one. Thus at steady state neither model turns off, and in the absence of directional sources the two models are equivalent in the sense that they both have omnidirectional antenna patterns.

The differential equations describing the average behavior of the weights for the two models are rather similar and are given by

$$\text{S1:}\ \frac{dw}{dt} + \alpha R_x w = \alpha z \ ; \ w(0) = \begin{bmatrix} \delta \\ 0 \\ \vdots \\ 0 \end{bmatrix} \tag{7-19}$$

$$\text{S2:}\ \frac{dw}{dt} + \alpha R'_x w = \alpha r \ ; \ w(0) = \begin{bmatrix} 0 \\ 0 \\ \vdots \\ 0 \end{bmatrix} \tag{7-20}$$

where the $(m-1)\times(m-1)$ matrix $R'_x$ and the $m-1$ dimensional vector $r$ are given respectively by

$$R'_x = E\left\{ \begin{bmatrix} x_2 \\ \vdots \\ x_m \end{bmatrix} \begin{bmatrix} x_2^*, \ldots, x_m^* \end{bmatrix} \right\} \tag{7-21}$$

$$r = E\left\{ x_1^* \begin{bmatrix} x_2 \\ \vdots \\ x_m \end{bmatrix} \right\} \tag{7-22}$$

### 7.3.1 Analysis of Model S1

To ascertain the trajectory of the weights and in fact the behavior of the array in a narrowband environment we will again consider the effect of one strong jammer and a weak desired signal and compare the responses of the arrays. We first focus on Model S1. The weight trajectory for this model can be computed from equation (7-19) and is given by

$$w(t) = [e^{-\alpha\lambda_1 t} + \frac{\delta}{\lambda_1}(1-e^{-\alpha\lambda_1 t})]E_1 w_o + [e^{-\alpha\lambda_2 t} + \frac{\delta}{\lambda_2}(1-e^{-\alpha\lambda_2 t})]E_2 w_o$$

$$+ [e^{-\alpha\lambda_3 t} + \frac{\delta}{\lambda_3}(1-e^{-\alpha\lambda_3 t})]E_3 w_o \tag{7-23}$$

with the resulting output signal power, jamming power and thermal noise given by

$$P_S = S\left|\langle w, v_1\rangle\right|^2 \tag{7-24}$$

$$P_J = J\left|\langle w, v_2\rangle\right|^2 \tag{7-25}$$

and

$$P_{n_t} = \sigma^2 \left\| w \right\|^2 \tag{7-26}$$

Since $\lambda_1 >> \lambda_2$ and since $E_3 v_1 = E_3 v_2 = 0$, we can easily see that after a short period of time the output powers are given by

$$P_S = S \left| \frac{\delta}{\lambda_1} <E_1 w_o, v_1> + [e^{-\alpha\lambda_2 t} + \frac{\delta}{\lambda_2}(1-e^{-\alpha\lambda_2 t})] <E_2 w_o, v_1> \right|^2 \tag{7-27}$$

$$P_J = J \left| \frac{\delta}{\lambda_1} < E_1 w_o, v_2> + [e^{-\alpha\lambda_2 t} + \frac{\delta}{\lambda_2}(1-e^{-\alpha\lambda_2 t})] < E_2 w_o, v_2> \right|^2 \tag{7-28}$$

Thus, the signal and jamming power approach steady state at a rate dependent primarily on $\lambda_2$ which is primarily proportional to the desired signal power. Thus, the stronger the jammer the less effect it has on the rate at which the output powers reach steady state. As $t \to \infty$ the model reaches steady state which for this system is given by

$$P_S = S\delta^2 \left| \frac{1}{\lambda_1} < E_1 w_o, v_1> + \frac{1}{\lambda_2} < E_2 w_o, v_1> \right|^2 \tag{7-29}$$

$$P_J = J\delta^2 \left| \frac{1}{\lambda_1} < E_1 w_o, v_2> + \frac{1}{\lambda_2} < E_2 w_o, v_2> \right|^2 \tag{7-30}$$

Upon substitution of the eigenvalues and evaluation of the innerproducts, we arrive at

$$P_S = \frac{S\left(\frac{\delta}{\sigma^2}\right)^2 \left\{ 1 + 2\left(\frac{mJ}{\sigma^2}\right)\left[1 - \frac{<v_1, v_2>}{m}\cos(\phi_2 - \phi_1)\right] + \left(\frac{mJ}{\sigma^2}\right)^2 \left[1 + \frac{<v_1, v_2>^2}{m^2} - 2\frac{<v_1, v_2>}{m}\cos(\phi_1 - \phi_2)\right]\right\}}{\left[1 + \frac{mS}{\sigma^2} + \frac{mJ}{\sigma^2} + \left(\frac{mS}{\sigma^2}\right)\left(\frac{mJ}{\sigma^2}\right)\left(1 - \frac{<v_1, v_2>^2}{m^2}\right)\right]^2} \tag{7-31}$$

$$P_J = \frac{J\left(\frac{\delta}{\sigma^2}\right)^2 \left\{ 1 + 2\left(\frac{mS}{\sigma^2}\right)\left[1 - \frac{<v_1, v_2>}{m}\cos(\phi_2 - \phi_1)\right] + \left(\frac{mS}{\sigma^2}\right)^2 \left[1 + \frac{<v_1, v_2>^2}{m^2} - 2\frac{<v_1, v_2>}{m}\cos(\phi_1 - \phi_2)\right]\right\}}{\left[1 + \frac{mS}{\sigma^2} + \frac{mJ}{\sigma^2} + \left(\frac{mS}{\sigma^2}\right)\left(\frac{mJ}{\sigma^2}\right)\left(1 - \frac{<v_1, v_2>^2}{m^2}\right)\right]^2} \tag{7-32}$$

It is interesting to note from these two equations that if $J/\sigma^2$ and $S/\sigma^2$ are large, then

$$\frac{P_S}{P_J} \approx \frac{J}{S} \quad .$$

That is, at steady state the output signal-to-jammer power ratio is inversely proportional to signal-to-jammer power at one antenna element. Hence, under this assumption, we will have certainly achieved our goal of providing a favorable condition for matched filter detection provided that $P_S$ is not buried below the output thermal noise. However, under this given assumption

$$P_S \approx \frac{S\left(\frac{\delta}{\sigma^2}\right)^2\left[1 - 2\frac{\langle v_1, v_2\rangle}{m}\cos(\phi_1 - \phi_2) + \frac{\langle v_1, v_2\rangle^2}{m^2}\right]}{\left[1 + \frac{mS}{\sigma^2}\left(1 - \frac{\langle v_1, v_2\rangle^2}{m^2}\right)\right]^2} \tag{7-33}$$

which approaches the value

$$P_J = \frac{\frac{\delta}{m}\left(\frac{\sigma^2}{mS}\right)^2\left[1 - 2\frac{\langle v_1, v_2\rangle}{m}\cos(\phi_1 - \phi_2) + \frac{\langle v_1, v_2\rangle^2}{m^2}\right]}{\left(1 - \frac{\langle v_1, v_2\rangle^2}{m^2}\right)^2} \tag{7-34}$$

as $S/\sigma^2$ becomes large. Thus, the larger the desired signal the smaller the output signal power. The same is true, of course, for the jammer. Hence, it appears that unless the output thermal noise is becoming small $P_S$ may well be below $P_{n_t}$ at steady state. To ascertain whether or not this is the case we shall now obtain an approximate solution for $P_{n_t}$ at steady state under the assumption that $S/J$ is much less than one.

Consider the following chain of equalities

$$P_{n_t} = \sigma^2 \|w\|^2 \tag{7-35}$$

$$= \sigma^2\delta^2 \langle R_x^{-1} w_o, R_x^{-1} w_o\rangle = \sigma^2 \langle w_o, R_x^{-2} w_o\rangle \tag{7-36}$$

$$= \sigma^2\delta^2 \langle w_o, \frac{1}{\lambda_1^2} E_1 w_o + \frac{1}{\lambda_2^2} E_2 w_o + \frac{1}{\lambda_3^2} E_3 w_o\rangle \tag{7-37}$$

where $E_i$ again represents the orthogonal projection on the $i^{th}$ eigenspace. Simplifying this equation we arrive at

$$P_{n_t} \cong \frac{\delta^2}{\sigma^2} \left\{ 1 - \left[ \frac{2\left(\frac{J}{\sigma^2}\right) + m\left(\frac{J}{\sigma^2}\right)^2}{1 + 2m\left(\frac{J}{\sigma^2}\right) + \left(\frac{mJ}{\sigma^2}\right)^2} \right] - \right.$$

$$\frac{\left(1 - 2\frac{\langle v_1, v_2\rangle}{m}\cos(\phi_1 - \phi_2) + \frac{\langle v_1, v_2\rangle^2}{m^2}\right)\left[2\left(\frac{S}{\sigma^2}\right) + m\left(\frac{S}{\sigma^2}\right)^2\left(1 - \frac{\langle v_1, v_2\rangle^2}{m^2}\right)^2\right]}{\left(1 - \frac{\langle v_1, v_2\rangle^2}{m^2}\right)\left[1 + 2m\left(\frac{S}{\sigma^2}\right)\left(1 - \frac{\langle v_1, v_2\rangle^2}{m^2}\right) + \left(\frac{mS}{\sigma^2}\right)^2\left(1 - \frac{\langle v_1, v_2\rangle^2}{m^2}\right)^2\right]} \tag{7-38}$$

As the signal power increases it is easily seen that $P_{n_t}$ approaches the nonzero value

$$P_{n_t} = \frac{\delta^2}{\sigma^2} \left\{ 1 - \frac{2\left[1 - \frac{\langle v_1, v_2\rangle}{m}\cos(\phi_1 - \phi_2)\right]}{m\left(1 - \frac{\langle v_1, v_2\rangle^2}{m^2}\right)} \right\} . \tag{7-39}$$

Thus, it is evident that for a desired signal input power, which is much larger than the input sensor noise, the output signal-to-thermal-noise power may be very small. One approach to overcome this difficulty would clearly be to decrease the depth of the nulls on both the desired signal as well as the jammer in order to raise $P_S$ and $P_J$ above output thermal noise at steady state. That is, we shall rectify this bad situation by forcing the antenna pattern to be more omnidirectional. This is precisely the purpose of the bias signal $\eta$. By inserting the bias signal into each adaptive loop we are essentially increasing the effective thermal noise. Mathematically, this can be seen by evaluating the differential equations with the presence of bias. Consider for example the $k^{th}$ loop, the equation describing its behavior is given by

$$\frac{dw_k}{dt} = -\alpha x_k^* \langle x, w\rangle - \alpha\eta w_k + \alpha z_k \; ; \; k = 1, \ldots, m . \tag{7-40}$$

In vector form these equations become

$$\frac{dw}{dt} = -\alpha(R_x + \eta I)w + \alpha z \ , \tag{7-41}$$

hence, an effective covariance matrix can be written as

$$R_{eff} = R_x + \eta I = (\sigma^2 + \eta) I + S v_1 v_1^* + J v_2 v_2^* \ . \tag{7-42}$$

If $\eta$ is made very large then $R_{eff}$ is essentially diagonal which then yields a steady state antenna pattern which is omnidirectional. Thus, by varying $\eta$ we can vary the depth of the spatial nulls placed on both emitters with slight effect on the output thermal noise, as well as vary the convergence time of the array.

The effect of the bias can be seen by replacing $\sigma^2$ with $\sigma^2 + \eta$ in equations (7-31) and (7-32), and evaluating the resulting output signal power and jamming power. If S/J is much less than one and $S/\sigma^2$ is large compared to one, then the output power ratio can be varied from

$$\frac{P_S}{P_J} = \frac{J}{S} \quad \text{for} \quad \eta = 0 \tag{7-43}$$

to

$$\frac{P_S}{P_J} = \frac{S}{J} \quad \text{for} \quad \eta = \infty \ . \tag{7-44}$$

Thus, the price we pay for improving the ratio of $P_S/P_{n_t}$ is the reduction of $P_S/P_J$. However, even if $P_S/P_J$ were somewhat less than one, there would normally be an adequate amount of processing gain in the matched filter to provide acquisition.

With these concepts in hand let us consider a situation where $\eta$ is chosen so that $S/(\sigma^2+\eta)$ is now much less than one whereas $J/(\sigma^2+\eta)$ is still much greater than one. Again by replacing $\sigma^2$ with $\sigma^2+\eta$ in equations (7-31) and (7-32) and making the obvious approximations we arrive at

$$P_S \cong S\left(\frac{\delta}{\sigma^2+\eta}\right)^2 \left[1 - 2\frac{\langle v_1, v_2\rangle}{m} \cos(\phi_1 - \phi_2) + \frac{\langle v_1, v_2\rangle^2}{m^2}\right] \tag{7-45}$$

$$P_J \cong \frac{\delta^2}{m^2 J} \tag{7-46}$$

whereas the output thermal noise can be shown to be

$$P_{n_t} = \left(\frac{\sigma\delta}{\sigma^2+\eta}\right)^2 (1 - 1/m) \tag{7-47}$$

Thus, it is evident that the output signal-to-jammer power ratio can be wrriten as

$$\frac{P_S}{P_J} \approx \left(\frac{mS}{\eta}\right)\left(\frac{mJ}{\eta}\right)\left[1 - 2\frac{\langle v_1, v_2\rangle}{m}\cos(\phi_1 - \phi_2) + \frac{\langle v_1, v_2\rangle^2}{m^2}\right] \tag{7-48}$$

with a signal-to-thermal-noise power ratio of

$$\frac{P_S}{P_{n_t}} = \frac{S}{\sigma^2}\;\frac{\left[1 - 2\frac{\langle v_1, v_2\rangle}{m}\cos(\phi_1 - \phi_2) + \frac{\langle v_1, v_2\rangle^2}{m^2}\right]}{1 - 1/m}\,. \tag{7-49}$$

From equations (7-48) and (7-49) we can conclude that if $J/S \gg 1$ then a bias signal bounded by

$$S \ll \eta \leq m\sqrt{SJ} \tag{7-50}$$

will ensure that

$$P_S > P_J\left[1 - 2\frac{\langle v_1, v_2\rangle}{m}\cos(\phi_1 - \phi_2) + \frac{\langle v_1, v_2\rangle^2}{m^2}\right]. \tag{7-51}$$

Thus, if the bias signal is chosen to be somewhat larger than the desired signal power entering a sensor, then regardless of how large the jammer, a very favorable power ratio exists for acquisition both in terms of $P_S/P_J$ and $P_S/P_{n_t}$. This is of course provided that the two emitters are separated far enough so that

$$\left[1 - 2\frac{\langle v_1, v_2\rangle}{m}\cos(\phi_1 - \phi_2) + \frac{\langle v_1, v_2\rangle^2}{m^2}\right] \tag{7-52}$$

is not close to zero. Recall that Figure 7-6 illustrates the effect of this term for a four element linear array with half wavelength spacing. From Figure 7-8 we see the response of the array with the addition of the steering vector with $\frac{\delta}{\sigma^2} = 1$ and no bias whereas Figure 7-9 illustrates the array response with $\frac{\delta}{\sigma^2} = 100$ and a bias signal of $\eta = 100$.

### 7.3.2 Analysis of Model S2

In this section we will focus our attention on Model S2 and determine the transient and steady state performance for the two emitter environments considered previously and compare the results obtained for Model S1. If we initially make $\eta$ zero, then recalling the differential equation for this model is given by

$$\frac{dw}{dt} + \alpha R_x' w = \alpha r \quad ; \quad w(0) = \begin{bmatrix} 0 \\ 0 \\ \cdot \\ \cdot \\ 0 \end{bmatrix} \tag{7-53}$$

we can easily write down the solution as

$$w(t) = \frac{1}{\lambda_1}(1 - e^{-\alpha\lambda_1 t}) E_1 r + \frac{1}{\lambda_2}(1 - e^{-\alpha\lambda_2 t}) E_2 r + \frac{1}{\lambda_3}(1 - e^{-\alpha\lambda_3 t}) E_3 r \tag{7-54}$$

where r is given by equation (7-22).

To simplify our discussion we shall select as our reference point the geometrical center of the m-1 antenna elements with unconstrained weights and assume that these antennas are symmetrical about this point. In this case r is given by

$$r = e^{i\phi_{11}} S v_1 + e^{i\phi_{21}} J v_2 \tag{7-55}$$

where

$$v_1 = \begin{bmatrix} e^{-i\phi_{12}} \\ \cdot \\ \cdot \\ \cdot \\ e^{-i\phi_{1m}} \end{bmatrix} \quad ; \quad v_2 = \begin{bmatrix} e^{-i\phi_{22}} \\ \cdot \\ \cdot \\ \cdot \\ e^{-i\phi_{2m}} \end{bmatrix}$$

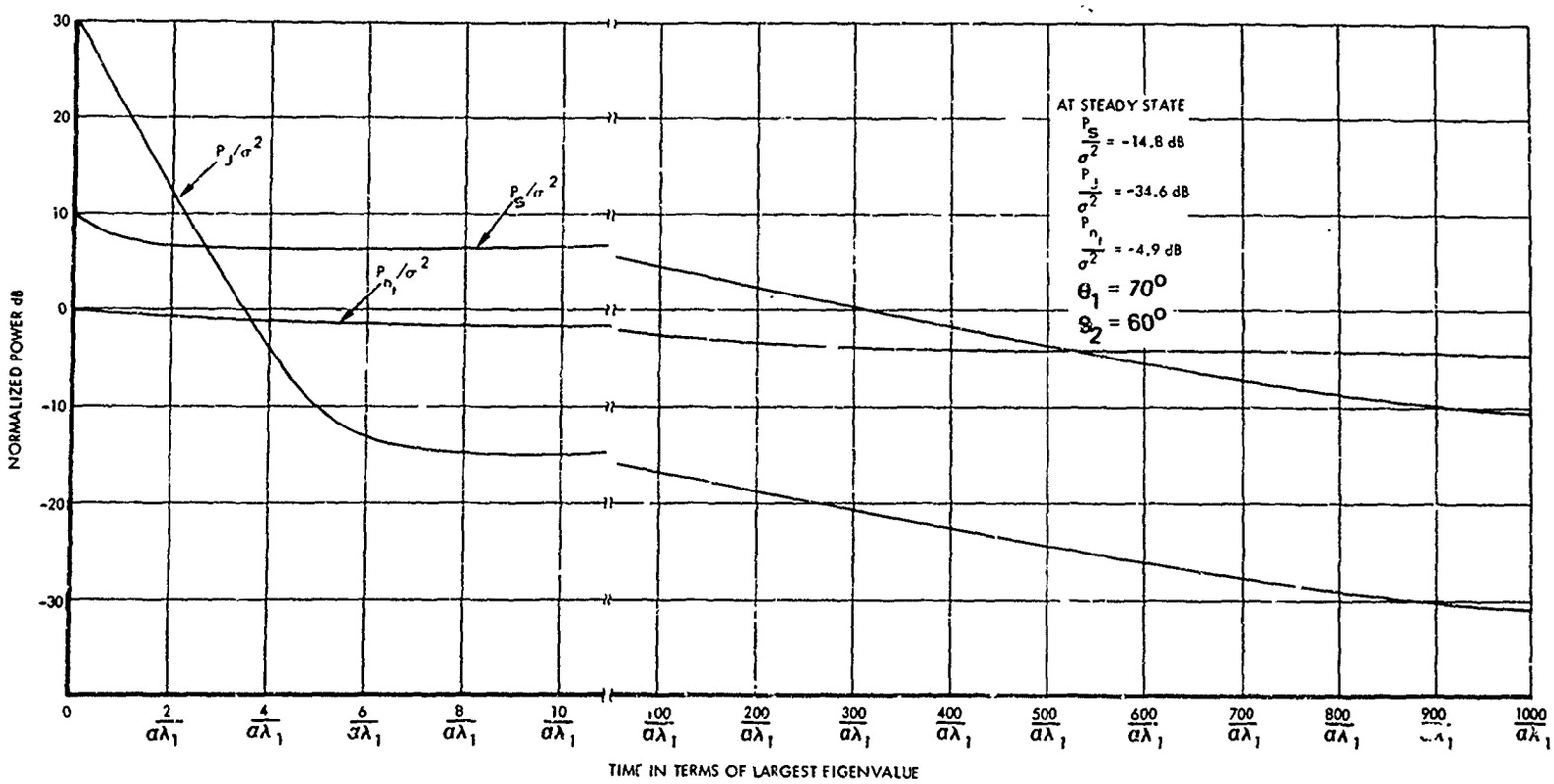


Figure 7-8. Transient Response of Model S1 for Very Narrowband Signals with $\frac{\xi}{\sigma^2} = 1$ and $\eta = 0$

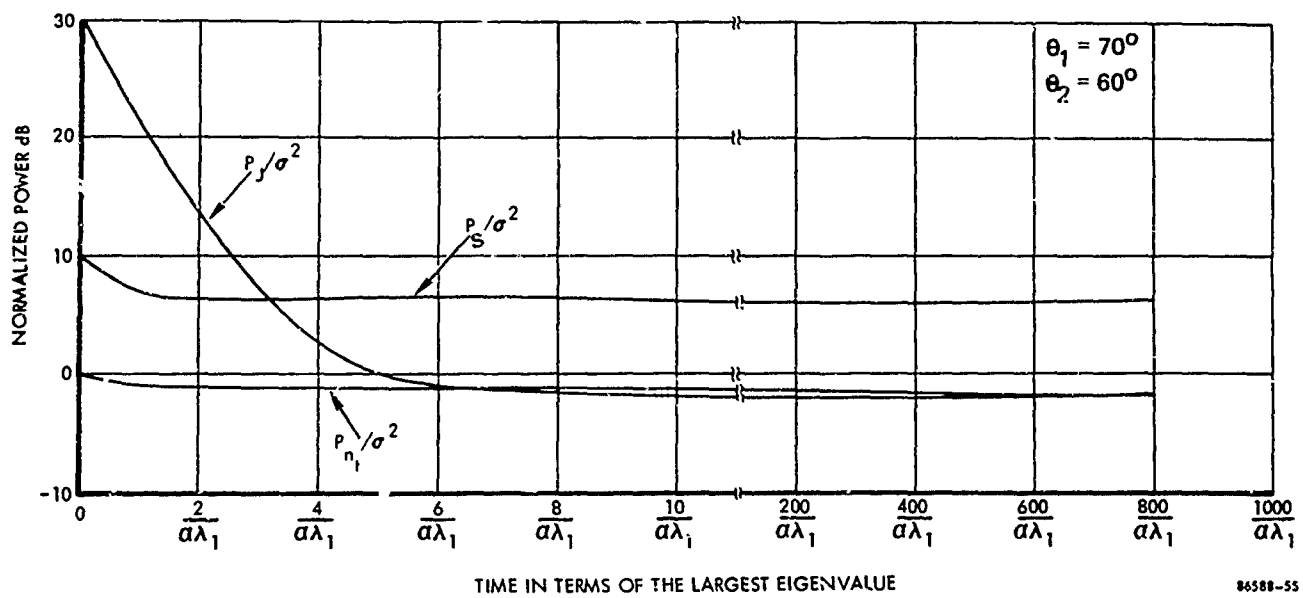


Figure 7-9. Transient Response of Model S1 for Very Narrowband Signals with $\frac{\delta}{\sigma^2} = 100$ and $\eta = 100$

where $\phi_{ij} = \frac{2\pi}{\lambda_c} < a_i, b_j >$, and where the eigenvalues and eigenvectors can be obtained from equations (7-37) through (7-40) with m replaced with m-1. The corresponding time response of this system is very similar to model S1 when only the steering vector with $\frac{S}{\sigma^2} = 1$ is applied, as is evident from Figure 7-10. The steady state powers are very nearly the same also. To demonstrate this analytically we recall that

$$P_S = S\left|<w, v_1> - e^{+j\phi_{11}}\right|^2 = S\left|<\frac{1}{\lambda_1}E_1 r + \frac{1}{\lambda_2}E_2 r + \frac{1}{\lambda_3}E_3 r, v_1> - e^{+j\phi_{11}}\right|^2 \tag{7-56}$$

$$P_J = J\left|<w, v_2> - e^{+j\phi_{21}}\right|^2 = J\left|<\frac{1}{\lambda_1}E_1 r + \frac{1}{\lambda_2}E_2 r + \frac{1}{\lambda_3}E_3 r, v_2> - e^{+j\phi_{21}}\right|^2 \tag{7-57}$$

and

$$P_{n_t} = \sigma^2 \left(1 + \|w\|^2\right). \tag{7-58}$$

Performing the indicated innerproducts we obtain

$$P_S = \frac{S\left[1 + 2\frac{m'J}{\sigma^2}\left[1 - \frac{<v_1, v_2>}{m'}\cos(\phi_{11} - \phi_{21})\right] + \left(\frac{m'J}{\sigma^2}\right)\left(1 - 2\frac{<v_1, v_2>}{m'}\cos(\phi_{11} - \phi_{21}) + \frac{<v_1, v_2>^2}{m'^2}\right)\right]}{\left[1 + \frac{m'S}{\sigma^2} + \frac{m'J}{\sigma^2} + \left(\frac{m'S}{\sigma^2}\right)\left(\frac{m'J}{\sigma^2}\right)\left(1 - \frac{<v_1, v_2>^2}{m'^2}\right)\right]^2} \tag{7-59}$$

$$P_J = \frac{J\left[1 + 2\frac{m'S}{\sigma^2}\left[1 - \frac{<v_1, v_2>}{m'}\cos(\phi_{11} - \phi_{21})\right] + \left(\frac{m'S}{\sigma^2}\right)^2\left(1 - 2\frac{<v_1, v_2>}{m'}\cos(\phi_{11} - \phi_{21}) + \frac{<v_1, v_2>^2}{m'^2}\right)\right]}{\left[1 + \frac{m'S}{\sigma^2} + \frac{m'J}{\sigma^2} + \left(\frac{m'S}{\sigma^2}\right)\left(\frac{m'J}{\sigma^2}\right)\left(1 - \frac{<v_1, v_2>^2}{m'^2}\right)^2\right]} \tag{7-60}$$

and for the large jammer-to-signal power ratios the output thermal noise is

$$P_{n_t} = \sigma^2 \left\{1 + m'\left[\left(\frac{S}{\sigma^2}\right) + 2\left(\frac{S}{\sigma^2}\right)\left(\frac{J}{\sigma^2}\right)\frac{<v_1, v_2>}{m'}\cos(\phi_{11} - \phi_{21}) + \left(\frac{J}{\sigma^2}\right)^2\right] - \right.$$

$$m' \frac{2\left(\frac{m'J}{\sigma^2}\right)+\left(\frac{m'J}{\sigma^2}\right)^2}{1+2m\left(\frac{J}{\sigma^2}\right)+\left(\frac{m'J}{\sigma^2}\right)^2}\left[\left(\frac{J}{\sigma^2}\right)^2+2\left(\frac{J}{\sigma^2}\right)\frac{\langle v_1, v_2\rangle}{m'}\cos(\phi_{11}-\phi_{21})+\left(\frac{S}{\sigma^2}\frac{\langle v_1, v_2\rangle}{m'^2}\right)\right]-$$

$$m'\left(\frac{S}{\sigma^2}\right)^2\left[1-2\frac{\langle v_1, v_2\rangle}{m'}\cos(\phi_{11}-\phi_{21})+\frac{\langle v_1, v_2\rangle^2}{m'^2}\right]\left[2\left(\frac{m'S}{\sigma^2}\right)\left(1-\frac{\langle v_1, v_2\rangle^2}{m'^2}\right)+\left(\frac{m'S}{\sigma^2}\right)^2\bullet\right.$$

$$\left.\left(1-\frac{\langle v_1, v_2\rangle^2}{m'^2}\right)^3\right] \qquad (7\text{-}61)$$

where $m'$ denotes m-1. Comparing equations (7-59) and (7-60) with equations (7-31) and (7-32) we note that they have exactly the same form and thus model S2 behaves in almost exactly the same way as model S1 at steady state. Thus model S2 has a similar acquisition performance with the addition of the bias signal as does S1. Figure 7-11 illustrates the behavior of model S2 with a bias signal in the two emitter environments. It is of interest to compare this result with that of model S1 given in Figure 7-8 and note how similor they are.

Throughout all of our analysis in this section we have focused on signals whose complex envelopes are very narrow band. The reason for this restriction was the fact that the covariance matrices had a very unique structure which was utilized to our fullest advantages. As the bandwidth increases the signals diffuse across the array, the matrix becomes more sparse, making an analytical approach very difficult if not impossible for an arbitrarily large array. It was hoped that the analysis presented here would lend some insight into environments consisting of wider band emitters. Although a detailed analysis of the behavior of adaptive arrays in wideband environments will be presented in the next chapter we now present the time behavior of model S2 in an environment of two wideband emitters. These emitters have a constant power spectral density over a relative bandwidth of 10 percent, with respect to the carrier. The total power relative to thermal noise per sensor for the jammer is 1000 whereas that of the desired signal is 10. Figure 7-12 shows the time response for model S2 with a bias of 100 with Figure 7-13 illustrating the time behavior of the antenna pattern. We see that even for this case acquisition is still possible even though the effects of the wider bandwidth relatively deteriorated the model's performance.

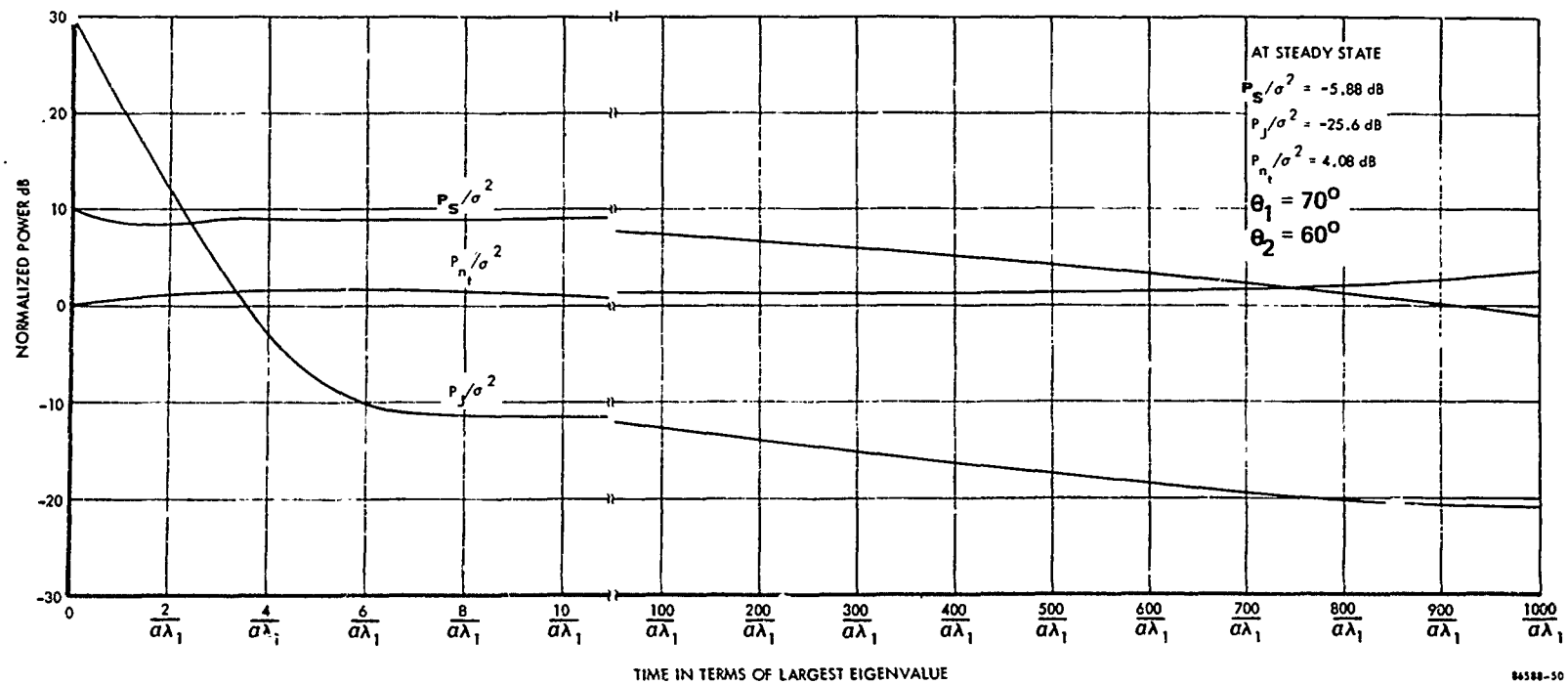


Figure 7-10. Transient Response of Model S2 for Very Narrowband Signals with $\eta = 0$

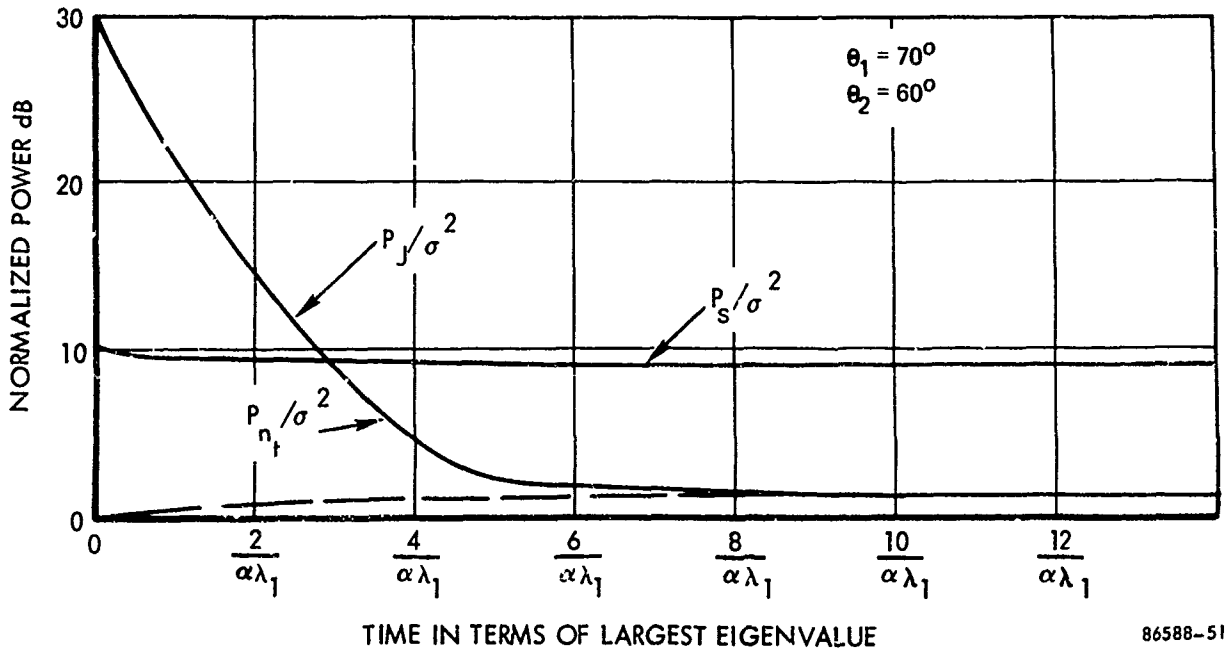


Figure 7-11. Transient Behavior of Model S2 for Very Narrowband Signals with $\eta = 100$

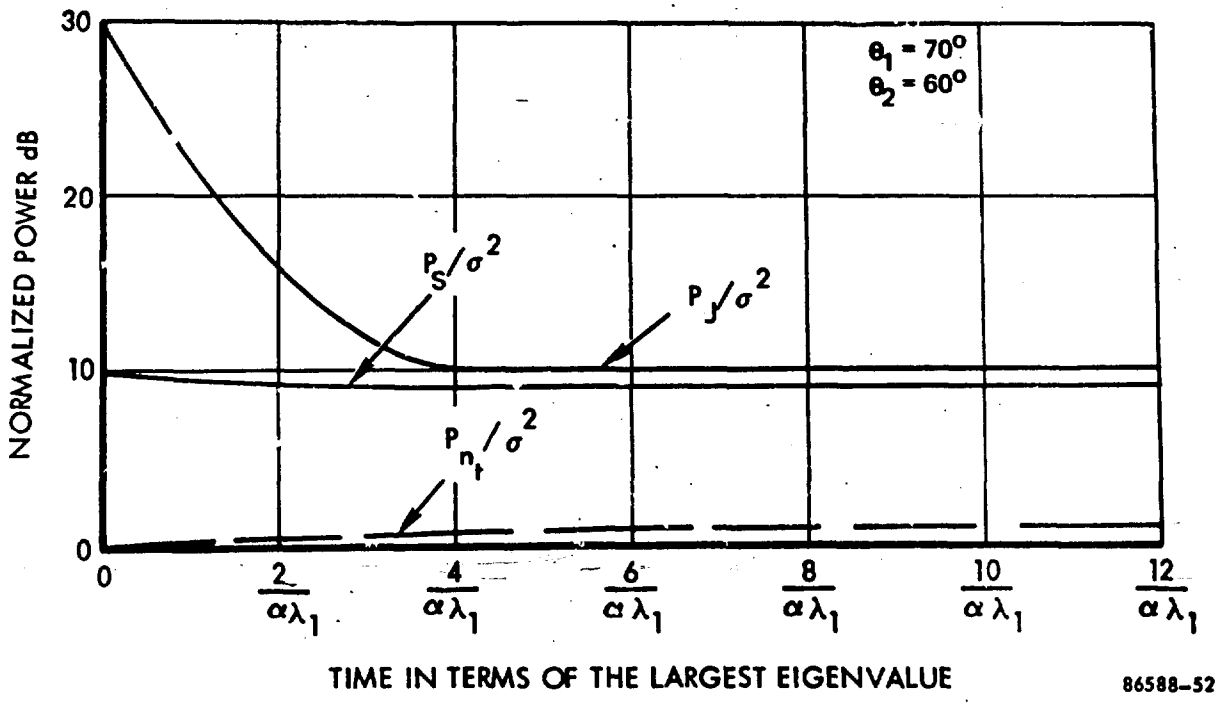


Figure 7-12. Transient Behavior of Model S2 for Signals of 10% Bandwidth with $\eta = 100$

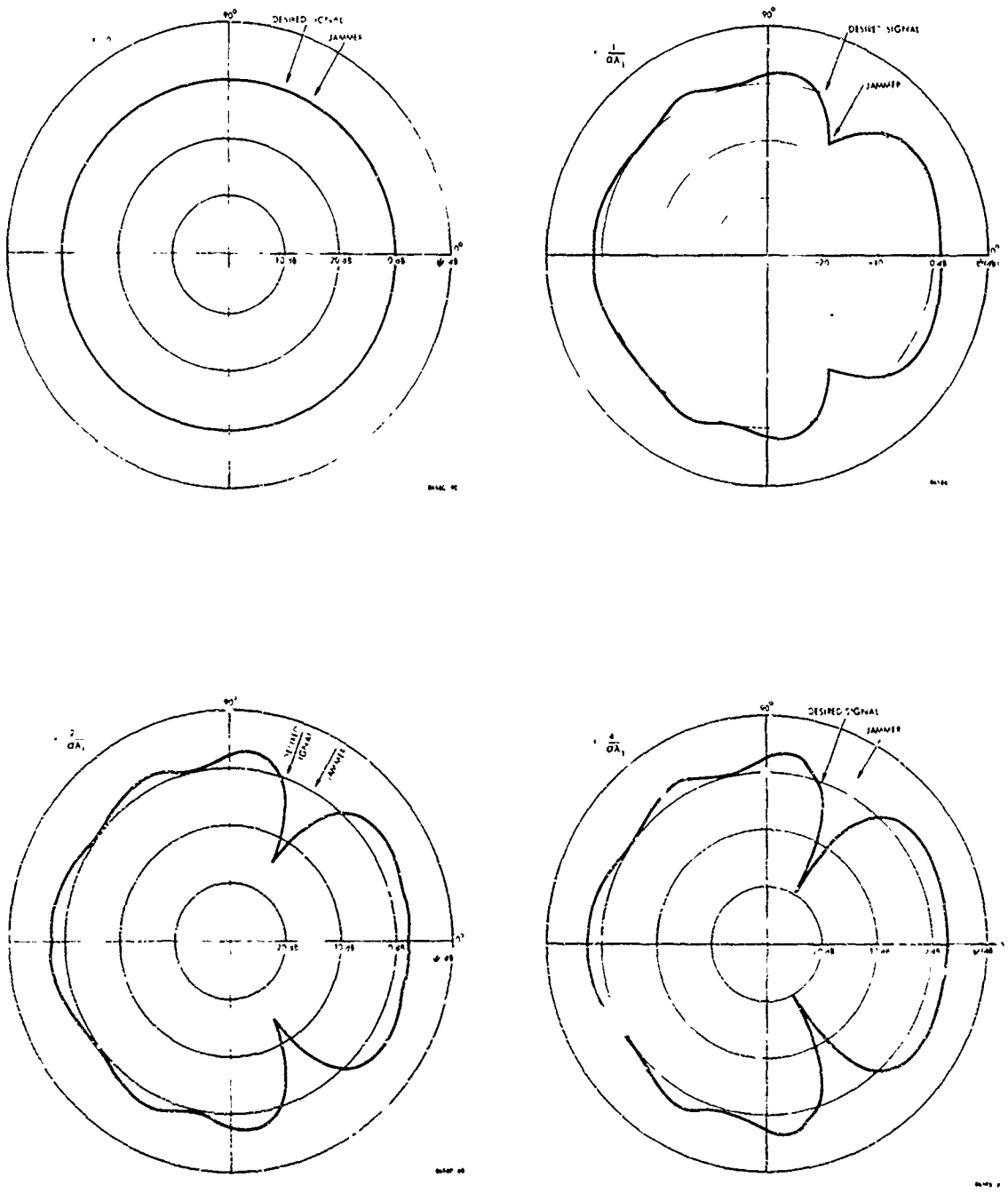


Figure 7-13. Antenna Pattern Time Behavior for 10% Bandwidth Signals

# CHAPTER 8

# PARAMETRIC STUDIES OF ADAPTIVE ARRAYS

## 8.0 PARAMETRIC STUDIES OF ADAPTIVE ARRAYS

In the preceding chapters, the theoretical basis for adaptive null-steering arrays was covered, and some numerical examples were given. It is the purpose of this chapter to show more detailed and numerous numerical studies of the effects of the various parameters of an adaptive null-steering array. In particular some parameters will be emphasized.

a. Bandwidth

b. Jamming power

c. Signal power when present

d. Angle(s) of arrival

e. Multiplicity of jammers

f. Number of array elements

g. Bias level

The case of a single jammer will be emphasized because this simple (but very important) case will illustrate the basic response of an adaptive array; the multiple jammer studies shown bear out that jammer null depth is not seriously affected by multiple jammers.

Also, for simplicity, one weight constraint was used almost exclusively in this study, that of the left weight fixed at one value (-1). Chapter 7 has covered the relation between this fixed weight constraint and other possible constraints or forcing functions used to keep the weighrs from going to zero. Also, the initial condition is always $w_o = (-1.0, 0.0, 0.0)$, unless otherwise stated.

As a final simplification, most of this chapter will concentrate on the Biased Jammer Suppression Technique for suppressing a dominant jammer before a signal is acquired. The reasons for this emphasis are:

a. The acquisition period is the most difficult time to make use of the null steerer.

b. The "Known-Signal" algorithms (such as the LMS array) have already been investigated to some extent, whereas the Jammer Suppression concept is new.

c. Control of nulls on jammers is much simpler and more straightforward when the jammer can be isolated, such as in the error signal of an LMS algorithm; in the Jammer Suppression technique, the tradeoff between signal and jammer loss is more critical.

d. There are time delay problems with implementing LMS algorithms, especially for many coded signal sources, while the biased suppression technique appears much simpler to implement.

Several significant simplifications in the parametric studies can be made. It has been shown theoretically and numerically that if a jammer is much larger than a desired signal (i.e., "dominant jamming power") and angularly separated from the signal, then the transient and steady state behavior of the output jamming power is essentially unaffected by the small signal level. Thus, for the jammer suppression technique, a jammer may be studied without the signal present and, most important, without categorizing signal parameters. This is not true for the Widrow algorithm, which must maximize the signal. It also does not apply when the number of unremoved signals exceeds the number of array elements.

The following paragraphs will cover:

8.1 Transient Behavior of the Biased Jammer Suppression Technique

8.2 Steady State Jammer Null De in the Biased Jammer Suppression Technique

8.3 Steady State Output Signal and Signal-to-Noise Improvement with the Biased Suppression Technique

8.4 Known-Signal (LMS Algorithm) Adaptive Array Behavior

8.5 Overspecified Arrays (Numerous Unremoved Signals)

8.6 Polarization Considerations

The calculations done in this chapter were done with programs developed on internal research and not part of this contract, although results of these programs are being made available herein. The basic transient computation is a numerical eigenvalue calculation and the steady state values are from numerical calculations of the Wiener-Hopf equation. The numerical solutions were required because the analytical solution approach of Chapters 6 and 7 cannot be used for finite bandwidth or numbers of emitters greater than 2-3.

## 8.1 Transient Behavior Biased Jammer Suppression

Although most of the results in this chapter deal with steady state performance, it is important to begin with several examples of transient performance in addition to those provided in Chapter 7.

### 8.1.1 Typical Results Using Eigenvalue Solutions (vs Angle, Bandwidth and Bias)

An example of the effect of angle-of-arrival on transient performance of an adaptive array using the Jammer Suppression Technique is shown in Figure 8-1. This plot is similar to those in Chapter 7. Relative output power vs relative time is shown for both the signal and jammer. The powers are relative to output thermal noise, $P_{n_t}$, which is plotted at 0 dB. Note that some plots in Chapter 7 and a few in this section are relative to input thermal noise, $\sigma^2$. The time is relative to the fastest (smallest) time constant in the eigenvalue solution, $\tau = \frac{1}{\alpha\lambda_1}$. This time will be related to absolute time later in this section. Time is plotted linearly to 10 units, then logarithmically to $10^4$ units. In this example, signal is plotted starting at 10 dB while jamming starts at 30 dB. These starting values represent the input values, $\frac{S}{\sigma^2}$, $\frac{J}{\sigma^2}$ at each omnidirectional element, with the initial condition of only one element "ON" (one non-zero weight). Two cases of jammer angle are plotted in Figure 8-1, $\theta_j = 45^\circ$ and $60^\circ$. For both cases, as shown, the number of elements m = 3*, the signal angle $\theta_s = 70^\circ$, the bandwidth BW = .12. In both, the jammer is quickly suppressed to about the signal level. The signal behavior depends upon the jammer-signal separation angle and initial signal-to-noise ratio, as discussed in the very narrow band case in Chapter 7. For the jammer at $60^\circ$, the signal is quickly suppressed 5 dB along with the jammer; for the $45^\circ$ jammer, signal actually rises slightly for the first ten time constants.

However, neither the signal nor jammer output is close to the steady state values at 10-100 time constants, as shown in the right-hand portion of Figure 8-1. Both signal and jammer experience ≈ 15 dB further loss to below thermal noise with very slow time constants being controlled by the very small eigenvalues which are related to thermal noise.

In summary, three significant points are to be noted from Figure 8-1:

a. The dominant jammer is rapidly suppressed to the desired signal level in this and most other cases. Thus, after a short time, signal acquisition using matched filter gain becomes more feasible.

* Throughout this section the number of elements is denoted by either m or M interchangeably.

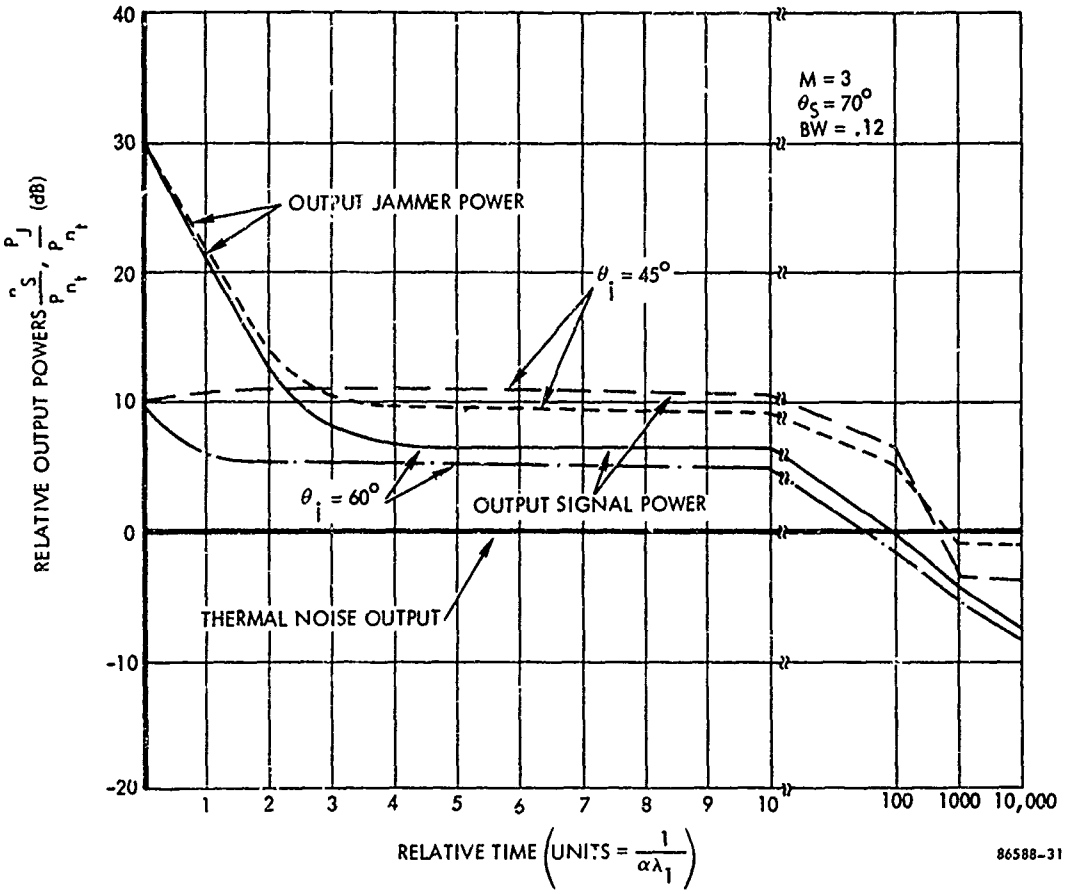


Figure 8-1. Output Powers vs Time Effect of Angle of Arrival (Biased Jammer Suppression, M = m = number of elements, $\eta = 0$)

b. After several hundred time constants, both signal and jammer are suppressed below thermal noise. Thus, simply calculating signal-to-jammer ratios in the steady state is not indicative of whether the signal can be acquired. Thermal noise must be included in the calculation.

c. If the signal and jammer are close together, the signal will be suppressed more rapidly and further than if it were widely separated from the jammer. This is because the signal is in the null being formed on the jammer.

The same kind of plot is used in the next six figures. Figure 8-2 shows the effect upon biased suppression of bandwidth changes. In this case, nine elements were used and a jammer 40 dB above thermal noise was assumed. The bias level was made approximately equal to the signal level to prevent deep signal nulling in the steady state. The bias level probably makes little difference on the first part of the transient behavior; however, a bandwidth change from 1 percent to 12 percent with nine elements drastically changes the initial behavior of the jammer suppression. With a 1 percent bandwidth, the jammer is suppressed rapidly to the signal level, as in most cases studied. With a 12 percent bandwidth, the jammer is suppressed only 10 dB until 100 time units. An explanation for this may be clearer later when a frequency response plot of a null is shown; simply put, the null is not wideband enough to prevent some dispersed jamming energy from entering the array. This dispersed energy appears to act like thermal noise, without a direction of arrival; just as high thermal noise causes jamming to level off at a high value, the jamming in this case levels off initially at a very high level.

The effect of transient performance upon bias level changes is shown in Figure 8-3, for the case of $m = 9$, $\theta_s = 70^\circ$, $\theta_j = 45^\circ$, and BW = .01. Bias level, $\eta$, relative to thermal noise, is in the three cases 0, $9\sigma^2$, and $99\sigma^2$, so that $\frac{S}{\sigma^2+\eta} = 10$ dB, 0 dB, and -10 dB, respectively.

The three cases show essentially the same performance, except in the steady state, where signal is much greater with respect to jamming and thermal noise as bias is increased.

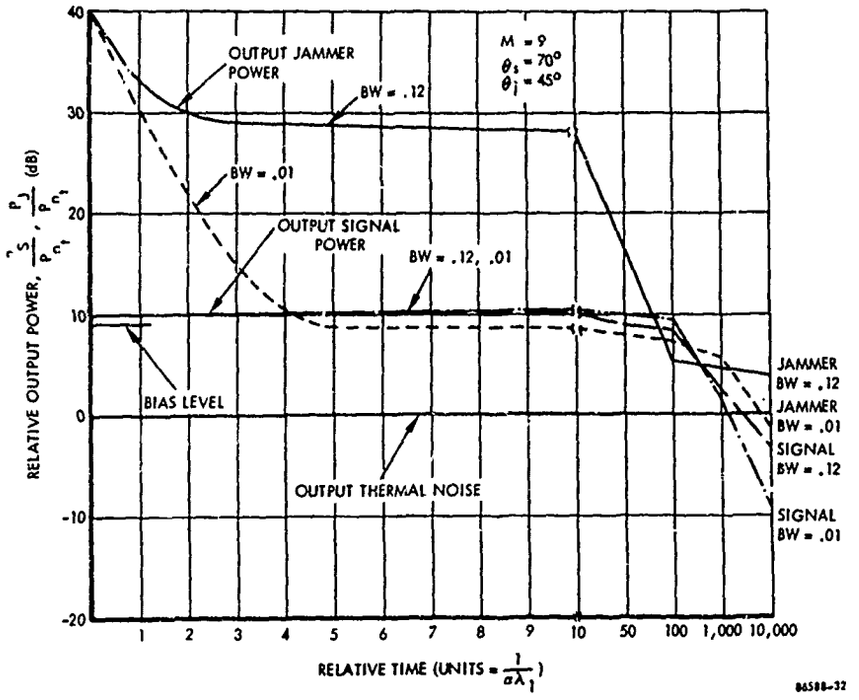


igure 8-2. Output Powers vs Time -Effect of Bandwidth (Biased Jammer Suppression Technique Bias $\eta = 9\sigma^2$)

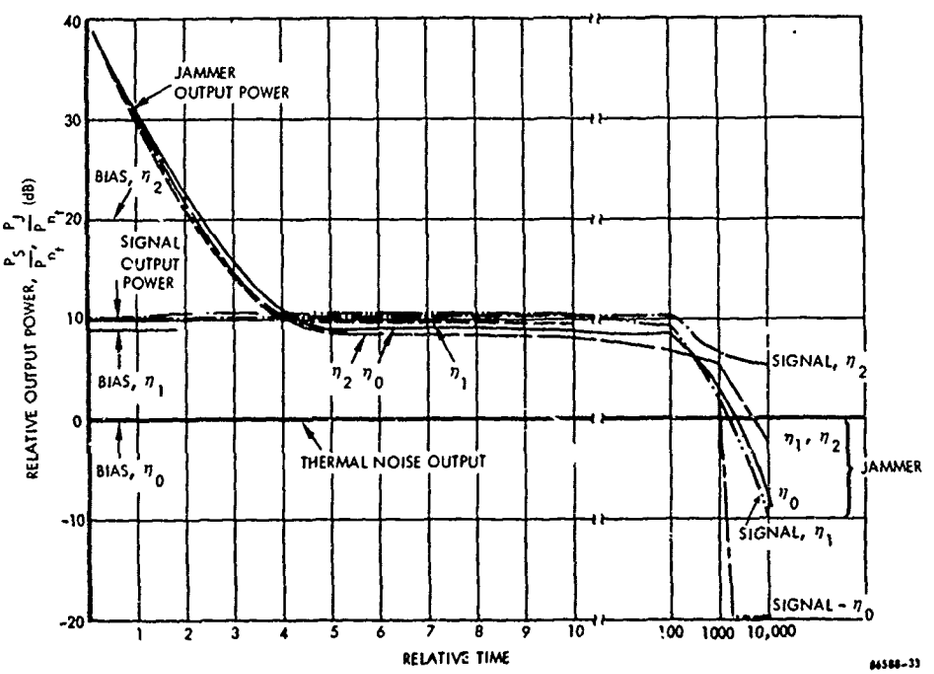


Figure 8-3. Output Power vs Time - Effect of Bias ( m = 9, $\theta_s$ = 70°, $\theta_j$ = 45°, BW = .01) (time units $1/\alpha\lambda_1$)

### 8.1.2 Typical Simulation Results

The previous examples were the result of numerically computed eigenvalue solutions. Complete results for very long averaging times are possible. However, another way of computing adaptive array performance is with digital simulations of both signal waveforms and adaptive array processing. Such a simulation is described in Chapter 9 to characterize a null steerer in a TDMA environment. Results of several such simulations are shown in Figure 8-4. Bandwidth is .001 and there are three elements. In the top figure, the signal is a broadside ($\theta_s = 90°$); in the bottom figure, at endfire ($\theta_s = 0°$). The input jammer level is $J/\sigma^2 = 30$ dB, and the signal is at 10 dB in one case and 20 dB in the other case. The jammer angle is set at 70°, 80°, and 85°. For all cases of jammer angle, the jammer is suppressed rapidly as predicted by the eigenvalue solutions. The signal is not suppressed much at $\theta_j = 70°$, but is increasingly at 80° and 85°, since the signal is falling into the jammer's null. Nevertheless, in most cases, output S/N is improved over the initial -20 dB input S/N. In the bottom figure, the signal at endfire is seen to be much more sensitive to even relatively large jammer-signal separation angles. The endfire signal location is obviously a poor arrangement for adaptive arrays, as it is for ordinary phased arrays. The endfire case is not emphasized because it would not be used operationally. Circular arrays or some form of elements with near "broadside" capabilities in all operational directions is clearly advisable. The linear array here is used only as an initial, simply analyzed array for investigation.

These simulations demonstrate that the expected value equations give the same results as the actual circuitry, in which only instantaneous quantities (not averaged) are multiplied and supplied to the integrator. The simulations are expensive to run, and do not show the steady state values predicted by the expected value equations with the few iterations and the rather large convergence constants (large loop bandwidths) used. An important corollary is that analog circuits with significant loop bandwidths may not achieve these steady state values either.

An analysis of the effect of large loop bandwidth is shown by Brennen, et al. [13] who calculate the total output variance (noise) of an adaptive array as the sum of the noise and jammer variance used in the calculations of this report, plus an additional output variance due to the variance of the weights caused by the finite loop bandwidth. Even though deep suppressions are predicted in the noise and jamming variance output, the weight variance can cause significant reductions in the steady stat null depth predicted by the expected value differential equation solutions plotted in 8-1. In other words, the steady state null depths predicted in 8-1 are only approached with very narrow control loop bandwidths.

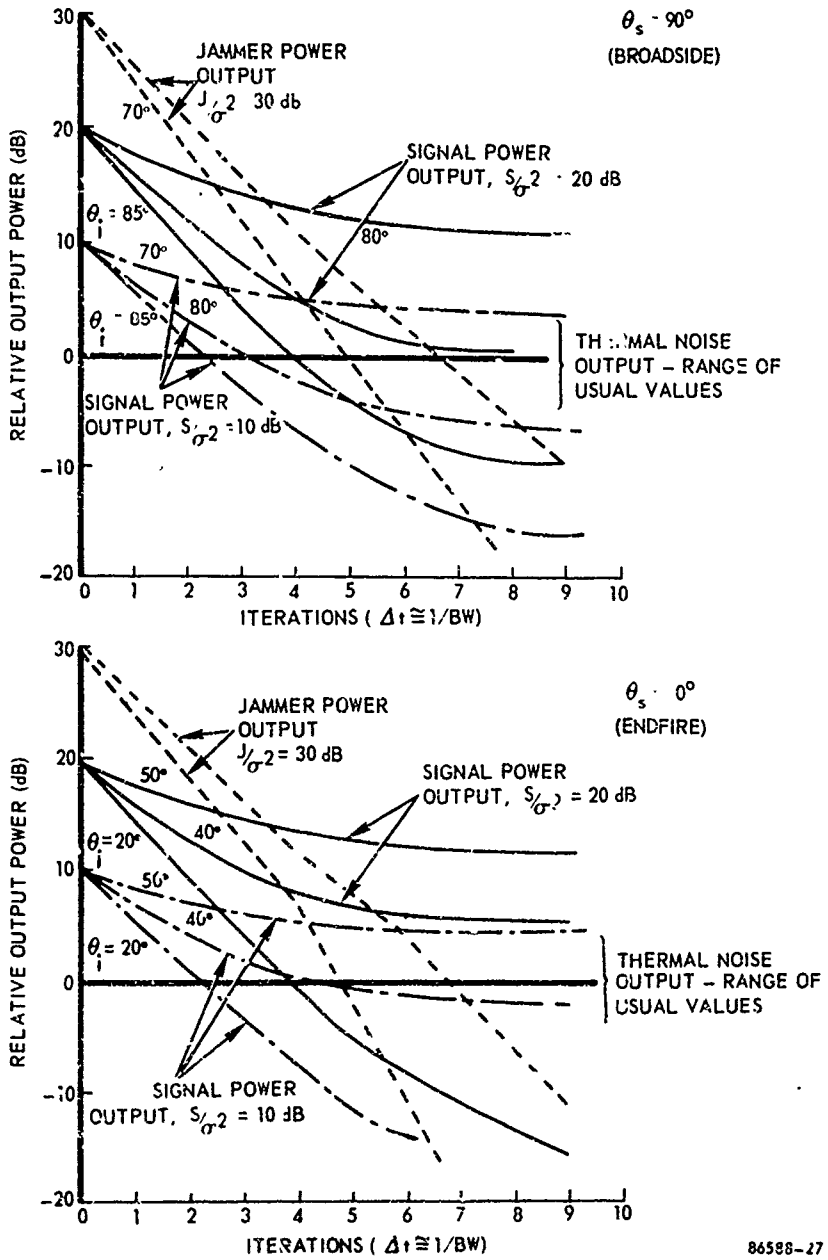


Figure 8-4. Computer Simulations of Acquisition Behavior - Interference Suppression (Linear Array, Fixed Center Weight Constraint, Unbiased, BW = .001)

### 8.1.3 Absolute Time

Throughout this report, time is normalized to the time constant of the largest eigenvalue ($\tau = \frac{1}{\alpha \lambda_1}$), or to a iteration count. Just how fast such loops can operate in real time is not given, although the relative timing of the initial jammer suppression to later suppression is correct.

Actually, the equation can give little clue to how fast such loops can operate, since they only describe a system of first order differential equations which is unconditionally stable for any $\alpha$ (integrator gain); thus $\tau$ can be made arbitrarily small in the expected value equations.

The actual limitations in maximum speed of the loop are:

a. Mathematical; the expected value equations hold only when the loop bandwidth of the control circuit is small compared to the input bandwidth, so that many independent values of the instantaneous signal and jammer multiplications are averaged to control a variation in the weight, thus allowing the cross correlation matrix to describe the system. As loop bandwidth is widened, weight jitter becomes unacceptable. Thus, for a 10 MHz input bandwidth, a maximum loop bandwidth of 10-100 kHz is expected. A simulation to be shown, with only one jammer present, demonstrates that much wider loop bandwidths can be used in some cases; the expected value equations, of course, do not apply.

b. Circuit limitations, such as the gains that can be practically achieved without second order effects causing oscillations, and other degradations.

In one simulation used at Radiation, a time waveform is generated and sampled. Real time is used throughout. Although there can be stability problems in this sampled feedback loop due to the digital nature of the simulation, such simulations can show minimum speeds attainable. Figures 8-5 and -6 show relative powers of jammer and signal vs. time in milliseconds and microseconds. In Figure 8-5, the broadside signal case is shown. Gains have been used that are close to the stability limit, thus the nonsmooth time history curve. The endfire signal case of Figure 8-6 is known to be a poor geometry in that the signal is suppressed even for fairly large jammer-signal separation angles. Acquisition does occur within 30-60 μs, or 60-120 inverse input bandwidths for this 2 MHz input bandwidth case.

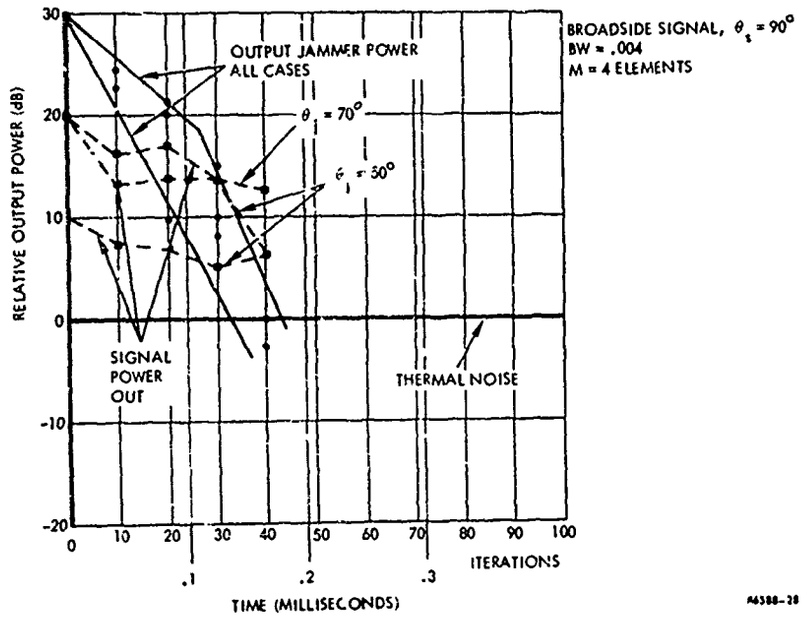


Figure 8-5. Direct Simulation - Jammer Suppression (FM Signal and Jammer, "TSM2" Program)

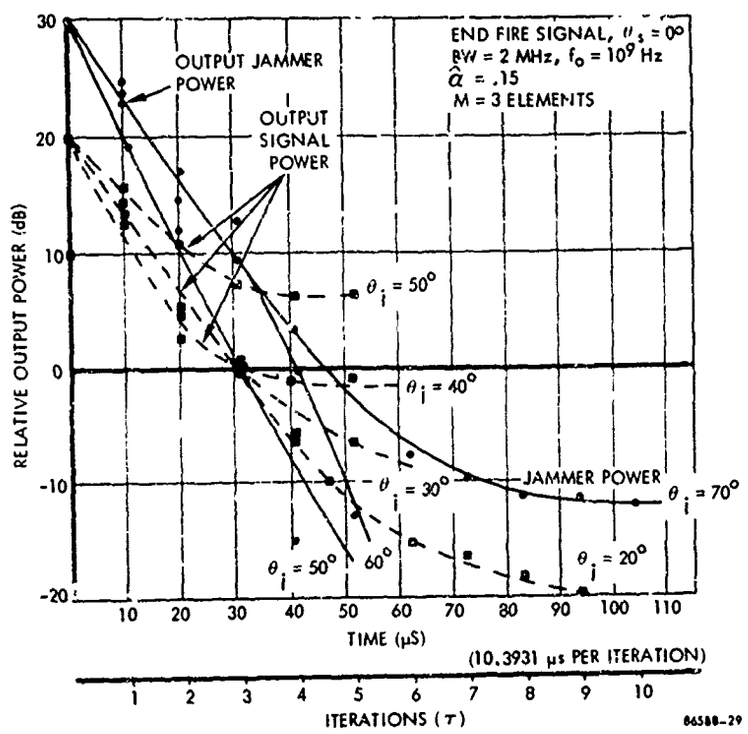


Figure 8-6. Direct Simulation - Jammer Suppression (FM Signal and Jammer, $\hat{\alpha}$ = Normalized Convergence Constant)

Finally, in the case of one completely dominant jammer, a null can be placed on the jammer as fast as its relative phase shift between elements can be estimated. Theoretically, this could occur in one RF cycle or less if enough jammer energy is present. A simulation was run of this case, as shown in Figure 8-7. Initial jammer suppression is seen to take place within 6-10 ns, where the RF frequency is 1 GHz, corresponding to 1 ns RF period. The input jammer-to-thermal noise ratio was assumed to be only 30 dB; however, the processing bandwidths being simulated are on the order of .1-1 GHz for these speeds, so that the equivalent jammer-to-thermal noise within a 10 MHz signal processing bandwidth would have to be at least on the order of 40-50 dB.

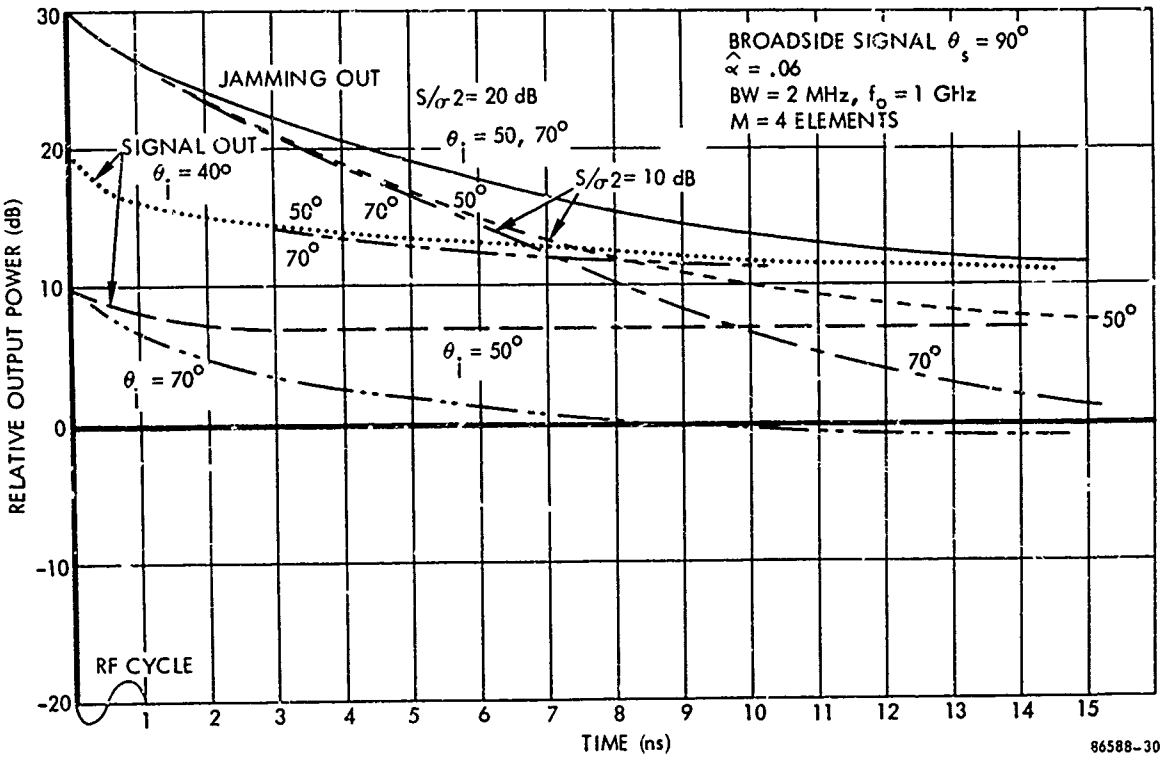


Figure 8-7. Fast Initial Jammer Suppression (FM Signal Simulation; Initial Condition $w_o$ = (0.0, 1.0, 0.0))

## 8.2 Steady-State Jammer Null Depth for the Jammer Suppression Technique

Having shown several examples of the transient behavior of null steering arrays, it will be convenient to plot only steady state values of the output powers of the signal and jammer, or the array null depth on these sources. Null depth or array gain has been chosen as the major dependent variable, defined as:

$$ND_J \triangleq \frac{P_J/P_{n_t}}{J/\sigma^2} = \frac{P_J}{J} \bullet \frac{1}{\sum_i |w_i|^2} = G_J$$

$$ND_S \triangleq \frac{P_S/P_{n_t}}{S/\sigma^2} = \frac{P_S}{S} \bullet \frac{1}{\sum_i |w_i|^2} = G_S$$

where

| | |
|---|---|
| $ND_J, ND_S$ | = Null depths on jammer and signal, respectively (Note, null depth < 1 or negative dB, like gain) |
| $P_J, P_S$ | = Power output of the jammer and signal, respectively |
| $J, S$ | = Power input of the jammer and signal, respectively |
| $\sigma^2$ | = Equivalent thermal noise variance input at each element |
| $P_{n_t}$ | = Thermal noise output $= \sigma^2 \sum_i |w_i|^2$, where $w_i$ is the ith weight |
| $G_J, G_S$ | = Absolute gains, with respect to isotropic, toward the jammer and signal, respectively |

Since the definition of absolute antenna gain in a given direction is the signal-to-noise improvement over the isotropic case, null depth = absolute gain.

### 8.2.1 Effect of Bandwidth

The major factor limiting jammer null depth is array dispersion, the effect of the jamming bandwidth. When the jammer is off axis, the time delay of the jammer received in successive elements causes the modulation envelope in successive channels to be slightly out of alignment, so that perfect cancellation between channels is not possible. Described in the frequency domain, dispersion causes the phase to not be the same function of frequency in each element, so that the sum channel has a nonlinear phase vs frequency curve; i.e., the envelope delay is not constant. Thus, the array, viewed as a filter function, is dispersive. Array bandwidth is a well known phenomenon of course, but a null is a much more sensitive function of bandwidth than the peak of a main beam, where array bandwidth has usually been considered. Cancellations of 40-50 dB calls for very exacting alignment of signals in each channel.

The examples to follow usually use the jammer angle of $45^{\circ}$, almost a worst-case for dispersion. Figure 8-7 shows the effect of bandwidth upon the null depth toward a single jammer, of strength $J/\sigma^2 = 30$ dB, angle $\theta_j = 45^{\circ}$. The jammer suppression technique is used in this example and throughout this section. The curves are plotted for the number of elements m = 3, 4, 7, and 9. It can be seen that

a. bandwidth must be less than .001 (.1%) in order to achieve deep nulls of -50 dB or more

b. the curves are not a strong function of the number of elements

c. at narrow bandwidths (.001 - .01) the null still decreases as the number of elements increases, due to the increased dispersion over many elements. For extremely narrow bandwidths ($<10^{-4}$), this relationship reverses, as discussed in Chapter 7, so that jammer null depth then increases with the number of elements.

Details of a null versus small frequency deviations are shown in Figure 8-8. In all curves, the array weights are optimized to reject a wideband (BW = .12) jammer, pictured as the bar at the top of figure. The narrow-band frequency response (i.e., filter response) of the array is then plotted, for the optimum weight cases where the number of elements m = 2, 3, 4, and 9. For m = 2, a very narrow null is seen. For m = 4, a much flatter bandpass response is noted. For m = 9, a ripple bandpass function is formed. Evidently, the increased dispersion of larger arrays is being compensated for by the increased number of degrees of freedom that are available to form a better bandpass function.

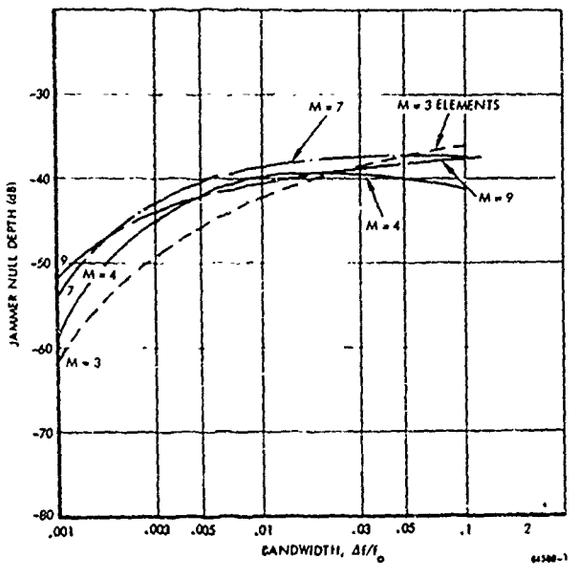


Figure 8-7. Single Jammer Null Depth vs Bandwidth ($J/\sigma^2$ = 30 dB, $\theta_j$ = 45°, S = 0, Jammer Suppression, Fixed Left Weight Constraint, $\eta$ = 0)

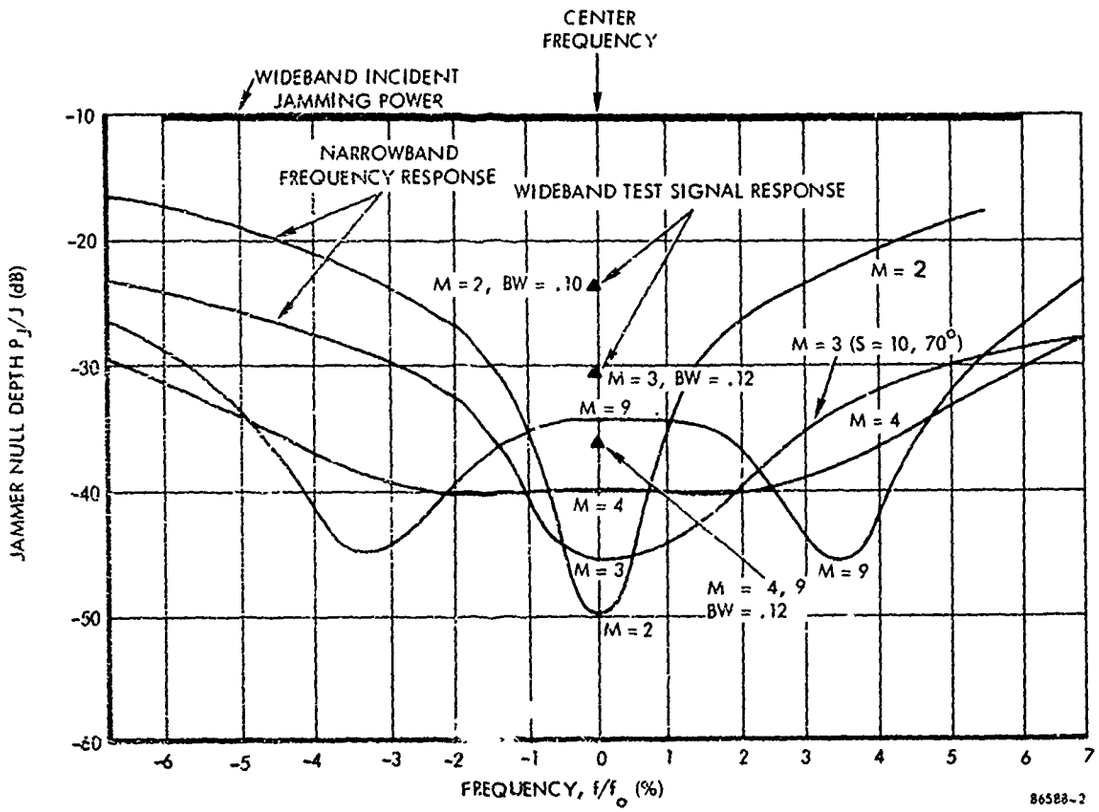


Figure 8-8. Frequency Response of Adaptive Array Null (Weights Optimized for $J/\sigma^2$ = 1000, $\theta_j$ = 45°, BW = .12, S = 0, Fixed Left Weight $\eta$ = 0)

### 8.2.2 Effect of Input Jammer Power

The jammer null depth is a very strong function of the input jammer power, normalized to thermal noise, $J/\sigma^2$. Chapter 7 discusses the very narrow-band case, in which the null depth is inversely proportional to the square of the input jamming power, so that as input jamming power is increased, output jammer power decreases. For moderate and wideband cases (BW = .01 and .12) null depth is plotted vs input jamming power in Figure 8-9. In this case, the jammer power is normalized with respect to the sum of thermal noise and dc bias signal, $(\sigma^2 + \eta)$, because both noise and bias have the same effect on null depth (see Chapter 7). If bias $\eta = 0$, then the line on the top right represents the jammer null depth that would give output jamming $P_J$ equal to output thermal noise, $P_{n_t}$. The null depths are always below this level.

If the null depth is multiplied by the normalized input jammer power, $J/\sigma^2$, then the normalized output jamming power, $P_J/P_{n_t}$ is obtained and plotted in Figure 8-10 versus input jamming power (BW = .01). For zero bias the output power rises to 10 dB below thermal noise before a good null is formed. As the null becomes deeper, the jamming power decreases. If the bandwidth were zero, the jamming power would then go to zero. For any finite bandwidth, it has been shown, and is discussed briefly in Chapter 7, that the jammer power eventually increases again. Once the null is well formed, the finite jammer power "leaks through" the null proportional to the input jammer power. For bias greater than zero, e.g. $9\sigma^2$ and $99\sigma^2$, so that $\sigma^2+\eta = 10$ and 100 respectively, the ratio $\frac{J}{\sigma^2 + \eta}$ becomes smaller for a given J, and thus the null depth is less, as shown in Figure 8-9. As a result, more jamming appears at the output, giving the higher curves shown in Figure 8-10.

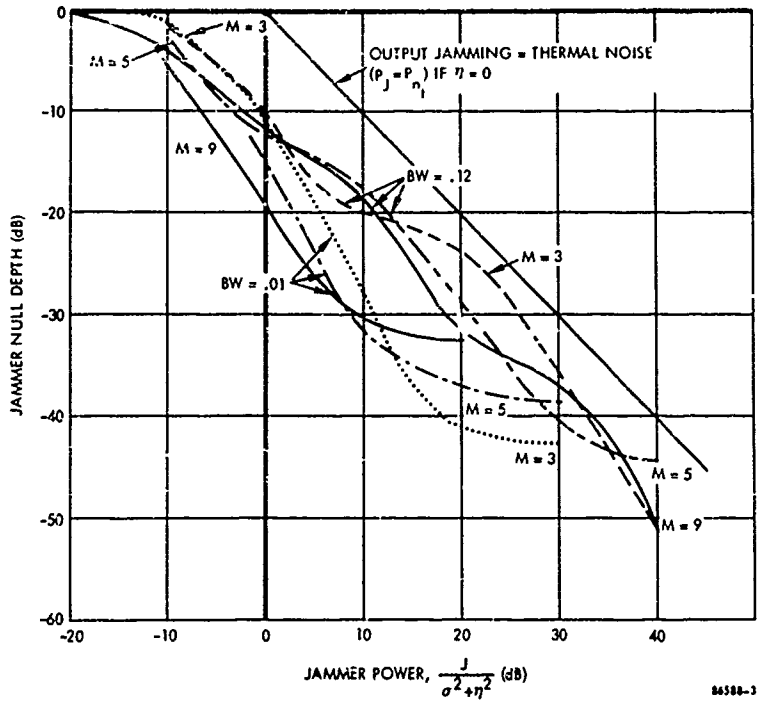


Figure 8-9. Jammer Null Depth vs Jammer Power ($\theta_1 = 45^\circ$, Jammer Suppression, Fixed Left Weight, S = 0, $\eta = 0$)

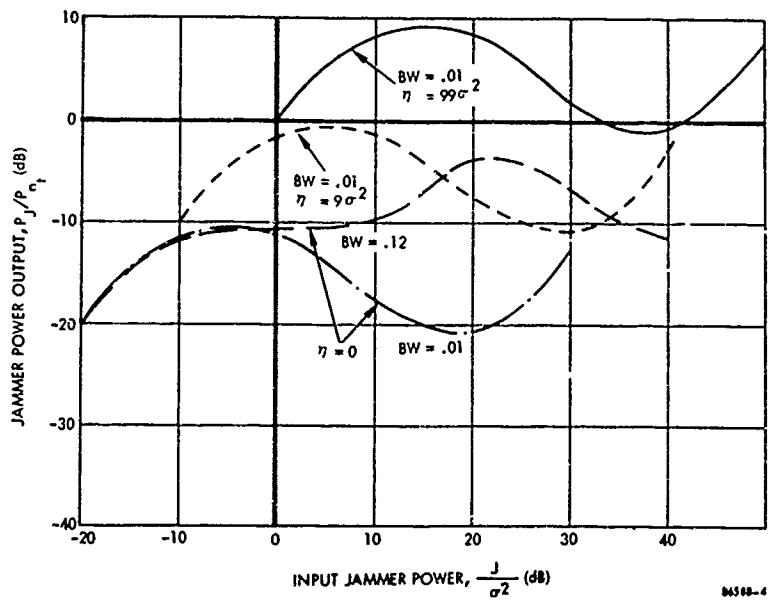


Figure 8-10. Jammer Power Output vs Power Input (M = 3)

### 8.2.3 Effect of Jammer Angle

All of the preceding curves have been for the jammer at 45° from the array axis, to emphasize any dispersive effects. If the jammer is at 90° (from the array axis), or normal to the array, there are no dispersive effects because there are no differential time delays between elements. The effect of jammer angle vs null depth is shown in Figure 8-11 for the number of elements m = 3 and 5, and Figure 8-12 for m = 7 and 9. In each set of curves, the solid lines are for BW = .12 and the dashed lines for BW = .01. The parameter on each curve is the normalized jammer power $J/\sigma^2$. For all curves where $J/\sigma^2 > 0$ dB, the jammer null depth dips sharply as the jammer approaches 90°, as expected, and is deeper for narrower bandwidths, also as expected. Since dispersion is less for narrower bandwidths, the null depth curve is less sharp for smaller bandwidths. Finally, an unexpected phenomenon occurred which has not been explained. For m = 5, and especially m = 7 and 9, the null depth decreases near 85° before the null at 90°.

If nulling a wideband jammer becomes a problem off axis, these figures indicate that considerable improvement in null depth could be obtained by turning the array to within 5° from normal to the jammer, to reduce dispersion. This may be possible in a higher frequency, high-gain array in a radome. Another solution is the general tapped delay line wideband array mentioned in Chapter 2. Obviously rather fine delay increments would be required to approximate nondispersive delay to within a few mechanical degrees.

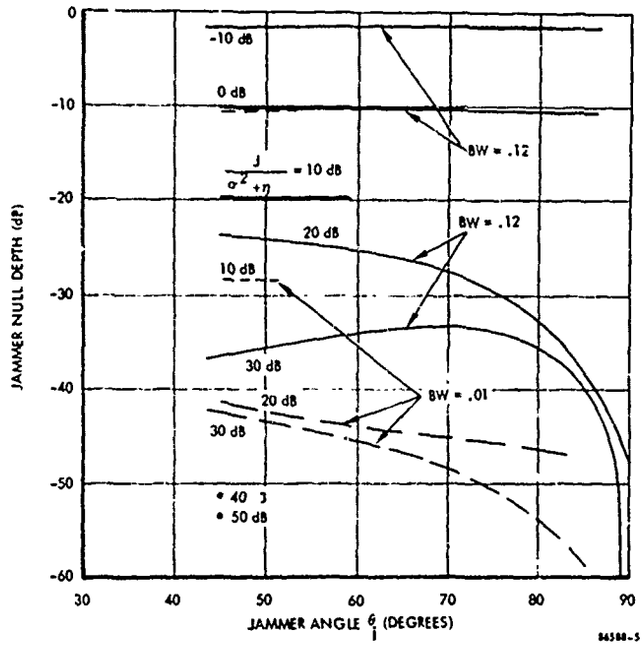


(a) M = 3

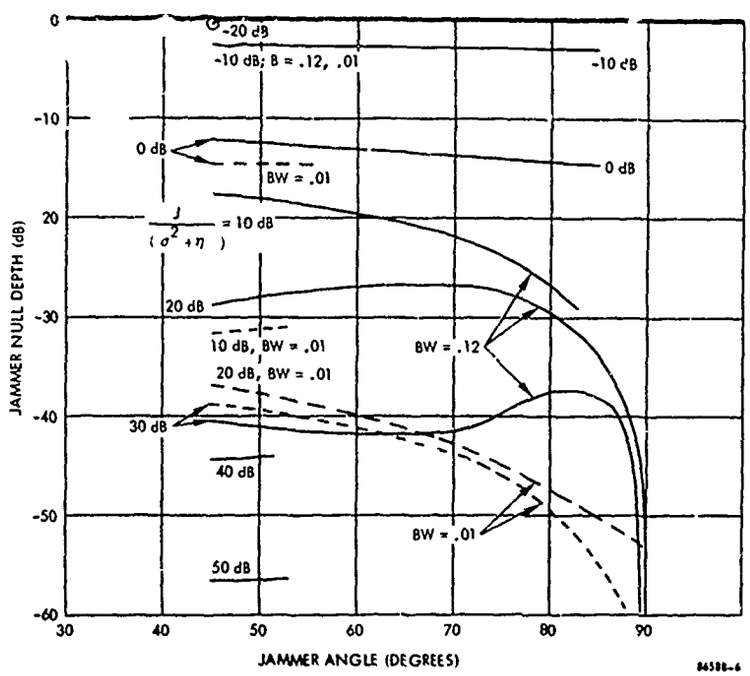


(b) M = 5

Figure 8-11. Jammer Null Depth vs Angle of Arrival (Jammer Suppression, Fixed Left Weight)

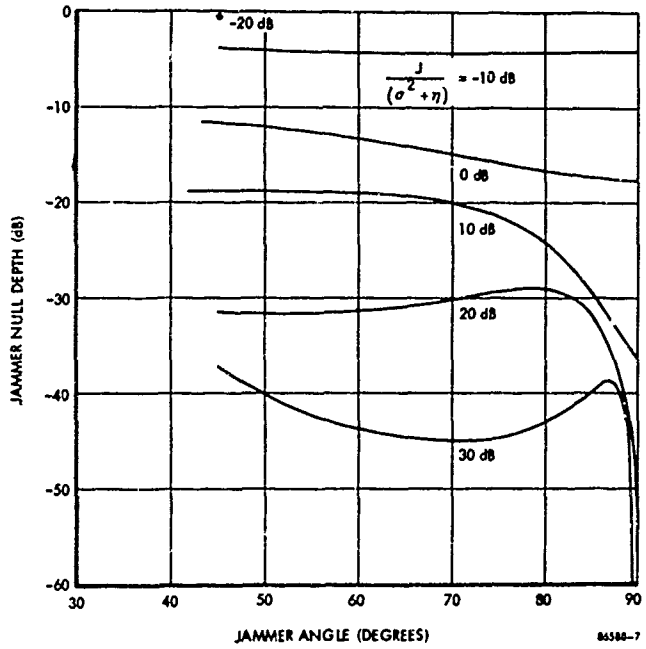


(a) M = 7

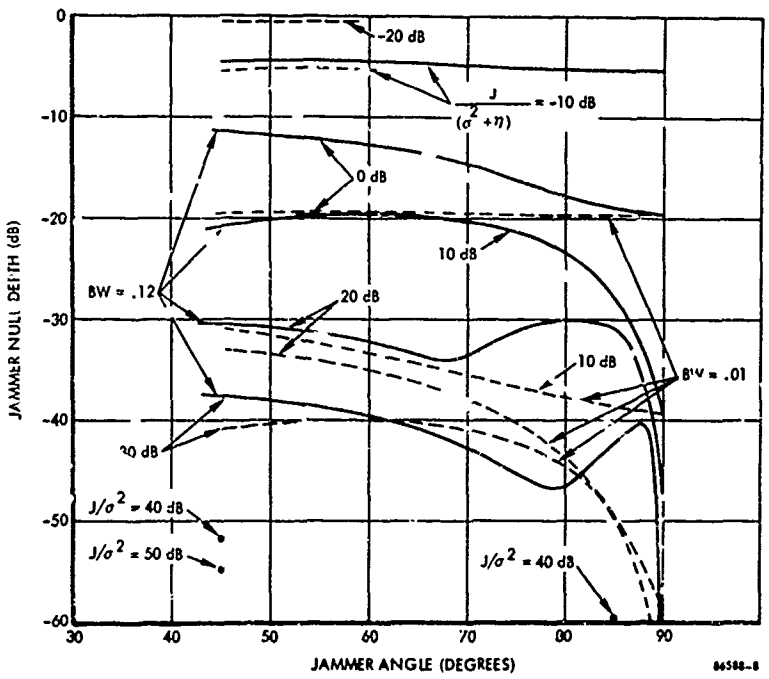


(b) M = 9

Figure 8-12. Jammer Null Depth vs Angle of Arrival (BW = .12, Jammer Suppression, Fixed Left Weight)

### 8.2.4 Effect of Multiple Jammers

It was stated at the beginning of this section that single jammers would be considered, but multiple jammer cases were very similar. Several multiple jammer cases are shown in Figure 8-13 for wide bandwidth (BW = .12), with m = 9 (part a) and 5 elements (part b). In these figures the null depth is plotted versus the number of jammers. As the graph is read from the left, jammers are added, $J_1$ ($\theta = 45^\circ$), $J_2$ ($\theta = 135^\circ$), etc. Null depth on each jammer is shown. Also, a desired signal was included in the calculations. The input J/S = 30 dB. The bias was set 10 dB above the signal ($\frac{S}{\sigma^2 + \eta}$ = 10 dB) so that very little signal would be lost. In Figure 8-13a, for m = 9, the jammer null depth continued at -25 dB or better until the number of jammers exceeded 5. In this case, the simple rule that the number of nulls = the number of elements less one is not true. Signal loss is only a few dB or less; remember that all these curves are for the biased jammer suppression case in which some signal loss can be expected. In Figure 8-13b, for m = 5, same bandwidth as in part a, the number of emitters exceeded the number of elements, with no significant degradation. It must be that some special angles are involved that allow the array to perform these nulls.

Figure 8-14 shows two more cases, one with BW = .01, m = 5 and another with BW = .12, m = 3. In the first case, Figure 8-14a, the null depth is degraded somewhat with 4 jammers but is still better than 25 dB at 6 jammers. Little signal loss is recorded. With m = 3, some degradation is seen with the number of jammers equal to 3, in Figure 8-14b.

In summary, the multiple jammer cases compare very well with the single jammer cases as long as the number of jammers is considerably less than the number of elements, although in some cases, even more jammers may be nulled.

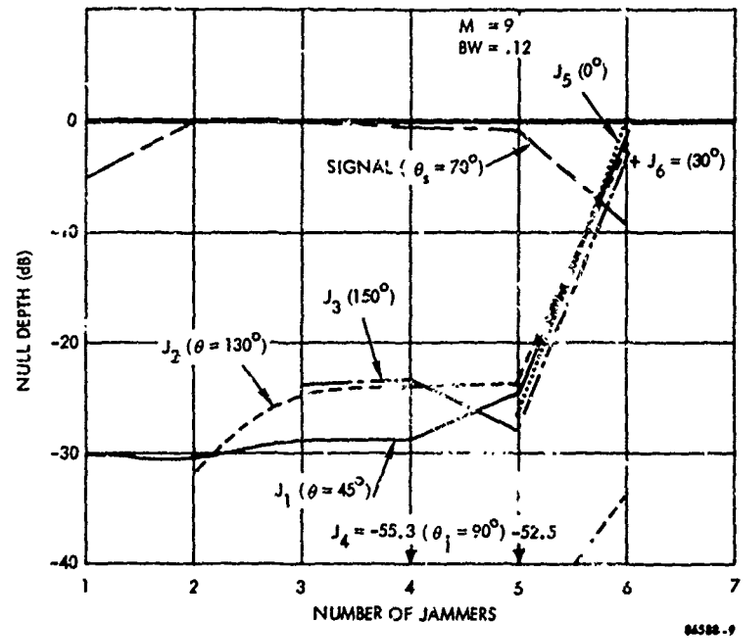


(a) M = 9

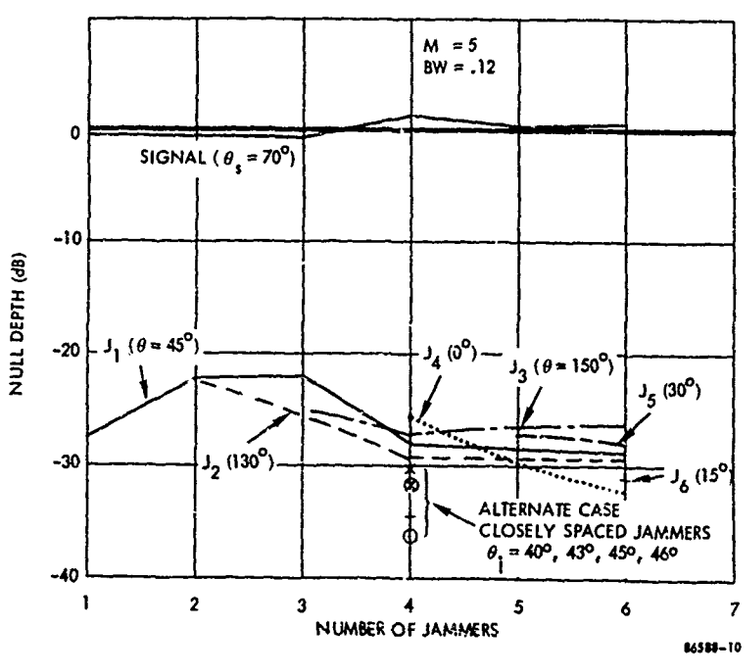


(b) M = 5

Figure 8-13. Effect of Multiple Jammers (Biased Jammer Suppression, $\frac{S}{\eta + \sigma^2} = -10$ dB, J/S = 30 dB)

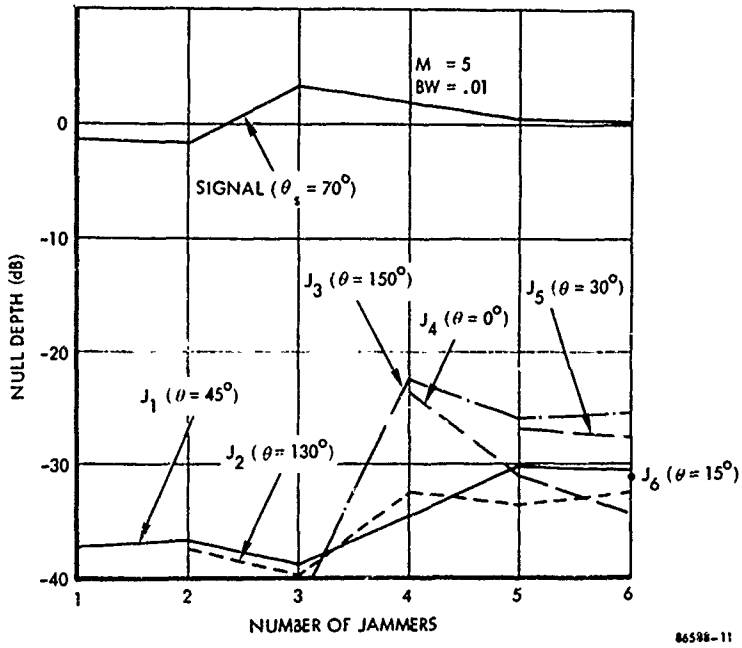


(a) M = 5

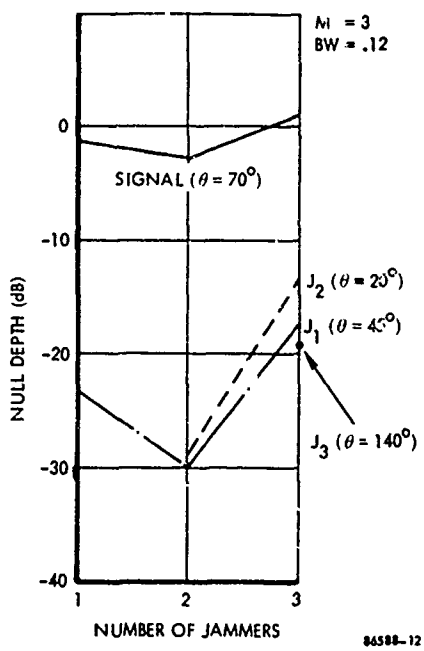


(b) M = 3

Figure 8-14. Effect of Multiple Jammers (Biased Jammer Suppression, $\frac{S}{\sigma^2 + \eta}$ = 10 dB, J/S = 30 dB)

## 8.3 Steady State Output Signal and S/N Improvement-Jammer Suppression Technique

In the Biased Dominant Jammer Suppression technique, the signal is suppressed to some extent, as well as the jammer. This (or the loss in jammer null depth that can be traded off) is the price paid for not having to estimate and remove the signal from the error channel.

### 8.3.1 Null Depth on Signal with Biased Suppression

Figures 8-15 through -18 show the signal null depth (absolute gain on the signal) versus normalized signal power, $\check{S} \triangleq \frac{S}{\sigma^2 + \eta}$, where S is the input signal power to an isotropic element, $\sigma^2$ is thermal noise input to each element, and $\eta$ is the dc bias. It is very important to normalize the signal to bias + noise because it will be seen, as discussed in Chapter 7, that bias can prevent signal loss. Figure 8-15 shows the signal null depth vs. input signal power for m = 3 elements, jammer angle $\theta_j = 45^\circ$, bandwidths BW = .12 (Figure a) and .01 (Figure b), for various normalized jammer powers, $\check{J} = \frac{J}{\sigma^2 + \eta}$ and signal angles, $\theta_s$. Figure a (BW = .12) shows less than -2 dB signal null depth if bias + noise is 10 dB greater than the signal $\left(\frac{S}{\sigma^2 + \eta} < -10 \text{ dB}\right)$ in those cases where $\theta_s > 80^\circ$ ($\theta_s - \theta_j > 35^\circ$). For $\theta_s > 70^\circ$, null depths less than -6 dB are obtainable with the same bias + noise. As the signal approaches the jammer to within 5-15° ($\theta_s = 50^\circ$, $60^\circ$), the nulls on the signal increase drastically because the signal is in the jammer null. The null for this wide bandwidth and jammer angle is quite wide (~9°). Although jammer power, $\check{J}$, is a significant parameter for large $\check{S}$, it has little effect on signal null depth as $\check{S}$ decreases below -10 dB. Figure 8-15, for a narrower bandwidth (BW = .01), shows much less signal loss for $\theta_s = 50^\circ$, $60^\circ$, and $70^\circ$, and a sharper fall off of signal output (null depth and gain) as input signal increases. The null is narrower in the narrow bandwidth case, causing less signal loss in nearby signals.

Figure 8-16 shows the same plots for m = 5 elements with BW = .12 (Figure a) and .01 (Figure b). A sharper falloff of signal output with signal input is to be noted, compared to the previous case in which m = 3. Still, when $\check{S} < -10$ dB and $\theta_s > 70^\circ$, signal loss is very small, less than 3 dB. Again, when $\theta_s = 50^\circ$, signal suppression is much greater than with the narrower bandwidth, because of the wider null in the wideband case. Figure 8-17 is for the 9-element case, and again shows sharper signal dropoff, with increased signal level, than with fewer elements, and less than 5 dB loss for large bias + noise.

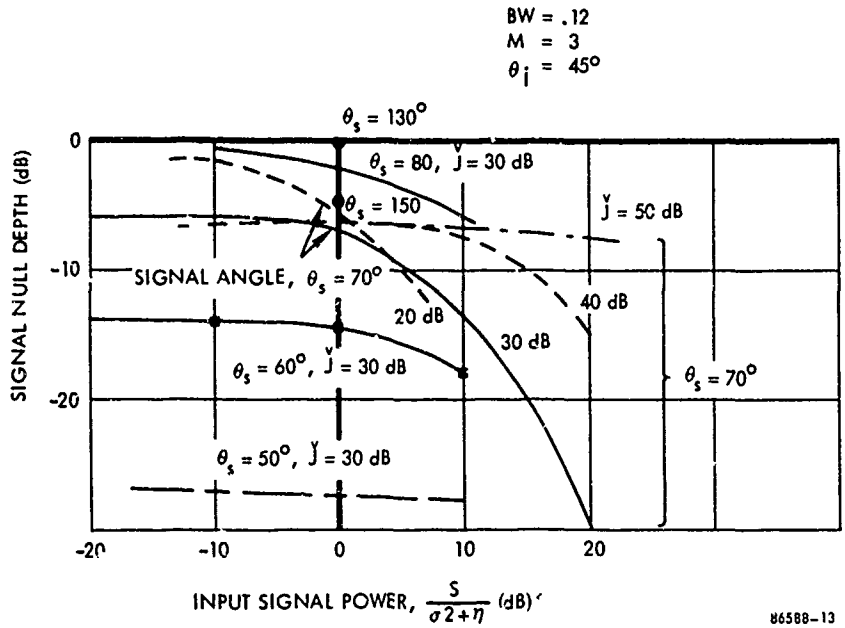


(a) BW = .12

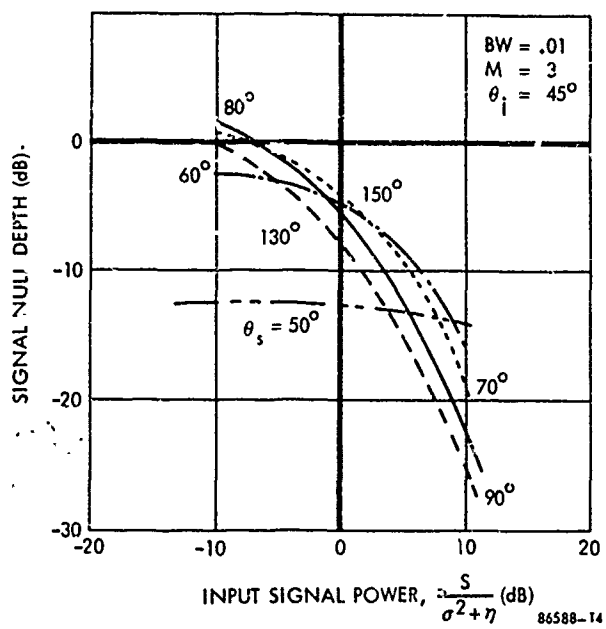


(b) BW = .01
$\check{J}$ = 30 dB

Figure 8-15. Steady State Signal Null Depth vs Signal Power (Biased Jammer Suppression Technique, $_i$ = 45°, J = $\frac{J}{\sigma^2+\eta}$

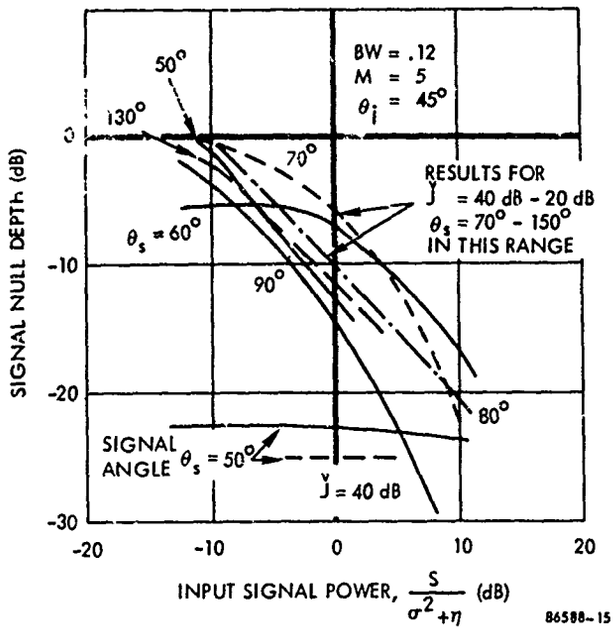


(a) BW = .12
$\check{J}$ = 30 dB

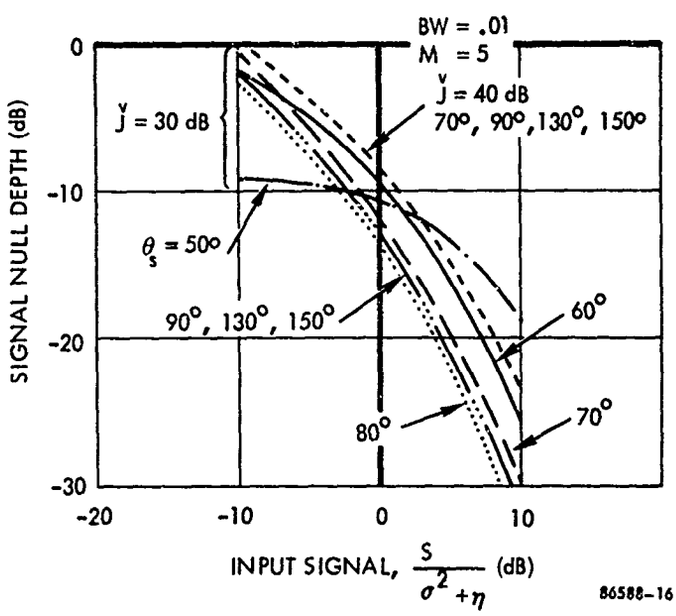


(b) BW = .01

Figure 8-16. Steady State Signal Null Depth vs. Signal Power (Biased Suppression, $\check{J} = \frac{J}{\sigma^2+\eta}$)

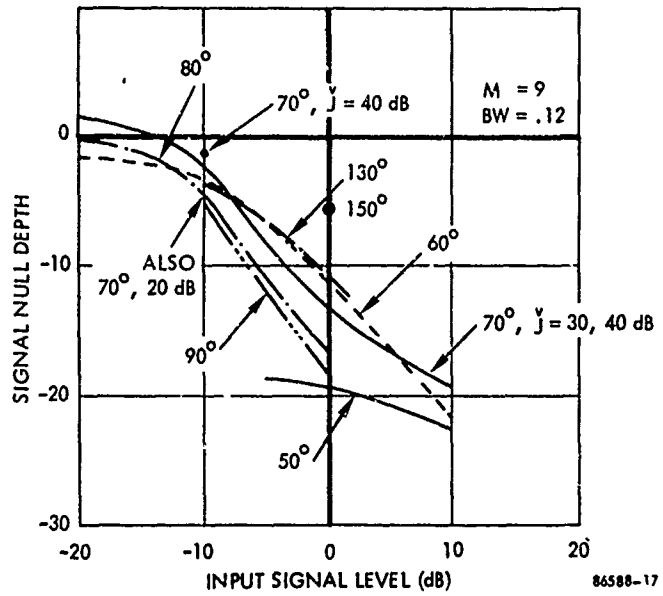


(a) BW = .12

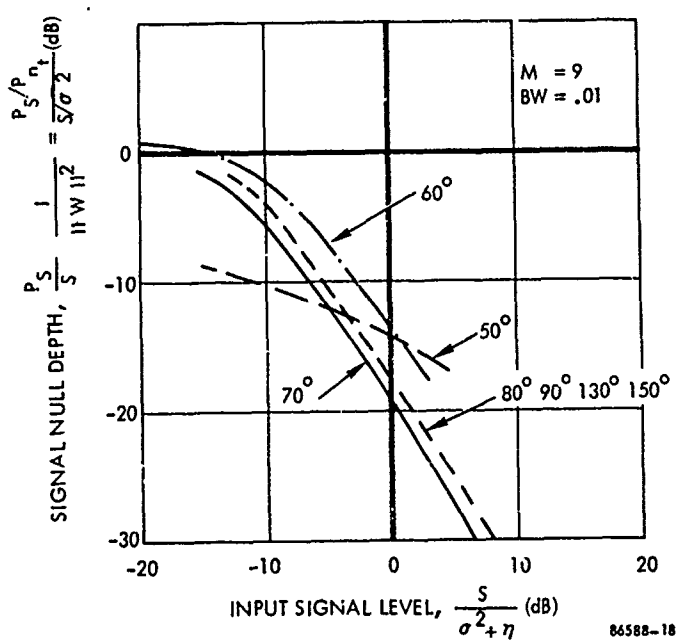


(b) BW = .01

Figure 8-17. Steady State Null Depth vs. Signal Power
(Biased Suppression, $\check{J} = \frac{J}{\sigma^2 + \eta} = 30$ except as shown)

To further investigate the effect on a signal close to a jammer, Figure 8-18 shows several cases of signal null depth vs. signal angle. Figure 18a shows a jammer at either 45° or 85°, with strength $\frac{J}{\sigma^2 + \eta} = 30$ dB. For the 85° jammer, ($\frac{J}{\sigma 2 + \eta} = 30$ dB and 10 dB), the signal must be 5° away to lose less than 2 dB with .12 bandwidth. For the 45° jammer, the wideband can cause 20 dB loss at 5° separation, BW = .12; 10 dB for .01 bandwidth. Figure 8-18b, with null depth plotted vs. input signal level, for several signal angles near the jammer angle, shows 10 dB loss for 5° separation. Note that angular sensitivities are proportional to the total size of the array; a larger array could discriminate between signal and jammer at smaller separation angles. In larger arrays, separations are often normalized to the beamwidth of the array.

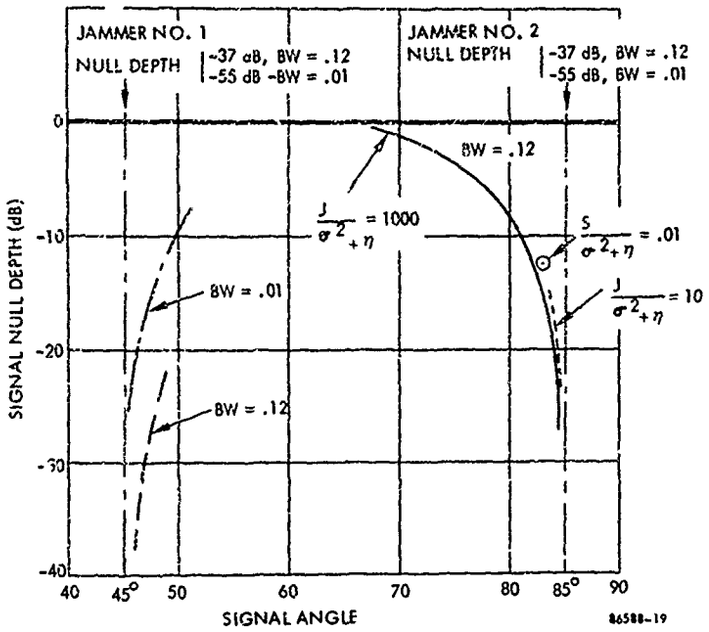


(a) vs $\theta_s$

$$\frac{S}{\sigma^2+\eta} = 0.1$$

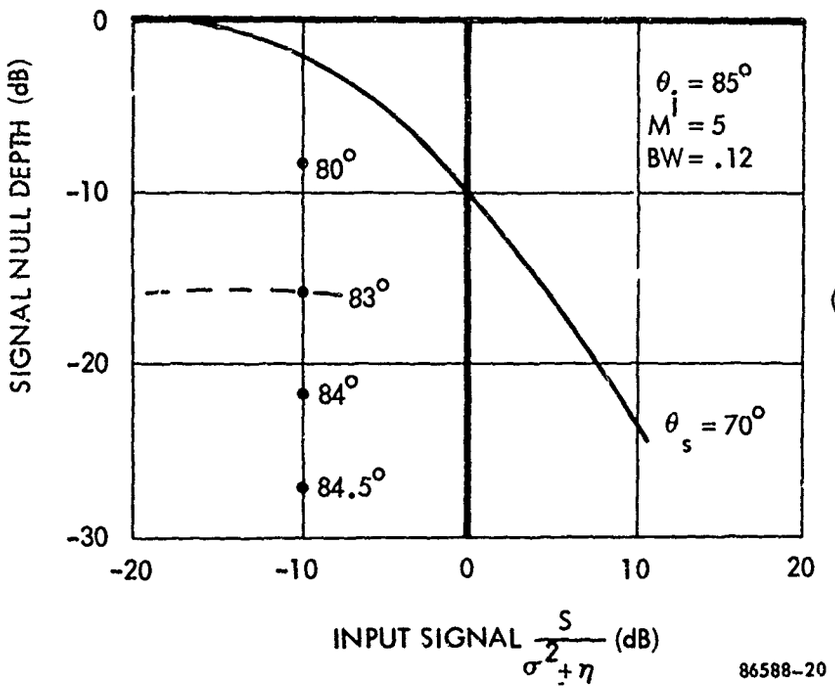


(b) vs $\frac{S}{\sigma^2+\eta}$

Figure 8-18. Signal Null Depth for Signal Close To Jammer (Biased Jammer Suppression, M = 5)

## 8.3.2 Signal-to-Jammer Ratio-Biased Suppression

In Sections 8.2 and 8.3.1 the null depths on the jammer and the signal were treated separately. It was evident from the curves that each was relatively independent of the other. The effect of bias + noise was very evident on the null depth of the signal; bias + noise had to be at least 10 dB higher than the signal for minimum signal loss; for less bias + noise, the signal loss was approximately inversely proportional to bias + noise. The effect of bias + noise on the jammer was also important; the jamming loss was approximately inversely proportional to bias + noise for bandwidths BW = .01 to .12. Since both signal and jamming were found to be inversely proportional to bias + noise for this range of bandwidths, one would expect the output signal-to-jammer ratio to be approximately constant, which is approximately the case for a narrow range of bias + noise $\approx$ S.

Figure 8-19 shows the output signal-to-jammer ratio as a function of bias + noise-to-signal ratio (called bias-to-signal in the diagram to emphasize that bias is expected to be much higher than noise in biased suppression).

Figure 8-19a plots the case m = 5, BW = .12. In the range -10 to 10 dB of the abscissa, the output signal-to-jamming ratio is approximately constant, -1 to -2 dB, for a wide range of the parameter, jamming-to-signal ratio, J/S. Two exceptions were for J/S = 10 dB and 30 dB where the output $P_S/P_J$ rises above 0 dB for the bias level equal to the signal. There is no clear explanation why the case for J/S = 20 dB does not more closely resemble the values for J/S = 10 dB and 30 dB; however, the jammer null depth curves have many changes in slope, particularly for the wideband case BW = .12.

In Figure 8-19b, for m = 9 and BW = .12, a very similar behavior of signal-to-jamming ratio occurs, but with no output values above 0 dB. Finally, Figure 8-19c, for m = 9 and BW = .01, a greater range of $P_S/P_J$ values is noted, most above 0 dB, with the notable exception where the parameter J/S = 30 dB. No explanation for the variations is obvious, other than the variation in jammer null depth already seen. It must be kept in mind that once dispersion and fairly large bandwidths are taken into account, the curves become rather complex, since the adaptive array is adapting to the changing conditions as best as it can.

Reciprocal suppression, discussed in Chapter 7 for zero bandwidth, does not occur for these relatively large bandwidths; at least not for significant bias levels. Suppresssion of the jammer to approximately the signal level is about the most that can be done. If the curves had been continued to the left for very small bias and large J/S, they might rise considerably more towards reciprocal suppression, at least for BW < .01. However, if one desires to minimize signal loss, in order to keep the signal above thermal noise in the steady state, bias must be at about the signal level, so that reciprocal suppression is not very useful.

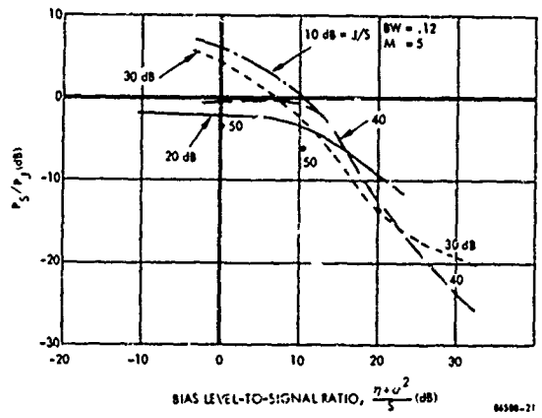


(a) M = 5

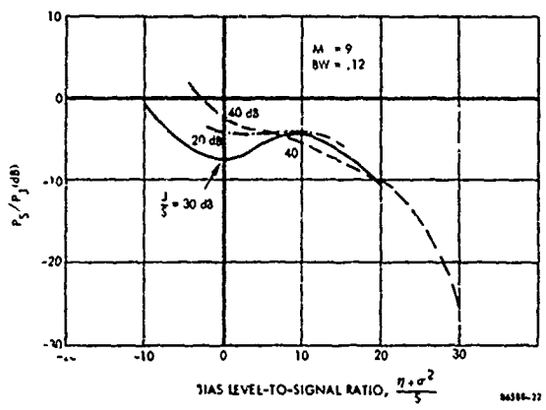


(b) M = 9

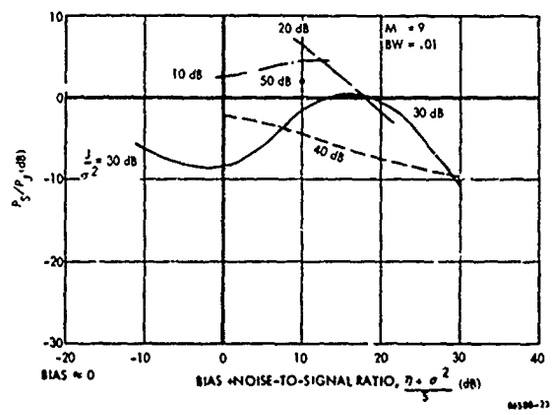


(c) M = 9

Figure 8-19. Signal-To-Jammer Ratio vs. Bias Level
($\theta_j = 45^o$, $\theta_s = 70^o$)

### 8.3.3 Signal-to-Total Noise Ratio-Biased Suppression

The most important measure of the performance of the Biased Suppression Technique is, of course, the signal-to-total noise ratio output, $P_S/P_N$. Some curves of this measure vs. bias + noise-to-signal ratio are plotted in Figure 8-20, for various input J/S ratios. Again, as in most previous figures, the widest bandwidth, BW = .12, and a jammer angle of $\theta_j = 45^\circ$ cause almost worst-case output.

Keep in mind that both the narrowband performance in Chapter 7 and the transient performance (before deep nulls are formed on the signal) yield less signal loss and better signal-to-total noise ratios. Figure 8-20a, for 5 elements and 12 percent bandwidth, shows that the output signal-to-total noise ratio rises to a broad maximum of approximately zero dB (before processing and front end filtering) for essentially all input J/S ratios. The bias level for maximization is from 0-10 dB above the signal. For higher bias levels, the jamming null becomes less, causing output signal-to-total noise to go down. For very small bias, the null formed on the signal reduces the output signal-to-total noise. Similar results for m = 9 and BW = .12 are shown in Figure 8-20b, except that output $P_S/P_N$ never rises above -5 dB. The added elements actually hurt the performance, apparently due to the increased dispersion for this wide bandwidth. For a narrower bandwidth, BW = .06 and m = 9, Figure 8-20c again shows increased $P_S/P_N$ up to the 0 dB, except for $J/S \geq 40$ dB. Remember that the input signal-to-noise ratio for this case is <-40 dB.

In conclusion, for the case where the number of emitters is less than the number of elements, biased suppression can be used to greatly improve very small signal-to-jamming ratios, from extremely small values up to approximately 0 to -10 dB. Signal processing must then be used to raise this array output signal-to-noise value to a level where detection can occur. Rather modest signal processing values like 6 to 20 dB will clearly suffice.

Although spread spectrum signal processing may immediately come to mind as a means for signal improvement, the more mundane multichannel receiver is also applicable. If the array steers nulls based on the whole input bandwidth of the receiver, the output signal-to-noise ratio of the array, which is the input signal-to-noise ratio at the receiver over the whole bandwidth, can be made approximately zero dB for the cases considered so far where the number of emitters is less than the number of array elements. The channelized receivers then can improve the signal-to-noise since the channel bandwidth is smaller than the input bandwidth. If the bias is adjusted so that jammer is suppressed well below the thermal noise, the signal processing gain is the ratio of input bandwidth to channel bandwidth; if the jamming is heavily concentrated in one channel's bandwidth, this signal processing gain cannot be achieved because as thermal noise is reduced by the bandwidth ratio, the jamming will not be reduced. Such a jammer, of course, leaves the other channels in the clear, so that this form of jamming appears unlikely.

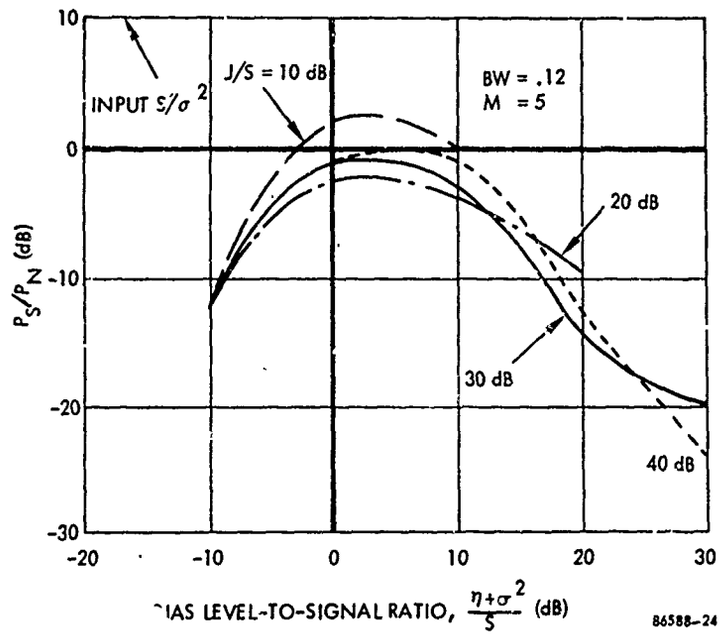


(a) M = 5

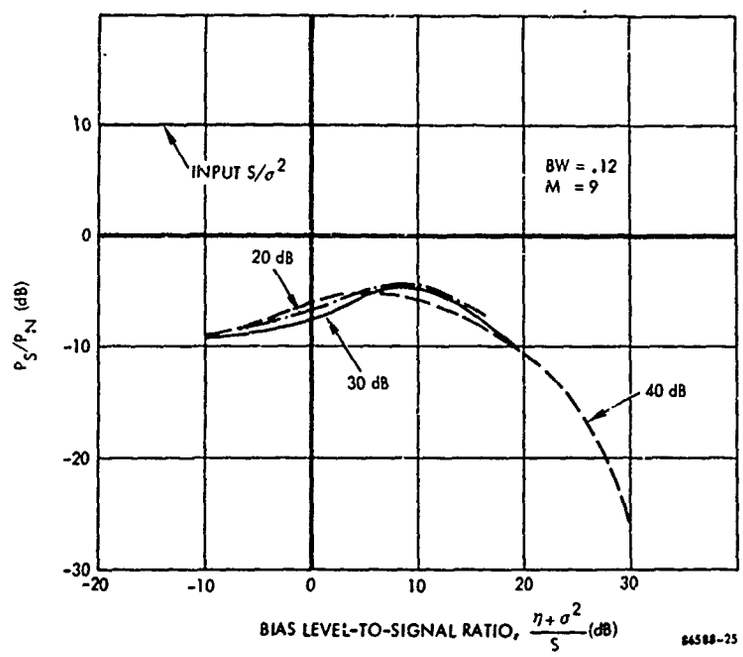


(b) M = 9

Figure 8-20. Output Signal-To-Total Noise vs. Bias Level

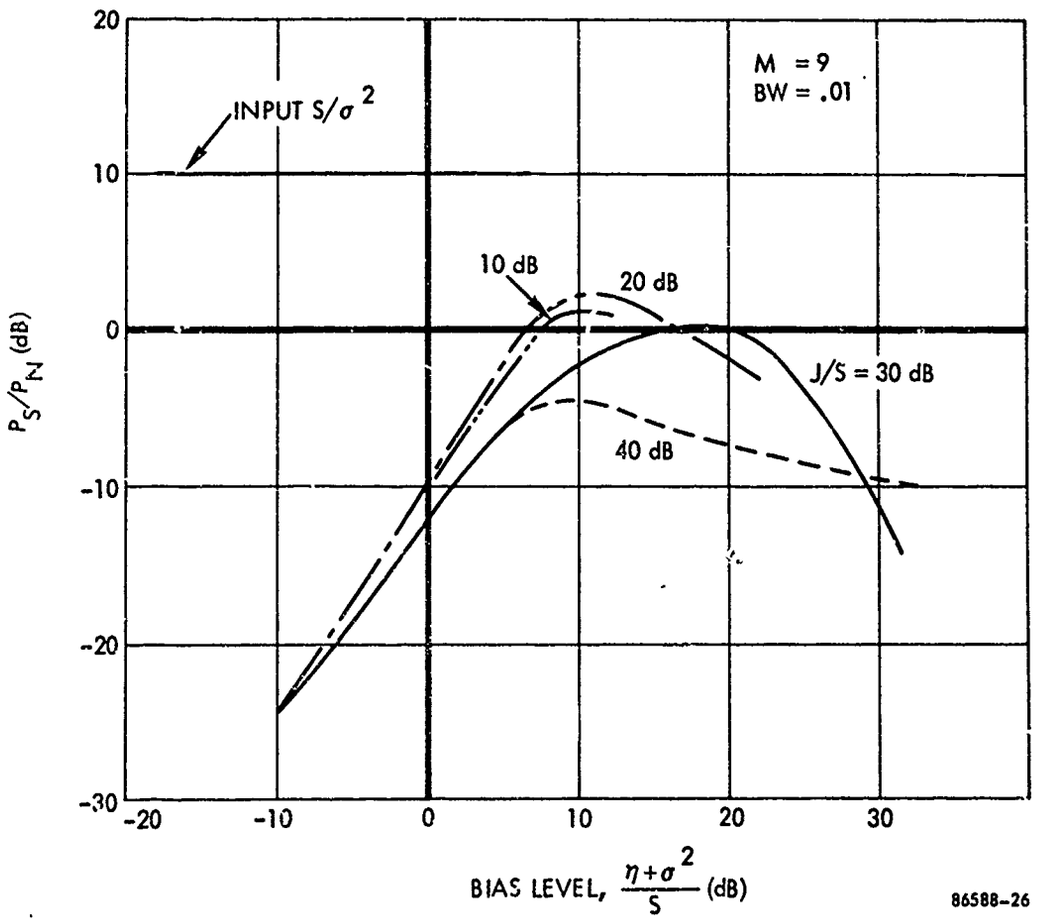


Figure 8-20c. Output Signal-To-Total Noise vs. Bias Level (Biased Jammer Suppression, $\theta_i = 45^\circ$, $\theta_s = 70^\circ$, $S/\sigma^2 = 10$ dB)

Another common signal processing improvement is via duty cycles. The adaptive array results for output S/N are for average signal power. For a low duty cycle signal, the peak S/N ratio is increased by this factor, if the interference is continuous.

For communication purposes, given continuous white noise interference, the average signal power-to-noise ratio determines the communication rate, since the bit error rates can be calculated from $E_b/N_o$, the energy per bit divided by the spectral density of the noise.

## 8.4 Several LMS Array Results (Having Signal Removal)

The LMS array has been rather thoroughly covered in Chapter 6, in the literature, and in work at Radiation by Butcher (17, 18) that will not be covered in this report. One set of curves, shown in Figure 8-21, relates jammer null depth and signal gain to jammer power input, for 4 elements and several bandwidths. For rather narrow bandwidths, such as BW = .001 (and even .01) greater than -40 dB jammer null depths (gains toward the jammer) are shown. However, for wide bandwidths (BW = .12), null depths of approximately 27 dB are shown, due to the dispersions. Signal gains shown in the dashed lines at the top, and read on the right-hand scale, are approximately 4-6 dB. For 4 elements, 6 dB is the maximum gain; thus, little gain has been lost; only 1-2 dB at the widest bandwidth.

## 8.5 Overspecified Arrays (The Numerous Signal Case)

One area of importance that was omitted in this study was the case where there are many more weak signals than elements in the array, but only a few jammers (the case of more jammers than elements has been covered). From several recent cases examined, it appears that the signals are not suppressed in a jammer suppression mode, even though they are 10 dB or more over thermal noise. This is, of course, because the array is overspecified; it simply cannot null all the sources. It appears (on the basis of only a small amount of data) that each signal source is not nulled more than 5 dB, but the average jamming power is reciprocally suppressed below the average total signal power. That is, at least for one jammer,

$$\frac{P_S}{P_J + P_{n_t}} \cong \frac{J}{\sum_i S_i}$$

One of the conclusions of this chapter (that signal null depth is critical and must be controlled with bias) is based on the assumption that the number of signals is less than the number of elements. When the number of signals is greater than the number of elements, nulls cannot form on all the signals. It does appear that output signal-to-total noise (jamming + thermal noise) is still in the -10 to +10 dB range, as is shown in Figure 8-20, but thermal noise is no longer a major factor.

## 8.6 Polarization Considerations

There is another parameter that is a potentially very powerful discriminant between signal and jamming, namely polarization. It is well known that different

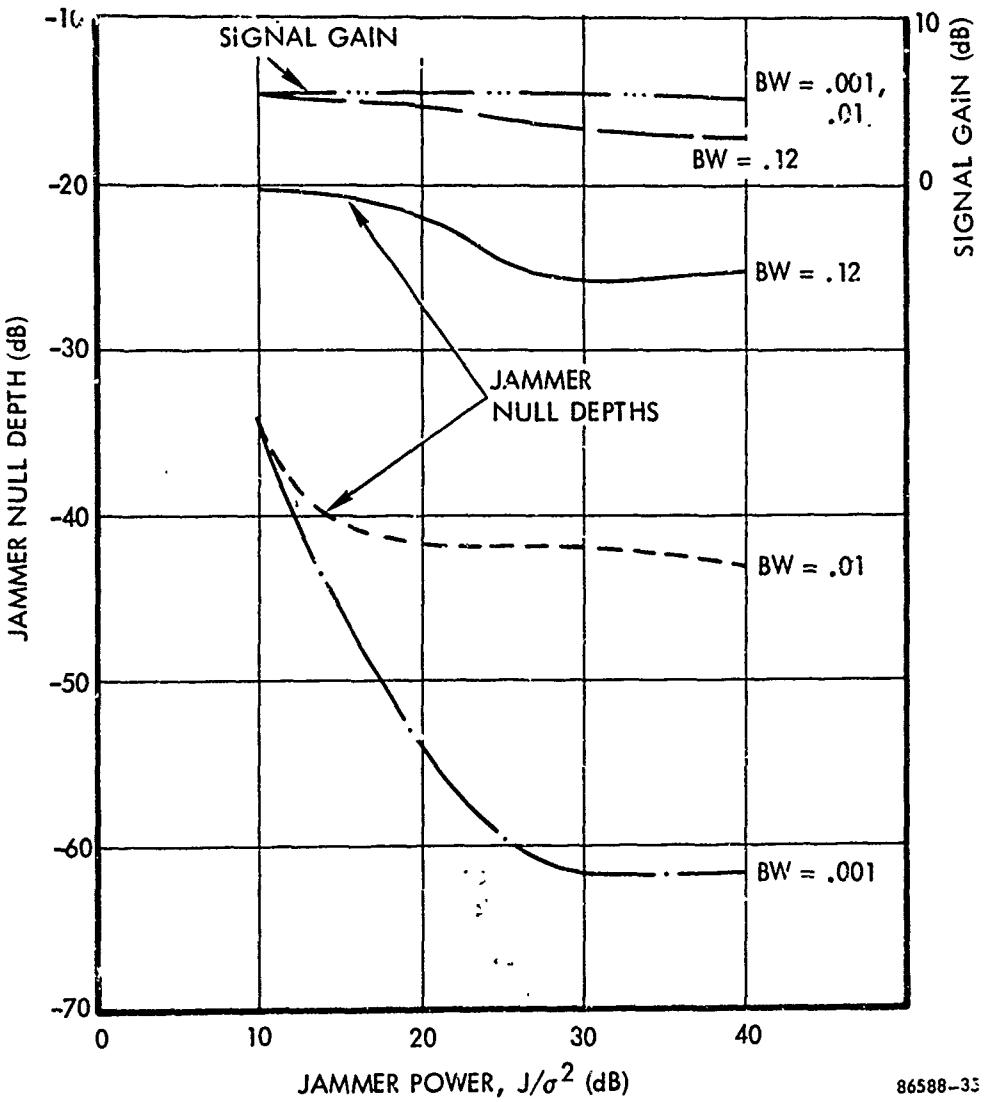


Figure 8-21. Known Signal (LMS) or Signal DOA Algorithm (Signal $S/\sigma^2 = 10$ dB, $M = 4$)

patterns exist for different polarizations; usually the two orthorgonal polarizations are plotted separately, either horizontal and vertical or left and right circular polarization. However, in null steering, plots of nulls in a given direction have usually been drawn without regard to polarization. In particular, when a null exists in the jammer direction, it has often been assumed that a colocated signal could not be received.

The jammer polarization can be described at any given time by a specific elliptical polarization; the signal can be decomposed into this elliptical polarization and the orthogonal polarization. A general null steerer that uses elements with orthogonal polarizations would steer a null on the jammer with exactly the jammer polarization; the antenna pattern with the other polarization need not have a null toward the jammer or signal. Thus, a colocated signal could be received with the power of the signal that was in the elliptical polarization orthogonal to the jammer (in general a significant amount).

In a general LMS algorithm which maximizes the signal, the polarization orthogonal to the jammer will be maximized, since this clearly provides the optimum signal-to-noise ratio output. On the other hand, for a Biased Jammer Suppression mode, it is not as clear what the orthogonal polarization's gain toward the signal would be.

Polarization has not been adequately treated in this study, but must be considered carefully in any application.

# CHAPTER 9

# A UNIFIED TDMA COMMUNICATION - NULL STEERING SYSTEM

## 9.0 A UNIFIED TDMA COMMUNICATION - NULL STEERING SYSTEM

### 9.1 Introduction

This Chapter describes a null steering system designed for use with a TDMA communication network. In order to help clarify the description, specific message length, amount of PN coding, message preamble length, maximum range bet en users, etc., have been assumed. It is emphasized that these values are not critic . to the system design and may be adjusted over wide ranges.

Organization of this Chapter is as follows: Section 2 is a description of the assumed system configuration. Assumed message formats, geometric distribution of emitters, and basic system properties are discussed. Section 3 covers properties of the adaptive null steering array to be used with the system. This array has been designed with three operational modes, suppression, synchronization and reception; these modes are discussed in the light of system details. Finally, Section 4 contains a block diagram and descriptions of the adaptive array error formation circuit, a critical part of the communication-null steering system. The description of a computer program designed to simulate the system is presented in Appendix B.

### 9.2 System Model

#### 9.2.1 Geometric Configuration

It is assumed that the electromagnetic environment consists of friendly emitters, hostile emitters and thermal noise. The assumed geometric configuration is illustrated in Figure 9-1. The emitters are more or less isotropically distributed, and only a few hostile emitters are present (or significant). Due to the physical separation of the emitters, non-negligible and more or less unpredictable time delays exist in propagation time between two arbitrary emitters. The maximum time delay is set by the maximum possible range of communication.

#### 9.2.2 Mode of Transmission

Friendly emitters transmit and receive signals from one another on a cooperative basis whereby each friendly emitter has an assigned transmit slot in a TDMA system. Each friendly emitter listens to all other emitters. Emitter "i" directs a communication to emitter "j" by transmitting j's address in a preamble to the message. Information is transmitted at 10 Mb/s for this example.

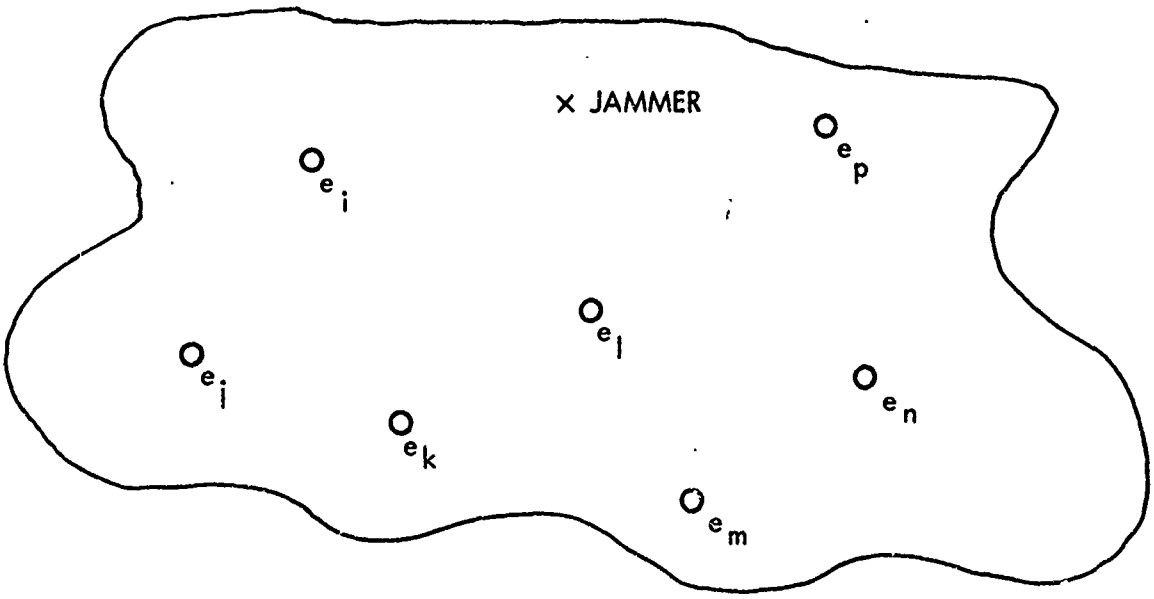


THE e 's REPRESENT FRIENDLY EMITTERS
THE × REPRESENTS A JAMMER

86258-1

Figure 9-1. Assumed System Geometry

### 9.2.3 Recognition of Friendlies

Due to the fact that hostile emitters exist, it is necessary that the friendlies be able to discriminate one another's emission from that of a hostile. Therefore, each preamble contains an exactly known a priori coded message. For this example, it has been assumed that an exactly known 127 bit code is used. Thus, a matched filter capable of compressing this code into one bit will provide a friendly to hostile recognition advantage of 21 dB.

Due to the possibility that a hostile emitter might repeat this preamble and thus be erroneously identified as a friendly, it is probably necessary that a time variable code be used. This problem involves both synchronization and matched filter design areas. Although solutions appear to be available, they represent a complexity that is additional to and detracts from the adaptive array aspects and so will not be considered at this time.

### 9.2.4 Message Coding

A 10 dB PN coding of message details is provided for intermodulation and multipath protection as well as for some protection against jamming. Synchronization to this code is discussed later.

### 9.2.5 Message Format

The assumed message format is shown in Figure 9-2. The 127 bit preamble is followed by a 10 dB PN coded message block. A very long code is assumed. The first 70 bits of this block are decoded into 7 "address" bits which uniquely identify one of the 127 friendly emitters. (The one for whom the message is intended.) The remaining message is slightly less than 20 ms duration. Given a 100 user system, about 2 seconds elapse between transmissions of a given user.

### 9.2.6 Jammer Characteristics

A hostile emitter (jammer) is assumed to use any appealing strategy except repetition (as discussed earlier). Since a given emitter uses only one TDMA slot and it is almost certainly the case that a jammer cannot ascertain which individual friendly he is jamming, then the most effective strategy would be continuous jamming. Noise modulation is a strong candidate. The subject of jammer strategies is discussed in greater detail in Section 9.3.3. The jammer is assumed to exceed signal strength by at least the coding gain, otherwise coding gain alone is sufficient for signal reception.

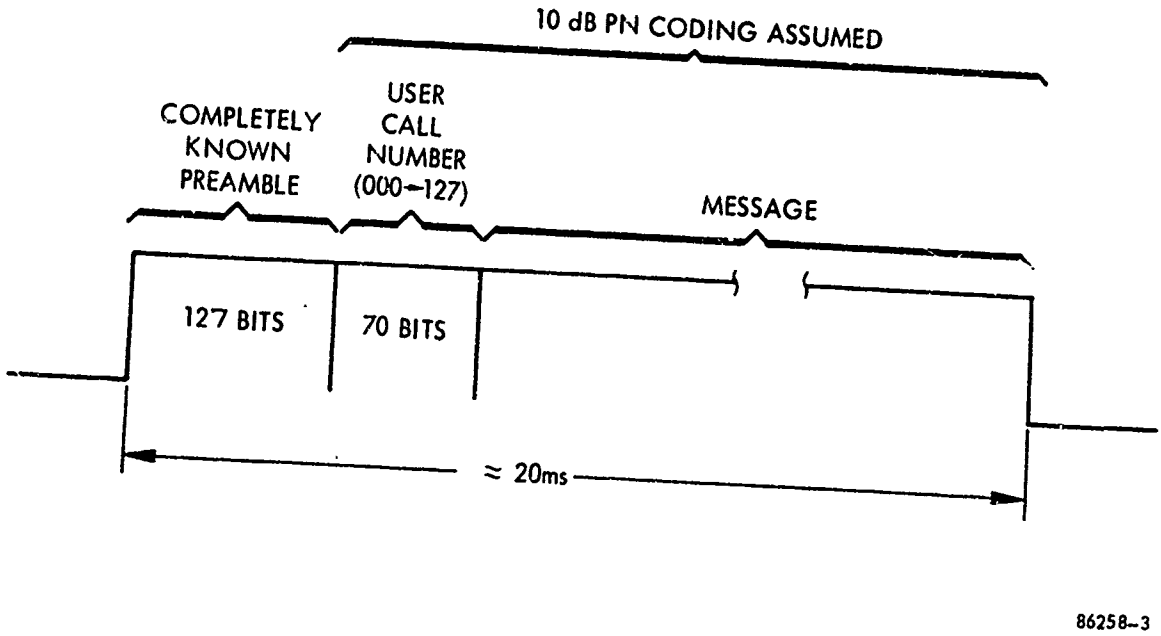


Figure 9-2. Assumed Message Format

### 9.2.7 System Synchronization

Continual user resynchronization is necessary due to unknown friendly locations, hence, propagation times. This synchronization is provided by the same completely known 127 bit preamble that is used for friendly identification. If a friendly to hostile power ratio sufficiently large exists, then a detectable pulse of about 1 bit duration will issue from the matched filter. This pulse is used to advance or retard the user's PN code generator to what we refer to as as a "flag point" (or message sync point). Flag points are illustrated in Figure 9-3.

If a maximum communication range of 300 miles is assumed, then a 1.5 ms maximum timing error could exist due to propagation. By prearrangement, the very long completely known PN code has been flagged at (approximately) 20 ms intervals. The flag points are used sequentially one per 20 ms interval. Receipt of a 127 bit preamble compressed to 1 bit (called a pointer) directs a user to move immediately to the nearest flag point (a move $\leq 1.5$ ms). Pointers missed for any reason do not affect the PN code timing. If the local clock is sufficiently accurate that an 18.5 ms drift does not occur before the next pointer is received, then continual synchronization is assured. (A crystal clock should be quite adequate.)

Since the 1 bit duration pointer locates a flag point to within 1 bit, then no searching is necessary in synchronization of the PN clock.

(Due to the relatively long time between uses of the 127 bit matched filter and the ease of maintaining expected flag point times within 18.5 ms, it appears simple to pseudorandom program the matched filter so as to combat repetition jamming.)

## 9.3 Desired Adaptive Array Properties

Briefly stated, the array is to minimize the system noise (thermal and hostile), maximize response to a desired friendly and do nothing to undesired friendlies. Different operational modes are used depending upon friendly to hostile power ratios at the array's output.

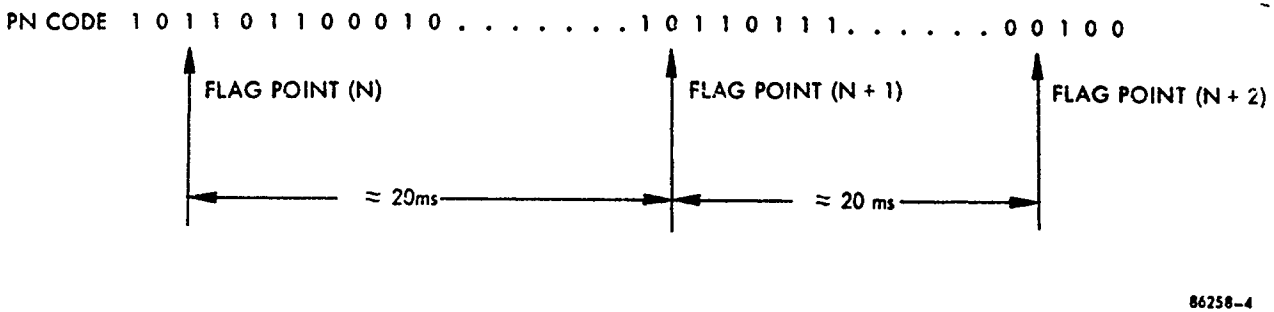


Figure 9-3. Assumed PN Code Form

### 9.3.1 Modes of Operation

Three principal modes of operation are envisioned. These modes will be discussed in detail later. They are:

1. Suppression mode. This mode is used whenever $S/N < -10$ dB.* In this mode, the array seeks to suppress received energy from the various powerful hostile emitters, thus improving S/N. The object of this mode is to provide sufficient S/N improvement for initiation of the sync mode.

2. Synchronization mode. The sync mode is used when $-10 \text{ dB} \leq S/N \leq 0 \text{ dB}$. Intelligent decoding of friendly messages is not possible in this S/N range, but since sync (and friendly signal recognition) can be provided by the preamble, a null steering mode whereby only hostile emissions are reduced is possible. The sync mode is used to improve S/N until intelligent decoding of friendly messages is possible.

3. Receive mode. Intelligent reception becomes possible if $S/N > 0$ dB. Two different receive functions are planned: Friendly reception and desired friendly reception. Desired friendly reception entails minimization of interference and maximization of the desired signal. Friendly reception entails only minimization of interference.

Although reference is made to selection of modes based on S/N, this "selection" is an implicit property of the chosen circuits. If one assumes that the system is operating, and that no mechanical faults have occurred, then failure of the matched filter to clearly produce "pointer" outputs is indicative of $S/N < -10$ dB (assuming that a 10 dB margin is necessary for pointer identification). If $S/N \geq -10$ dB mode switching occurs automatically when the pointer synchronizes the PN code generator.

### 9.3.2 Suppression Mode

If $S/N < -10$ dB then reception of the desired signal cannot occur until null steering has improved the S/N ratio. Since synchronization has not occurred, one cannot rely upon any a priori knowledge of the signal.

* In this section the symbol S/N will mean the usual output signal-to-noise ratio.

The suppression mode capitalizes upon an inherent property of adaptive arrays to reduce stronger interferences more rapidly than weak ones. Since the desired signal is unrecognized, it, as well as jamming, is treated as interference by the array. (In order that interference is not minimized by simply setting all weights to zero, it is necessary to constrain the array weights. A method of doing this uses one unity weighted antenna input.) As the array proceeds to reduce the stronger interference (jamming) more rapidly than the weaker signal, the S/N ratio improves. The sync mode begins whenever $S/N \geq -10$ dB.

Meanwhile, questions arise as to whether one can reasonably expect to reach $S/N = -10$ dB in the suppression mode. Guarantee of this condition requires one to examine all possible jammer strategies. As a reasonable compromise, one of the worst cases is discussed in the next section.

First there are two important points to be made regarding array size and configuration. The array should have about the number of degrees of freedom (weights) necessary to accommodate jammer nulling; too much flexibility can result in undesired friendly signal nulling. Secondly, waveform dispersion resulting from widely spaced elements or end elements in a multi-element array has the effect of reducing those element's effectiveness in either beam forming or nulling. From economic standpoi ts, the marginal benefits of additional elements becomes even less due to their additional cost. As a rough guide, then, a minimal element closely spaced array is suggested.

### 9.3.3 Jammer Strategies

If the hostile emitters wish to deny one or more particular users from receiving information, then jamming must be applied with a unity duty cycle; otherwise information from any one user destined for any other user could be relayed through a third unjammed user (since transmit slots are fixed). Clearly, this is at a penalty of reduced overall data rates and may be a mode not planned for this system, but even then it seems to present an unacceptable risk of failure to the hostile emitters. While it is conceivable that an effective unity duty cycle could be obtained from numerous pulsed and possibly synchronized hostile emitters, a more effective strategy would use the same number of emitters transmitting continuously. Thus, it seems reasonable to postulate continuously transmitting jammers. Finally, we assume that a jammer exceeds the signal in power at least as much as the coding gain. If it does not, coding gain alone is sufficient protection.

#### 9.3.3.1 A Possible Worst-Case

The null steerer equalization mode is designed to minimize the energy received from spatially discrete emitters. Thus, a worst-case configuration with regard

to S/N occurs if all desired signals appear to emanate from the same direction, each jammer is in a different direction from the array, and equal power is available from all emitters. (This situation is equivalent to a continuous signal emission.)

It is well established that the adaptive array is dominantly influenced by the most powerful emitters. Thus, the initial array response is to reduce the powerful emitters. The array produces more or less the following result due to correlation products at a given weighting circuit:

$$\left(P_{in}\ P_{out}\right)_i \approx \left(P_{in}\ P_{out}\right)_k \tag{9-1}$$

where $(P_{in})_i$ is the element input power and $(P_{out})_i$ is the array output power due to the $i^{th}$ emitter. (The above equation should be modified to account for lack of input-output correlation when wideband signals are considered.) This relationship appears to hold to about the number of terms as there are weights and with the significant terms being selected by power.

Contrary to biased suppression results which have been applied mostly to the "more elements than emitters" case, the weaker, or signal emitter(s), are not necessarily reduced to or below thermal noise. If the array has only enough flexibility to suppress the powerful jammers, then the signal output power is about equal to input power and the input-output product about equal to that of the jammers. Of course, if signal and a jammer are too close in angle (and polarization), then as far as the array is concerned, only one emitter seems to be present - the jammer; both signal and jammer will be suppressed.

Applying these arguments to a three element, two jammer, one signal case where signal-to-thermal noise is 20 dB and jammer-to-thermal noise 30 dB gives

$$\left(P_{out}\right)_{i_1} \sim \left(P_{out}\right)_{i_2} \sim 10\left(P_{out}\right)_{sig} \tag{9-2}$$

Signal-to-noise ratio is then about 7 dB. Actual signal output power is pattern dependent (established by jammer nulls) but about 20 dB is expected.

An example of these effects is given in Table 9-1 where steady state results are given for two jammers held fixed in azimuth with the signal azimuth varied. A three element linear array with half wavelength spacing and 10 percent bandwidths is considered. Signal power is 20 dB relative to thermal noise and jamming 30 dB. A relatively large signal power is chosen to simulate the "worst-case" mentioned earlier for all signals in one direction. It is found that as long as the signal is not close in azimuth to a jammer, Equation 9-2 and $S/N \approx 7$ dB holds true. Signal out is about 20-25 dB and thermal noise about 3 dB.

Table 9-1

| SIGNAL AZIMUTH | $45^\circ$ | $60^\circ$ | $80^\circ$ | $90^\circ$ |
|---|---|---|---|---|
| SIGNAL OUTPUT POWER, dB | 19 | 25 | 24 | 20 |
| $JAMMER_1$ OUTPUT POWER, dB | 15 | 16 | 15 | 14 |
| $JAMMER_2$ OUTPUT POWER, dB | 3 | 10 | 14 | 10 |
| S/N | 3 | 7 | 7 | 4 |

$JAMMER_1$ AZIMUTH = $30^\circ$, $JAMMER_2$ AZIMUTH = $100^\circ$

At low azimuth angles, reduced correlations due to dispersion upset the simple relationships as do close signal-jammer approaches in azimuth.

In one final note for this case, a transient analysis indicates that steady state is reached extremely rapidly due to jammer correlations rather than signal or thermal noise controlling the smallest eigenvalue. For the 90 degree signal azimuth case, the two eigenvalues are:

$$\lambda_1 = 2221$$

$$\lambda_2 = 1982$$

In a signal or thermal noise controlled case, much smaller second eigenvalues are found. Eigenvalues are discussed in Section 6-1. These particular eigenvalues are obtained. numerically as mentioned in Section 8.0.

### 9.3.3.2 An Expected Case

Under the more expected conditions the desired emitters are isotropically distributed and equal power is not received from each jammer. Isotropic distribution of

the friendlies coupled within their time multiplexed emissions is much like irreducible isotropic thermal noise to the array if the array's adaptation time (in the suppression mode) is long compared to emission slot time. Due to the duty cycle (1/M, where M is the number of friendly users) and Equation (9-1), we expect an S/N improvement equal to M over the continuous emission case. If there are 100 time slots, then M = 100 and a 20 dB advantage is gained. This advantage strictly applies when the number of weighted array elements, N, satisfies N = K +1 where K is the number of powerful jammers. Again, it is noted that the antenna pattern is principally controlled by the jammers; if desired signals are too near, they will fail into the jammer null.

Table 9-2 is a summary of power outputs for a three element, eight signal, and one jammer example. It is notable that the pattern is essentially established by the jammer and that signals are not suppressed even though relatively large average signal powers are assumed (all 10 dB relative to thermal noise in the first two columns, 0 dB in the third). Jammer power is 30 dB relative to thermal noise and 10 percent bandwidth is assumed. If we assume a 20 dB peak to average signal power, it is clear that no signal reception problems exist for this case.

Table 9-2. Summary of Power Outputs

| JAMMER AZIMUTH | $-30^\circ$ | $90^\circ$ | $70^\circ$ (0. dB Signals) |
|---|---|---|---|
| JAMMER POWER | 11.0 | 1.0 | 3.27 |
| SIGNAL$_1$ ($40^\circ$) | 2.0 | 12.5 | 2.2 |
| SIGNAL$_2$ ($80^\circ$) | 13.7 | 8.5 | -2.0 |
| SIGNAL$_3$ ($120^\circ$) | 13.4 | 14.2 | 3.7 |
| SIGNAL$_4$ ($160^\circ$) | 7.5 | 7.7 | 1.0 |
| SIGNAL$_5$ ($200^\circ$) | 7.5 | 7.7 | 1.0 |
| SIGNAL$_6$ ($240^\circ$) | 13.4 | 14.2 | 3.7 |
| SIGNAL$_7$ ($280^\circ$) | 13.7 | 8.5 | -2.0 |
| SIGNAL$_8$ ($320^\circ$) | 2.5 | 12.3 | 2.2 |
| OUTPUT THERMAL NOISE | 1.8 | 1.8 | 2.0 |

Expected adaptation waveforms for the array are illustrated in Figure 9-4. Power from a strong jammer is reduced more quickly than power from the weaker friendlies as the array is seeking to suppress powerful directionally received energy. Reference to Figure 9-4 when the remaining modes are discussed will be helpful.

The equalization mode is terminated at S/N $\approx$ -10 dB at which point the sync mode is instituted. In the sync mode, the friendly emissions are no longer minimized and a desired friendly is maximized. Considerations relating to this mode are the subject of the next section.

### 9.3.4 Sync Mode

The sync mode function is to improve the array's output S/N from -10 dB to 0 dB. This mode is entered automatically at the time S/N output of the matched filter following preamble reception is sufficiently great to locate a PN sequence flag point to within one bit. It is important to note that a desired friendly is treated the same as a friendly in the sync mode. This is because a desired friendly cannot be identified unless the first 70 message bits can be decoded, and intelligent decoding of message bits requires a larger S/N than the -10 dB available when the sync mode is entered.

Attainment of synchronization means that the bandspread message can be despread into a much narrower band of frequencies by mixing with the PN code. Since the jamming is not coherent with the PN code, it will not be despread. A narrowband reject filter centered about the despread signal is used to remove friendly signal energy from the error channel. However, most of the frequency spread energy from the jammer passes. In order to reestablish the jammer amplitude, frequency, and phase characteristics present before the signal despreading operation, the energy resultant from the filtering operation is respread by a second mixing with the PN code. This gives an array error output which has essentially no signal terms but essentially all of the jamming. (If serious time delays result, despreading at each element rather than respreading the output may be required, or compensating time delays might be used.) The array minimizes this error output which means that nulls are steered toward the jammers and friendlies are disregarded. Accordingly, S/N will improve for two reasons, (1) jamming continues to be reduced and (2) since friendlies are disregarded, partial nulls previously placed on them will be released and used for jammer rejection, improving signal response.

### 9.3.5 Receive Mode

The receive mode is attained automatically when S/N $\geq$ 0 dB and consists of two functions depending upon whether a friendly or a desired friendly is calling. The strategy is for one to do nothing (do not maximize or minimize array response) to a

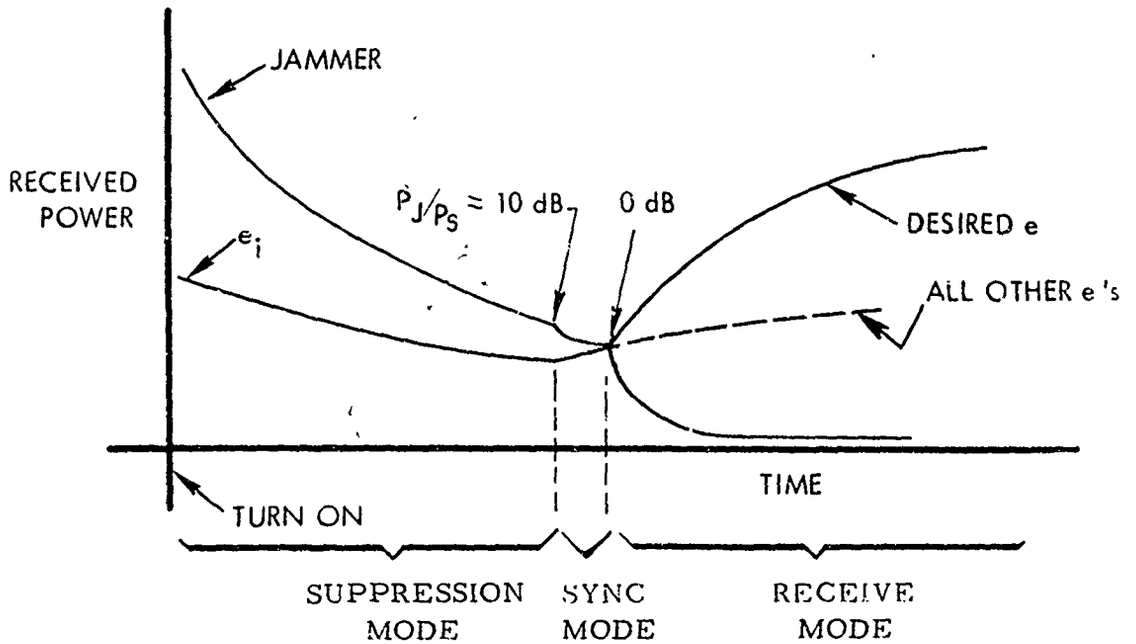


Figure 9-4. Expected Adaptation Waveforms for the Array

friendly (whose signal is not desired) and to maximize a desired friendly. The array achieves this first function by blocking friendly signals from the error channel exactly as done in the sync mode and will not receive additional attention here. The second function is realized by subtracting a desired response from the error channel in the conventional "Widrow" manner. Desired signal maximization requires formation of a "desired response," d(t), and a subtractive error forming circuit rather than the simple signal blocking used in the other modes. This mode is useful only when S/N is relatively high, due to difficulty in forming d(t).

When $S/N \geq 0$ dB, intelligent message decoding becomes possible, thus, a desired signal can be identified. Additionally, a desired response can be derived by decoding the desired signal, making hard decisions as to one or zero message bits, and producing a "clean" constant power waveform from these bits. Although errors will be made in estimating d(t), it nevertheless will be mostly derived from the desired signal. This derived d(t) is subtracted from the instantaneous array output in the conventional manner, giving $\left[\xi(t) - d(t) + \text{jamming}\right]$ in the error output and leading to maximization of $\xi(t)$ and minimization of jamming. Note that the estimated d(t) improves as the array adapts.

## 9.4 Circuit Description

The adaptive array circuit designed to produce the responses just described is illustrated in Figure 9-5. An array with the usual elements and weights (except perhaps for one input with a constant weight) is used. The major difference and the one illustrated is in the error formation circuits.

Conventional arrays obtain the error output $\epsilon(t)$, by subtracting a desired response, d(t), from the sum of weighted inputs, $\gamma(t)$. The circuit illustrated functions in the equalization mode if d(t) = 0, in the friendly receive mode if d(t) = 0 and $\xi(t)$ is blocked from $\gamma(t)$, and in the desired friendly receive mode when d(t) = constant power function of $\xi(t)$.

### 9.4.1 Suppression Mode

Assume that $S/N < -10$ dB. With reference to Figure 9-5, the array output $\gamma(t)$ is applied to a matched filter suitable for preamble detection and to a mixer (multiplier). Due to the poor S/N a "pointer" output will not be obtained from the matched filter. Therefore, the PN code generator continues to operate on the internal clock with no change in timing. Application of the PN code, referred to as c(t), to the previously

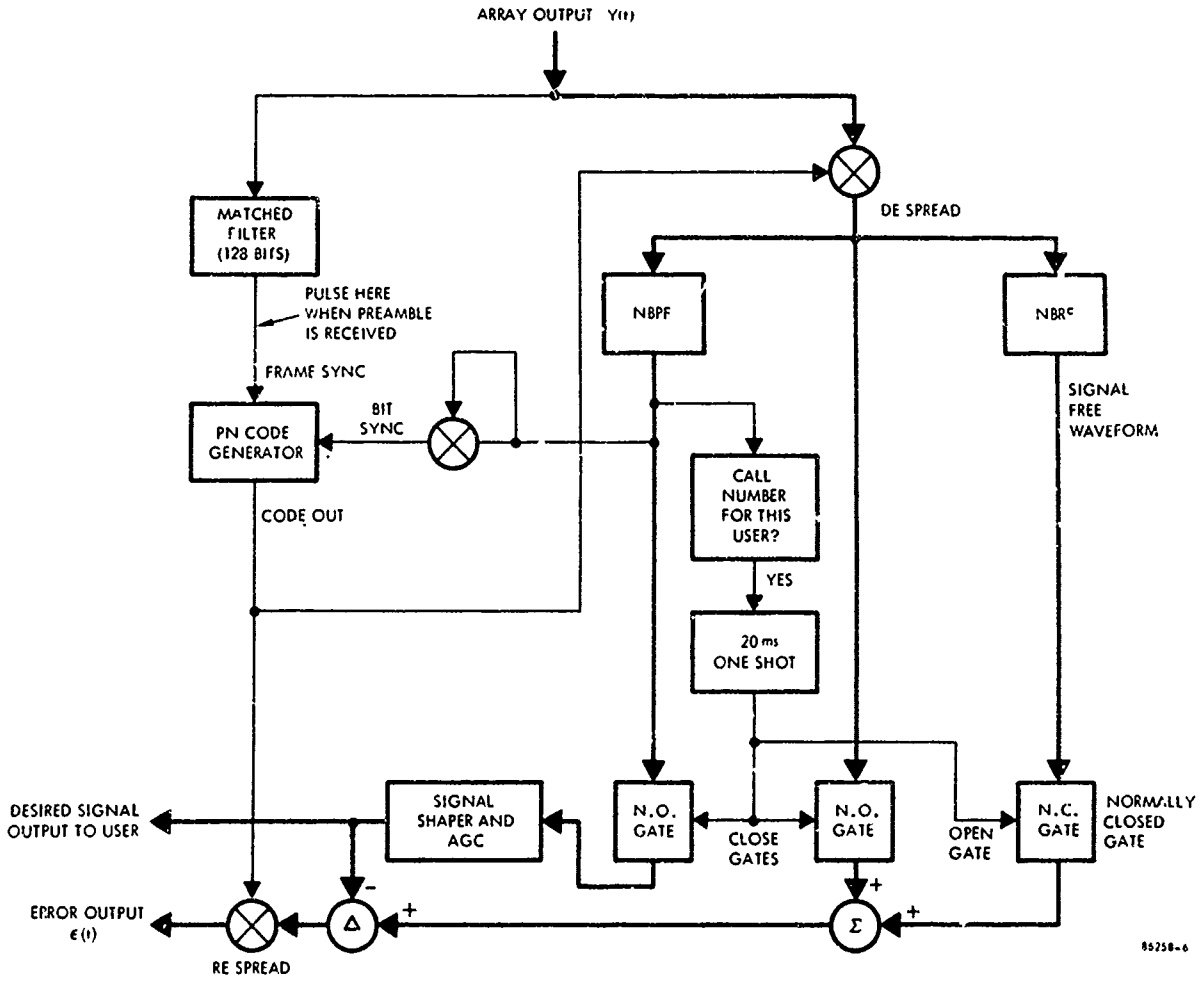


Figure 9-5. Block Diagram of Error Formation, TDMA

mentioned mixer causes a frequency spreading of all waveforms in $\gamma(t)$. This spread waveform, $\gamma(t)$, is applied to three channels.

The left most channel illustrated contains a narrowband pass filter (NBPF) which blocks all but a small part of the waveforms. If the code generator were synchronized, this filter would pass signal terms and block jamming. However, in this case both jamming and signal are spread, thus the filter output is essentially meaningless. Regardless, even if by chance the PN code generator were synchronized, the 10 dB S/N improvement provided by the NBPF would be insufficient to allow intelligent decoding of the signal. Consequently, a user call number cannot be ascertained and output from the left most and middle channels is blocked by normally open gates (NO).

Only signals in the right most of the three illustrated channels are allowed to pass (through the normally closed (NC) gate). The narrowband reject filter (NBRF) in this channel is designed to reject the same signal terms passed by the NBPF if synchronization existed. However, in this case both signal and jamming are passed.

This frequency spread and slightly filtered version of the array output is routed to a summing combiner and then a differencing combiner, but each of the other combiner inputs are zero (due to the NO gates). The waveform is applied to a second mixer which again is driven by c(t). Thus we get approximately $c^2(t)\gamma(t)$. A property of the PN code we will select is that $c^2(t) = 1$ (this is obtained if c(t) is composed of (+) and (-) bits). Thus, the error output, $\epsilon(t)$, is equal essentially to $\gamma(t)$.

Minimization of $\epsilon(t)$, as discussed previously, leads to improvement in the S/N ratio. Eventually, S/N has improved such that a clearly detectable pulse is obtained from the matched filter whenever a friendly's 127 bit preamble is obtained. This pulse synchronizes the PN code generator. As before, c(t) is multiplied with $\gamma(t)$, but due to synchronization having been obtained, the array automatically enters the sync mode.

### 9.4.2 Sync Mode

Due to the still poor S/N, call number identification is not yet possible and the various gate positions are unchanged.

With regard to the incoming waveforms, it is instructive to examine the $c(t)\gamma(t)$ despreading mixer output. Let $\xi(t) = c(t)m(t)$, where $m(t)$ is the information-containing uncoded modulation. Then we get

$$c(t)\gamma(t) = c(t)\left[\xi(t) + \text{jamming}\right] = m(t) + c(t)\,(\text{jamming}) \qquad (9\text{-}3)$$

Recall that $c^2(t) = 1$. Since we have assumed a 10 dB coding, $m(t)$ is despread into a frequency band 10 times less than the original band. The NBPF improves S/N by 10 dB but at the switchover to receive mode, this improved $S/N \approx 0$ dB.

The NBRF rejects $m(t)$ and a small part of the spread jamming. As before the error output, $\epsilon(t)$ is formed but due to synchronization and the signal blocking filter, we get

$$\epsilon(t) \approx c^2(t)\,(\text{jamming}) = (\text{jamming}) \qquad (9\text{-}4)$$

Note that the PN code generator should be frequency stable enough that sync is approximately maintained without bit sync correction during the 20 ms message period. Since the error output contains essentially jamming, the array output S/N will improve with time.

### 9.4.3 Receive Modes

The two different receive mode functions are determined, as discussed previously, by S/N and secondarily by detection of a particular user call number.

When $S/N \geq 0$ dB, the filtered output in the left most channel illustrated in Figure 9-5 will be sufficient to enable acceptably noise free reception of a friendly transmission. If the particular call number is not received, gate positions do not change, but a third mixer forms the product $m^2(t)$. The squaring result is like that of $2\cos^2(t)$, yielding a unity term and a second harmonic. The second harmonic of $m^2(t)$ is used to help maintain bit sync in the PN code generator. (This corrective sync may be unnecessary.)

The desired friendly reception mode occurs whenever the user call number is received. The call number identifier enables a monostable multivibrator (one shot) to turn on. This one shot's period is set to be that of the message duration, 20 ms. The gates NO are closed and the gate NC is opened. As can be seen from the figure, the despread array output is passed directly via the center channel to the summer which again has only one non zero input. However, the difference combiner negative input, $d(t)$, is now non zero.

The term d(t) is formed from the NBPF output which is nearly m(t). A signal shaper and AGC produce a "clean" and constant power waveform giving a second mixer input of $c(t)\left[\xi(t) + \text{jamming} - d(t)\right]$. Thus, for the error output we get

$$\epsilon(t) = \xi(t) - d(t) + \text{jamming} \qquad (9\text{-}5)$$

This expression is the form required for maximization of S/N.

Finally, the signal shaper output is also routed to the user, providing a decoded desired signal.

### 9.4.4 Important Response Times

Several important response times are inherent to this approach. If necessary they can be changed with acceptance of performance penalties or by system modification.

#### 9.4.4.1 Null Forming Time

In order to take advantage of possible friendly emitter isotropy (or at least non-colinear formations), it is necessary to average emissions for a time greater than one emission slot time. If one accepts that nulling within a 20 ms emission is not necessary, then one might null form for a second or so. (Since a given desired friendly transmits only once per 2 seconds.)

In order to accommodate more than one desired friendly per frame, one would want to reduce the null forming time. Depending upon this and other system considerations one may wish to null form in 40 to 100 ms.

#### 9.4.4.2 Beam Forming Time

Once relatively good nulls have been formed, it is desirable to quickly form a beam in the direction of the desired friendly. The speed in which this occurs may easily be regulated by properly setting the amplitude of d(t). However, if the constant power d(t) amplitude is set too large, excessive variance in weights will result.

In a final comment about response time, it is notable that the array can be expected to assume different response times as different power friendlies are received as a function of slot times The array may be in a suppression mode during one slot, desired friendly receive mode the next, etc. Consideration needs to be given to whether a jammer might advantageously use this "conditions variable" feature of the array.

# CHAPTER 10

# IMPLEMENTATIONS OF ADAPTIVE ARRAYS

## 10.0 IMPLEMENTATIONS OF ADAPTIVE ARRAYS

In the previous chapters only idealized complex weights, idealized perfect multipliers, and antennas have been shown in the array discussions. Of course, these examples are meant to portray only simplified systems that can be readily analyzed. In practice, we are faced with a receiver design type of problem plus many additional problems. In particular, the following areas must be carefully considered in designing an actual null-steering array:

a. RF vs IF weighting (whether or not IF strips are going to be used behind each element).

b. Types of Weights (including tapped delay line or different amplitude-phase types)

c. Types of Correlation

d. Weight Control

e. Weight Constraints

f. Amplitude and Convergence Rate Control

g. Signal Removal - (especially spread spectrum signal removal)

h. Unavoidable Time Delays and Phase Shifts

i. Antenna Element Type and Location

### 10.1 RF Versus IF Processing

One of the first design choices that must be made is whether the weighting will be done at RF or IF, as shown in Figure 10-1.

#### 10.1.1 RF Weighting

The main advantage of RF weighting (Figure 10-1a) is that no modification of an existing single-antenna receiver is necessary; multiple IF strips are avoided. All antenna signals are combined into one RF channel connected to the receiver. For this reason, most conventional command-steered phased arrays use RF phase shifters as weights. The disadvantages of RF weighting for adaptive arrays are:

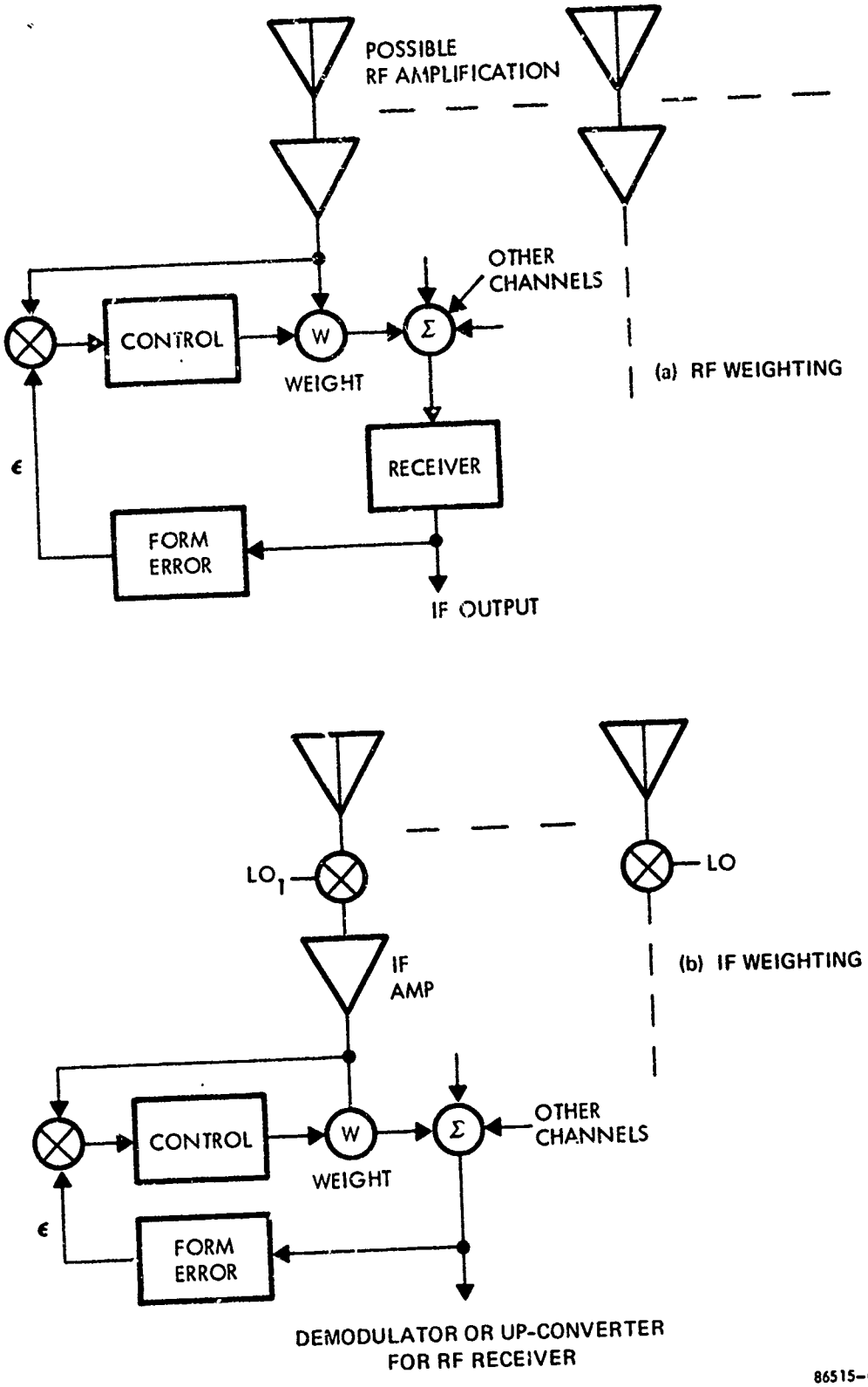


Figure 10-1. RF Versus IF Weighting and Combining

a. The amplitudes of weights using most conventional controls have a large dynamic range, depending upon the particular geometry and signal levels entering the array. Without prior amplification, serious losses in signal-to-thermal noise ratio would be encountered, due to the adaptive weight attenuations, as well as inherent resistive losses.

b. RF weighting usually requires RF correlation, which appears more difficult and expensive than IF correlation with presently available hardware.

### 10.1.2 IF Weighting

The need for amplification and filtering in much of the control circuitry, especially before and after correlation and matched filtering, makes the use of some IF processing almost essential. Although this does not preclude RF weighting, it makes all-IF-processing and weighting potentially useful, and possibly cheaper than RF weighting, especially if RF amplification is required to compensate for RF weighting losses. Figure 10-1b shows RF weighting; the local oscillator and RF amplifier are the IF strip of a receiver, and must be repeated for each element unless some time shared use is made of one processor. Since jamming can be expected to be much larger than the thermal noise, the noise figure quality of the receiver IF strips need not be as good as conventional receivers; other characteristics, however, such as dynamic range may have to be as good or better than conventional receivers.

Many microwave integrated circuit arrays, such as Texas Instruments MERA and RASSR, have these separate IF strips for each element of the array. At very high microwave frequencies, such as X-band or high power L-S band, such arrays are very expensive. At the lower VHF-UHF frequencies, where only a few elements are involved, the expense may not be great.

## 10.2 Types of Weights

Many possible weight types are shown in Figure 10-2. Since both amplitude and phase of a signal must be controlled, one can either control the amplitude of two quadrature phase components of the signal, or use a phase shifter to control the phase with one amplitude control. The first part of Figure 10-2 shows quadrature amplitude control with either double balanced mixers (four quadrant multipliers), variable gain amplifiers, or variable attenuators. The second section of Figure 10-2 shows amplitude and phase control with phase control from either phase shifters or mixers (employing a phase - shifted local - oscillator frequency).

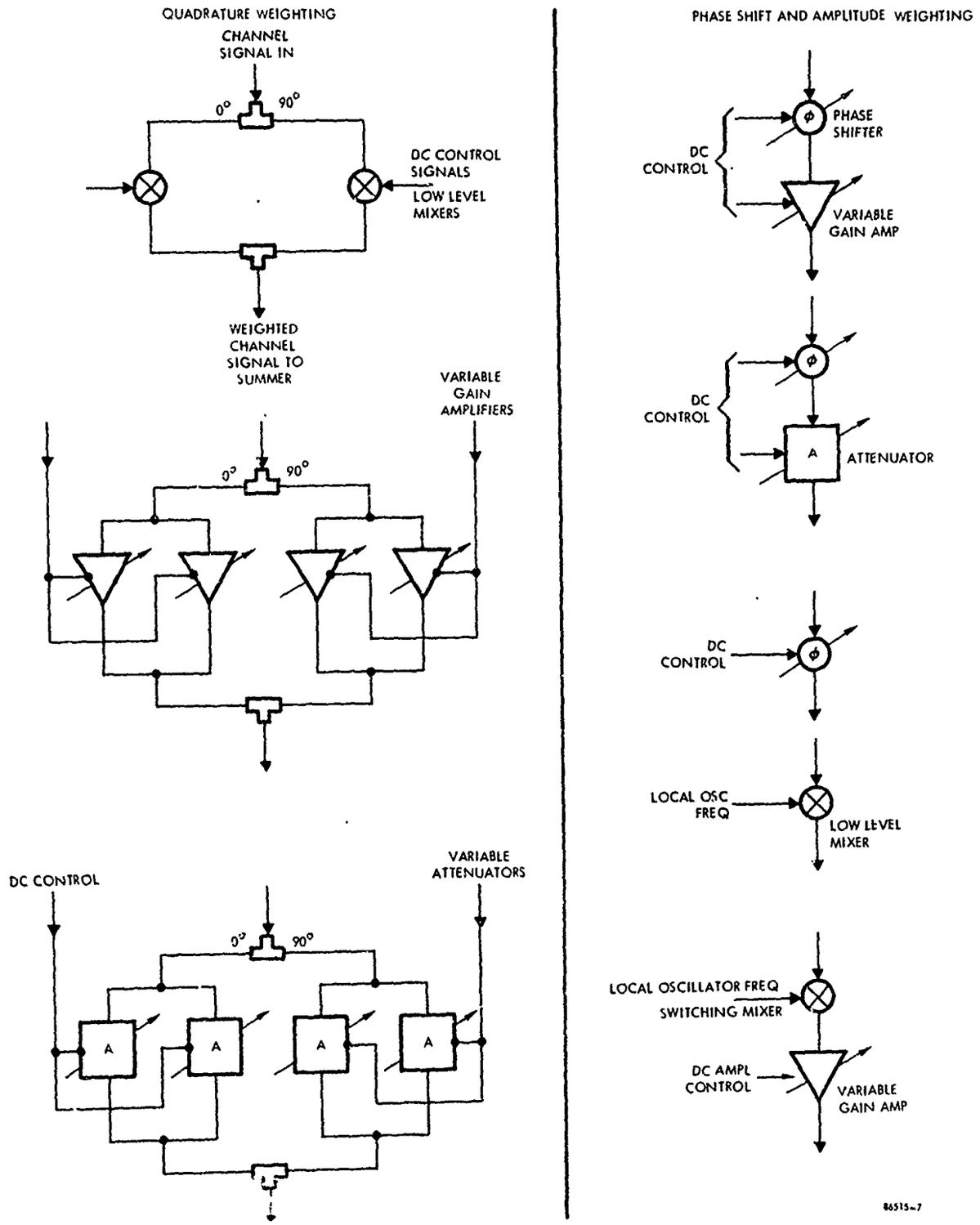


Figure 10-2. Possible Weight Types

## 10.3 Types of Correlation

The correlation shown in Figure 10-1a is usually between an RF frequency (the channel signal, $x_i$) and an IF frequency (the error) to yield a correlation signal at another "local oscillator" frequency. The output correlation would contain both amplitude and phase on the local oscillator carrier frequency. If the error was fed back at the RF frequency and at a high power level relative to the channel signal, leakage and oscillation would be difficult to prevent. With IF weighting, using IF amplification first, two high power level signals $x_i$ and $\epsilon$ are available for correlation; thus correlation can be performed with both signals at the same frequency, and output at dc. Since a dc signal cannot carry both amplitude and phase, correlations with dc output must be performed for both quadrature components of a narrow band signal.

## 10.4 Weight Control

The weight control circuitry and the amplification of the weights may be performed in many different ways; three basic ways are shown in Figure 10-3. In the first two ways shown, correlation output at dc is assumed, which requires correlation of the error with two quadrature components of the signal or vice versa. The correlation output at dc is integrated (low pass filtered) to form the voltages that control the two quadrature weights. In Figure 10-3a, the quadrature weights are applied to the signal channel directly. Compton [61,26] uses this method. In Figure 10-3b, they are applied to the low-level local oscillator, which in turn applies amplitude and phase weighting to the signal. Finally, Figure 10-3c shows a correlator output at some local oscillator frequency being narrowband filtered and mixed directly with the signal to apply amplitude and phase weighting. Applebaum [5] uses this technique in some of his sidelobe cancellers. The narrowband filter is not integral control, but much smoothing is available with a very narrowband filter. One serious problem with this technique is alignment of many very narrowband filters, if much smoothing (integration time) is required. Tracking filters, such as VCO's, may be used to alleviate alignment of passive narrowband filters, although additional complexity and expense results.

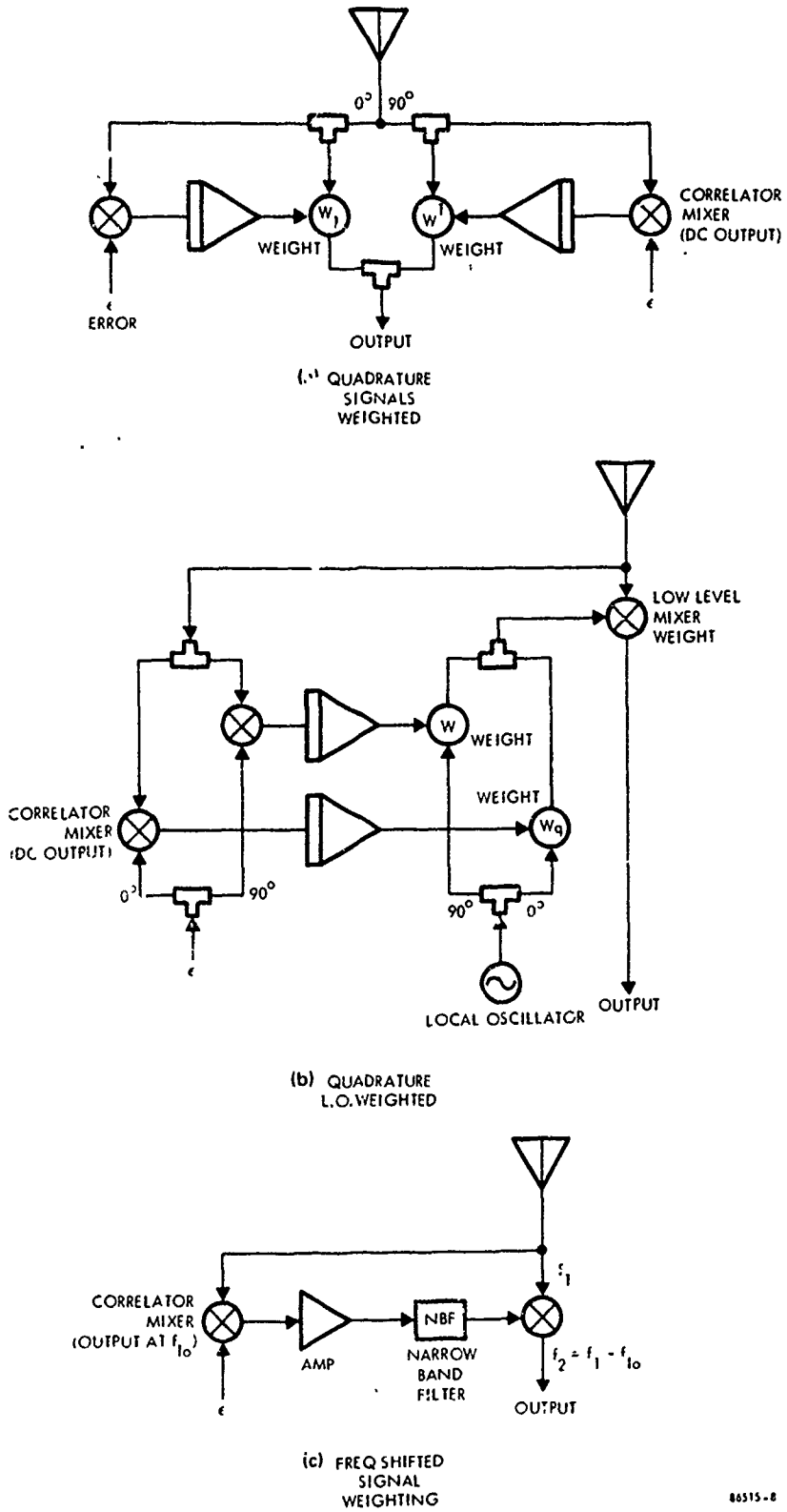


Figure 10-3. Weight Control

## 10.5 Weight Constraints

In order to understand the various adaptive arrays being discussed, it is important to list the possible weight constraints.

### 10.5.1 Before Signal Acquisition

For the acquisition case neither signal nor signal DOA may be known. With the "Strong Jammer Suppression" acquisition algorithm, the weights may be constrained as follows:

a. Unconstrained - The weights, in this case, go to a steady state value of zero (shut-off), but at a sufficiently slow rate so that signal acquisition can take place after the jammer is nulled. The report by Zahm[79] and the simulation program TSM2 uses this unconstrained case.

b. One Weight Fixed - In this case, the weights cannot go to zero since one weight is fixed. Thus, shut-off of the array is prevented, although, in the steady state, both jammer and signal are often well below thermal noise. Most examples in Chapter 8 use this constraint. Analytical solutions have also been obtained for this case.

c. Constant Norm of Weights, Sum of the Weights, Power Input, to the Processor or Output - Automatic Gain Control or a similar method could be used to keep the power input to the processor or output equal to a constant or to keep the sum of the squares of the weights or the sum of the weights fixed. It is probable that a fixed input power is a preferred one, because the eigenvalues and time constants of the system are proportional to input power.

d. Additive Forcing Function - The use of a forcing function, such as that discussed in Chapter 7, is similar in results, to fixing one weight.

### 10.5.2 After Signal Acquisition

After signal acquisition no explicit weight constraints are required, because the operations to optimize the signal implicitly constrain the weights:

a. Signal subtraction, for the "Known-Signal" algorithm, in which the signal is maximized and the weights are automatically constrained by forcing the output signal to be equal to the reference signal, see Widrow[76].

b. Signal Correlation subtraction for the "Known Signal- DOA" algorithm, in which the signal is again maximized and the weights constrained by forcing the output signal correlation to be equal to the subtracted correlation; see Applebaum[5], Griffiths[43].

c. Sum of Weights = Constant - This is the weight constraint used in the "projection gradient" algorithm. It is a "DOA-Known" algorithm in which signal correlation is derived and removed via a main beam pointed at the signal.

In addition, explicit weight constraints may be used, such as AGC, but only with care if the optimum solution is to be preserved.

## 10.6 Amplitude and Convergence Rate Control

It has been shown in Chapter 7 that the initial convergence rate of nulls on a dominant jammer was dependent upon the largest eigenvalue, $\lambda_1$. Most plots were normalized to the time constant $\tau = \frac{1}{\alpha\lambda_1}$. It is known that this eigenvalue is closely approximated by twice the total input power. Although the total input power is not known in an operational situation, the power in each channel is known,

$$P_{x_i} = \overline{x_i^2} \ .$$

Controlling these powers will control the convergence rate.

It is desired to control the convergence rate. Since the input power may have a very large dynamic range (due mainly to the varying range to emitters) some form of amplitude control is required. In addition, the limited dynamic range in correlators and weights make amplitude control necessary. Three controls are commonly used for amplitude control:

a. Automatic Gain Control (AGC)

b. Limiting

c. Logarithmic Amplification (Log-Amp)

A simplified figure showing such controls is shown in Figure 10-4.

Automatic gain control will clearly regulate the power entering the array processing. If this total power is held constant, then the integrator or filter gain $\alpha$ can be chosen for a desired initial convergence rate. Several disadvantages of AGC are the finite settling time and the suppression of very weak signals if instantaneous dynamic range is limited. For these and other antijamming reasons, AGC control is not used as much as it used to be in many applications; either limiting or log-amplification is preferred.

Limiting or clipping is also potentially very useful for amplitude control. It would not have the disadvantage inherent in AGC, such as settling time and limited dynamic range. The main question is how well a correlator would perform using signals that had been limited. It appears as if the effects of limiting in null steering is not yet clearly understood. The resulting correlation would be equivalent to phase detection. Thus, amplitude would be lost. The phase information would permit the crucial phase shift weighting in each channel, which would allow some nulling of the jamming. If very hard limiting were not employed, then the correlation could go into a linear range when most of the jamming was removed from the error channel. Initial experimentation has verified that such soft limiting can be used successfully in a null steerer, but that convergence was, in one realization, very slow during the time that limiting occurred, possibly due to the loss of amplitude error information.†

The use of logarithmic amplifiers is also possible, but has not been explored or reported on to our knowledge. Of course, antilog operation would also be necessary before array summation because a linear combination of array channels is required to cancel jamming. Otherwise, non-linearities, different in each channel, would change the signals differently in each channel, making cancellation impossible.

---

†More detail of limiting is found in Technology Services Corp. "Adaptar, Space-Time Processing in Airborne Radars," Feb. 71, AD881462 (U).

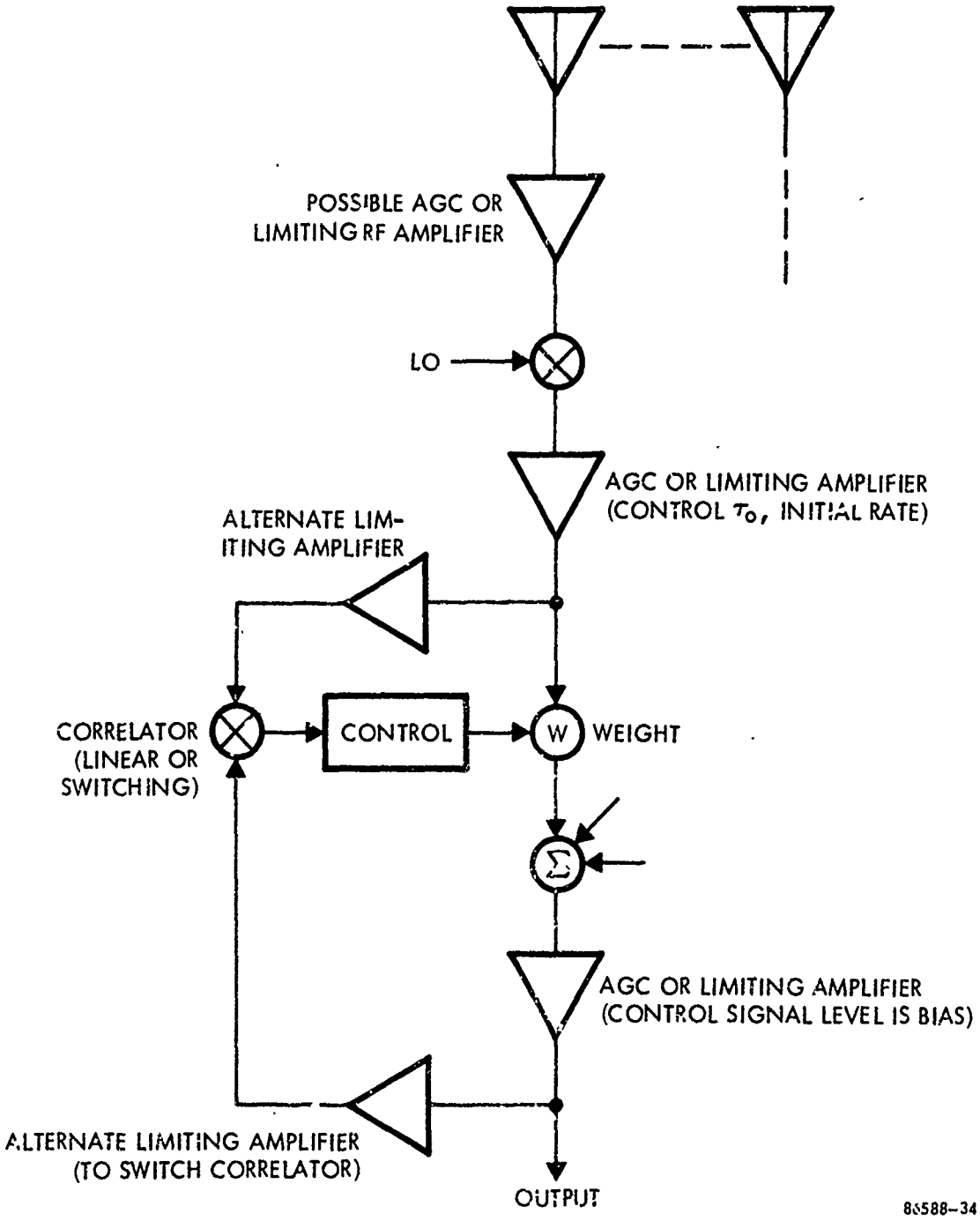


Figure 10-4. Amplitude Control for Convergence Rate and Bias Control

## 10.7 Signal Removal of Spread Spectrum Signals

It was discussed in Chapter 8 that signal removal from the error channel may not always be required, but is generally desirable to prevent signal degradation or to provide antenna gain toward a signal. For some situations, especially those in which only a few signals are present having long acquisition and transmission times, partial signal removal after initial signal acquisition is relatively simple. However, in the case of many simultaneous spread spectrum signals, considerable difficulties arise in removing the signals from error channel. A serious problem is time delay through the matched filters (or correlator systems). Since the signal cannot be known a priori, the signal must be detected via matched filters at the receiver output, which make correlation with the input signal $x_i$ more difficult. These matched filters must have a delay of approximately the information bit in order to make a decision on any spread spectrum sequence of "chips." For a spread spectrum signal of 10 MHz and assuming a surface wave matched filter with roughly 10 μs length is the maximum available (as is presently the case), approximately 20 dB of spread spectrum processing improvement is available; however, delay of $\approx 10$ μs are encountered in the matched filter. In order for correlation over 10 MHz bandwidth with the ith input channel signal, $x_i$, it too must be delayed 10 μs (note, in each channel). Such delays could be expensive and lossy. If larger processing gains, such as 40-50 dB, are used with a 10 MHz bandwidth, delays of 1-10 msec are needed which are extremely difficult to achieve.[††] Digital sampling, processing, and storage techniques might be required, or other techniques such as biased suppression or "DOA-Known" types could be used that do not require signal estimation.

Two possible techniques of spread-spectrum-signal removal using matched filters are shown in Figure 10-5. In part (a) of the figure, identical banks of matched filters are used in both the error and ith signal channel, one filter in each bank for each signal sequence to be detected. Since the signal energy in the output of each matched filter is concentrated with a high peak pulse, this signal energy may be partly removed by clipping the signal at about the detection threshold. Noncoded jamming and noise will be spread in time and unclipped. Thus, correlation will be done mainly on jamming, transformed by the matched filter almost identically in the two channels. As in all "Separable Jamming" techniques, signal is not maximized by this array processing.

[††] Latest information available indicates that delays on the order of up to 100 μsec are now available.

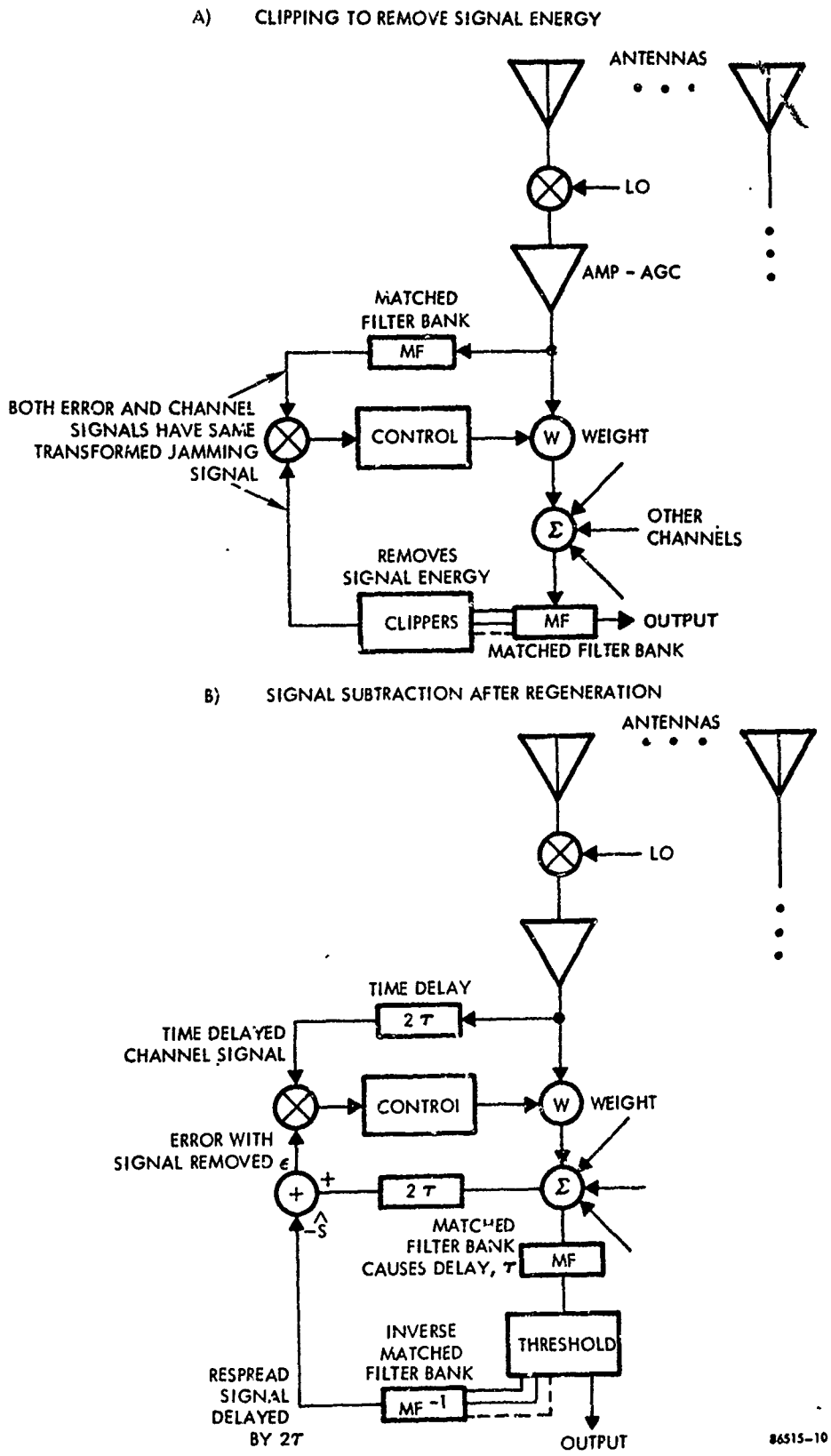


Figure 10-5. Spread Spectrum Signal Removal Techniques Using Matched Filters

by clipping the signal at about the detection threshold. Noncoded jamming and noise will be spread in time and unclipped. Thus, correlation will be done mainly on jamming, transformed by the matched filter almost identically in the two channels. As in all "Separable Jamming" techniques, signal is not maximized by this array processing.

The outstanding difficulty with this signal removal technique is that the matched filter band must be repeated for each channel. For two matched filters (for a 0 and 1), this is not too difficult. However, if a different matched filter is used for each sensor, or for a group of sensors in order to allow simultaneous communication with many sensors, then the technique probably requires too many matched filters to be practical.

Another signal removal technique, shown in Figure 10-5b shows a technique of signal subtraction, which will maximize signals, since it is a "Known-Signal" thresh-technique like Widrow's [76] "mode 1" array. In this technique, the output of the old detector that follows each output matched filter will trigger an identical matched filter to regenerate each coded signal. The composite coded signal is then subtracted from the output to form the error channel as in the "Known-Signal" adaptive array. Single time delays, instead of banks of duplicate matched filters, are now required in the output before signal subtraction, and in the ith signal channel.

If, instead of matched filters, synchronized reference sequences are used to correlate and despread the spread spectrum signals, then similar techniques for spread spectrum signal removal have been developed and are shown in Figure 10-6. In Figure 10-6a, the synchronized reference sequence is correlated with the input signal to produce a narrowband signal, but uncoded jamming remains spread over the spectrum. Before narrowband filtering (which would eliminate most of the jamming that must control the adaptive array), the usual adaptive array is used, with the addition of a narrowband reject filter in the error channel for signal removal. This technique is a more sophisticated, spread-spectrum version of the simple "Separable Jammer" technique of filtering and separating out-of-band jamming for use in null-steering. The delay and distortion of the narrowband reject filter is probably minimal and can be compensated for, but the disadvantage of different codes for each different sensor remains; a different coded, synchronized reference signal is needed for each signal. The synchronization problem itself appears very difficult, even for a conventional single channel signal processing system.

A similar scheme, due to Compton, for signal removal is shown in Figure 10-6b. A PSK signal is assumed after despreading. Squaring this signal results in a double frequency carrier which may be removed in a very narrowband reject filter in the error channel. Thus, a "carrier" portion of the signal has been removed, which may prevent nulling of the signal.

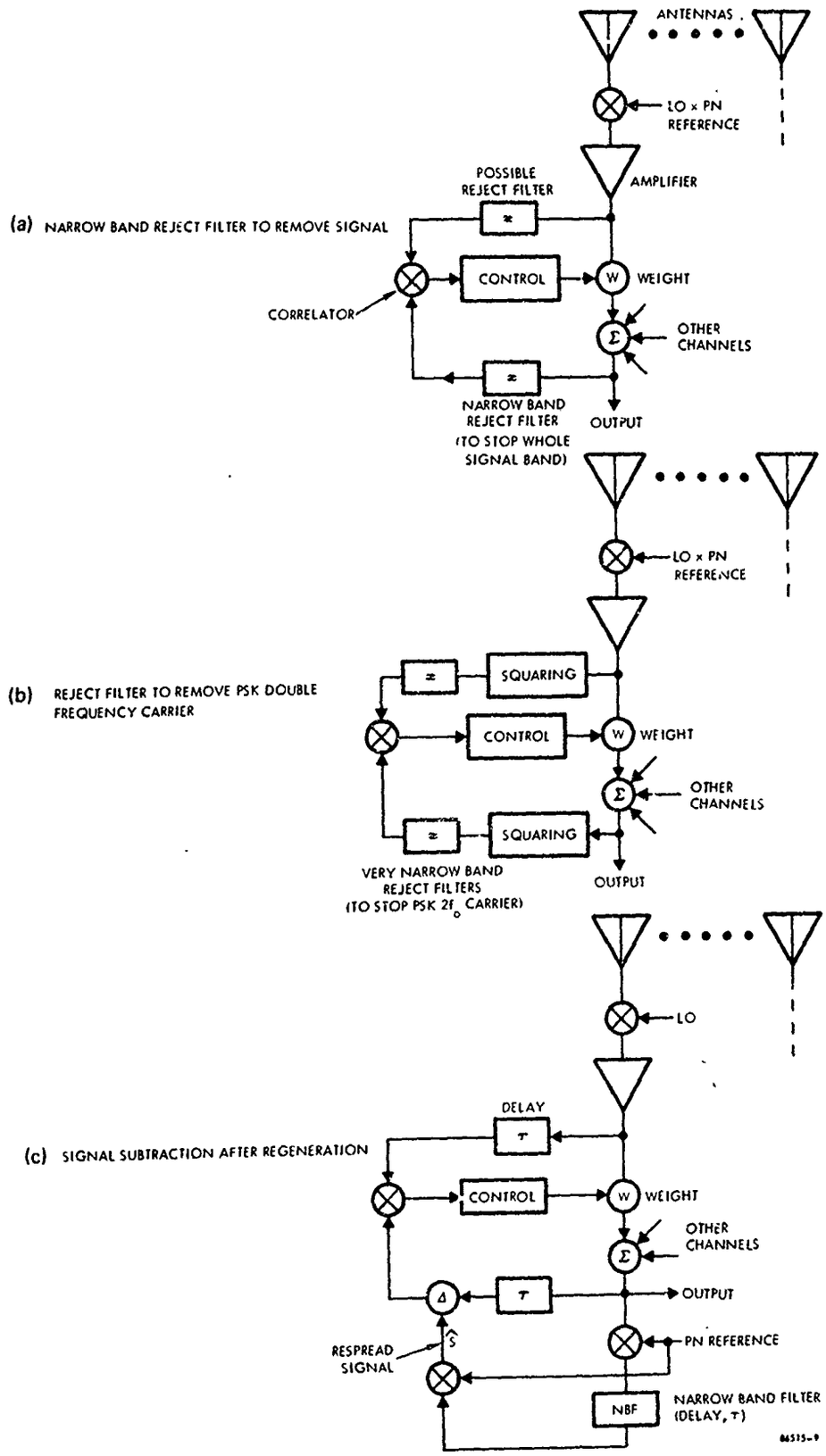


Figure 10-6. Spread Spectrum Signal Removal Using Correlation With a Reference

A third technique, also due to Compton and others, filters out the despread signal through the narrowband filter in the signal channel, then regenerates the coded signal by spreading it with the reference sequence. This forms a signal estimate, delayed by the narrowband filter. With compensating delays, a "Known-Signal" adaptive array technique can be used. There is still difficulty in signal distortion through the narrowband filter causing an error in the correlation of the error with the channel signal, $x_i$. Compton has recently reported, in private communication, that he was limited to a 4:1 spread spectrum bandwidth reduction which is believed due to the delay and distortion in the narrowband filter; although he recognizes the need for a delay, it is believed that he did not use a compensating delay in the above experiment.

# CHAPTER 11

# BREADBOARD DESIGNS AND DESIRABLE EXPERIMENTS

## 11.0 BREADBOARD DESIGNS AND DESIRABLE EXPERIMENTS

The preceding chapter discussed possible implementations of the general functions (correlation, weighting, etc.) that are needed in adaptive arrays. The "best" implementation is not known, but designs for adaptive circuits and even adaptive arrays, have been implemented in the past. Several designs do look most promising.

In this chapter, designs that presently look most desirable will be presented along with experiments that must be run to determine the best design for communication purposes, especially with spread spectrum signals and many users.

There are two objectives in these experiments: (a) finding the best implementation(s) via a flexible breadboard, which is emphasized herein, and (b) applications experiments with the best implementation(s).

### 11.1 Preferred Implementations

There are two preferred basic designs based on studying the apparent complexity of the various implementations in Chapter 10 and on what past experience has been published in this area. These basic designs utilize the following weighting techniques:

a. Quadrature Channel Weights

b. Complex Weighting

as shown in Figure 11-1. Figure 11-1a shows dc correlation and integrator control of quadrature weight channels. There are several weight types that need to be evaluated with this basic implementation, namely diode double balanced mixers, variable attenuators (such as PIN diode attenuators), and transistor multipliers (double balanced mixers) such as Compton uses.

Figure 11-1b shows a basic IF correlation scheme with narrowband pass filtering replacing the integration. The weight will probably be a double balanced mixer, run at a level low enough to give both amplitude and phase weighting, such as done for diversity combining by Raytheon [80], and for sidelobe cancellers[6]. Another possibility is using the mixer only for phase shifting, and amplitude weighting with an amplifier or variable attenuator.

There are, of course, other designs that may be important, such as one that would control RF phase shifters directly. However, the above two basic designs, with variations due to different weighting schemes, are ones that there is some experience to base confidence upon, and that can be evaluated with the same basic test bed to be described.

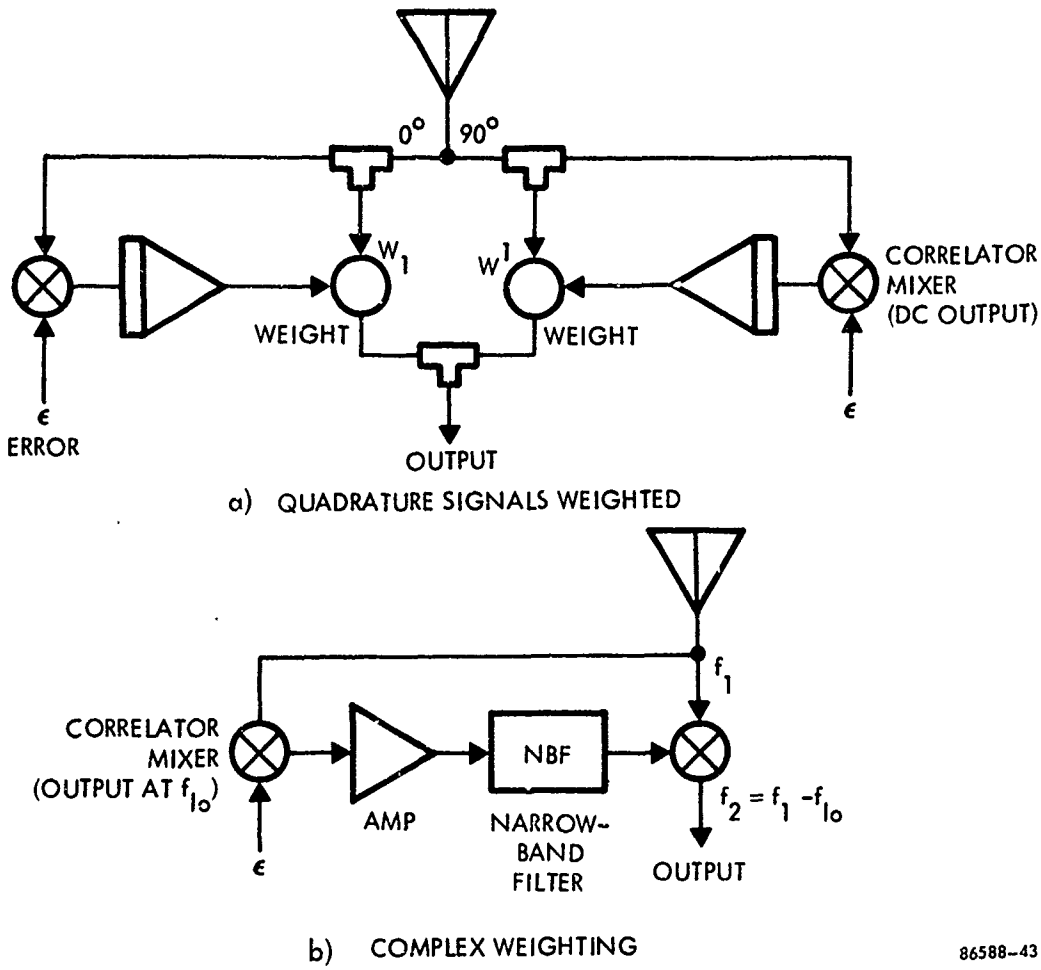


Figure 11-1. Preferred Implementations

## 11.2 Breadboard Experiments

Given the basic preferred designs, there are then a host of design problems that must be answered. The construction of a very flexible breadboard or test bed would allow one to measure and compare the performance of several different designs, especially using different weight types. It is felt that there are three basic steps in building such a breadboard:

a. A basic two-channel test bed, which would have one variable weight channel and one fixed weight channel, in order to test the weight type as cheaply and quickly, as possible. It would steer one null on one jammer.

b. A 3-5 element array using several, or at least the best, weighting technique decided upon during the two channel experiments above.

c. A signal removal breadboard to test the various techniques for removing spread spectrum signal effects from the null-steering control. The most promising technique should then be tried in the two-channel test bed, and then the 3-5 element array. Because of the strong potential of using biased jammer suppression without removing the spread spectrum signal, it is felt that this experiment can be run separately, and not seriously affect the basic null-steering breadboard.

Note that the two channel test bed is not being called an array, although it can null one jammer and is potentially quite useful. The two channel testbed is to test the correlator, control circuitry, weight, dynamic range problems of amplifiers, and a host of other circuit component problems associated with controlling the array.

For each of the two basic designs in Figure 11-1, a more detailed design will be given to show the potential cost and complexity of the experiment. It should be clear that the equipment is relatively inexpensive and straightforward to build. By using coax throughout at 60-70 MHz IF, a very flexible test bed could be built.

### 11.2.1 Quadrature Channel Experiments

Figure 11-2 shows the basic three-element array that will be constructed. One fixed weight (straight-through connection) is used, both as a practical weight constraint to prevent weight shut-off, and to conserve on parts while allowing three elements. The weighted channel on the left consists of an antenna, mixer, bandpass filter and amplifier; i.e., an IF strip. The power is then split into quadrature channels ($0^o$, $90^o$) to provide amplitude control alone in each channel and vary both amplitude and phase of

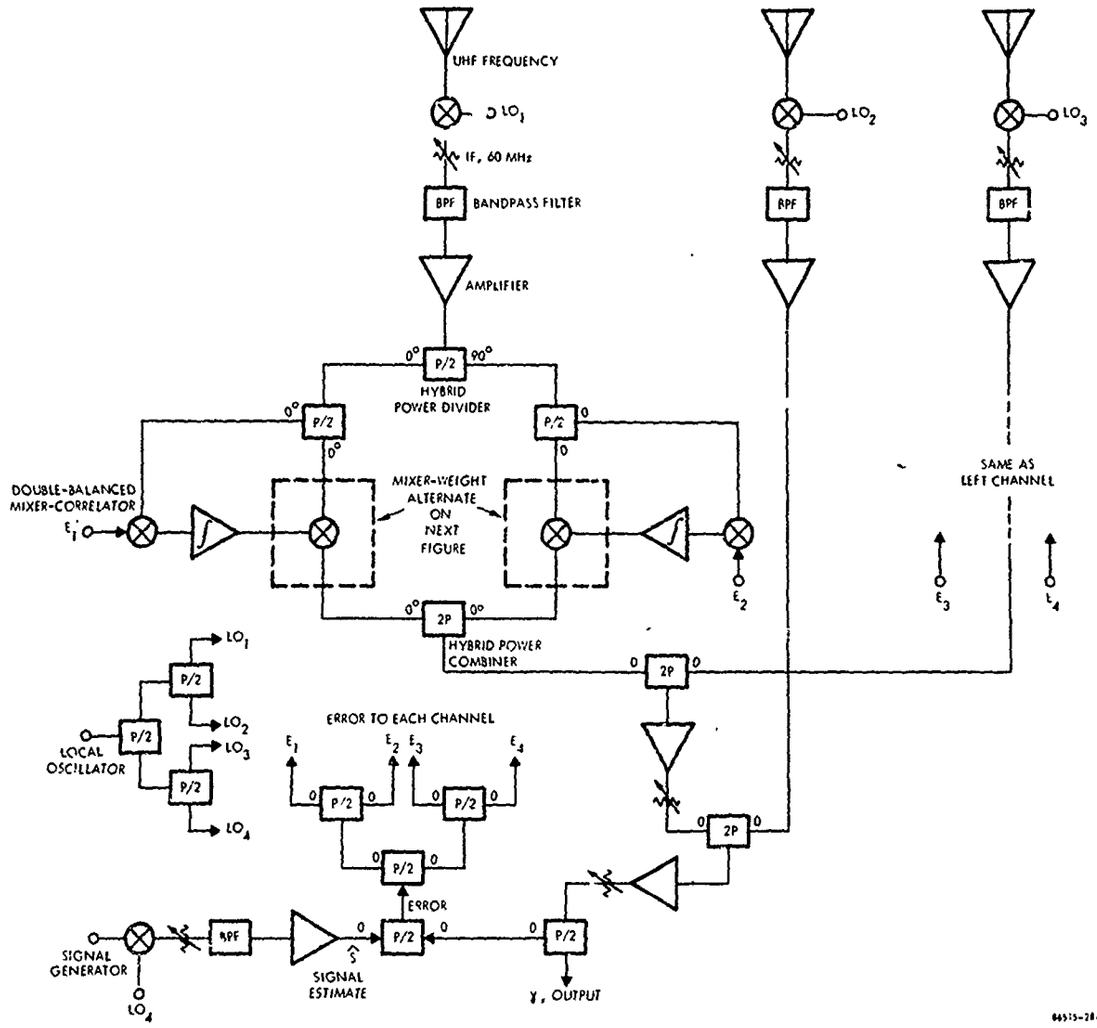


Figure 11-2. Laboratory Breadboard (Quadrature Channel Mixer Weighting)

the entire channel's signal. Considering only the $0^{\circ}$ channel, this is then split into a signal going to the correlator and one going to the mixer weight. The correlator drives an integrator, whose output voltage is the control voltage on a double-balanced mixer attenuation weight. The amplitude of the output of the mixer is proportional to the control voltage applied, thus multiplying the IF signal by the weight. Both quadrature channels are thus weighted and added together then added again to the signal from the right hand channel. These two channels are the only two weighted channels, and since the attenuation of the mixer operated in its multiplying range is rather large (-25 dB), amplification and amplitude trimming is provided before addition to the unweighted channel. Finally, the sum of the three channels is amplified again, and split into an output signal ($\gamma$) and a signal to be fed back to form error. A local oscillator signal generator is split into four channels for use as shown in the diagram. A signal generator, which will be the source of the incoming desired signal, is mixed with the fourth channel of the local oscillator to form a "desired signal estimate" at the output IF, and is subtracted from the feedback output signal to form an error signal. The error signal is split into four parts for the correlators in the weight control circuitry. This diagram then forms a simple realization of the basic Widrow ("mode 1") LMS algorithm. One of the advantages of double-balanced mixers is that the dc voltage multiplying the signal may be either plus or minus. The minus automatically reverses the phase ($180^{\circ}$) in the signal channel. With 0 to $\infty$ attenuators, phase reversal must be performed another way. The amplifiers shown are required to bring the low input signal levels up to values needed in the correlator ($\sim$ -25 dBm). In addition, other amplifiers are needed after the mixers to make up for the natural loss in multiplying two low-level signals. The correlators will also be double-balanced mixers, because of their wide bandwidth and good rejection of unbalanced signals from each individual channel.

Both transistorized and diode double-balanced mixers should be tried. Recent work by Compton[28], shows good success with transistorized multipliers (mixers), as shown in Figure 11-3a. Good isolation is an advantage of active circuits. Figure 11-3b shows a quadrature attenuator weighting scheme that is also planned for testing. It can be inserted in place of the balanced mixer weights. The attenuators will be PIN diode attenuators commonly used in microwave and IF equipment. Drivers will be required for each PIN diode, and of course two different attenuators in $0^{\circ}$ and $180^{\circ}$ lines of a hybrid will be required for both in-phase and quadrature components of the signal in each channel.

In addition to the antenna inputs, it is planned to have a laboratory bench power splitter and delay method to provide test signals that simulate a signal and jammer arriving from different directions. A block diagram of this equipment is shown in Figure 11-4.

So far the design is detailed enough to get an approximate part count for a two channel test bed or a three element array. This circuitry should steer nulls if proper amplitude levels are set at the input so that the dynamic range of the components is not exceeded. The mixers, used both as weights and correlators in Figure 11-2, have a very good dynamic range; some are advertised as having over 50 dB. However, the

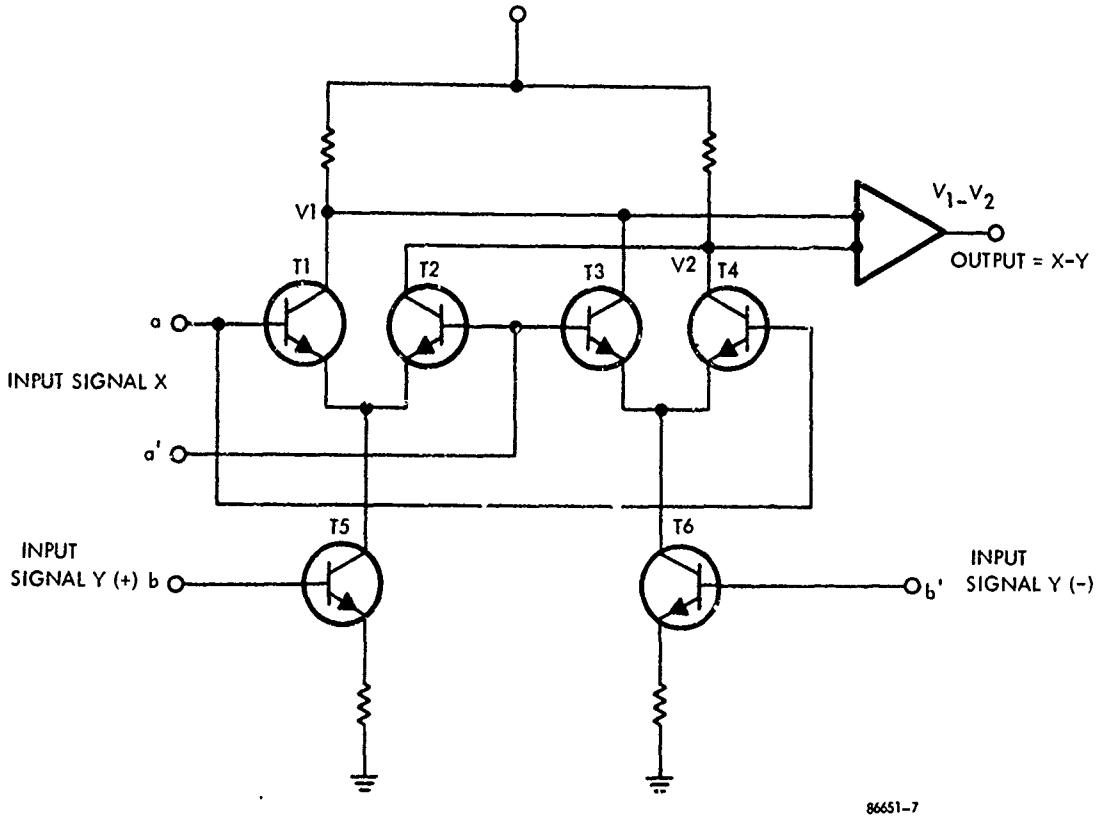


a) Transistorized Multipliers (Mixers)

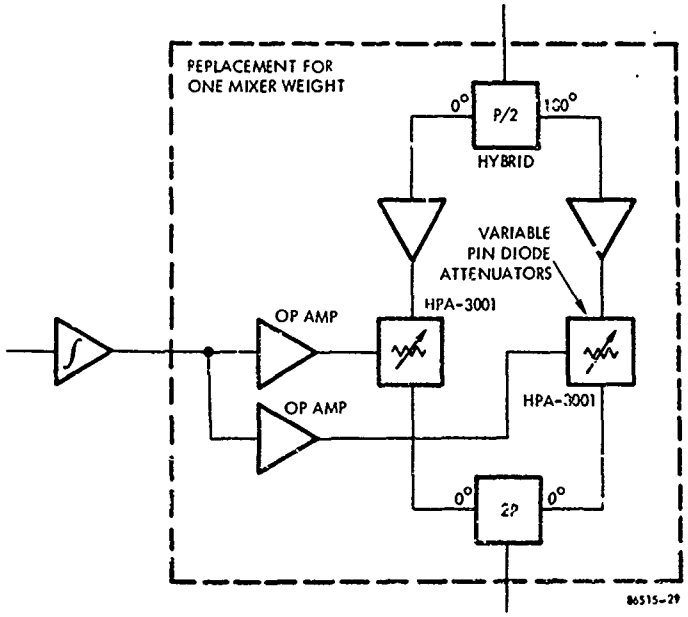


b) Quadrature Attenuator Weighting

Figure 11-3. Variable Gain Weight

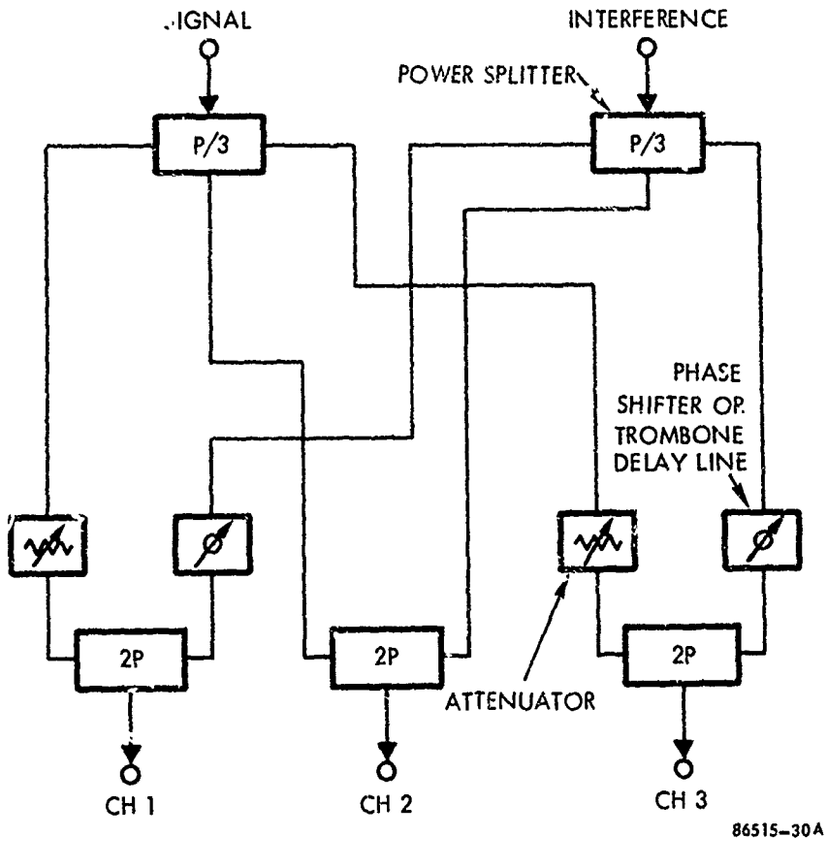


Figure 11-4. IF Test Signal Power Splitter

**Preceding page blank**

amplitude and convergence constant controls discussed in Chapter 10 are not included in the basic design. Either AGC amplifiers or limiter-amplifiers were good possibilities for this control. At least two amplifiers of each type should be obtained for a two channel test bed to measure the impact of these important real components upon null steering capability. Initially, it would be possible to put a limiter after the input amplifier to obtain limiting action. For the AGC amplifier, it could be adequately simulated by manually setting the approximate total input power level.

As discussed at the beginning of this chapter, the signal processing that might be used to obtain a Widrow algorithm is considered as a separate experiment, and is thus not included in the basic breadboard design.

### 11.2.2 Complex Weight With IF Correlation

A more detailed design of the basic "complex weighting" scheme of Figure 11-1b is shown in Figure 11-5. This figure is considered an addition to the basic breadboard, Figure 11-2; local oscillator distribution, etc. is assumed the same. The left channel, as in Figure 11-2, begins with an IF strip, and then splits to a correlator and to a weight. However, this time the weight will be "complex," that is, both an amplitude and a phase weight combined, without quadrature channels. This complex weight is formed by the correlation, through the double-balanced mixer shown, of the error signal at 70 MHz and the channel signal, $x_1$, 100 MHz. The narrowband filter at 30 MHz passes the difference frequence only, which carries both the phase difference between $x_1$ and the error $E_1$ and the amplitude of the correlation. This 30 MHz signal then multiplies the $x_1$ channel signal through the double-balanced mixer weight. The 30 MHz weighting signal acts as a 2nd local oscillator, but is not allowed to hard-switch the mixer. The signals from the left and right channels are then added, amplified, added to the unweighted channel, amplified again, and split between the output signal and the signal used to form the error. All of this is similar to Figure 11-2, and can use essentially the same equipment, except for the 100 MHz first IF. If necessary, the first IF could be left at 70 MHz, and the second IF could be lowered to 60 MHz or less. The frequencies shown are not firm, and depend on exactly what the implementation of the narrowband filter will be.

The narrowband filter is the crux of this design. It could be a crystal filter, if two or more exactly matching crystals can be found or tuned for the various channels. Although this is a simple implementation, the smoothing time of the filter is limited (milliseconds) by the narrowbandwidth obtainable.

A more flexible filtering scheme is the so-called "tracking-filter" shown in Figure 11-6. It is a normal phase-locked loop whose feedback filter bandwidth may be made very small, resulting in long smoothing times. The vco itself generates the output

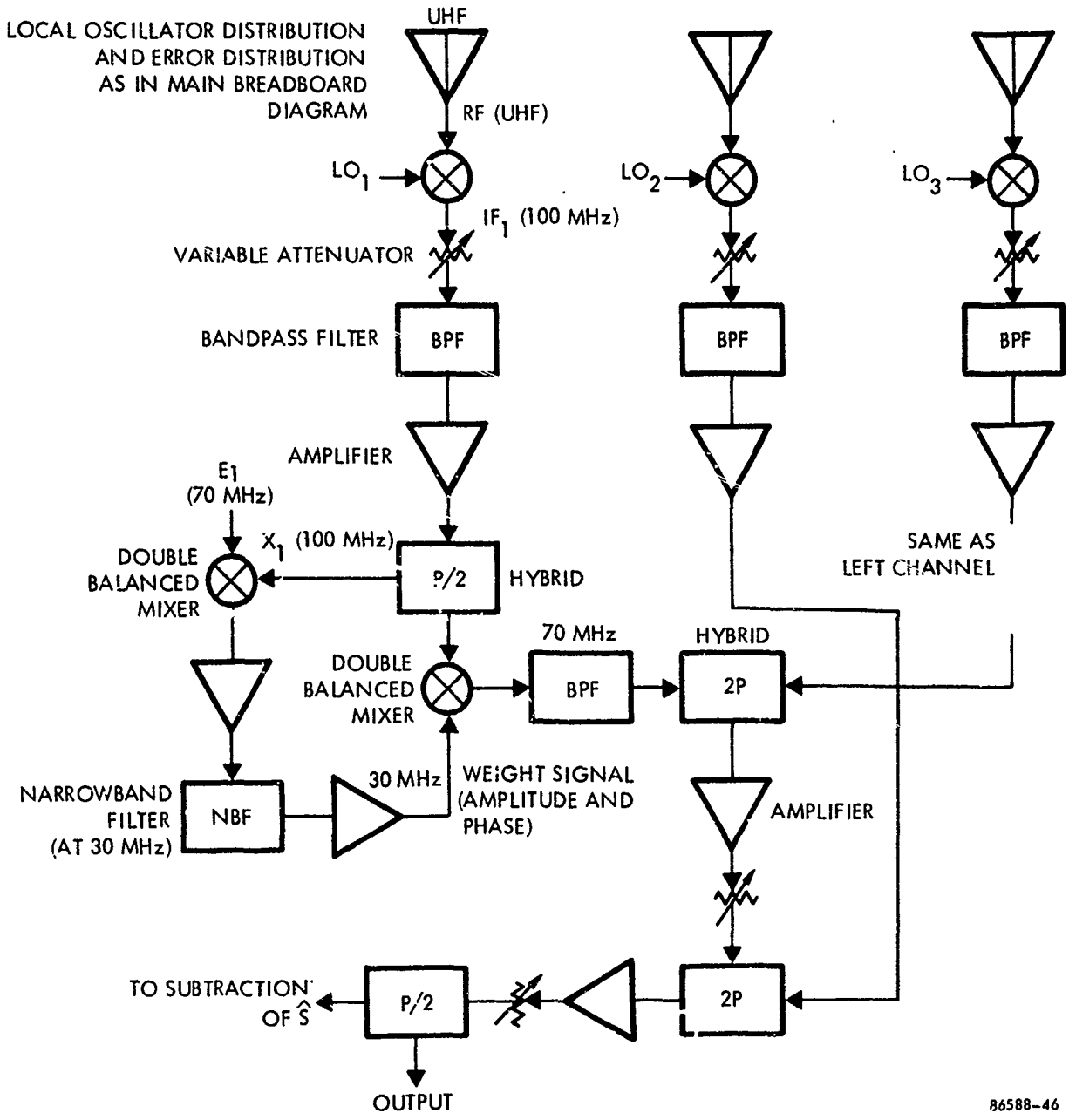


Figure 11-5. Modification of Breadboard for Complex Mixer Weight

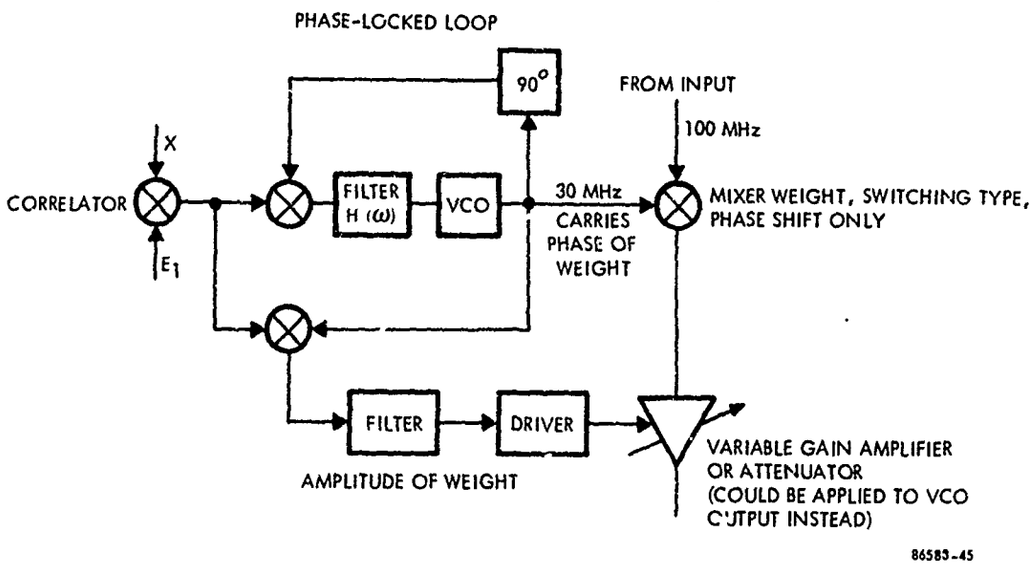


Fig. 11-6 . Possible Tracking-Filter Replacement for Narrow-Band Filter

weighting signal, with a phase equal to the input phase. Usually, however, the output is limited or saturated, so that amplitude information is lost. Amplitude information (modulation) can be obtained by an in-phase detection of the output with the input, as shown. This amplitude can then be used to "weight" the vco output before it weights the signal channel. In the figure, however, an alternate scheme is shown that allows the vco to "switch" the mixer, thus applying only a phase shift to the signal. Amplitude weighting is applied separately with a PIN diode attenuator or variable gain amplifiers.

## 11.3 Spread Spectrum Signal Removal Experiments

The spread spectrum signal removal experiments should be considered a separate experiment, because:

a. Biased suppression techniques do not require signal removal.

b. It may be very difficult, and much too expensive, to remove spread spectrum signals, because of the time delay problems encountered in matched filters. This should not be allowed to hold up the null-steering experiments.

Because of the simplicity, a coded reference decorrelation method of spread spectrum demodulation was chosen rather than a matched filter, although if such are available, they should also be tested. Figure 11-7 shows a basic breadboard for suggested experiments. The UHF signal generator, upper left, is modulated (perhaps at the signal generator), then spread spectrum modulated with a simple PN sequence derived from a shift register. This signal is added to a modulated "jamming" source to form the transmitter output. Synchronization is assumed perfect in this experiment; the PN signal is hard-wired to the array to modulate the local oscillator, which in turn mixes the received signals. The rest of the array is the basic breadboard array except for band-stop filters in both channels leading to each correlator. These filters block the narrow-band demodulated desired signal while passing most of the jamming.

Other techniques of signal removal should be tried as well; however, some would require substantially more equipment, and might raise the price of the effort considerably. Nevertheless, it may be essential to find an adequate method of signal effect removal, if the nulls obtained by biased suppression are not satisfactory.

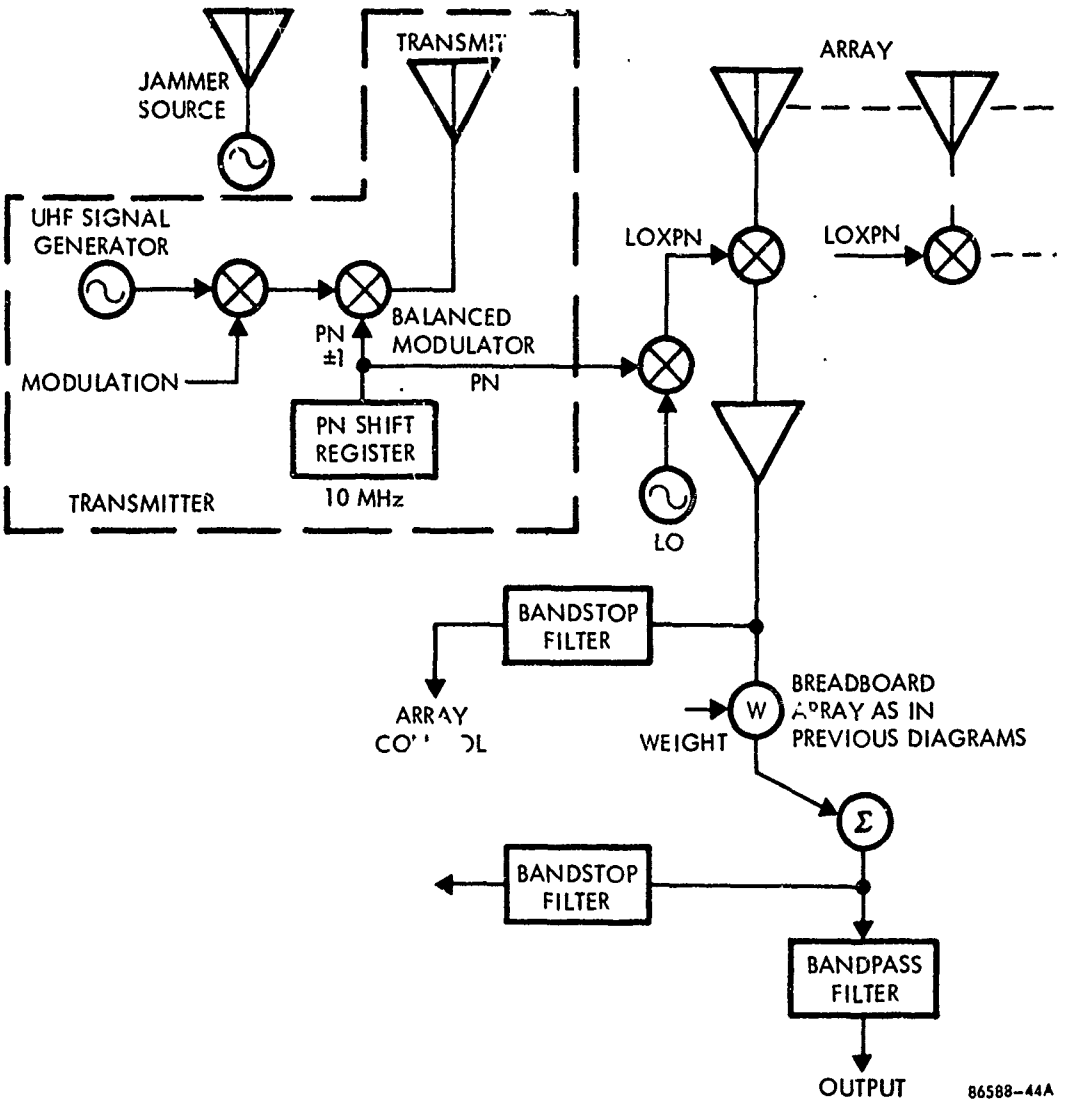


Figure 11-7. Spread Spectrum Signal Experiment Addition to Breadboard Array

# CHAPTER 12

# CONCLUSIONS

## 12.0 CONCLUSIONS

### 12.1 Summary of Results

At the outset of this study the work was conceived of as a two phase effort. The first phase involved the compilation and critical examination of those adaptive null-steering techniques which appeared applicable to RF communications problems, particularly the multiple user TDMA type system. This involved the comparative analysis of a large amount of existing technology. The second phase was to perform a more detailed analysis of at least one of the more promising procedures studied during the first phase effort. The work has essentially proceeded along these original lines, with the exception that the second phase effort has become more involved. Due to the inadequacy of the previously developed methods examined in the first phase, particularly in application to practical communication problems, the second phase effort has entailed the expanded task of both the development of practical acquisition techniques and their more detailed analysis.

In the first phase of the study the many technology areas and mathematical methods applicable to the RF null steering problems were examined. Major areas of interest were

1. The choice of an appropriate mathematical model for the general problem formulation and the adaptive array processor.

2. The selection of appropriate performance measures to define the optimal weights.

3. Derivation and comparison of the optimal weights for the various performance measures.

4. Compilation and critical examination of iterative-adaptive optimization methods to determine the best procedure for use in real-time computation for RF communication arrays.

5. Compilation and critical examination of those adaptive algorithms which have been previously suggested.

Some of the results of the first phase effort are:

1. The choice of a complex weight model for the relatively narrow band problem under study.

2. Identification of four appropriate performance measures; mean square error, signal-to-noise ratio, the likelihood function, and output noise variance.

3. Derivation of optimal complex weights for the four criteria.

4. Demonstration that for narrow band problems the minimum mean square error solution factors into a linear matrix filter, which is common to all four solutions, followed by scalar processing gains which contain all the other optimal solutions.

5. As a result of 4., it is shown that each optimal solution takes the form

$$w_{opt} = \beta R_n^{-1} r_{x\xi} \tag{12-1}$$

where $\beta$ is a scalar gain, and hence, for the narrow band case, all solutions yield identical output signal-to-noise ratios.

6. Selection of the steepest descent optimization method as the obvious choice for practical computation of the optimal solutions.

7. Demonstration, through both stochastic approximation ideas and intuitive relative bandwidth arguments, that the performance measure gradients needed in the steepest descent algorithm can be computed using instantaneous quantities readily available at the array.

8. Demonstration that the more practical algorithms suggested previously differ primarily in how desired signal effects are removed from the control circuitry. Consequently, using stochastic approximation arguments, they all obey the same general form of differential equation, namely,

$$\frac{d\overline{w}}{dt} + \alpha R_x \overline{w} = \alpha \hat{r}_{x\xi} \tag{12-2}$$

From this work it is apparent that not only are the steady state optimal solutions essentially identical, but that the algorithms developed to construct these solutions will exhibit the same general transient behavior. This, of course, also depends on how the desired signal approximation or direction of arrival estimates are acquired. Herein lie the basic differences and difficulties associated with these methods. They do not represent practical solutions, since they do not deal with the acquisition problem, however, they do dictate the basic control loop form, contingent on how the acquisition is obtained.

The first phase effort has placed the large, and therefore perhaps confusing, background of applicable techniques and algorithms in the adaptive array area within the context of the RF communication problem. It has been shown that many of the separately presented past results lead to equivalent algorithms for our problem, and that they do not actually represent practical solutions. Consequently, the second phase effort has become not only a detailed analysis, but also a development of practical acquisition techniques. This effort has proceeded primarily in the following areas:

1. Analysis of basic differential equations (Equation 12-2) using spectral decomposition techniques.

2. A detailed study of the "Dominant Jammer Reciprocal Suppression" technique for signal acquisition, in the face of very powerful jamming or interference, including: (a) analytical transient solutions for the zero-bandwidth, one-jammer case and (b) computer simulations and analysis for arbitrary parameters.

3. A detailed study of the "Biased Dominant Jammer Suppression" technique (a generalization of the "Equalization" phenomenon that Compton noted).

4. A less detailed analysis of the LMS algorithm, including analytical and some general computer results.

5. Studies of techniques for discrimination of signal and jamming in realistic scenarios. Since the techniques vary with a priori knowledge, the classification of different adaptive processing techniques by the a priori knowledge was done.

6. Studies of the various implementations of adaptive arrays, with some analysis of the hardware problems that might result.

7. Decisions for a basic breadboard design, including the several most promising implementations of weights, correlator controls, amplitude constraints and signal estimation methods that should be tested on the breadboard.

8. Statement of the recommended general approach to the breadboard tests.

Specific results have been obtained from the first four study areas cited above. Although it is difficult to summarize these results in a few lines, the major conclusions appear to be:

1. The LMS algorithm can produce at least -41 dB gain (null depth) on 1 percent bandwidth jammers, and at least -27 dB gain (null depth) on 12 percent bandwidth jammers, while losing essentially none of the full array gain on the signal in the first case, and only 2 dB in the second. Very narrow band interference or jamming can be nulled much more: over 60 dB for .1 percent bandwidth.

2. An important adaptive array property called "Dominant Jammer Reciprocal Suppression" was discovered. This property suppresses a dominant jammer very quickly, compared to a weak desired signal, without the signal being suppressed significantly. The output signal-to-jamming ratio is the reciprocal of the input signal-to-jamming ratio. Two important cases exist:

   a. Number of signals > number of elements > number of jammers. In this case, this Reciprocal Suppression result is approximately true in the steady state, at least for bandwidth < 10 percent.

   b. Number of emitters < number of elements. In this case, the reciprocal effect is true after the first transient period, at least for very narrow band; however, after this transient, the signal can be suppressed well below thermal noise. The transient period for signal acquisition was usually found to be several hundred times as long as the initial jammer suppression period. There is a very real possibility of signal acquisiton during this transient period. The reciprocal suppression result can be obtained before signal processing improvement.

3. An important signal acquisition and communication technique called "Biased Jammer Suppression" or "Equalization " allows the potential of suppressing powerful interference down to the signal level, or below it, in the steady state. The resulting output signal-to-total noise ratios approach 0 dB (for the case where the number of emitters < number of elements) just from spatial processing before signal processing. No a priori information is required about the interference sources or the signal. Note that,

   a. This technique, which does not maximize the signal or provide gain toward it, can be used for initial signal acquisition. The LMS algorithm, which requires signal estimation or signal DOA estimation, can be used later.

   b. In addition, this technique could be used for signal communication with large numbers of signal sources without signal maximization,

if approximately isotropic gain toward the signal is acceptable and some signal processing (perhaps 6-10 dB) is available.

4. Multiple jammer and multiple signal cases show little degradation over the single jammer and signal cases that form the bulk of this report.

5. In implementation study results, the three basic methods that appear most promising emphasize three different weighting techniques:

   a. Quadrature channel amplitude weighting.

   b. "Complex" weighting by using a mixer for both phase and amplitude weighting.

   c. Control of RF phase shifters, probably digitally.

6. The recommended breadboard design can test the quadrature and complex weighting techniques above with several different methods of amplitude weighting suggested: dc mixers or variable gain amplifiers or attenuators. The third technique, control of RF phase shifters, is very appealing for modifying an existing array, especially where an existing computer is available, but these assumptions, plus being totally different from the first two techniques, have eliminated it from the breadboard recommendations.

## 12.2 Recommendations for Future Work

The recommendations stem primarily from two sources. First, during the course of this study certain topics, not directly related to this effort, could only be touched upon briefly. Secondly, much of the work which has been conducted could be very profitably extended. This section presents some of these ideas.

### 12.2.1 Additional Computer Simulation

Additional computer simulations could be conducted, not only continued performance of the parameter studies already conducted, plus the consideration of additional parameters, but equally important, the development of more realistic simulations. For instance, the control loop transient behavior has been simulated using solutions to the differential equations governing the idealized control loop. This assumes perfect

integrators, summers, multipliers, etc., and does not account for even the most obvious circuit nonlinearities. Other aspects of the computer simulations could also benefit from more realistic hardware assumptions. Another area of interest would be more detailed analysis of convergence behavior and convergence control. The use of AGC or nonlinear amplifiers at the input channel, to control power and thus convergence rate, could benefit from computer analysis. Also, the use of controlled bias insertion requires additional simulation. For a given problem situation the use of the standard Widrow-Griffiths LMS algorithm would require detailed simulation study, particularly the techniques used to form effective signal or DOA estimates.

### 12.2.2 Breadboard Tests

At this point in the development of RF communication adaptive array technology, the design and construction of preliminary breadboard implementations is not only an obvious extension of the theoretical and computer analysis, but is a necessary step towards the further development of this important technology. This encompasses the construction of both specific breadboard circuitry for particular applications and the development of more general test bed configurations useful in a wide variety experimental programs. A discussion of some of the details of such programs is included in Chapters 10 and 11 of this report.

### 12.2.3 Alternative Algorithm Investigations

The present effort has been confined to the study of algorithms based on standard iterative-adaptive optimization techniques, particularly those using steepest descent gradient methods. Recently, a new class of adaptive algorithms, based on recursive estimation methods, and applicable to the control of null-steering arrays, has been introduced. These were discussed in Section 4.6 and offer several potentially important advantages over the standard adaptive methods studied here. It is important to develop these new methods to the point where reasonable comparative analysis with the standard adaptive algorithms is feasible, thereby providing the rationale for the making of trade-offs between the two methods in a given problem application. Development of this new algorithm is presently being conducted at Radiation Systems Division.

### 12.2.4 Studies for Specific Applications

Many specific applications need to be investigated for the application of adaptive arrays, for example:

a. More specific work on TDMA systems

b. Simple RF interference of UHF-VHF communications, especially at aircraft and satellite platforms.

c. Multi-path elimination, for VHF-UHF between high platforms.

d. Sensor, sonobuoy and other applications where very large numbers of signal sources exist.

e. Near - Far problem elimination in PN - spread-spectrum as well as multichannel applications.

# APPENDIX A

# DESCRIPTION OF COMPUTER SIMULATION ROUTINES

## APPENDIX A

This Appendix serves to give a block diagram representation and description for three computer programs being submitted in this report.

Program 1: Equalization mode for an adaptive array with one weight initialized to one in the jammer suppression mode.

In this program, we submit Figure A-1 as the flow diagram with the following table giving equivalence relation between the symbols used as input parameters of the program and the report.

| Program Input Symbols | Report Symbols |
|---|---|
| S1 | S |
| S2 | J |
| T1 | $\theta_1$ |
| T2 | $\theta_2$ |
| D | $\rho$ |
| N | m |
| GAM | $\delta$ |
| B | $\eta$ |

The remaining input parameters not listed here are well defined in the program. The program first compiles the electrical angles of arrival and the spatial factor given by suppression mode.

$$T11 = 2\pi D \cos (T1) \tag{1}$$

$$T22 = 2\pi D \cos (T2) \tag{2}$$

$$\langle V_1, V_2 \rangle = Q = (\sin (N/2\,(T11-T22)))/\sin (1/2(T11-T22)) \tag{3}$$

These parameters are then used to compute the weight vector

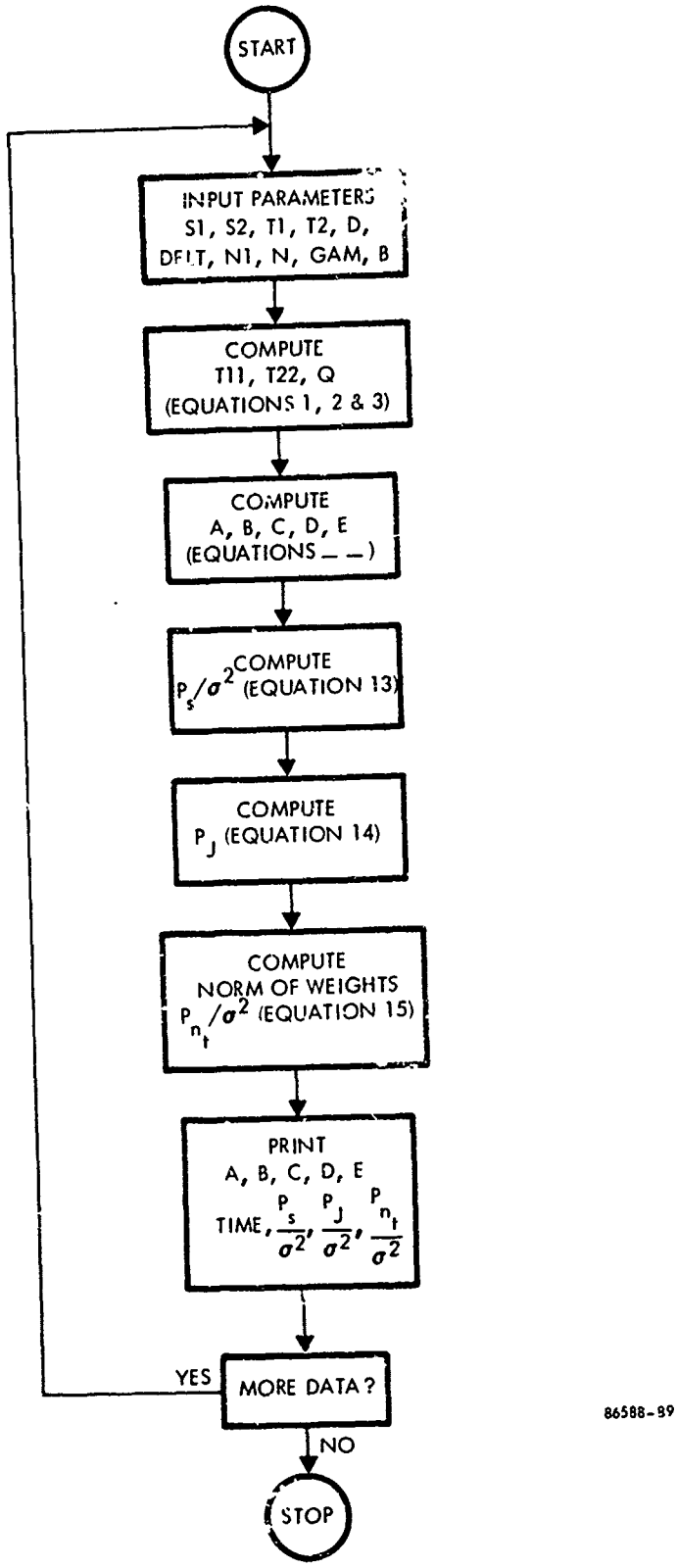


Figure A-1. Flow Diagram for the Program Equalization Mode for an Adaptive Array With One Weight Initialized to One in the Jammer Suppression Mode

$$w(t) = [A(t) + jD(t)]\, v_1 + [B(t) + jE(t)]v_2 + c(t)w_o \tag{4}$$

where

$$A(t) = \mathrm{Re}\left\{\left[e^{-\alpha\lambda_1 t} - e^{-\alpha\sigma^2 t} + \frac{1}{\lambda_1}(1-e^{-\alpha\lambda_1 t}) - \frac{1}{\sigma^2}(1-e^{-\alpha\sigma^2 t})\right]\right.$$

$$\left.\frac{\langle c_1, w_o\rangle}{\|c_1\|^2} B1\right\} + \mathrm{Re}\left\{\left[e^{-\alpha\lambda_2 t} - e^{-\alpha\sigma^2 t} + \frac{1}{\lambda_2}(1-e^{-\alpha\lambda_2 t}) - \frac{1}{\sigma^2}\right.\right.$$

$$\left.\left.(1-e^{-\alpha\sigma^2 t})\right] \frac{\langle c_2, w_o\rangle}{\|c_2\|^2} B2\right\} = \mathrm{Re}\,\hat{A}(t) \tag{5}$$

$$B(t) = \mathrm{Re}\left\{\left[e^{-\alpha\lambda_1 t} - e^{-\alpha\sigma^2 t} + \frac{1}{\lambda_1}(1-e^{-\alpha\lambda_1 t}) - \frac{1}{\sigma^2}(1-e^{-\alpha\sigma^2 t})\right]\right.$$

$$\left.\frac{\langle c_1, w_o\rangle}{\|c_1\|^2}\right\} + \mathrm{Re}\left\{\left[e^{-\alpha\lambda_2 t} - e^{-\alpha\sigma^2 t} + \frac{1}{\lambda^2}(1-e^{-\alpha\lambda_2 t}) - \frac{1}{\sigma^2}\right.\right.$$

$$\left.\left.(1-e^{-\alpha\lambda^2 t})\right] \frac{\langle c_2, w_o\rangle}{\|c_2\|^2}\right\} = \mathrm{Re}\,\hat{B}(t) \tag{6}$$

$$C(t) = e^{-\alpha\sigma^2 t} \tag{7}$$

$$D(t) = \mathrm{Im}\,\hat{A}(t) \tag{8}$$

$$E(t) = \mathrm{Im}\,\hat{B}(t) \tag{9}$$

$$t = \frac{DELT}{\alpha \lambda 1} \tag{10}$$

$$B1 = \frac{m(S-J) + \left[m^2(S-J)^2 + 4SJ < v_1, v_2 >^2\right]^{\frac{1}{2}}}{2J < v_1, v_2 >} \tag{11}$$

$$B2 = \frac{m(S-J) - \left[m^2(S-J)^2 + 4SJ < v_1, v_2 >^2\right]^{\frac{1}{2}}}{2J < v_1, v_2 >} \tag{12}$$

From these equations, the power due to the weak desired signal, the jammer and thermal noise are determined for an m ($m > 2$) element linear array given by

$$\frac{P_s}{\sigma^2} = S|< w, v_1 >|^2 = \left(\frac{(S)}{\sigma^2}\right)\left|[A(t) + jD(t)]m + [B(t) + jE(t)] < v_1, v_2 > \right.$$

$$\left. + C(t) < w_o, v_1 >\right|^2 \tag{13}$$

$$\frac{P_J}{\sigma^2} = J|< w, v_2 >|^2 = \left(\frac{J}{\sigma^2}\right)\left| \left[A(t) + jD(t)\right] < v_1, v_2 > + \left[B(t) + jE(t)\right]\right.$$

$$\left. m + C(t) < w_o, v_2 >\right|^2 \tag{14}$$

$$\frac{P_{n_t}}{\sigma^2} = \left\| \left[A(t) + jD(t)\right] v_1 + \left[B(t) + jE(t)\right] v_2 + C(t)\, w_o \right\|^2 \tag{15}$$

A printout of the program is shown in Figure A-2 with a sample run in Figure A-3.

```
100        PRINT,"EQUALIZATIØN MØDE FØR AN ADAPTIVE ARRAY WITH
110& ØNE WEIGHT INITIALIZED TØ"
120        PRINT,"ØNE,IN THE JAMMER SUPPRESSIØN MØDE."
130     1 PRINT 12
140    12 FØRMAT("0","RELATIVE DESIRED SIGNAL PØWER=")
150        INPUT,S1
160        PRINT,"RELATIVE JAMMING PØWER="
170        INPUT,S2
180        PRINT,"DIRECTIØN ØF ARRIVAL ØF DESIRED SIGNAL(DEGREES)="
190        INPUT,T1
200        PRINT,"DIRECTIØN ØF ARRIVAL ØF JAMMER(DEGREES)="
210        INPUT,T2
220        PRINT,"ANTENNA SPACING IN WAVELENGTHS="
230        INPUT,D
240        PRINT,"SAMPLE TIME IN TERMS ØF SMALLEST TIME CØNSTANT="
250        INPUT,DELT
260        PRINT,"NUMBER ØF TIME SAMPLES DESIRED="
270        INPUT,N1
280        PRINT,"NUMBER ØF ANTENNA ELEMENTS="
290        INPUT,N
300       PRINT,"RELATIVE MAGNITUDE ØF FØRCING FUNCTIØN Z="
310        INPUT,GAM
320        PRINT,"BIAS SIGNAL ETA="
330        INPUT,B
340        PI=3.1416
350        T1=PI*T1/180.
360        T2=PI*T2/180.
370        T11=2.*PI*D*CØS(T1)
380        T22=2.*PI*D*CØS(T2)
390        IF(T11-T22)2,3,2
400      2 Q=(SIN(N/2.*(T11-T22)))/(SIN(1./2.*(T11-T22)))
410        GØ TØ 4
420        3 Q=N
430      4 A1=N*(S1-S2)/(2.*S2*Q)
440        A2=(1./(2.*S2*Q))*SQRT(N*N*(S1-S2)**2+4.*S1*S2*Q*Q)
450        B1=A1+A2
460        B2=A1-A2
470        B3=B1*B1*N+2.*B1*Q+N
480        B4=B2*B2*N+2.*B2*Q+N
490        C1=CØS(PI*D*(N-1)*CØS(T1))
500        C2=SIN(PI*D*(N-1)*CØS(T1))
510        C3=CØS(PI*D*(N-1)*CØS(T2))
520        C4=SIN(PI*D*(N-1)*CØS(T2))
530        AL1=1.+B+N*(S1+S2)/2.+SQRT(.25*N*N*(S1-S2)**2+S1
540&*S2*Q*Q)
550        AL2=1.+B+N*(S1+S2)/2.-SQRT(.25*N*N*(S1-S2)**2+S1*S2*Q*Q)
560        PRINT 10
570   10 FØRMAT("0",5X,"TIME",13X,"THERMAL",12X,"SIGNAL",11X,"JAMMER")
580       PRINT 11
590   11 FØRMAT(" ",21X,"NØISE(DB)",9X,"PØWER(DB)",9X,"PØWER(DB)")
```

Figure A-2. Equalization Mode for an Adaptive Array with One Weight Initialized to One in the Jammer Suppression Mode Program

```
600        DØ 5 I=1,N1
610        T=(I-1)*DELT
620        D1=(EXP(-T))*(1.-GAM/AL1)+GAM/AL1
630        D2=(EXP(-T*(1.+B)/AL1))*(1.-GAM/(1.+B))+GAM/(1.+B)
640        D3=(EXP(-T*AL2/AL1))*(1.-GAM/AL2)+GAM/AL2
650        RW1=(D1-D2)*(B1*C1+C3)*B1/B3+(D3-D2)*(B2*C1+C3)
660&*B2/B4
670        RW2=(D1-D2)*(B1*C1+C3)/B3+(D3-D2)*(B2*C1+C3)/B4
680        RW3=D2
690        AIW1=-(D1-D2)*(B1*C2+C4)*B1/B3-(D3-D2)*(B2*C2+C4)*B2/B4
700        AIW2=-(D1-D2)*(B1*C2+C4)/B3-(D3-D2)*(B2*C2+C4)/B4
710        PN=N*(RW1**2+AIW1**2)+2.*Q*(RW1*RW2+AIW1*AIW2)+2.*(C1
720&*(RW1*RW3)-C2*RW3*AIW1)+N*(RW2**2+AIW2**2)+2.*(C3*(RW2
730&*RW3)-C4*RW3*AIW2)+D2**2
740        PS=S1*((D1*((N*B1+Q)/B3)*(B1*C1+C3)+D3*(B2*C1+C3)
750&*(N*B2+Q)/B4)**2+(D1*(B1*C2+C4)*(N*B1+Q)/B3+D3*(B2*C2+C4)*
760&(N*B2+Q)/B4)**2)
770        PJ=S2*((D1*(B1*C1+C3)*(B1*Q+N)/B3+D3*(B2*C1+C3)*(B2*Q
780&+N)/B4)**2+(D1*(B1*C2+C4)*(B1*Q+N)/B3+D3*(B2*C2+C4)*(B2
790&*Q+N)/B4)**2)
800        PN1=10.*ALØG10(PN)
810        PS1=10.*ALØG10(PS)
820        PJ1=10.*ALØG10(PJ)
830     PRINT 6,T,PN1,PS1,PJ1
840       PRINT 7,RW1,RW2,RW3,AIW1
850     5 PRINT 8,AIW2
860       7 FØRMAT(" ","A=",E12.5,2X,"B=",E12.5,2X,"C=",E12.5,2X
870&"D=",E12.5)
880      8 FØRMAT(" ","E=",E12.5)
890     6 FØRMAT("0",F11.2,10X,F8.3,10X,F8.3,10X,F8.3)
900        GØ TØ 1
910        STØP
920       END
```

Figure A-2. Equalization Mode for an Adaptive Array with One Weight Initialized to One in the Jammer Suppression Mode Program (Continued)

```
EQUALIZATIØN MØDE FØR AN ADAPTIVE ARRAY WITH ØNE WEIGHT INITIAL
IZED TØ ØNE, IN THE JAMMER SUPPRESSIØN MØDE.

RELATIVE DESIRED SIGNAL PØWER=?10

RELATIVE JAMMING PØWER=?1000

DIRECTIØN ØF ARRIVAL ØF DESIRED SIGNAL(DEGREES)=?90

DIRECTIØN ØF ARRIVAL ØF JAMMER(DEGREES)=?84

ANTENNA SPACING IN WAVELENGTHS=?.5

SAMPLE TIME IN TERMS ØF SMALLEST TIME CØNSTANT=?1

NUMBER ØF TIME SAMPLES DESIRED=?11

NUMBER ØF ANTENNA ELEMENTS=?4

RELATIVE MAGNITUDE ØF FØRCING FUNCTIØN Z=?100

BIAS SIGNAL ETA=?100

     TIME              THERMAL            SIGNAL            JAMMER
                       NØISE(DB)          PØWER(DB)         PØWER(DB)

       0.                0.                10.000            30.000
A= 0.            B= 0.            C= 0.10000E+01   D= 0.
E= 0.

      1.00             -1.049             4.962             21.675
A=-0.16781E-02   B=-0.13451E+00   C= 0.99976E+00   D=-0.37642E-03
E= 0.72616E-01

      2.00             -1.229             3.574             13.902
A=-0.25479E-02   B=-0.18372E+00   C= 0.99953E+00   D=-0.11497E-02
E= 0.99907E-01

      3.00             -1.265             3.393              7.306
A=-0.31139E-02   B=-0.20157E+00   C= 0.99930E+00   D=-0.20527E-02
E= 0.11051E+00

      4.00             -1.277             3.378              2.615
A=-0.35619E-02   B=-0.20788E+00   C= 0.99908E+00   D=-0.29876E-02
E= 0.11496E+00
```

Figure A-3. Sample Computer Run

```
      5.00            -1.286            3.374            -0.029
A=-0.39603E-02  B=-0.20995E+00  C= 0.99886E+00  D=-0.39189E-02
E= 0.11712E+00

      6.00            -1.294            3.366            -1.242
A=-0.43345E-02  B=-0.21047E+00  C= 0.99865E+00  D=-0.48338E-02
E= 0.11844E+00

      7.00            -1.301            3.357            -1.734
A=-0.46940E-02  B=-0.21043E+00  C= 0.99844E+00  D=-0.57281E-02
E= 0.11943E+00

      8.00            -1.308            3.347            -1.923
A=-0.50425E-02  B=-0.21018E+00  C= 0.99824E+00  D=-0.66005E-02
E= 0.12029E+00

      9.00            -1.315            3.337            -1.993
A=-0.53813E-02  B=-0.20987E+00  C= 0.99805E+00  D=-0.74510E-02
E= 0.12109E+00

     10.00            -1.321            3.327            -2.020
A=-0.57112E-02  B=-0.20953E+00  C= 0.99785E+00  D=-0.82799E-02
E= 0.12185E+00
```

Figure A-3. Sample Computer Run (Continued)

Program 2: Antenna Pattern Routine - This program utilizes the parameters A, B, C, D, and E generated in program 1 to determine the antenna pattern of an m $(m > 2)$ element linear array. A flow diagram of this program is given in Figure A-4.

The program computes the output power of the array given by a unity power source as described by equation

$$\psi = \left|\langle w, v_\mu\rangle\right|^2 = \left|\left[A(t) + jD(t)\right]\langle v_1\, v_\mu\rangle + \left[B(t) + jD(t)\right]\langle v_2, v_\mu\rangle + C(t)\langle w_o, v_\mu\rangle\right|^2$$

where

$$\langle v_1, v_\mu\rangle = \left\{\operatorname{Sin}\frac{m}{2}\left[2\pi D \operatorname{Cos}(T1 - T3)\right]\right\} \Big/ \operatorname{Sin}\frac{1}{2}\left[2\pi D \operatorname{Cos}[T1 - T3]\right]$$

where T3 is the angle of arrival of the unity power source. A listing of the program is shown in Figure A-5 with a sample run in Figure A-6.

Program 3: Optimal Antenna Patterns - This program computes the optimal antenna pattern for an m element linear array with an electronic environment consisting of a desired emitter with known direction of arrival and two jammers. The block diagram representation of this program is shown in Figure A-7. This program is basically the same as program 2 except that the weights are computed from

$$W_{opt} = \frac{S R_n^{-1} v_1}{1 + S\langle v_1, R_n^{-1} v_1\rangle}$$

where

$$Rn = \sigma^2 I + J_1 v_2 v_2^* + J_2 v_2 v_2^*$$

The antenna pattern can then be written as

$$\psi = \left|\langle w, v_\mu\rangle\right|^2 = \left[\frac{S}{1 + S\langle v_1, R_n^{-1} v_1\rangle}\right]^2 \left|\langle R_n^{-1} v_1, v_\mu\rangle\right|^2$$

A program listing is shown in Figure A-8 with a sample run in Figure A-9. The input parameters are well defined in the program and can be seen in Figure A-8.

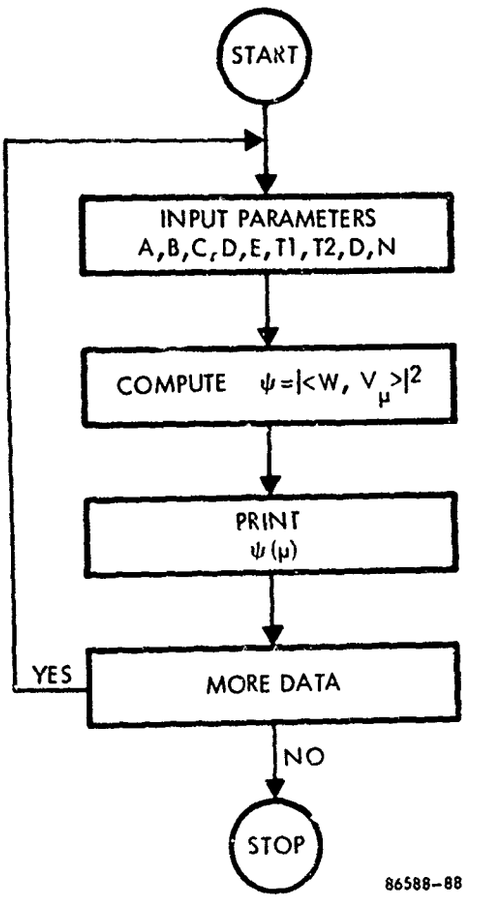


Figure A-4. Flow Diagram for "Antenna Pattern Routine"

```
100        PRINT,"ANTENNA PATTERN RØUTINE"
110    1    PRINT 12
120   12 FØRMAT("0","A=")
130      INPUT,RW1
140      PRINT,"B="
150      INPUT,RW2
160      PRINT,"C="
170      INPUT,RW3
180      PRINT,"D="
190      INPUT,AIW1
200      PRINT,"E="
210      INPUT,AIW2
220      PRINT,"ANGLE ØF ARRIVAL ØF DESIRED SIGNAL(DEGREES)="
230      INPUT,T1
240      PRINT,"ANGLE ØF ARRIVAL ØF JAMMER(DEGREES)="
250      INPUT,T2
260      PRINT,"ANTENNA SPACING IN WAVELENGTHS="
270      INPUT,D
280      PRINT,"NUMBER ØF ANTENNA ELEMENTS="
290      INPUT,N
300      PI=3.1416
310      T1=PI*T1/180.
320      T2=PI*T2/180.
330      T11=2.*PI*D*CØS(T1)
340      T22=2.*PI*D*CØS(T2)
350      PRINT 11
360   11 FØRMAT("0",1X,"DEGREES",12X,"GAIN(DB)")
370      DØ 8 I=1,91
380      A3=(I-1)*2.
390      T3=PI*A3/180.
400      PH=2.*PI*D*CØS(T3)
410      IF(T11-PH)2,3,2
420    2 Q1=(SIN(N/2.*(T11-PH)))/(SIN(1./2.*(T11-PH)))
430      GØ TØ 4
440    3 Q1=N
450    4 IF(T22-PH)5,6,5
460    5 Q2=(SIN(N/2.*(T22-PH)))/(SIN(1./2.*(T22-PH)))
470      GØ TØ 7
480    6 Q2=N
490    7 X1=RW1*Q1+RW2*Q2+RW3*CØS(PI*D*(N-1)*CØS(T3))
500   X2=AIW1*Q1+AIW2*Q2-RW3*SIN(PI*D*(N-1)*CØS(T3))
510      PSI=X1**2+X2**2
520     APSI=10.*ALØG10(PSI)
530     8 PRINT 9,A3,APSI
540    9 FØRMAT(F8.2,10X,F9.3)
550     GØ TØ 1
560      STØP
570      END
```

Figure A-5. Antenna Pattern Routine Program

```
ANTENNA PATTERN RØUTINE

A=?-0.57112E-02

B=?-0.20953E+00

C=?.99785E+00

D=?-0.82799E-02

E=?0.12185E+00

ANGLE ØF ARRIVAL ØF DESIRED SIGNAL(DEGREES)=?90

ANGLE ØF ARRIVAL ØF JAMMER(DEGREES)=?84

ANTENNA SPACING IN WAVELENGTHS=?.5

NUMBER ØF ANTENNA ELEMENTS=?4
```

| DEGREES | GAIN(DB) |
|---|---|
| 0. | -0.616 |
| 2.00 | -0.622 |
| 4.00 | -0.641 |
| 6.00 | -0.672 |
| 8.00 | -0.717 |
| 10.00 | -0.777 |
| 12.00 | -0.853 |
| 14.00 | -0.946 |
| 16.00 | -1.057 |
| 18.00 | -1.187 |
| 20.00 | -1.337 |
| 22.00 | -1.505 |
| 24.00 | -1.688 |
| 26.00 | -1.882 |
| 28.00 | -2.078 |
| 30.00 | -2.264 |
| 32.00 | -2.424 |
| 34.00 | -2.538 |
| 36.00 | -2.584 |
| 38.00 | -2.545 |
| 40.00 | -2.407 |
| 42.00 | -2.172 |
| 44.00 | -1.851 |
| 46.00 | -1.467 |
| 48.00 | -1.048 |
| 50.00 | -0.624 |
| 52.00 | -0.221 |
| 54.00 | 0.137 |

Figure A-6. Sample Computer Run

| | |
|---|---|
| 56.00 | 0.431 |
| 58.00 | 0.642 |
| 60.00 | 0.756 |
| 62.00 | 0.758 |
| 64.00 | 0.632 |
| 66.00 | 0.360 |
| 68.00 | -0.081 |
| 70.00 | -0.720 |
| 72.00 | -1.601 |
| 74.00 | -2.739 |
| 76.00 | -4.392 |
| 78.00 | -6.613 |
| 80.00 | -9.895 |
| 82.00 | -15.611 |
| 84.00 | -32.019 |
| 86.00 | -16.031 |
| 88.00 | -10.061 |
| 90.00 | -6.673 |
| 92.00 | -4.390 |
| 94.00 | -2.745 |
| 96.00 | -1.531 |
| 98.00 | -0.637 |
| 100.00 | 0.001 |
| 102.00 | 0.427 |
| 104.00 | 0.669 |
| 106.00 | 0.748 |
| 108.00 | 0.681 |
| 110.00 | 0.485 |
| 112.00 | 0.176 |
| 114.00 | -0.227 |
| 116.00 | -0.697 |
| 118.00 | -1.200 |
| 120.00 | -1.690 |
| 122.00 | -2.113 |
| 124.00 | -2.418 |
| 126.00 | -2.566 |
| 128.00 | -2.551 |
| 130.00 | -2.393 |
| 132.00 | -2.134 |
| 134.00 | -1.820 |
| 136.00 | -1.492 |
| 138.00 | -1.176 |
| 140.00 | -0.892 |
| 142.00 | -0.649 |
| 144.00 | -0.452 |
| 146.00 | -0.299 |
| 148.00 | -0.189 |
| 150.00 | -0.118 |
| 152.00 | -0.081 |
| 154.00 | -0.073 |

Figure A-6. Sample Computer Run (Continued)

| | |
|---|---|
| 156.00 | -0.089 |
| 158.00 | -0.124 |
| 160.00 | -0.172 |
| 162.00 | -0.230 |
| 164.00 | -0.292 |
| 166.00 | -0.356 |
| 168.00 | -0.417 |
| 170.00 | -0.474 |
| 172.00 | -0.523 |
| 174.00 | -0.563 |
| 176.00 | -0.592 |
| 178.00 | -0.610 |
| 180.00 | -0.616 |

Figure A-6. Sample Computer Run (Continued)

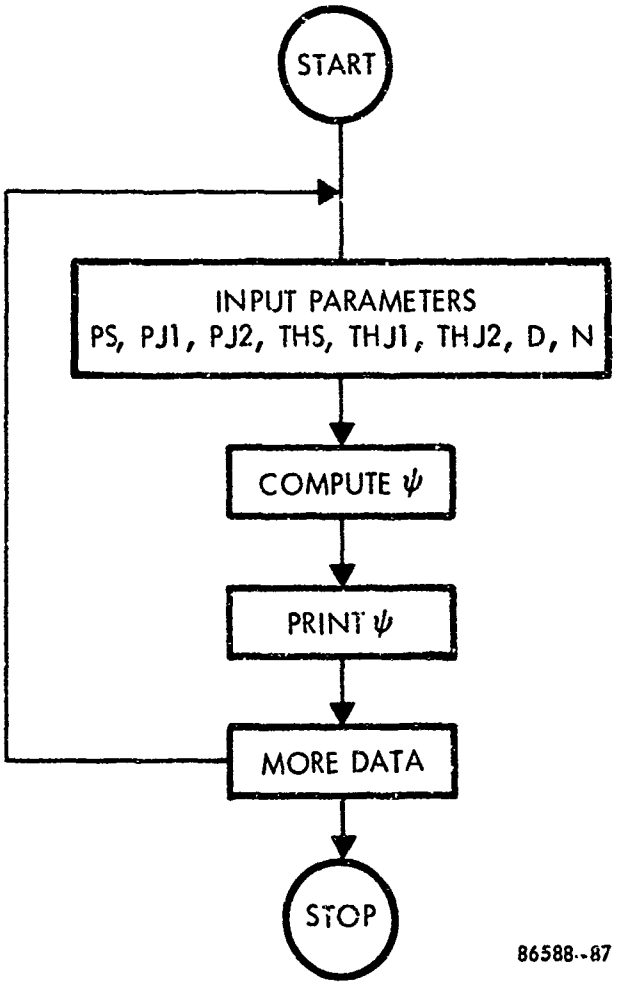


Figure A-7. Optimal Antenna Patterns

```
100        PRINT,"ØPTIMAL ANTENNA PATTERNS"
110    1    PRINT 12
120    12   FØRMAT("0","RELATIVE DESIRED SIGNAL PØWER=")
130        INPUT,PS
140        PRINT,"FIRST RELATIVE JAMMER PØWER="
150        INPUT,PJ1
160        PRINT,"SECØND RELATIVE JAMMER PØWER="
170        INPUT,PJ2
180        PRINT,"DIRECTIØN ØF ARRIVAL ØF DESIRED SIGNAL(DEGREES)="
190        INPUT,THS
200        PRINT,"DIRECTIØN ØF ARRIVAL ØF FIRST JAMMER(DEGREES)="
210        INPUT,THJ1
220        PRINT,"DIRECTIØN ØF ARRIVAL ØF SECØND JAMMER(DEGREES)="
230        INPUT,THJ2
240        PRINT,"ANTENNA SPACING IN WAVELENGTHS="
250        INPUT,D
260        PRINT,"NUMBER ØF ANTENNA ELEMENTS="
270        INPUT,N
280        PI=3.1416
290        THJ1=THJ1*PI/180.
300        THJ2=THJ2*PI/180.
310        THS=THS*PI/180.
320        PHS1=2.*PI*D*CØS(THS)
330        PHJ1=2.*PI*D*CØS(THJ1)
340        PHJ2=2.*PI*D*CØS(THJ2)
350        B1=1.+N*PJ1*(1.-(1./N*PAT(PHS1,PHJ1,N))**2)+N*PJ2*(1.
360       &-(1./N*PAT(PHS1,PHJ2,N))**2)
370        B2=N*N*PJ1*PJ2*(1.-(1./N*PAT(PHJ1,PHJ2,N))**2-(1./N*
380       &PAT(PHS1,PHJ1,N))**2-(1./N*PAT(PHS1,PHJ2,N))**2+(2./
390       &(N**3))*PAT(PHS1,PHJ1,N)*PAT(PHJ1,PHJ2,N)*PAT(PHJ2,P
400       &HS1,N))
410        DEN=1.+N*PJ1+N*PJ2+N*N*PJ1*PJ2*(1.-(1./N*PAT(PHJ1,PHJ
420       &2,N))**2)
430        B3=(PS/(1.+N*PS*(B1+B2)/DEN))**2
440        B4=(1./(N*(B1+B2)/DEN))**2
450        B33=10.*ALØG10(B3)
460        B44=10.*ALØG10(B4)
470        GØ=10.*ALØG10((PJ1+PJ2+1.)*N*(B1+B2)/DEN)
480        GC=10.*ALØG10(N*N*(1.+PJ1+PJ2)/(N+PJ1*(PAT(PHS1,PHJ1
490       &,N))**2+PJ2*(PAT(PHS1,PHJ2,N))**2))
500        C1=(-PJ1*(1.+N*PJ2)*PAT(PHJ1,PHS1,N)+PJ1*PJ2*PAT(PHJ1
510       &,PHJ2,N)*PAT(PHJ2,PHS1,N))/DEN
520        C2=(-PJ2*(1.+N*PJ1)*PAT(PHJ2,PHS1,N)+PJ1*PJ2*PAT(PHJ1
530       &,PHJ2,N)*PAT(PHJ1,PHS1,N))/DEN
540        C3=N*(1.+C1*C1+C2*C2)+2.*C1*PAT(PHJ1,PHS1,N)+2.*PAT(
550       &PHJ2,PHS1,N)*C2+2.*C1*C2*PAT(PHJ1,PHJ2,N)
560        C33=10.*ALØG10(1./C3)
580        B6=C33-B44
590        B5=B33-B44
600        SNØ=GØ-10.*ALØG10(PJ1+PJ2+1.)+10.*ALØG10(PS)
```

Figure A-8. Optimal Antenna Patterns Program

```
610        SNC=GC-10.*ALØG10(PJ1+PJ2+1.)+10.*ALØG10(PS)
620        PRINT 13,GØ
630   13   FØRMAT(" ","GAIN ØF ØPTIUM ARRAY(DB)=",F7.2)
640        PRINT 14,GC
650   14 FØRMAT(" ","GAIN ØF CØNVENTIØNAL ARRAY(DB)=",F7.2)
660        PRINT 15,SNØ
670   15 FØRMAT(" ","SIGNAL TØ NØISE RATIØ ØF ØPTIUM ARR
680&AY(DB)="F7.2)
690        PRINT 16,SNC
700   16 FØRMAT(" ","SIGNAL TØ NØISE RATIØ ØF CØNVENTIØNAL ARRA
710&Y(DB)=",F7.2)
740        PRINT 18
750    18 FØRMAT("0",1X,"DEGREES",12X,"PATTERN GAIN(DB)")
760     DØ 5 M1=1,91
770        PHS=2.*PI*D*CØS(2.*(M1-1)*PI/180.)
780     AN1=2.*(M1-1)
790        A1=PAT(PHS,PHS1,N)
800        A2=-PJ1*PAT(PHS1,PHJ1,N)*PAT(PHJ1,PHS,N)
810        A3=-PJ2*PAT(PHS1,PHJ2,N)*PAT(PHJ2,PHS,N)
820        A4=PAT(PHS1,PHJ1,N)*PAT(PHJ1,PHS,N)
830        A5=PAT(PHS1,PHJ2,N)*PAT(PHJ2,PHS,N)
840        A6=-1./N*PAT(PHS1,PHJ1,N)*PAT(PHJ1,PHJ2,N)*PAT(PHJ2,PHS
850       &,N)
860        A7=-1./N*PAT(PHS1,PHJ2,N)*PAT(PHJ2,PHJ1,N)*PAT(PHJ1,P
870       &HS,N)
880        A8=A2/DEN
890        A9=A3/DEN
900        A10=-(N*PJ1*PJ2*(A4+A5+A6+A7))/DEN
910        PSI=(A1+A8+A9+A10)**2
920        PSI4=10.*ALØG10(PSI)+B33
930    5 PRINT 6,AN1,PSI4
940    6 FØRMAT(F8.2,15X,F9.3)
950        GØ TØ 1
960        STØP
970        END
980        FUNCTIØN PAT(PH1,PH2,L)
990     IF(PH1-PH2)2,3,2
1000     2 PAT=(SIN(L/2.*(PH1-PH2)))/(SIN(1./2.*(PH1-PH2)))
1010       GØ TØ 4
1020     3 PAT=L
1030     4 RETURN
1040       END
```

Figure A-8. Optimal Antenna Patterns Program (Continued)

```
ØPTIMAL ANTENNA PATTERNS

RELATIVE DESIRED SIGNAL PØWER=?10

FIRST RELATIVE JAMMER PØWER=?100

SECØND RELATIVE JAMMER PØWER=?1000

DIRECTIØN ØF ARRIVAL ØF DESIRED SIGNAL(DEGREES)=?90

DIRECTIØN ØF ARRIVAL ØF FIRST JAMMER(DEGREES)=?95

DIRECTIØN ØF ARRIVAL ØF SECØND JAMMER(DEGREES)=?80

ANTENNA SPACING IN WAVELENGTHS=?.5

NUMBER ØF ANTENNA ELEMENTS=?4

GAIN ØF ØPTIUM ARRAY(DB)=  15.29
GAIN ØF CØNVENTIØNAL ARRAY(DB)=   1.56
SIGNAL TØ NØISE RATIØ ØF ØPTIUM ARRAY(DB)=  -5.13
SIGNAL TØ NØISE RATIØ ØF CØNVENTIØNAL ARRAY(DB)= -18.86
```

| DEGREES | PATTERN GAIN(DB) |
|---|---|
| 0. | -11.871 |
| 2.00 | -11.708 |
| 4.00 | -11.237 |
| 6.00 | -10.506 |
| 8.00 | -9.579 |
| 10.00 | -8.523 |
| 12.00 | -7.393 |
| 14.00 | -6.234 |
| 16.00 | -5.078 |
| 18.00 | -3.948 |
| 20.00 | -2.859 |
| 22.00 | -1.821 |
| 24.00 | -0.840 |
| 26.00 | 0.080 |
| 28.00 | 0.936 |
| 30.00 | 1.726 |
| 32.00 | 2.448 |
| 34.00 | 3.102 |
| 36.00 | 3.684 |
| 38.00 | 4.195 |
| 40.00 | 4.631 |
| 42.00 | 4.989 |
| 44.00 | 5.268 |
| 46.00 | 5.463 |
| 48.00 | 5.569 |
| 50.00 | 5.582 |

Figure A-9. Sample Computer Run

| | |
|---|---|
| 52.00 | 5.495 |
| 54.00 | 5.301 |
| 56.00 | 4.990 |
| 58.00 | 4.551 |
| 60.00 | 3.970 |
| 62.00 | 3.228 |
| 64.00 | 2.301 |
| 66.00 | 1.155 |
| 68.00 | -0.257 |
| 70.00 | -2.008 |
| 72.00 | -4.218 |
| 74.00 | -7.104 |
| 76.00 | -11.153 |
| 78.00 | -17.908 |
| 80.00 | -50.882 |
| 82.00 | -19.252 |
| 84.00 | -14.538 |
| 86.00 | -12.552 |
| 88.00 | -11.979 |
| 90.00 | -12.579 |
| 92.00 | -14.618 |
| 94.00 | -19.513 |
| 96.00 | -51.780 |
| 98.00 | -17.349 |
| 100.00 | -10.774 |
| 102.00 | -6.776 |
| 104.00 | -3.908 |
| 106.00 | -1.706 |
| 108.00 | 0.042 |
| 110.00 | 1.452 |
| 112.00 | 2.594 |
| 114.00 | 3.515 |
| 116.00 | 4.247 |
| 118.00 | 4.814 |
| 120.00 | 5.233 |
| 122.00 | 5.518 |
| 124.00 | 5.679 |
| 126.00 | 5.725 |
| 128.00 | 5.661 |
| 130.00 | 5.492 |
| 132.00 | 5.221 |
| 134.00 | 4.850 |
| 136.00 | 4.381 |
| 138.00 | 3.811 |
| 140.00 | 3.140 |
| 142.00 | 2.362 |
| 144.00 | 1.471 |
| 146.00 | 0.458 |

Figure A-9. Sample Computer Run (Continued)

| | |
|---|---|
| 148.00 | -0.692 |
| 150.00 | -1.999 |
| 152.00 | -3.493 |
| 154.00 | -5.220 |
| 156.00 | -7.254 |
| 158.00 | -9.722 |
| 160.00 | -12.872 |
| 162.00 | -17.302 |
| 164.00 | -25.243 |
| 166.00 | -35.018 |
| 168.00 | -21.867 |
| 170.00 | -17.461 |
| 172.00 | -15.014 |
| 174.00 | -13.496 |
| 176.00 | -12.555 |
| 178.00 | -12.036 |
| 180.00 | -11.870 |

Figure A-9. Sample Computer Run (Continued)

# APPENDIX B

# SIMULATION PROGRAM TDNS

## 1.0 INTRODUCTION

This Appendix is a users tuide to and description of the computer program "TDNS" which simulates the TDMA - Null Steering system described in Chapter 9. The presentation is organized into three parts; the first part is a brief description of the program including special assumptions made. The second part is a presentation and explan-explanation of the program flow diagram combined with accompaning explanations of the various printouts and requests for data as they are encountered during a run. The last part of the presentation is a discussion of a variety of considerations relating to the program.

## 2.0 PROGRAM DESCRIPTION

The program model has been designed to be as much like the system model as possible without requiring excessive computation time or program complexity. The program model was also designed to be suitable for an interactive computing system as opposed to batch processing.

Consider the assumed system geometry shown in Chapter 9, Figure 1. The program geometry model is very similar to this with the exception that individual emitters in the figure are regarded as flights of aircraft in the program model, each flight being composed of an arbitrary number of individual friendly signals. Given any significant range between flights and identical aircraft parameters within a flight, all signals within a flight may be regarded as having equal transmitter power and equal azimuths. This approximation is used in the program model. Rather than specify range and transmitter power, the program model asks the program user to specify relative signal power at the receiving null steering array. The program assumes the geometry to be unchanging.

The program assumes that one emitter wishes to communicate with the null steering array site (the program user) as in the system described in Chapter 9. Transmission from the user is not a program parameter (it can be approximately accomodated by assuming that the null steerer and receiver are gated off during transmission). Program selection of the desired signal is accomplished by specifying a desired flight number; account is taken within the program so as to produce only one desired signal per frame even though signal emissions equal in number to the number of aircraft per flight occur from each flight per frame.

Each desired emitter is assumed to have a pulse like transmission. The transmission may be broken into an arbitrary number of pulses at the program user's discretion, depending upon whether interest is directed principally to detailed array response to a single emitter or to overall array response on a frame basis. User compromise is required here - that assignment of an excessively large number of pulses per transmission would require excessively long computation times per frame.

Message PN coding and preamble detection by matched filter is incorporated into the program through use of user specified processing gains and error rate assumptions based on the array output S/N. Specifically, if array output S/N after applying the PN coding gain exceeds 10 dB, then zero error rate is assumed, otherwise a 100 percent rate applies. Users of the TDMA system obtain synchronism through use of matched filter detection of a message preamble. In the program, perfect synchronization is assumed if the S/N after application of the matched filter gain exceeds 10 dB, otherwise the preamble is not recognized and synchronization is not obtained.

Zero percent bandwidths are assumed. Modification of the program for the finite bandwidth case is feasible.

A nine isotropic element cruciform array geometry has been selected. Elements are equally spaced, but spacing is a program variable, and the user selects which of the nine elements will be used in a particular problem. Any one of the selected elements may be used as an initial condition isotropic element (unity weight on the selected element, all other weights zero). This weight can be specified as fixed or it can be allowed to respond to algorithm adjustment.

The algorithm used is based on the desired system response discussed in Chapter 9. In effect, a differential equation using the expected value differential equation discussed in Chapter 7 is solved iteratively. One could have used closed form solutions rather than the iterative ones but quite a large number of different solutions used piecewise in time would have been required to accomodate the switching nature of the system.

## 3.0 PROGRAM FLOW DIAGRAM AND USER'S GUIDE

A simplified Program Flow Chart is presented in Figure 1. Some program flow details are not discussed in order to expedite the users familiarization. A listing of the Program is given in Figure 3; reference to this listing is useful in understanding the program flow. The first eight major blocks, approximately the first quarter of the program, indicate establishment of initial conditions and data read in steps. Roughly the next quarter of the program deals with calculation of correlation products used in the differential equation solution while the third quarter is a "logic" section specifying how these correlation terms will be used. The remaining quarter of the flow diagram deals with loop control logic, printing control logic, and logic for user control of the program.

The program begins by asking

#FL, #S/FL, #J ?

where the symbols have the following meaning:

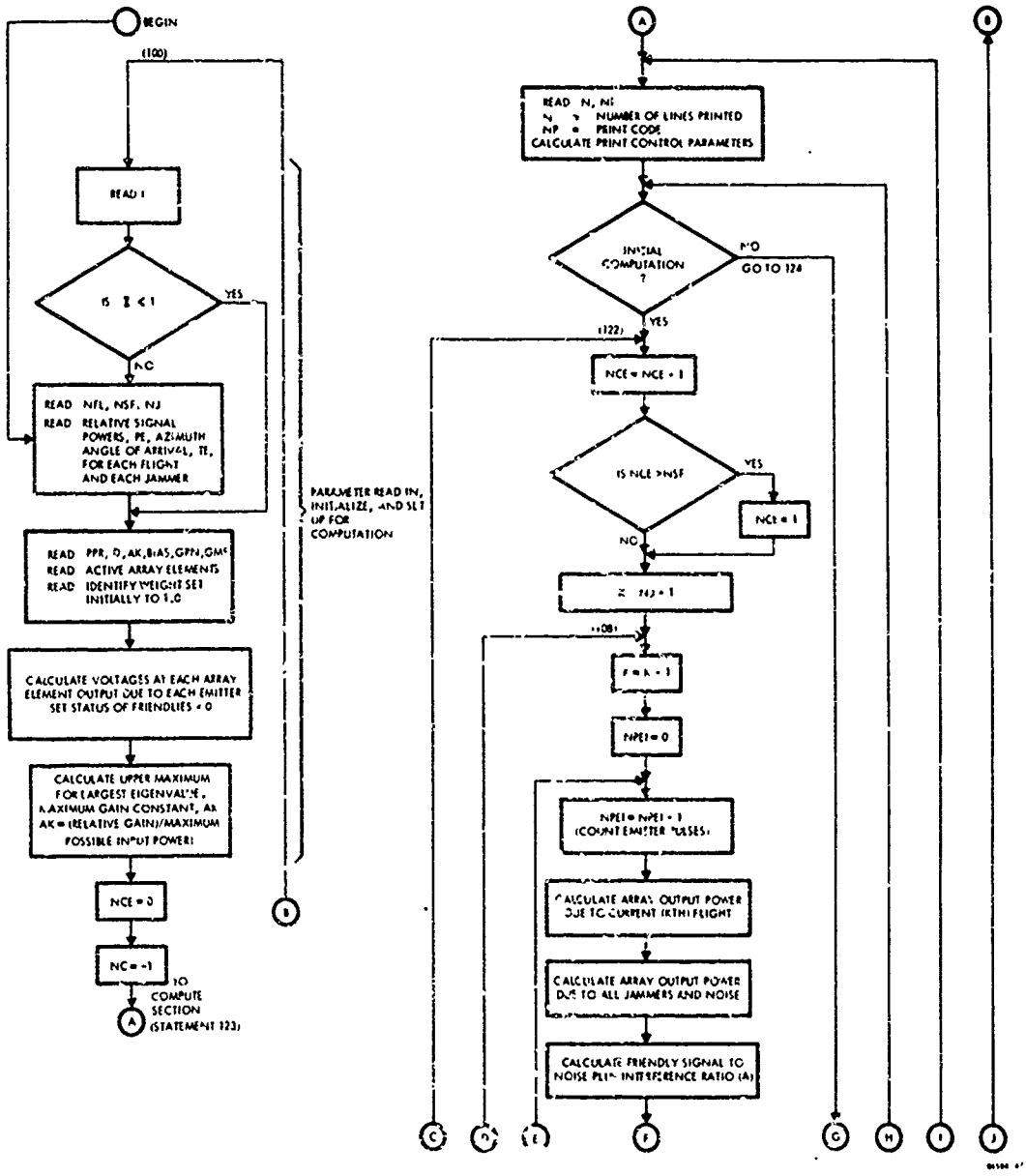


Figure 1. Program "TDNS" Flow Diagram

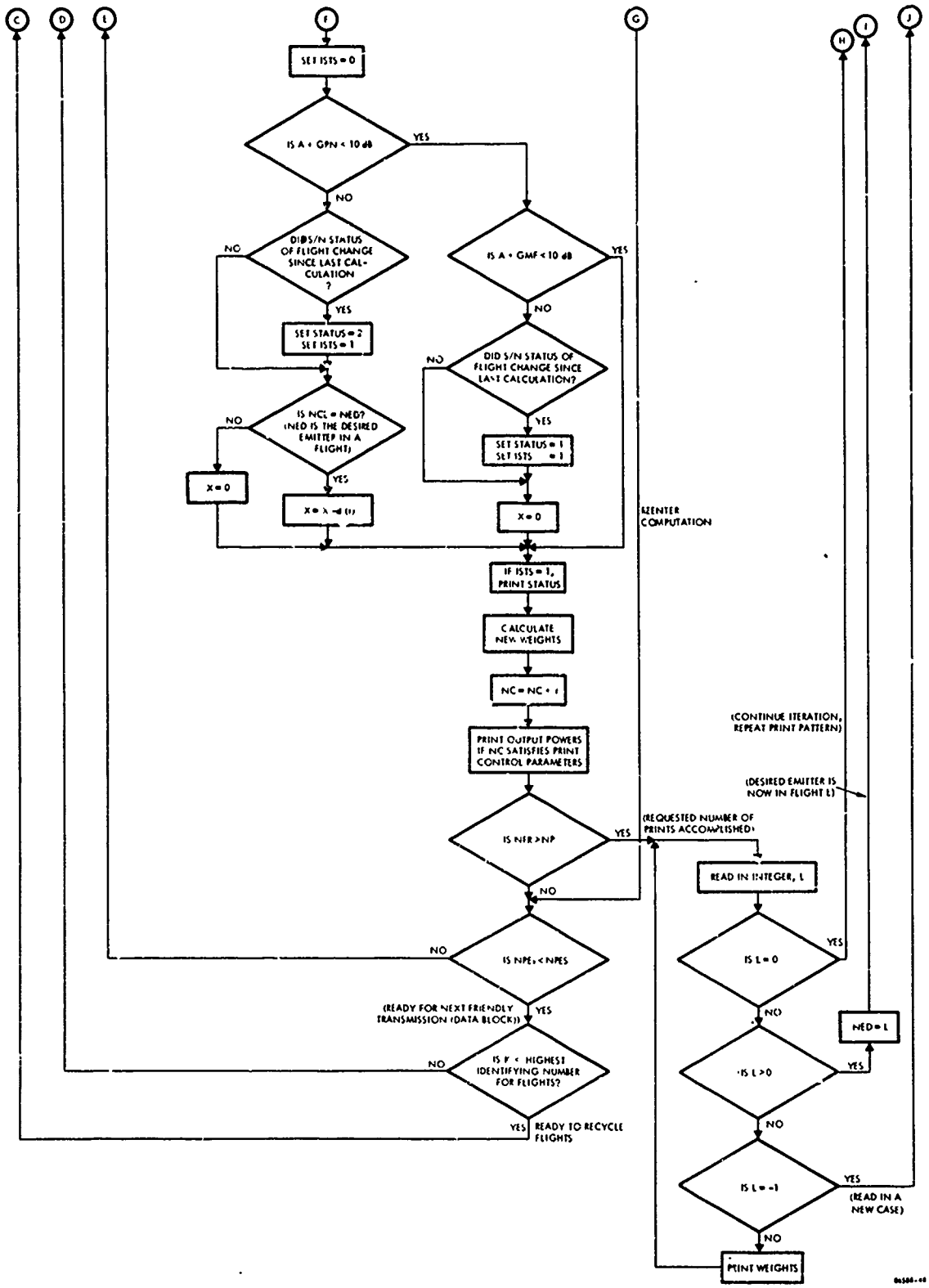


Figure 1. Program "TDNS" Flow Diagram (Continued)

#FL - Number of flights (max = 8).

#S/FL - Number of signals (aircraft) per flight.

#J - Number of Jammers (max = 3).

The number of flights plus the number of jammers is arbitrarily limited to 11 by dimension statements. The suggested maximums above are imposed by output formats, and minor program modification will permit more flexible mixes. A possible user response to the above request might be

6,5,2

(Computer and user responses are illustrated in Figure 2 for this program checkout example). As indicated on the flow diagram, Figure 1, and seen in the example run, Figure 2, the program requests the user for details about the emitters.

PJ1, T1 ?

This request has the following meaning:

PJ1 - Normalized power in watts/watt received by an isotropic antenna element at the users location due to jammer number 1 relative to thermal noise. (Thermal noise is always assumed to have a value of unity.)

T1 - Azimuth angle theta of Jammer 1 expressed in degrees and measured from a line passing through antenna elements 1, 2, 3, 4, and 5.

In the example run, the user response 1000, 90 is made, indicating that received jammer number 1 power is 30 dB above thermal noise and at an azimuth angle of $90^{\circ}$. Since #J is greater than 1, the program requests data for the second jammer by printing "PJ2, T2". In this example, the reply 500, 60 was given. Now that jammer parameters have been specified, the program asks,

PS1, T1 ?

These terms have meanings essentially the same as those just discussed, except now signal parameters are requested. In the example, the response "20, 5" was made indicating a S/N (thermal) = 20=13 dB at an azimuth of $5^{\circ}$. (Incidentally, these relative received signal and jammer powers could have resulted from a close weak jammer and a distant strong signal or in any number of other ways. When the user specifies these powers, it

```
#FL,#S/FL,#J?6,5,2
PJ1, T1?1000,90
PJ2, T2?500,60
PS1, T1?20,5
PS2, T2?20,15
PS3, T3?100,50
PS4, T4?10,85
PS5, T5?10,-50
PS6, T6?20,-55

PPS,D,AK,BIAS,GPN,GMF?2,.5,.5,0,10,20

ACTIVE ARRAY ELEMENTS, L-R(5),T-B(4)?01010,1000

FL# DESIRED,INIT W#, +FIX,-FLOAT?1,-6

N,NP (N PRINTS. PRINT PER P-1,FL-2,CY-3,FR-4)?16,1
  T     PN    PJ1    PJ2
  0     0.    30.0   27.0 PF1= 13.0
  1   -1.3    26.3   24.5 PF1= 13.2
  2   -2.1    22.5   22.1 PF1= 13.3
  3   -2.5    18.7   19.9 PF2= 10.7
STATUS FL 2 IS 1
  4   -2.8    14.5   17.8 PF2= 10.5
STATUS FL 3 IS 1
  5   -2.9    10.1   15.9 PF3= 11.8
  6   -3.0     5.2   14.2 PF3= 10.8
  7   -3.0    -0.8   12.5 PF4=-13.9
  8   -3.1    -9.1   10.9 PF4=-12.5
STATUS FL 5 IS 1
  9   -3.1   -30.5    9.5 PF5=  7.9
```

Figure 2. Example Program Run

```
 10  -3.1 -13.6   8.1 PF5=  7.9
STATUS FL 6 IS 2
 11  -3.1  -9.8   6.7 PF6= 10.8
 12  -3.1  -8.4   5.4 PF6= 10.8
STATUS FL 1 IS 2
 13  -3.1  -8.0   4.2 PF1= 12.9
 14  -3.1  -8.1   3.0 PF1= 12.9
STATUS FL 2 IS 2
 15  -3.1  -8.5   1.8 PF2=  9.9
 16  -3.1  -9.1   0.6 PF2=  9.9
FL# DESIRED (=0 MØRE, -1 NEW CASE, -2 WEIGHTS)?2

N,NP (N PRINTS. PRINT PER P-1,FL-2,CY-3,FR-4)?16,4
  T    PN   PJ1   PJ2   PF1   PF2   PF3   PF4   PF5   PF6
STATUS FL 3 IS 2
STATUS FL 4 IS 1
STATUS FL 5 IS 2
 60  -3.2 -56.9 -48.9  12.5   9.7   4.2  -9.0   8.3  11.1
120  -3.2 -87.9 -79.9  12.5   9.7   4.2  -9.0   8.3  11.1
180  -3.2 -88.0 -80.0  12.5   9.7   4.2  -9.0   8.3  11.1
240  -3.1 -88.0 -80.0  12.5   9.7   4.2  -9.0   8.3  11.1
300  -3.1 -88.1 -80.0  12.5   9.7   4.2  -9.0   8.3  11.1
360  -3.1 -88.0 -80.0  12.6   9.7   4.2  -9.0   8.3  11.1
420  -3.1 -88.0 -80.0  12.6   9.7   4.2  -8.9   8.3  11.2
480  -3.1 -88.0 -80.0  12.6   9.7   4.3  -8.9   8.3  11.2
540  -3.1 -88.1 -80.1  12.6   9.7   4.3  -8.9   8.4  11.2
600  -3.1 -88.1 -80.1  12.6   9.8   4.3  -8.9   8.4  11.2
660  -3.1 -88.1 -80.1  12.6   9.8   4.3  -8.9   8.4  11.2
720  -3.1 -88.1 -80.1  12.6   9.8   4.3  -8.9   8.4  11.2
780  -3.0 -88.1 -80.1  12.6   9.8   4.3  -8.9   8.4  11.2
840  -3.0 -88.1 -80.1  12.6   9.8   4.3  -8.9   8.4  11.2
900  -3.0 -88.1 -80.1  12.7   9.8   4.3  -8.9   8.4  11.2
960  -3.0 -88.1 -80.1  12.7   9.8   4.3  -8.8   8.4  11.2
FL# DESIRED (=0 MØRE, -1 NEW CASE, -2 WEIGHTS)?
```

Figure 2. Example Program Run (Continued)

is presumed that he has in mind specific signal and jammer ERP's and ranges.) As can be seen in the example, program requests are answered by the user until all signals are described by received power and azimuth.

As noted on the flow-chart, the computer now requests,

PPS, D, AK, BIAS, GPN, GMF

where we have:

PPS - Pulses per signal. This number is not limited by the program, but excessively large numbers will greatly lengthen computation time. (Large PPS values permit microscopic examination of array response to a given signal; small values emphasize the macroscopic array response.)

D - Array element spacing measured in wavelengths.

AK - Relative algorithm gain constant. AK= 1 will cause the algorithm to converge as rapidly as possible without instability. Usually, a value of 0.5 or 0.1 is selected. (Actually, a choice of AK slightly greater than 1.0 is sometimes possible. Refer to the following discussion regarding maximum eigenvalue approximation.)

BIAS - Bias. As discussed in Chapter 7, array acquisition behavior may sometimes be enhanced by lessening the relative strength of signal and jammer correlation terms. Normally, these terms are referenced to thermal noise power. In this algorithm, the correlation terms are referenced to BIAS + thermal noise.

GPN - Gain of the Pseudo Noise Code in dB.

GMP - Gain of the preamble detecting matched filter in dB.

In the example run, the user response was "2, .5, .5, 0, 10, 20".

Specification of the array configuration and active array elements is next in the program flow. The program asks:

ACTIVE ARRAY ELEMENTS, L-R(5), T-B(4) ?

Request is being made for the user to specify which of the 9 array elements will be used in this problem. This printout reminds that five elements are numbered left to right, and

the remaining four from top to bottom. The elements are assumed to be numbered as follows:

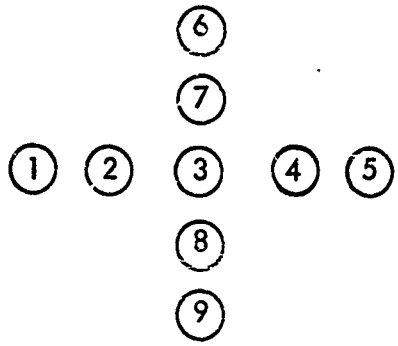


The user response identifies which of these elements are to be used. Let us assume that the following array configuration is desired:

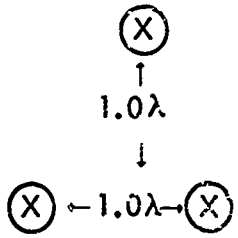


For this, the user types "01010, 1000". This input specifies that elements 2, 4, and 6 will be used and that 1, 3, 5, 7, 8, and 9 are inactive. Note that a comma (or any other separator) is required between the horizontal and vertical element specifiers. Often, a desired array configuration may be obtained in numerous different ways-with different D values and with different active elements. For example, a 3 element horizontal array may be specified as "11100, 0000," "011100, 0000," "00111, 0000," or "10101, 0000."

After this specification, the program types:

FL# Desired, INIT W#. + FIX, -FLOAT ?

The user is asked to specify two integers: the flight number within which the desired signal is located (NSD) and secondly, which array element will have an initial weight of unity when computation commences. (All other weights are set to zero. This initial weight specification ensures that all emitter signals will be initially received by the array and none will initially fall within an array factor null.) If the identifying number of an inactive element is chosen, all weights will be initially zero. If the element identifying number is positive, the weight identified is not adjusted by the algorithm-it remains fixed at 1.0. However, a negative identifying number allows the algorithm to adjust this weight as well as the others. The example user's response was "1, -6" thus the desired signal is an aircraft located in flight number 1 and element 6, the upper

element in the previous diagram, is initially weighted unity while elements 1 and 5 are weighted zero. As time progresses, all three weights will be adjusted by the algorithm.

As indicated on the flow diagram, prepatory calculations are carried out at this time. An array of numbers representing the normalized phase voltage at the output of each element due to each signal and each jammer is calculated. (Element output due to thermal noise is 1.0 and is not calculated.) Voltages for elements in a horizontal line are expressed as

$$VEM(\ell, I, k) = e^{-j2\pi D \cos (T(I) * 2\pi/180^{\circ})}$$

where VEM is the name of the array storing the phase voltages, $\ell = 1$ for storage of the real part of the expression or $\ell = 2$ for storage of the imaginary part. (This notation is used throughout the program. Ordinarily, automatic complex arithmetic would be used, but allowance is made here for limited computer compiler capacity.) The parameter "I" identifies the emitter while "k" specifies the element number. Similar expressions are obtained for vertically aligned elements except that Sin rather than Cos is used as an arrangement for the exponential. Note that the center element (3) is used as reference and has a unity normalized voltage.

Before the initialization phase of the program is ended, the "Status" of all flights is set equal to zero. The term "Status" is used to denote the relative received strength of a "friendly" signal. The following definitions are made:

| Status | Condition |
|---|---|
| 0 | Friendly is not receivable (Suppression mode refered to in Chapter 9). |
| 1 | Friendly's preamble is received error free by the matched filter and the local PN code generator is synchronized, but reception of message data is not possible. (Sync mode refered to in Chapter 9). |
| 2 | Friendly's message can be received error free (Receive mode of Chapter 9). |

Calculation of the unnormalized algorithm gain constant can be realized by approximating the maximum eigenvalue of $R_x$ by the sum of all incident power at each element times the number of active elements (bias is a psuedo power and must be included in this sum). We have

AK (unnormalized) = AK (normalized to maximum)/largest eigenvalue

Since the array differential equations are known to have solutions of the form

$$e^{-(AK)(\lambda)t}$$

a normalized time, $\tau$, is defined for convenience. We require

$$\tau = t(AK)(\lambda)$$

For this program, the iteration number, refered to here as T, is printed rather than $\tau$. The parameter $\tau$ can be obtained by the user through the expression

$$\tau = T(AK \text{ normalized})$$

Lastly, as indicated on the program flow diagram, the parameters NCE and NC are initialized. NCE has no external meaning - it is used in the program to ensure only one desired friendly emission per frame. The term NC is the iteration count and is printed under the identifier "T" just mentioned. An initial value of -1 is used to accomodate the time=zero condition. Other statements within the mostly arithmitic sections also provide special computation for this first time through situation but are not shown on the flow diagram.

At this point the program request print control parameters N and NP. The example shows the following print:

N, NP (N PRINTS. PRINT PER P-1, FL-2, CY-3, FR-4)?

The first parameter, N, specifies how many lines of array output data will be printed. The second parameter, NP, establishes at what points within the computation printout will occur.

NP

1 (P) Array output power in dB is printed for every pulse of a friendly signal. (Every iteration)

2 (FL) Array output power is printed at the end of iterations for a friendly signal. This is the same as the end of transmissions for a flight (FL). If PPS=1, then the effect of NP=1 is the same as NP=2.

3 (CY) This program simulation of the TDMA system is based upon friendly signals emanting successively from flights in sequence. One cycle (CY) is a complete set of emissions, one from each flight. NP=3 will cause array output power to be printed once per cycle. Note that a cycle is not a frame unless the parameter #S/FL=1.

4. (FR) Array Power output printout occurs once per frame (FR) for NP=4.

In the example run, "16, 1" was the user response, thus 16 output data lines are to be printed, one for every signal pulse (algorithm iteration). All output power is expressed in dB.

The major part of computation begins soon after this point in the program flow (statement number 123), but first print control parameters are calculated and headings are printed. A decision is made at statement 127 as to whether computation on a previous problem is being continued or whether this is a new case. If calculations are being continued, control is transferred to statement 124 where computation begins again where it was left off. If this is a new case, a major program loop is entered at statement 122, where the parameter NCE is incremented. If NCE exceeds the number of signals per flight, NCE is reset to 1; this occurs once per time frame completion.

The parameter K identifies friendly emitter storage locations. Since all emitters are stored sequentially with jammers first, the first K is the number of jammers plus one; the last is equal to the total number of emitters, NE. A second major loop is entered at statement 108 where computation for sucessive emitters (K) is entered. The final major loop is preceeded with NPEI=0. This loop counts emitter pulses. All iterative computation for weights occurs within this loop; correlations for all jammers, thermal noise, and the $K^{th}$ friendly signals are calculated for use in the algorithm.

Normalized array output for the $K^{th}$ signal is calculated first. We use "X" for this term and get

$$X = \sum_{L} W(L) * VEM(K, L)$$

The actual expressions are slightly more complicated than the above expression indicates due to use of XR = Real part of X and XI = imiginary part of X in lieu of automatic complex arithmetic. It is recalled that the first parameter of VEM is either 1 or 2 respectively for real and imaginary parts. Emitter output power, PEO(K), is also calculated (in dB). Note that X is normalized to unity input power.

Calculations for jammer and thermal noise output are similarly performed with normalized complex jammer output being stored in the array JO and jammer power output in PEO(M).

Next, the $K^{th}$ signal (flight) to noise plus jamming ratio is calculated and eventually stored in variable "A" (between statements 110 and 118). An internally used flag, ISTS, is set to zero, and then tests are begun to establish the status of the $K^{th}$ flight. It is assumed that 10 dB S/N is required for adequate detection. If A+GPN

exceeds 10 dB, then the despread signal can be detected error free (by assumption). In this case, check of the $K^{th}$ flight status is made to see whether or not a change has occured and if so, the flag ISTS is set and the new status appropriately noted.

Now, if calculations are presently being made for the desired friendly emitter (correct flight and correct signal within the flight), the algorithm described in Chapter 9 specifies that a Widrow Type array is to be used and the term X-d(t) is formed. Due to an inability to adequately estimate d(t) if the S/N is too low, this computation for X is made only if the desired signal has a status of 2. It is assumed that the desired magnitude of the signal in the array output is 6 dB above that at an element (twice the voltage) and that d(t) is in phase with the output. Thus, we replace X with the following

$$X = X - 2 * (X/\text{Magnitude}(X))$$

(X is expressed above as a normalized complex quantity).

If the calculations are not being made for the desired emitter, the algorithm discussed in Chapter 9 requires that we simply remove all signal from the array output to prevent array nulling action. This is accomplished by setting X = 0.

Earlier the test of S/N was made for Status = 2; if this test was failed, a check for S/N meeting status 1 requirements is made (Preamble receivable with matched filter). If this test is passed, the current status is recorded and any status change noted. The term X is set to zero whether or not this calculation is made for the desired signal since adequate S/N for X-d(t) formation is not available.

If S/N is too low for Status 1, no signal recognition is possible and X is retained "as is" in the array output. Although it is not indicated or the flow diagram, status changes downward are also noted and recorded. If ISTS was set to 1 indicating a change, the new status of the present emitter is noted in a printout.

New weight calculations are undertaken next. The following expression for the normalized weight change is used:

$$DW(J) = \{ PE(K) * X * VEM(K, J) \} + \sum_{M} \{ PE(M) * JO(M) * VEM(M, J) \} + \{ BIAS * W(J) \}$$

The first brace is due to friendly signals, the second due to jammers and the third due to thermal noise and the psuedo noise, "bias" (note: the term BIAS is the sum of the BIAS value read in and the element expected noise value, 1.0). Finally, new weights are calculated according to the expression

$$W(J)_{t+1} = W(J)_t - AK * DW(J)$$

The program now enters a "bookkeeping" phase which controls looping and printout. The iteration counter NC is advanced and printout tests are made. A count is made of the number of lines printed, NPR. If the requested number of lines has not been printed, tests are made as to completion of the three major iteration loops. If on the other hand, the requested amount of computation has been finished, the program requests the user for new directions:

FL# DESIRED ( = 0 MORE, -1 NEW CASE, -2 WEIGHTS)

User response is to type in an integer. The following conditions apply:

0 Continue computation. The flight number within which the desired signal is located remains unchanged as do N and NP.

>0 Continue computation for the present case. The flight number of the desired signal is now the number typed in. The program requests new values for N and NP. If the user wishes to change N and NP without changing the flight number desired, he should type in the present flight number.

- 2 Present values of the weights are printed out with the real part first and the imaginary part second. The program then repeats its request for new direction.

- 1 No more data is sought for the present case. Control is transferred to statement 100 where the program begins reinitialization.

Reinitialization proceeds almost the same as the initialization phase described earlier. The difference is that the user has the option of retaining the same signals and jammers without re-reading them in: the computer asks:

NEW SIGS, 1

If retention of the previous data is desired, zero should be the input, otherwise type in 1.

In the example run, the user typed in 2 for the flight number desired (it was previously 1). Next N and NP were changed to 16, 4 and a printout format change is reflected in the new value of NP.

## 4.0 CONSIDERATIONS

Three important considerations are touched on here, the difficulty in reaching steady state with the program, the possibility of instability due to the beam forming algorithm, and the fact that the user modifications of the program may inadvertently affect proper program flow.

As has been mentioned previously, steady state is virtually unachievable with iterative computation even though output parameters may appear to be quite unchanging. An example of this is seen in the example run, Figure 2. Note that after the initial transient is over, several hundred more iterations were necessary to cause a 0.1 dB change in the desired signal output (Flight 1). However, there is a very interesting case where steady state is achievable iteratively - the "overspecified" case discussed in 9.3 wherein only enough elements as necessary for forming jammer nulls are used. As mentioned in Chapter 9, the eigenvalues are large and determined almost entirely by the jammers.

The possibility of computation instability exists under certain beam forming calculations. It is due to the fact that d(t) influences the maximum eigenvalues as well as array input power, yet account is not taken of this effect in normalizing AK. Part of the difficulty is that the program does not know in advance which signal will be desired. If instability occurs, selection of a smaller AK will solve the problem.

Finally, it is realized that user modification of the program will probably be desirable, and that this could create inadvertent errors. Additionally, programs often run differently on different machines. It is suggested that checkout of the program be made using known results such as the example run and/or data from the numerous transient curves presented earlier in this report.

```
100        DIMENSIØN PE(11),TE(11),PEØ(11),IE(9),ISTS(8)
110       &,W(2,9),VEM(2,11,9),DW(2,9),AJØ(2,9)
120        GØTØ129
130 100    PRINT,"NEW SIGS,1"
140        INPUT,I
150        IF(I.LT.1)GØTØ101
160 129    PRINT,"#FL,#S/FL,#J"
170        INPUT,NS,NSF,NJ
180        NE=NS+NJ
190        XK=0.
200        DØ102I=1,NE
210        J=I-NJ
220        IF(I.GT.NJ)PRINT302,J,J
230 301    FØRMAT("&PJ",I1,", T",I1)
240        IF(I.LE.NJ)PRINT301,I,I
250 302    FØRMAT("&PS",I1,", T",I1)
260        INPUT,PE(I),TE(I)
270        XK=XK+PE(I)
280        TE(I)=TE(I)*.017453293
290 102    CØNTINUE
300 101    CØNTINUE
310        PRINT,"PPS,D,AK,BIAS,GPN,GMF"
320        INPUT,NPE,D,AK,BIAS,GPN,GMF
330        BIAS=BIAS+1.
340        D=D*6.2831853
350        PRINT,"ACTIVE ARRAY ELEMENTS, L-R(5),T-B(4)"
360        INPUT201,(IE(I),I=1,9)
370 201    FØRMAT(5(I1),1X,4(I1))
380        PRINT,"FL# DESIRED,INIT W#, +FIX,-FLØAT"
390        INPUT,NED,NWF
400        DØ104I=1,NE
410        VEM(1,I,3)=1.
420        VEM(2,I,3)=0.
430        CI=D*CØS(TE(I))
440        CR=CØS(CI)
450        CI=-SIN(CI)
460        VEM(1,I,4)=CR
470        VEM(2,I,4)=CI
480        VEM(1,I,2)=CR
490        VEM(2,I,2)=-CI
500        VEM(1,I,5)=CR*CR-CI*CI
510        VEM(2,I,5)=2.*CR*CI
520        VEM(1,I,1)=VEM(1,I,5)
530        VEM(2,I,1)=-VEM(2,I,5)
540        CI=D*SIN(TE(I))
550        CR=CØS(CI)
560        CI=SIN(CI)
570        VEM(1,I,7)=CR
```

Figure 3. Listing of Program "TDNS"

```
580          VEM(2,I,7)=CI
590          VEM(1,I,8)=CR
600          VEM(2,I,8)=-CI
610          VEM(1,I,6)=CR*CR-CI*CI
620          VEM(2,I,6)=2.*CR*CI
630          VEM(1,I,9)=VEM(1,I,6)
640          VEM(2,I,9)=-VEM(2,I,6)
650 104      CØNTINUE
660          L=0
670          DØ105I=1,9
680          L=L+IE(I)
690          W(1,I)=0.
700 105      W(2,I)=0.
710          AK=AK/(L*(XK+BIAS))
720          J=IABS(NWF)
730          W(1,J)=1.
740          W(2,J)=0.
750          NC=-1
760          DØ121L=1,NS
770          PEØ(L+NJ)=0.
780 121      ISTS(L)=0
790          NCE=0
800 123      CØNTINUE
810          PRINT,"N,NP (N PRINTS. PRINT PER P-1,FL-2,CY-3,FR-4)"
820          INPUT,NP,NPP
830          IF(NP.LT.0)STØP
840          IF(NPP.EQ.1)NCP=1
850          IF(NPP.EQ.2)NCP=NPE
860          IF(NPP.EQ.3)NCP=NPE*NS
870          IF(NPP.EQ.4)NCP=NPE*NS*NSF
880          PRINT304
890 304      FØRMAT("&  T     PN")
900          DØ116I=1,NJ
910 116      PRINT305,I
920 305      FØRMAT("&    PJ",I1)
930          IF(NPP.LT.3)GØTØ127
940          DØ117I=1,NS
950 117      PRINT306,I
960 306      FØRMAT("&    PF",I1)
970 127      IF(NC.GT.0)GØTØ124
980          NPR=0
990 122      CØNTINUE
1000          NCE=NCE+1
1010          IF(NCE.GT.NSF)NCE=1
1020          K=NJ
1030 108      K=K+1
1040          NPES=NPE
1050          IF(NC.LT.0)NPES=NPES+1
```

Figure 3. Listing of Program "TDNS" (Continued)

```
      NPEI=0
  114 NPEI=NPEI+1
      PE0(K)=0.
      XR=0.
      XI=0.
      D0109L=1,9
      IF(IE(L).LT.1)G0T0109
      XR=XR+W(1,L)*VEM(1,K,L)-W(2,L)*VEM(2,K,L)
      XI=XI+W(2,L)*VEM(1,K,L)+W(1,L)*VEM(2,K,L)
  109 CONTINUE
      PE0(K)=4.3429*AL0G(REAL(PE(K)*(XR*XR+XI*XI)))
      PN=0.
      P=0.
      D0110M=1,NJ
      AJ0(1,M)=0.
      AJ0(2,M)=0.
      YR=0.
      YI=0.
      D0111L=1,9
      IF(IE(L).LT.1)G0T0111
      YR=YR+W(1,L)*VEM(1,M,L)-W(2,L)*VEM(2,M,L)
      YI=YI+W(2,L)*VEM(1,M,L)+W(1,L)*VEM(2,M,L)
      IF(M.EQ.1)PN=PN+W(1,L)*W(1,L)+W(2,L)*W(2,L)
  111 CONTINUE
      AJ0(1,M)=YR
      AJ0(2,M)=YI
      A=PE(M)*(YR*YR+YI*YI)
      P=P+A
      PE0(M)=4.3429*AL0G(A)
  110 CONTINUE
      P=4.3429*AL0G(P+PN)
      PN=4.3429*AL0G(PN)
      ISF=0
      A=PE0(K)-P
      L=K-NJ
      IF((A+GPN).LT.10)G0T0118
      IF(ISTS(L).NE.2)ISF=1
      ISTS(L)=2
      IF((NCE.GT.1).0R.(L.NE.NED))G0T0128
      CR=1.-2./(SQRT(XR*XR+XI*XI))
      XR=XR*CR
      XI=XI*CR
      G0T0120
  118 IF((A+GMF).LT.10.)G0T0119
      IF(ISTS(L).NE.1)ISF=1
      ISTS(L)=1
  128 XR=0.
      XI=0.
```

Figure 3. Listing of Program "TDNS" (Continued)

```
1540        GØTØ120
1550 119    IF(ISTS(L).NE.0)ISF=1
1560        ISTS(L)=0
1570 120    CØNTINUE
1580        IF(ISF.GT.0)PRINT307,L,ISTS(L)
1590 307    FØRMAT(" STATUS FL ",I1," IS ",I1)
1600        DØ112J=1,9
1610        IF(IE(J).LT.1)GØTØ112
1620        IF(J.EQ.NWF)GØTØ112
1630        DW(1,J)=(VEM(1,K,J)*XR+VEM(2,K,J)*XI)*PE(K)+W(1,J)*BIAS
1640        DW(2,J)=(VEM(1,K,J)*XI-VEM(2,K,J)*XR)*PE(K)+W(2,J)*BIAS
1650        DØ113M=1,NJ
1660        DW(1,J)=DW(1,J)+(VEM(1,M,J)*AJØ(1,M)+VEM(2,M,J)*AJØ(2,M)
1670       &)*PE(M)
1680        DW(2,J)=DW(2,J)+(VEM(1,M,J)*AJØ(2,M)-VEM(2,M,J)*AJØ(1,M)
1690       &)*PE(M)
1700 113    CØNTINUE
1710        W(1,J)=W(1,J)-AK*DW(1,J)
1720        W(2,J)=W(2,J)-AK*DW(2,J)
1730 112    CØNTINUE
1740        NC=NC+1
1750        J=(NC/NCP)*NCP
1760        IF(NPP.GT.2)GØTØ125
1770        IF((J.NE.NC).AND.(NC.GT.0))GØTØ124
1780        PRINT303,NC,PN,(PEØ(J),J=1,NJ)
1790        PRINT310,L,PEØ(K)
1800        GØTØ106
1810 310    FØRMAT("&PF",I1,"=",F5.1)
1820 125    IF(J.NE.NC)GØTØ124
1830        PRINT303,NC,PN,(PEØ(J),J=1,NE)
1840 303    FØRMAT(1X,I3,11(1X,F5.1))
1850 308    FØRMAT(1X,I3," PF",I1,1X,F5.1)
1860 106    CØNTINUE
1870        NPR=NPR+1
1880        IF(NPR.GT.NP)GØTØ126
1890 124    IF(NPEI.LT.NPES)GØTØ114
1900        IF(K.LT.NE)GØTØ108
1910        GØTØ122
1920 126    PRINT,"FL# DESIRED (=0 MØRE, -1 NEW CASE, -2 WEIGHTS)"
1930        INPUT,L
1940        IF(L.EQ.-1)GØTØ100
1950        IF(L.LT.-1)GØTØ130
1960        NPR=1
1970        IF(L.EQ.0)GØTØ124
1980        NED=L
1990        GØTØ123
2000 130    PRINT311,(I,W(1,I),W(2,I),I=1,9)
2010        GØTØ126
2020 311    FØRMAT(9(1X,"W",I1,G11.4,1X,G11.4,/))
2030        END
```

Figure 3. Listing of Program "TDNS" (Continued)

# REFERENCES

## REFERENCES


1. Adams, R. T., "An Adaptive Antenna System for Maximizing Signal-to-Noise Ratio," Wescon Conf., Sessions 24, pp. 1-4, 1966.

2. Allen, J. L., "The Theory of Array Antennas (with Emphasis on Radar Applications)," Massachusetts Institute of Technology, Lincoln Lab. Report 323, 25 July 1963.

3. Anderson, V. C., "DICANNE, a Realizable Adaptive Process," JASA, Vol. 45, No. 2, pp. 298-405, 1969.

4. Anderson, V. C. and P. Rudnick, "Rejection of a Coherent Arrival at an Array," JASA, Vol. 45, No. 2, pp. 406-410, 1969.

5. Applebaum, S. P., "Adaptive Arrays," SPL-TA-66-1, Syracuse University Research Corp., Syracuse, N. Y., August 1966.

6. Applebaum, S. P., et al., "Coherent Sidelobe Cancellation Techniques," 12th Annual Tri-Service Radar Symp. Rec., Syracuse University Research Corp., June 1966.

7. Baird, C. A., "A Recursive, Least Squares Algorithm for the Control of Array Antennas," Radiation Incorporated, APD Technical Memo, August 1970.

8. Baird, C. A., "Adaptive Processing Techniques for Antenna Arrays," Radiation Incorporated, TR-45, (RADC Contract #F30602-71-C-0173), November 1971.

9. Baird, C. A., and J. T. Rickard, "Recursive Estimation in Array Processing," Fifth Asilomar Conf. on Circuits and Systems, November 1971.

10. Baird, C. A., and C. L. Zahm, "Performance Criteria for Narrowband Array Processing," 1971 IEEE Conference on Decision and Control, Miami Beach, Florida, December 15-17, 1971.

11. Backus, M., J. Burg, D. Baldwin, and E. Bryan, "Wide Band Extraction of Mantle P Waves from Ambient Noise," Geophysics, Vol. 29, pp. 672-692, October 1964.

12. Becker, C. J., and B. F. Cron, "Optimum Array Gain for Directional Noise," USL Report No. 656, 5 October 1965.

13. Brennan, L. E., E. L. Pugh, and I. S. Reed, "Control-Loop Noise in Adaptive Array Antennas," IEEE Trans. on Aerospace and Electronic Systems, Vol. AES-7, No. 2, March 1971.

14. Brown, R. G., and J. W. Nilsson, "Introduction to Linear Systems Analysis," J. W. Wiley & Sons, N. Y., 1962.

15. Bryn, F., "Optimum Signal Processing of Three-Dimensional Arrays Operating on Gaussian, Signals and Noise," JASA, Vol. 34, #3, 1962.

16. Burg, J. P., "Three-Dimensional Filtering with an Array of Seismometers," Geophysics, Vol. XXIX, No. 5, pp. 693-713, October 1964.

17. Butcher, W. and R. J. Sims, "Application of Adaptive Algorithms to RF Antenna Arrays," Proc. of IEEE, Vol. 60, No. 3, March 1972.

18. Butcher, W., and R. J. Sims, "Adaptive Null Steering for RF Antenna Arrays," Array Antenna Conference, Naval Electronics Lab Center, San Diego, California, February 1972.

19. Capon, J., R. J. Greenfield, and R. J. Kolker, "Multidimensional Maximum-Likelihood Processing of a Large Aperture Seismic Array," Proc. of the IEEE, Vol. 55, No. 2, pp. 192-211, February 1967.

20. Chang, J. H., and F. B. Tuteur, "Adaptive Tapped Delay Line Filters," Third Princeton Conference on Information Sciences and Systems, March 1969.

21. Chang, J., and F. Tuteur, "Optimum Adaptive Array Processor," Proc. of Symp. on Computer Processing in Commu., Polytechnic Inst. of Brooklyn, pp. 695-710, April 8-10, 1969.

22. Chang, J. H., and F. B. Tuteur, "A New Class of Adaptive Processors," JASA, Vol. 49, No. 3, 1971.

23. Cheng, D. K., and F. I. Tseng, "Signal-to-Noise Ratio Maximization in Receiving Arrays," IEEE Trans. Ant. and Prop., Vol. AP-14, pp. 792-794, November November 1966.

24. Claerbout, J. F., "Detection of P Waves from Weak Sources at Great Distances," Geophysics, Vol. 29, pp. 197-211, April 1964.

25. Collin, R. E. and F. J. Zucher, "Antenna Theory," Parts I and II, McGraw-Hill, N. Y., 1969.

26. Compton, R. T., and R. L. Riegler, "Adaptive Antennas for Automatic Interference Rejection," URSI Fall Meeting, University of Texas, Austin, Texas, 1969.

27. Compton, R. T., "Adaptive Arrays: On Power Equalization with Proportional Control," Quarterly Report 3234-1, Naval Air Systems Command, Contract #N00019-71-C-0219, December 1971.

28. Compton, R. T., "Adaptive Antenna Arrays for Aircraft Communications Systems," Final Report 3098-2 Office of Naval Research, Contract #N00014-67-A-0232-0009, January 1972; Interim Report, 3098-1, July 1971.

29. Cox, H., "Optimum Arrays and the Schwartz Inequality," JASA, Vol. 45, No. 1, pp. 228-232, 1969.

30. Curry, G. R., "Interference Cancelling Using an Independent Reference," M.I.T. Lincoln Lab, Group Report 47.27, 16 July 1959 (U).

31. Daniell, T. P., "Adaptive Estimation with Mutually Correlated Training Samples," PhD Dissertation, Stanford University, 1968.

32. Davidson, W. C., "Variable Metric Methods for Minimization," A.E.C. Research and Development Report, ANL-5990 (rev), 1959.

33. Dvoretzky, A., "On Stochastic Approximation," Proc. Third Berkeley Symp. on Math Stat. and Prob., pp. 39-55, 1956.

34. Edelblute, D. J., J. M. Fisk, and G. L. Kinnison, "Criteria for Optimum Signal Detection Theory for Arrays," JASA, Vol. 41, No. 1, pp. 199-205, 1967.

35. Fagin, Samuel L., "Recursive Linear Regression Theory, Optimal Filter Theory, and Error Analyses of Optimal Systems," M. S. Thesis, New York University, 1964.

36. Faran, J. J., and R. Hills, "Wide-band Directivity of Receiving Arrays," Harvard University Acoustics Research Lab, Tech. Memo. No. 31, 1 May 1953.

37. Gaarder, A. T., "The Design of Point-Detection Arrays," Tech. Report, Stanford Research Inst.

38. Getty, W. D., "Noise Cancellation Using Amplitude and Phase Nulling Servo Loops," Internal Report 16, NOrd 14362, M.I.T. Res. Lab. of Elect., 1 October 1954 (U).

39. Gostin, J. J., "Matched Weighing - a Self-Optimizing Aperture Illumination Function," General Electric Report #R67 EMH38, November 1967.

40. Graham, J. W., "The Effect of Bandwidth Upon Noise Cancellation by Phase Balancing," Internal Report 15, NOrd 14362, M.I.T. Res. Lab. of Elect., 1 October 1954 (U).

41. Griffiths, L. J., "Signal Extraction Using Real-Time Adaptation of a Linear Multichannel Filter," PhD Thesis, Stanford Univ., 1968.

42. Griffiths, L. J., "Minimum Mean Square Error Array Processing. An Interative Approach," Sym. on Computer Proc. 17 Comm., Poly. Inst. of Brooklyn, April 8-10, 1969.

43. Griffiths, L. J., "A Simple Adaptive Algorithm for Real-Time Processing in Antenna Arrays," Proc. of the IEEE, Vol. 57, No. 10, October 1969.

44. Halmos, P. R., "Finite Dimensional Vector Spaces," D. Van Nostrand Co., Inc., 1958.

45. Hanson, R. C., "Microwave Scanning Antennas," Vol. II "Arrays," Academic Pros., N. Y., 1964.

46. Huff, R. J., "Coherent Multiplexing and Array Techniques," Ohio State University, RADC-TR-70-34, AD 867946, March 1970.

47. Huff, R. J., "TDMA Space Communications Systems: Concepts and Practical Techniques," RADC-TR-71-255, November 1971.

48. Kelly, E. J., and M. J. Levin, "Signal Parameter Estimation for Seismometer Arrays," Lincoln Laboratory, Lexington, Mass., Technical Report 339, M.I.T. DDC 435489, January 1964.

49. Kelly, E. J., "A Comparison of Seismic Array Processing Schemes," Tech. Note 1965-21, M.I.T. Lincoln Laboratory, 14 June 1965.

50. Kiefer, J., and J. Wolfowitz, "Stochastic Estimation of the Maximum of a Regression Function," Annals of Math. Stat., Vol. 23, pp. 462-466, 1952.

51. Kowalik, J. and M. R. Osborne, "Methods for Unconstrained Optimization Problems," American Elsevier, N. Y., 1968.

52. LaCoss, R. T., "Adaptive Combining of Wideband Array Data for Optimal Reception," IEEE Trans. on Geo. Sci. Elect., Vol. GE-6, pp. 78-86, May 1968.

53. Levin, M. J., "Least-Squares Array Processing for Signals of Unknown Form," The Radio and Electronics Engr., pp. 213-222, April 1965.

54. Lintz, P. R., "Principles of Wiener Auto-Adaptive Filtering," Seismic Data Laboratory Report No. 224, Advanced Research Projects Agency, Nuclear Test Detection Office, Washington, D.C., 1968.

55. Liusternik, L. and V. Sobolev, "Elements of Functional Analysis," Frederick Ungar Pub. Co., N. Y., 1961.

56. Mantey, D. E., and L. J. Griffiths, "Iterative Least-Squares Algorithms for Signal Extraction," 2nd Hawaii Conference on System Science, January 1969.

57. Middleton, D., and H. Groginsky, "Detection of Random Acoustic Signals by Receivers with Distributed Elements," SJOR-297, Raytheon Co., August 1963.

58. Owsley, N. L., "Source Location with an Adaptive Array," Naval Underwater Systems Center, NUSC Report No. NL-3015, AD 719896, January 1971.

59. Pritchard, R. L., "Directivity of Acoustic Linear Point Arrays," Harvard University Acoustics Res. Lab., Tech. Memo No. 21, 15 January 1951.

60. Riegler, R. L., "Adaptive Optimization of Signal-to-Noise Ratio in Receiving Arrays," Ohio State University, TR2902-1, NASA grant NGL-36-008-138, July 1970.

61. Riegler, R. L., and R. T. Compton, "An Adaptive Array for Interference Rejection," Ohio State University, Columbus, Ohio, Report No. 2552-4, N70-25470, 16 February 1970.

62. Robinson, E. A., "Mathematical Development of Discrete Filters for the Detection of Nuclear Explosions," J. of Geophysical Research, Vol. 68, No. 19, pp. 5559-5567, October 1963.

63. Schneider, W. A., K. L. Larner, J. P. Burg, and M. M. Backus, "A New Data Processing Technique for the Elimination of Ghost Arrivals on Reflection Seismograms," Geophysics, Vol. XXIX, No. 5, pp. 783-805, October 1964.

64. Schweppe, F. C., "Sensor Array Data Processing for Multiple-Signal Sources," IEEE Trans. on Info. Theory, Vol. IT-14, No. 2, March 1968.

65. Seidman, L. P., "The Statistical Theory of Bearing Estimation - I - Literature Survey," Bell Telephone Laboratories Technical Memo No. MM68-4211-9, September 1968.

66. Senne, Kenneth, "Adaptive Linear Discrete-Time Estimation," PhD Dissertation, Stanford University, 1968.

67. Shor, S. W. W., "Adaptive Technique to Discriminate Against Coherent Noise in a Narrowband System," Journal of Acoustical Society of America, 39, pp. 74-78, January 1966.

68. Stradling, C. S., and A. B. Baggeroer, "Joint Active and Passive Sonar Signal Processing Using Arrays," Naval Underseas Research and Development Center, NUC TP121, December 1968.

69. Texas Instruments Inc., Science Services Division, Special Reports, Contract # AF33(65T)-12747, Air Force Tech. Appl. Center, VELA Seismological Center, June 1967.

70. Texas Instruments Inc., Science Services Division, Special Reports 1-14, Contract # F33657-67-C-0708-P001, ARPA, Nuclear Test Detection Office, December 1967.

71. Texas Instruments Inc., Science Services Division, Special Reports 1-10, Contract # F33657-68-C-0867, ARPA, Nuclear Test Detection Office, March 1969.

72. Van Trees, H. L., "A Formulation of the Space-Time Processing Problem for Sonar Systems," Project Trident Working Memo 208, A. D. Little, Inc., 4 December 1964.

73. Van Trees, H. L., "A Unified Theory of Array Processing," Department of the Navy, Naval Ship Systems Command, NObsr-93055, Arthur D. Little Report No. 4150866, August 1966.

74. Van Trees, H. L., "Optimum Processing for Passive Sonar Arrays," IEEE Ocean Engr. Symp., Hawaii, 1966.

75. Widrow, B., "Adaptive Filters 1: Fundamentals," Systems Theory Laboratory, Stanford Electronics Laboratories, Stanford University, Stanford, California, Report No. 6764-6, December 1966.

76. Widrow, B., P. E. Mantey, L. J. Griffiths, and B. B. Goode, "Adaptive Antenna Systems," Proc. of the IEEE, Vol. 55, No. 12, pp. 2143-2159, December 1967.

77. Wiggins, R. A., and E. A. Robinson, "Recursive Solutions to the Multichannel Filtering Problem," J. of Geophysical Research, Vol. 70, No. 8, pp. 1885-1891, April 1965.

78. Wilde, D., "Optimum Seeking Methods," Prentice-Hall, Chapter 6, 1964.

79. Zahm, C. L., "Application of Adaptive Arrays to Suppress Strong Jammers in the Presence of Weak Signals," Radiation Incorporated, Advanced Systems Operations Tech. Memo No. 44, February 1972.

80. Raytheon Co. Report (NASA-CR-728, N 67-27267) "Study of a Signal Processor Employing a Synthetic Phase Isolator," (Bickford, W. J., et al.), May 1967.